

# UC Davis

## UC Davis Electronic Theses and Dissertations

### Title

From basic to translational: investigating serotype I feline coronavirus biology, moving anticoronaviral therapeutics into cats with feline infectious peritonitis, and delivering feline erythropoietin into cells and rodents using viral vectors

### Permalink

<https://escholarship.org/uc/item/04g507dx>

### Author

Cook, Sarah E

### Publication Date

2022

Peer reviewed|Thesis/dissertation

From basic to translational: investigating serotype I feline coronavirus biology, moving anticoronaviral therapeutics into cats with feline infectious peritonitis, and delivering feline erythropoietin into cells and rodents using viral vectors

By

SARAH ELISABETH COOK  
DISSERTATION

Submitted in partial satisfaction of the requirements for the degree of

DOCTOR OF PHILOSOPHY

in

Integrative Pathobiology

in the

OFFICE OF GRADUATE STUDIES

of the

UNIVERSITY OF CALIFORNIA

DAVIS

Approved:

---

Brian G. Murphy, Chair

---

Amir Kol

---

Simon Anthony

Committee in Charge

2022

## Table of Contents

Title page	i
Table of Contents	ii
Acknowledgements	iii
Abstract	iv
Chapter 1.	1
Introduction and Review - <i>Coronavirus infections in companion animals: virology, epidemiology, clinical and pathologic features</i>	
Chapter 2.	24
<i>Serotype I and II feline coronavirus replication and gene expression patterns of feline cells – building a better understanding of serotype I FIPV biology</i>	
Chapter 3.	44
<i>Investigation of monotherapy and combined anticoronaviral therapies against feline coronavirus serotype II in vitro</i>	
Chapter 4.	56
<i>An optimized bioassay for screening combined anticoronaviral compounds for efficacy against feline infectious peritonitis virus with pharmacokinetic analyses of GS-441524, remdesivir, and molnupiravir in cats</i>	
Chapter 5.	75
<i>Assessing safety and efficacy of a lentivirus-vectored feline erythropoietin gene therapy strategy in tissue culture and rodent models</i>	
Chapter 6.	123
<i>Conclusion</i>	

## Acknowledgements

I have had the sincere honor of receiving mentorship from Brian Murphy for many years now. First, alongside the entire UC Davis Anatomic Pathology Service, as a valued and supportive teacher during my time in the UC Davis anatomic pathology residency program. Brian offered a balance of humor, realism, and the ability to never shy away from expressing his opinion. This transitioned into a position of research mentorship quickly as I initiated my residency research project with the Murphy lab during my first year of residency and subsequently continued my work in his lab when I entered the Integrative Pathobiology Graduate Group PhD program upon completion of the residency training. Brian always encouraged me to be comfortable making mistakes and to be independent. His tireless efforts demonstrated his investment in my success as a pathologist, a researcher, and a person. Thank you.

My qualifying exam committee: Kevin Woolard, Lark Coffey, and Sean Hulsebosch for their thoughtful questions, for challenging me, and guiding me through that pivotal transition into candidacy. My dissertation committee, Amir Kol, Simon Anthony, and Brian Murphy, for their encouragement, direction, and enthusiasm towards my research accomplishments and remaining goals. Further, I thank the many collaborators involved in the research presented within this dissertation for their individual and collective expertise that contributed to my success.

In addition, I would like to acknowledge Diego Castillo. His expertise and support were essential to my success, and he was always available to help with his vast skill set. Diego has been a friend for several years prior to commencing my graduate work. It was a relief to have a familiar and friendly face at the lab ready to guide me.

To my resident-mate and graduate school comrade, Charlie Alex. What a journey it's been! I can't think of another person with which to experience our residency years and graduate school.

Finally, I thank my family for their unwavering support over the many years of school, training, struggles, and achievements.

## Abstract

Coronaviruses are enveloped RNA viruses capable of causing a spectrum of diseases including respiratory, enteric, and/or systemic diseases in a wide variety of hosts. The major structural proteins of coronaviruses include the nucleocapsid (N), spike (S), membrane (M), and envelope (E) proteins. The viral Spike protein largely determines host range and tissue/cellular tropism and is responsible for promoting fusion of the viral and host cell membranes, leading to cell entry and infection. A literature review of coronaviruses in companion animals is included in this thesis (Chapter 1), which highlights the virology, epidemiology, clinical and pathologic features of coronaviruses of the cat, ferret, dog, horse, and alpaca.

Feline infectious peritonitis (FIP) is one of the most complex and interesting viral diseases of domestic cats, caused by the FIP virus (FIPV), a biotype of feline coronavirus (FCoV). FIP has an immune-mediated pathogenesis involving multiple host and virologic factors. FIP presents as a spectrum of clinical signs including cavitory effusions, anorexia, persistent fever, lymphopenia, and lesions of pyogranulomatous vasculitis and peri-vasculitis that may or may not include central nervous system or ocular involvement. Untreated, FIP is generally considered to be fatal once clinical signs appear.

FCoV includes two biotypes, feline enteric coronavirus (FECV) and FIPV. FIPV spreads systemically and is thought to arise from a discrete set of mutations in the more benign FECV, which is confined to the alimentary tract. These coronaviruses are further classified into serotypes I and II based on Spike-associated antigenic differences. Serotype II FCoV initially arose as the result of a series of recombination events between feline and canine coronavirus (CCoV) and is the *less* prevalent serotype naturally circulating in feline populations worldwide. As a result of recombination, the serotype II FIPV Spike protein has its origin in CCoV, which serves as the viral ligand for cell entry.

Although FIPV serotype I is the more prevalent viral serotype in cats with naturally occurring FIP, serotype II has been more extensively studied *in vitro* due to the relative ease in propagating this virus in

tissue culture systems. Consequently, more is known about the biology of serotype II FIPV than the more biologically relevant serotype I. Serotype II FIPV utilizes the cell surface protein feline aminopeptidase N, the ligand of the viral Spike protein, while the receptor for serotype I remains unknown. An understanding of viral receptor biology is a key facet in decoding viral pathogenesis, informing mechanisms of disease, viral dissemination, and potential vaccine strategies. The recent development of a feline cell line that effectively propagates serotype I FIPV, FCWF-4 CU, offers an opportunity to expand our understanding of serotype I FIPV biology. FCWF-4 CU is a culture adapted feline cell line derived from FCWF-4 cells available through the ATCC. Importantly, these two FCWF cell lines are variably permissive to the propagation of serotype I and II FIPV. In Chapter 2, we determined the targeted gene expression patterns in four feline cell lines, utilized normal feline tissues to determine the immunohistochemical expression patterns of two known coronavirus receptors, ACE2 and DC-SIGN, and compared the global transcriptomes of the two closely related FCWF-4 cell lines. We identified six differentially expressed transcripts with potential to explain the differential FIPV replication kinetics.

The discovery of effective, available, and affordable antiviral treatments has been a focus of veterinary research for more than 10 years and recent advances in antiviral therapies for HIV, hepatitis C virus, ebolavirus and SARS CoV-2 have paved the way for similar advances for FCoV. In Chapter 3, we screened 90 putative antiviral compounds for efficacy and cytotoxicity against FIPV serotype II (WSU-79-1146) using real-time RT-PCR based screens and identified 26 compounds with antiviral activity against FIPV representing differing drug classes and mechanisms of action. Further, based on the success of combinatorial therapy strategies in human patients with HIV or hepatitis C, we strategically combined different antiviral compounds in order to identify additive or synergistic effects (combined anticoronaviral therapy, or CACT). Although we demonstrated additive and/or synergistic effects for several antiviral combinations, ultimately a select few monotherapies demonstrated superior efficacy overall. In Chapter 4, we reappraised antiviral assessment using an improved biological colorimetric

assay and compared the antiviral efficacies of GC376, nirmatrelvir, remdesivir, GS-441524, molnupiravir (EIDD-2801), and  $\beta$ -D-N4-hydroxycytidine (EIDD-1931) against both serotype I and II FIPV, as monotherapies and CACT. We also determined the pharmacokinetic properties of three antiviral compounds, molnupiravir, GS-441524, and remdesivir in cats *in vivo* as a step towards establishing dose in an antiviral treatment protocol for clinical use.

An understanding of viral cell entry, dissemination and persistence are concepts that are also relevant to viral-vectored gene therapy. As a parallel adjunct study to the coronavirus projects, we created a lentiviral-vectored gene therapy approach to treating cats with chronic renal disease-associated anemia. Chronic renal disease (CRD) is a common disease of aged cats, often associated with clinically significant nonregenerative anemia as a result of reduced renal production of erythropoietin (EPO). Multiple approaches to the management of CRD-associated anemia have been attempted, including the use of gene therapy. In Chapter 5, we designed a series of third-generation lentivirus-based vectors to encode and produce the native feEPO protein in tissue culture experiments and in rodent models *in vivo*. The vectors were designed to include a pharmacologic safety mechanism through the incorporation of the “suicide gene” HSV-TK. This gene product allows for the pharmacologic termination of the therapeutic effect in the event of supraphysiologic polycythemia. We hypothesized that cells transduced *in vitro* by a lentiviral vector encoding native feline erythropoietin would express feEPO mRNA and biologically active feEPO protein and that this expression could be terminated by the administration of ganciclovir (GCV, the nontoxic substrate of HSV-TK). The *in vitro* assays facilitated optimization of the vector for three *in vivo* studies in rats and genetically modified anemic mice in which we demonstrated a significant elevation of blood packed cell volume in treated animals relative to control animals.

**Chapter 1: Review of coronavirus infections in companion animals: virology, epidemiology,  
clinical and pathologic features**

# Coronavirus Infections in Companion Animals: Virology, Epidemiology, Clinical and Pathologic Features

Christine Haake<sup>1,\*</sup> , Sarah Cook<sup>2</sup>, Nicola Pusterla<sup>3</sup> and Brian Murphy<sup>4</sup> 

<sup>1</sup> School of Veterinary Medicine, University of California, Davis, CA 95616, USA

<sup>2</sup> Graduate Group Integrative Pathobiology, School of Veterinary Medicine, University of California, Davis, CA 95616, USA; sestevens@ucdavis.edu

<sup>3</sup> Department of Medicine & Epidemiology, School of Veterinary Medicine, University of California, Davis, CA 95616, USA; npusterla@ucdavis.edu

<sup>4</sup> Department of Pathology, Microbiology, and Immunology, School of Veterinary Medicine, University of California, Davis, CA 95616, USA; bmurphy@ucdavis.edu

\* Correspondence: cjhaake@ucdavis.edu

Received: 28 July 2020; Accepted: 11 September 2020; Published: 13 September 2020



**Abstract:** Coronaviruses are enveloped RNA viruses capable of causing respiratory, enteric, or systemic diseases in a variety of mammalian hosts that vary in clinical severity from subclinical to fatal. The host range and tissue tropism are largely determined by the coronaviral spike protein, which initiates cellular infection by promoting fusion of the viral and host cell membranes. Companion animal coronaviruses responsible for causing enteric infection include feline enteric coronavirus, ferret enteric coronavirus, canine enteric coronavirus, equine coronavirus, and alpaca enteric coronavirus, while canine respiratory coronavirus and alpaca respiratory coronavirus result in respiratory infection. Ferret systemic coronavirus and feline infectious peritonitis virus, a mutated feline enteric coronavirus, can lead to lethal immuno-inflammatory systemic disease. Recent human viral pandemics, including severe acute respiratory syndrome (SARS), Middle East respiratory syndrome (MERS), and most recently, COVID-19, all thought to originate from bat coronaviruses, demonstrate the zoonotic potential of coronaviruses and their potential to have devastating impacts. A better understanding of the coronaviruses of companion animals, their capacity for cross-species transmission, and the sharing of genetic information may facilitate improved prevention and control strategies for future emerging zoonotic coronaviruses. This article reviews the clinical, epidemiologic, virologic, and pathologic characteristics of nine important coronaviruses of companion animals.

**Keywords:** feline infectious peritonitis; coronavirus; canine; ferrets; spike glycoproteins; SARS Virus; COVID-19; zoonoses

---

## 1. Introduction

Coronaviruses are spherical, enveloped, single-stranded, positive-sense RNA viruses within the family *Coronaviridae*, named for the ultrastructural “crown-like” (corona) appearance of the spike proteins on the virion surface. Coronaviruses infect humans as well as many other mammalian and avian species, generally causing variably severe intestinal, respiratory, neurologic, or systemic disease syndromes [1–4]. Genomically, coronaviruses are among the largest of the RNA viruses, with genomes spanning 27.6 to 31 kilobases (kb) in length [5], approximately three times the size of most retroviruses. On the basis of comparative genome sequence analyses, coronaviruses are subdivided into four genera: alphacoronavirus, betacoronavirus, gammacoronavirus, and deltacoronavirus. Alpha- and betacoronaviruses originate from bats and predominantly infect mammals, while gamma-

and deltacoronaviruses originate from birds and are capable of infecting both bird and mammal species [6]. Companion animals presently considered include cats, dogs, ferrets, horses, and alpacas. While not universally recognized as companion animals, alpacas and horses are considered by the authors to be companion animals and are therefore included in this review. Notable coronaviruses of companion animals include feline enteric coronavirus (FECV), feline infectious peritonitis virus (FIPV), canine enteric coronavirus (CCoV), ferret enteric coronavirus (FRECv), ferret systemic coronavirus (FRSCV), and alpaca respiratory coronavirus, which are alphacoronaviruses, and canine respiratory coronavirus (CRCoV), equine enteric coronavirus (ECoV), and alpaca enteric coronavirus, which are betacoronaviruses [7]. Phylogenetic relationships of these coronaviruses are shown in Figure 1, while clinical and pathologic features are summarized in Table 1. Other coronaviruses belonging to the betacoronavirus genus include SARS-CoV-1, MERS-CoV, and SARS-CoV-2, zoonotic coronaviruses that have recently transferred from animal to human populations and are capable of causing severe disease and death [8]. The ability of SARS-CoV-2 to initiate infections in companion animals is currently poorly understood, although preliminary studies have indicated that ferrets and cats are permissive for SARS-CoV-2 infection and replication, while the virus has been shown to replicate poorly in dogs, pigs, chickens, and ducks [9]. SARS-CoV-2 infection of horses and camelids has not been reported.

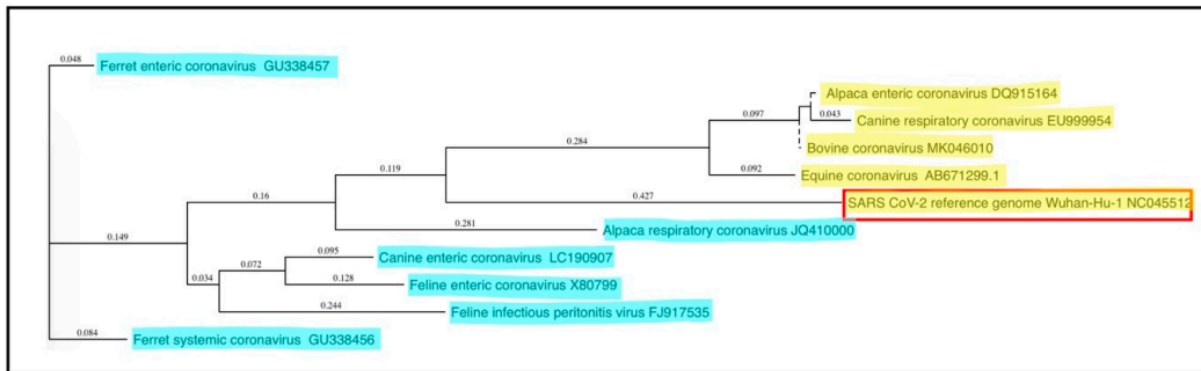


**Figure 1.** Phylogenetic relationships of coronaviruses of companion animals. The 3' portions of the coronaviral genomes encoding the spike and other non-structural proteins (~9 kb) were compared and plotted as a “guide tree” using MacVector software (ClustalW Multiple Sequence Alignment). Betacoronavirus sequences are highlighted in yellow, while alphacoronavirus sequences are highlighted in blue; the zoonotic SARS CoV-2 coronavirus is surrounded by a red box. GenBank submission numbers are indicated for each sequence.

Coronavirus genomes encode three classes of proteins: structural, accessory, and non-structural proteins. Major structural proteins of coronaviruses include the nucleocapsid (N), spike (S), membrane (M), and envelope (E) proteins [5]. The S protein is the primary viral binding protein and mediator of membrane fusion and viral entry. The N protein, in close association with genomic viral RNA (gRNA), forms the helical nucleocapsid, which is stabilized via binding to the M protein (Figure 2). The viral genome and helical nucleocapsid are surrounded by a host-derived lipid bilayer, in which the S, E, and M proteins are anchored. The transmembrane E and M proteins are involved in virion assembly and budding [10]. In addition to the four structural proteins, coronavirus genomes also encode a number of accessory proteins. While the roles of most of the accessory proteins remain poorly understood and may be dispensable for virus replication *in vitro*, certain accessory proteins appear to enhance viral virulence *in vivo*; for example, the SARS coronavirus encodes accessory proteins that antagonize the development of type I interferon (IFN) responses [11].

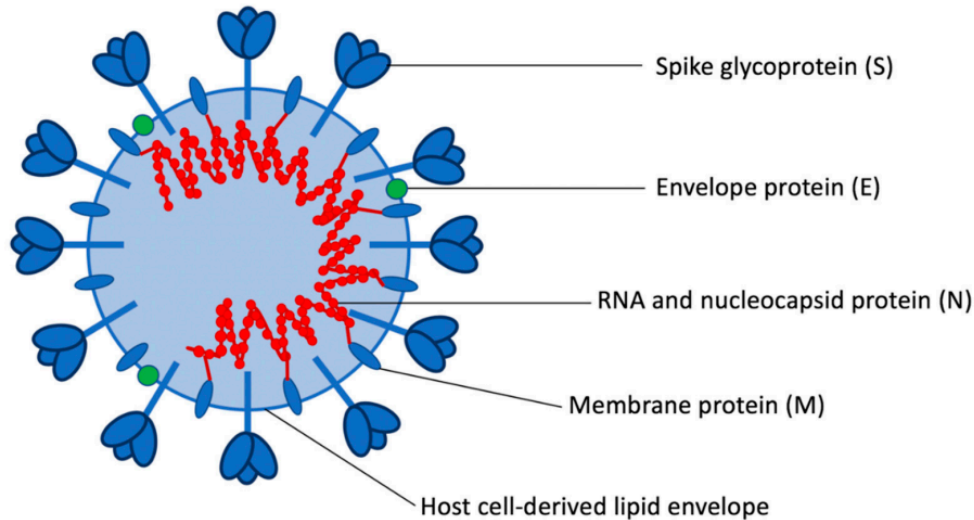


**Figure 2.** Coronavirus structural proteins.

Unlike alphacoronaviruses, a subset of betacoronaviruses are more structurally complex and have additional membrane glycoproteins, called hemagglutinin-esterase (HE) proteins, encoded by an additional gene roughly 1.2 kb in size [12]. Coronavirus HEs are thought to be acquired from an influenza virus C-like gene encoding a hemagglutinin-esterase fusion protein in a relatively recent horizontal gene transfer event [13]. While coronavirus HEs are able to bind to sialic acid, they are reported to serve primarily as receptor-destroying enzymes (RDE), which facilitates the reversibility of the virus-host cell attachment. For all coronaviruses, the S protein is thought to be the primary binding protein, responsible for attachment of coronavirus to the cell surface. However, the contribution of HEs to virion attachment and their role in tissue tropism and pathogenesis are currently not well understood [14].

The molecular events of the coronavirus replication cycle are complex and begin with virion attachment to the host cell, accomplished by binding of the viral S protein to a unique target receptor on the host cell surface. As the primary binding protein and mediator of virus-host cell membrane fusion and subsequent virus entry into the cell, the S protein is critical in determining the host species and tissue and cell tropism for each coronavirus [15]. Upon receptor binding, conformational changes in the S protein expose the fusion peptide, facilitating fusion of the viral and host cell membranes and subsequent release of the viral nucleocapsid into the host cell cytoplasm [10,16]. Upon cytoplasmic release of the viral nucleocapsid, the positive sense genomic RNA (+gRNA) serves as viral messenger RNA (mRNA) for the direct translation of the *replicase* gene complex utilizing the host cell's ribosomal machinery. The *replicase* gene complex consists of two large open reading frames (ORF) approximately 20 kb in total size [17], ORF1a and ORF1b, the latter transcribed via a ribosomal frameshift. The ORF1a and ORF1b mRNA are translated into polypeptides 1a or 1ab, which are subsequently cleaved by viral proteases to create sixteen nonstructural proteins (nsps). These nonstructural proteins reassemble to form a viral replicase-transcriptase complex, consisting of the RNA-dependent RNA polymerase (RdRp, nsp12), helicase (nsp13), nsps with accessory functions, such as the nsp14 exoribonuclease, as well as multiple membrane-spanning proteins that are thought to provide a membrane-associated scaffold for the assembly of the replicase-transcriptase complex [18–20]. As eukaryotic cells typically do not encode an RdRp, that is, they lack the ability to catalyze the formation of RNA using RNA as a substrate, the viral RdRp enzyme provides a useful target for antiviral therapeutics [21,22]. Within this group of nonstructural proteins is an exonuclease with proof-reading function, unusual for RNA viruses but perhaps important for ensuring the fidelity of the very large coronaviral RNA genome during replication [23].

The viral polymerase synthesizes complementary full-length negative-sense RNA copies of the genome, which serve as templates for full length positive-sense RNA genomes, generated via RdRp's replicase function. In addition to replicase activity, RdRp also has transcriptase activity; by discontinuous RNA synthesis directed by transcriptional regulatory sequences, RdRp creates a set of subgenomic RNAs (sgRNA) of different sizes [24], which are then copied by RdRp into positive-sense mRNAs, serving as templates for translation of viral proteins necessary for virion assembly, including the structural proteins S, E, M, and N. Translated viral proteins are inserted into the cell's endoplasmic reticulum and then transported to the site of viral assembly, the endoplasmic reticulum-Golgi intermediate compartment (ERGIC). Viral genomes (+gRNA) encapsidated by N proteins bud into the ERGIC membrane, forming fully assembled virions surrounded by a host-derived lipid bilayer [25]. Assembled virions are subsequently transported in vesicles to the plasma membrane, where they are released from the infected cell via exocytosis [26]. In some coronaviruses, the accumulation of S proteins on the surface of infected cells can result in fusion of adjacent cells and the formation of syncytia, facilitating rapid cell-to-cell spread of the virus [27].

The genetic diversity of coronaviruses is a consequence both of polymerase error-driven point mutations, as well as of genetic recombination between different strains and species of coronaviruses during coinfection within the same host cell [5,28]. Relative to other single-stranded RNA viruses, coronavirus mutation rates are moderate to high [29], despite the proof-reading function of the viral exonuclease [30]. Genetic recombination is a direct result of the discontinuous transcriptional activity of the coronaviral polymerase and likely contributes to the emergence of new viruses with altered virulence, novel host species range, and novel tissue tropism [18].

**Table 1.** Clinical and pathologic features of major coronavirus infections of companion animals.

Virus	Primary Target Organ(s)	Primary Host Cell	Disease/Symptoms	Transmission	Cellular Receptor
Genus Alphacoronavirus					
Feline enteric coronavirus (FECV)	GI tract	Enterocyte	Asymptomatic to mild gastroenteritis and diarrhea	Direct contact; fecal-oral, maternal shedding	Serotype I: unknown Serotype II: APN
Feline infectious peritonitis virus (FIPV)	Omentum, serosal/pleural surfaces, liver, kidneys, lymph nodes, eyes, brain	Monocyte, macrophage	Peritonitis, thoracic and abdominal effusions, CNS and ocular signs.	Rare to no horizontal transmission	Serotype I: unknown Serotype II: APN
Ferret enteric coronavirus (FRECV)	GI tract	Enterocyte	Epizootic catarrhal enteritis	Fecal-oral	Unknown
Ferret systemic coronavirus (FRSCV)	Spleen, mesenteric lymph nodes, intestines, kidneys, liver, lungs, brain	Unknown	Weight loss, anorexia, diarrhea, abdominal granulomas/masses, CNS signs	Unknown	Unknown
Canine enteric coronavirus (CECoV)	GI tract	Enterocyte	Mild gastroenteritis and diarrhea; rarely, severe enteritis and systemic signs	Fecal-oral	Serotype I: unknown Serotype II: APN
Alpaca respiratory coronavirus	Respiratory tract	Respiratory epithelia (presumed)	Mild to severe respiratory disease	Aerosol (presumed)	Unknown

**Table 1. Cont.**

Virus	Primary Target Organ(s)	Primary Host Cell	Disease/Symptoms	Transmission	Cellular Receptor
Genus Betacoronavirus					
Canine respiratory coronavirus (CRCoV)	Respiratory tract	Respiratory epithelia	Mild upper respiratory disease	Aerosol	Unknown
Equine coronavirus (ECoV)	GI tract	Enterocyte	Fever, anorexia, lethargy; less frequently, diarrhea, colic, neurologic signs	Fecal-oral	Unknown
Alpaca enteric coronavirus	GI tract	Enterocyte (presumed)	Enteritis, severe diarrhea	Fecal-oral (presumed)	Unknown

## 2. Feline Enteric Coronavirus and Feline Infectious Peritonitis Virus

### 2.1. Epidemiology, Clinical and Pathologic Features

Feline coronaviruses are separated into two distinct biotypes: feline enteric coronavirus (FECV) and feline infectious peritonitis virus (FIPV). FECV is endemic in domestic cat populations worldwide and primarily infects intestinal enterocytes, typically resulting in either mild enteric disease or a lack of clinical signs (subclinical infections). Experimental studies have demonstrated consistent shedding of FECV in the feces of infected cats from 2 days to 2 weeks post-infection, followed by a decrease in viral loads and intermittent shedding for up to 20 weeks after this period [31,32]. Subclinical carriers of FECV play an important role in shedding and transmitting the virus to other cats via the fecal-oral route, especially in those animals housed indoors in multi-cat environments [33]. FECV primarily infects the apical epithelial cells of the intestinal villi (enterocytes), from the distal duodenum to the cecum. Villous atrophy of the lining mucosa and sloughing and degeneration of epithelial cells at the villous tips occur in severe infections [34]. Shortening and fusion of intestinal villi and hyperplasia of crypt epithelia are also common pathological findings [3].

In contrast to the mild enteric disease or absence of clinical signs associated with FECV infection, the closely related FIPV biotype generally results in a highly inflammatory, systemic, and nearly 100% fatal disease once clinical signs develop. This clinical syndrome is called feline infectious peritonitis (FIP). The origin of FIPV is thought to arise from a select number of spontaneous mutations in the FECV genome, which confers a tropism switch from enterocytes to macrophages, facilitating systemic spread. These mutations are thought to arise *de novo* within each FECV-infected cat. Male cats, purebred cats, and those living in multi-cat environments are more likely to develop FIP [35]. Specific cat breeds at higher risk for the development of FIP include Abyssinian, Bengal, Birman, ragdoll, and rex cat breeds [36,37], likely due to inherited genetic factors in these breeds, leading to increased susceptibility to FIP [38]. FIP seems to preferentially occur in young, very old, or immunosuppressed individuals. An FIP-like disease has also been documented in a number of wild species of felids infected with coronaviruses, including African lions, cheetahs, mountain lions, leopards, jaguars, lynx, servals, caracal, European wild cats, Sand cats, and Pallas cats [39–47].

Key point mutations proposed to be responsible for the conversion of FECV to FIPV include two alternative amino acid differences in the gene encoding the fusion peptide of the spike (S) protein [48], substitutions in the furin cleavage site between receptor-binding (S1) and fusion (S2) domains of the spike protein [49], and mutations in open reading frame 3abc resulting in a truncated protein 3c protein [50]. It has subsequently been reported that one of the amino acid differences in the fusion peptide of the FECV spike protein, specifically, a methionine to leucine substitution at position 1058, is involved in systemic spread of FCEV from the intestine, rather than with the potential to cause FIP [51]. Mutations of 3c and S protein genes are often found in combination, but a single mutation in either S or 3c appears to be sufficient to dramatically alter the tropism of FECV, allowing for enhanced

internalization and replication of the virus within monocytes and macrophages, facilitating systemic, cell-associated dissemination of the virus [50].

Clinically, FIP typically manifests as one of two forms: “wet” (effusive) FIP, “dry” (granulomatous) FIP, or some combination of the two. Effusive FIP is the more common and classical form of disease and is generally associated with rapid disease progression and the exudation of fluid into the peritoneal or thoracic body cavities. The “dry”/granulomatous form of FIP generally lacks cavitory effusion and is instead characterized by multifocal granuloma formation in a variety of organs and a more insidious disease progression. As a result, the initial clinical signs of FIP are often nonspecific and may include anorexia, weight loss, and/or chronic fever [52,53]. Clinical neurologic signs, including ataxia, seizures, nystagmus, hyperesthesia, and/or cranial nerve deficits [54,55], as well as ocular disease may occur in some cats, with a higher frequency in those with the dry form of FIP than the wet form [56].

It has been hypothesized that a “strong and focused” cell-mediated immune (CMI) response directed to the coronavirus may prevent FIP disease development, while animals with a “weak” CMI in combination with a strong humoral immune response will likely develop wet FIP. Further, it has been hypothesized that animals with a “moderate” CMI will likely develop the dry form of FIP [57].

Grossly, the wet/effusive form of FIP is characterized by “straw-colored,” semi-translucent, protein-rich peritoneal or thoracic effusions and fibrinous and granulomatous serositis/pleuritis with variable involvement of parenchymal organs (Figure 3A) [56]. Virus-associated pyogranulomatous inflammation is focused on small and medium sized veins, resulting in vascular injury and leakage [58]. These vasculo-centric lesions can occur in the omentum and serosal surfaces of the liver, spleen, intestines, kidneys, and lungs, and are composed primarily of macrophage aggregates in combination with smaller numbers of neutrophils and lymphocytes (pyogranulomatous inflammation). Occasionally, pyogranulomatous nodular lesions extend beyond the serosal surfaces into underlying parenchyma. Coronaviral antigen can often be detected within intralesional macrophages using immunohistochemistry techniques; coronaviral antigen detection via immunohistochemistry is a commonly utilized diagnostic method.

The dry form of FIP is characterized grossly by variably sized parenchymal and serosal pyogranulomas in affected organs but lacks the exudation archetypal of wet FIP. Granulomatous lesions of dry FIP may extend from serosal surfaces into the parenchyma of affected organs, and lesions may be restricted to a single organ, such as the kidney, eye, or brain [59]. Other frequently affected organs in the dry form of FIP include the mesenteric and mediastinal lymph nodes, omentum, intestine, and liver. Perivascular inflammatory lesions contain aggregates of macrophages and fewer neutrophils, which are surrounded by dense infiltrates of primarily B lymphocytes and plasma cells extending into surrounding tissues, with or without the presence of vasculitis [47,59]. It is not uncommon for affected animals to demonstrate some combination of both effusive and granulomatous forms of the disease.

It has been hypothesized that immune-mediated type III and/or type IV hypersensitivity reactions may play a role in the perivascular granulomatous inflammation characteristic of FIP [60,61]. Type III hypersensitivity lesions feature the overproduction of immune complexes comprised of antibody bound to soluble antigen, and subsequent inflammatory pathway activation, deposition into vessel walls (e.g., vasculitis) and tissue injury [62]. FIPV-associated vascular lesions have been hypothesized as being caused by type III hypersensitivity based on studies demonstrating antibody, complement, and FCoV antigen within vascular lesions; however, a definitive connection between type III hypersensitivity and FIP-associated vasculitis/peri-vasculitis has not been unequivocally confirmed [60,63]. Alternatively, FIPV-associated vascular injury and subsequent permeability may be a result of virus-induced activation of monocytes and macrophages. This hypothesis is supported by the finding that vascular endothelial growth factor (VEGF) produced by FIPV-infected monocytes and macrophages causes vascular permeability and effusion in cats with FIP [64]. Matrix metalloproteinase 9 (MMP-9) has also been shown to be upregulated in activated monocytes and macrophages in FIP, contributing to the destruction of type IV collagen and degradation of the basal lamina of affected vessels in FIP vasculitis [58]. Type IV, or delayed-type hypersensitivity, is mediated by hyperstimulated T cells

and macrophages, which cause damage to surrounding tissue and may contribute to the granuloma formation characteristic of the dry form of FIP [65].

In a subset of wet and dry FIP cases, affected cats may present with ocular and/or neurologic involvement. In cases with ocular involvement, diffuse and multifocal inflammatory infiltrates may be found in the ciliary body, retina, and choroid as well as throughout the uvea and in the sclera, conjunctiva, and optic nerve. Ocular perivascular leukocytes are typically lymphoplasmacytic, composed mostly of B cells and plasma cells, with fewer numbers of T cells and macrophages [66]. Gross lesions of FIP in the central nervous system include ventricular dilation, flattening of cerebral gyri, and ependymal and meningeal congestion [67]. Mild to marked ventricular enlargement is associated with accumulation of inflammatory cells within the ventricles [54], with corresponding increased protein, increased cellularity, and presence of virus in cerebrospinal fluid [67]. Histopathological lesions in the brain consist of perivascular neutrophilic and lymphoplasmacytic infiltrates in the leptomeninges, the choroid plexus, the periventricular space, and/or the parenchyma of the spinal cord and brainstem [68]. Less common (atypical) manifestations of FIP include nodular dermatitis [69–71], rhinitis [72], orchitis [73,74], priapism [75], and syringomyelia associated with involvement of the fourth ventricle [76].

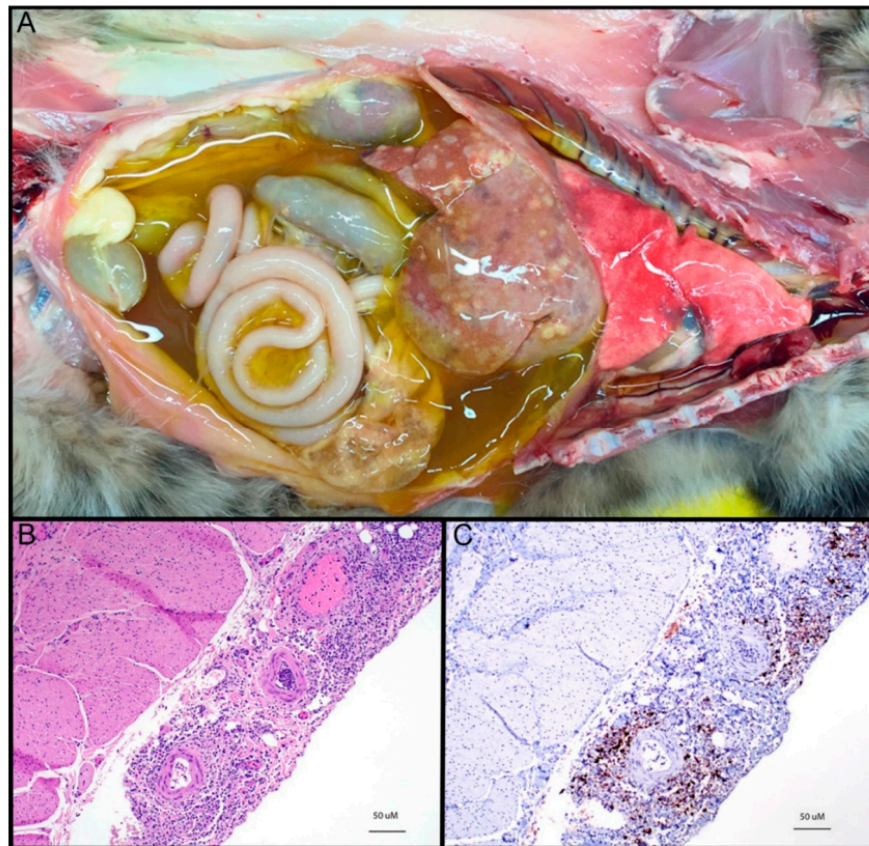


**Figure 3.** (A) Gross image of “wet” or effusive feline infectious peritonitis (FIP), thoracic and abdominal cavities, cat. Abundant semi-translucent “straw-colored”, proteinaceous peritoneal effusion with fibrinous and granulomatous serositis and multifocal granulomatous lesions in the liver. Gross image courtesy of Chrissy Eckstrand. (B) FIP, urinary bladder serosal surface, cat, hematoxylin and eosin (HE). Severe, necrotizing, pyogranulomatous and lymphoplasmacytic serositis and vasculitis. (C) FIP, urinary bladder serosal surface, cat, FCoV immunohistochemistry. Same lesion tissue as 3b with frequent, positive immunoreactivity for FCoV antigen (brown pigment).

## 2.2. Virology

Feline coronaviruses are alphacoronaviruses and are divided into two serotypes, type I and type II, based on genetic and antigenic properties [77]. Although both serotypes are capable of causing FIP [78], serotype I is much more prevalent in nature and is responsible for 80–90% of naturally occurring clinical cases [79,80]. Serotype II is comparatively rare, having emerged as a result of recombination events between feline coronavirus serotype I and canine enteric coronavirus serotype II, following cross-species transmission of CCoV to cats [81–83]. Although the feline serotype I is more prevalent, it is less well studied due to challenges in propagating this viral serotype in culture-adapted cell lines *in vitro*. The molecular events of the serotype II viral lifecycle are better understood due to the relative ease with which serotype II can be propagated and studied *in vitro*.

The target cell membrane receptor of serotype II feline coronaviruses has been identified as feline aminopeptidase N (fAPN) [84]. Feline APN is a membrane peptidase expressed on the brush border of small intestine and renal tubule microvilli, as well as by cells of myeloid origin, including monocytes, macrophages, and granulocytes [85]. Additional non-specific viral receptors, including the lectin molecule DC-SIGN, have also been proposed [41,78]. The primary cell receptor for the more prevalent serotype I FIPV has yet to be definitively identified [86]; however, studies have proposed DC-SIGN [87], as a potential host cell entry co-receptor. The Fc receptor CD16 (FcγRIII) has also been proposed as a potential cellular receptor [88]. Interestingly, antibodies directed to the spike protein of feline coronavirus have been shown to enhance virus infection both *in vitro* [89] and *in vivo* [63] through a mechanism known as antibody dependent enhancement (ADE). In ADE, antibodies facilitate the uptake of virus-antibody complexes by monocytes and macrophages using Fc receptors like CD16, resulting in more efficient infection than by virus alone [90,91].

Following binding to the target receptor on the cell surface, FIPV serotype II enters monocytes via clathrin and caveolae-independent and dynamin-dependent endocytosis [92]. Consistent with the initial distribution of lesions on serosal surfaces of abdominal organs, FIPV is thought to preferentially target peritoneal macrophages [88]. Once ensconced within these histiocytic cells, FIPV is able to seed the abdominal and thoracic cavities and, in some cases, spread to more distant sites, such as the brain and eye.

## 3. Ferret Enteric Coronavirus and Ferret Systemic Coronavirus

### *Epidemiology, Virology, and Clinical and Pathologic Features*

Similar to feline coronaviruses, infection with ferret coronaviruses can result in enteric or systemic disease [93]. First identified in the United States in 2000, ferret enteric coronavirus (FRECV) is associated with epizootic catarrhal enteritis (ECE), originally called “green slime disease” due to the development of profuse, foul-smelling, bright green mucus-laden diarrhea [94]. Clinically, ECE is associated with lethargy, anorexia, and vomiting. ECE is characterized by high morbidity but low mortality [95]. While juvenile ferrets develop mild to subclinical disease and can be subclinical carriers, ECE can cause more severe disease in older ferrets [96].

A genetically distinct coronavirus called ferret systemic coronavirus infection (FRSCV) was subsequently identified, which causes a systemic, progressive, and fatal pyogranulomatous inflammatory disease resembling the dry form of feline infectious peritonitis (FIP) in cats. The average age at the time of FRSCV diagnosis has been reported to be 11 months, and clinical signs include chronic weight loss, anorexia, diarrhea, palpable abdominal masses, and neurologic disease [97].

Both the enteric (FRECV) and systemic (FRSCV) ferret coronaviruses are alphacoronaviruses, related to feline coronavirus and canine enteric coronavirus, and most closely related to mink coronavirus. Complete genome sequencing of FRSCV and FRECV strains revealed a shared 89% nucleotide identity, but only 49.9–68.9% nucleotide identity with other known coronaviruses [98]. The pathogenic relationship of these two ferret coronaviruses, and whether FRSCV arises by mutation within ferrets infected with FRECV, has not been determined. The cellular entry receptors have also

not been identified. Many facets of the pathogenesis of the virulent systemic ferret coronavirus remain unknown, but as is true for FIPV, macrophages appear to play an important role in the inflammatory response. Furthermore, similarities in pathologic lesions suggest parallels in the pathogenesis of ferret systemic coronavirus and FIP.

FRECV is associated with lesions restricted to the gastrointestinal tract, which include lymphocytic enteritis, villous blunting, fusion, and atrophy, as well as vacuolar degeneration and necrosis of apical villous enterocytes, similar to FECV [94].

In contrast to FRECV, FRSCV is grossly associated with pale to white nodules (granulomatous inflammation) in multiple organs, including the spleen, kidneys, mesenteric lymph nodes, intestines, liver, lungs, and brain (Figure 4) [99,100]. Granulomas have a heterogeneous cellular composition including macrophages, T and B lymphocytes, and plasma cells. These granulomatous lesions are morphologically similar to FIP both in immune cell composition and presence of virus within the macrophage cytoplasm [101]. Interestingly, cavitory effusions and vasculitis, characteristic features of the wet form of FIP, have not been identified in the majority of ferrets infected with systemic coronavirus. Clearly, much remains to be learned about ferret coronavirus virology and pathology.

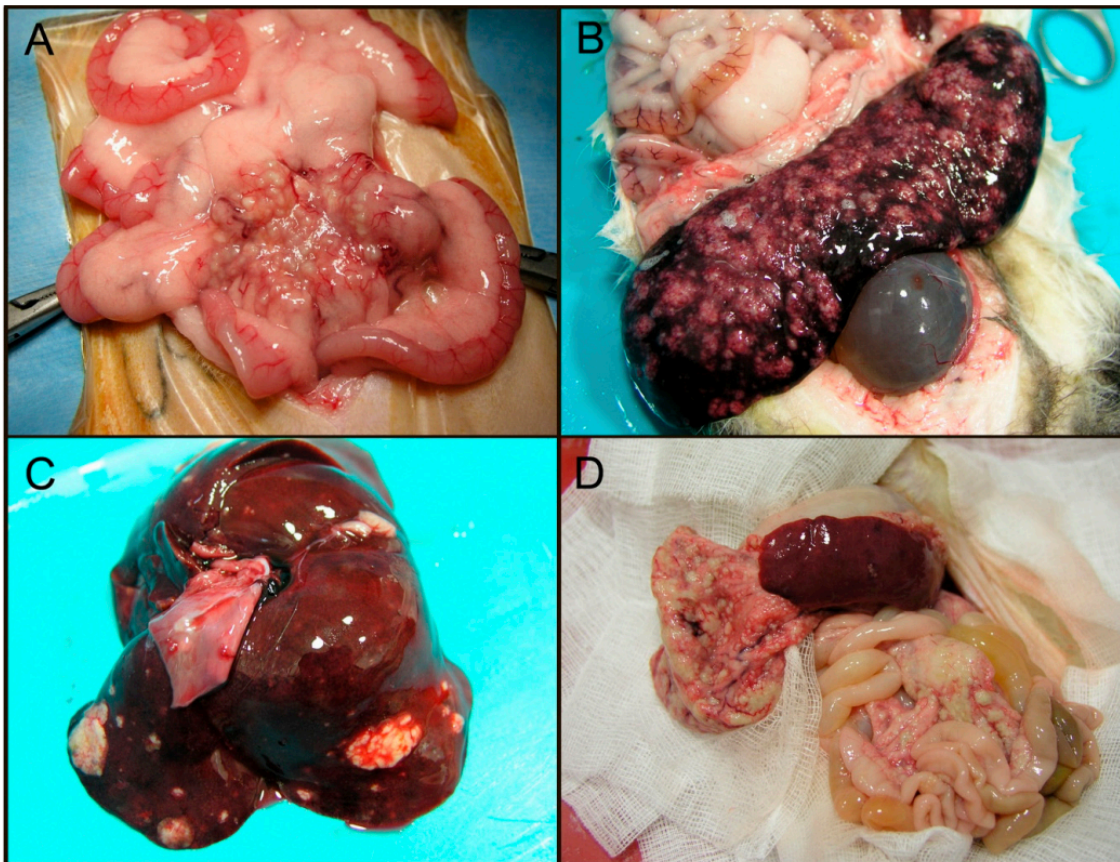


**Figure 4.** Gross lesions associated with ferret systemic coronavirus (FRSCV). (A) Ferret, coronavirus-associated granulomatous mesenteritis. Numerous, multifocal to coalescing, pale tan, firm nodular masses (granulomas) distributed throughout the mesentery, often corresponding to vasculature. (B) Ferret, coronavirus-associated serositis and splenitis. Numerous, multifocal to coalescing, pale tan nodules (granulomas) expanding the serosa with variable parenchymal involvement. (C) Ferret, coronavirus-associated hepatitis. Multifocal, pale tan, expansile nodular masses throughout the liver. (D) Ferret, coronavirus-associated peritonitis. Multifocal to coalescing, pale tan, nodular masses (granulomas) throughout the peritoneum. All images courtesy of Jordi Jimenez.

## 4. Canine Enteric Coronavirus

### 4.1. Epidemiology and Clinical Features

As is true of FECV, canine enteric coronavirus (CCoV) is a common infection of dogs with worldwide distribution. While not universally recognized as an important canine enteric pathogen, multiple independent studies have demonstrated that CCoV is significantly associated with diarrhea in dogs [102,103]. CCoV is transmitted via the fecal-oral route, with higher prevalence in dogs housed in dense populations such as in shelters or kennels [104]. First reported in 1971 in dogs in a canine military unit in Germany [105], CCoV generally causes mild, self-limiting diarrhea in dogs, especially in young puppies. More severe hemorrhagic disease associated with higher mortality has also been reported in combination with other pathogens [106], including canine parvovirus type 2 [107] and canine adenovirus type I [108]. CCoV infection has a synergistic effect with canine parvovirus type 2, increasing severity of enteric disease [109]. More virulent strains of CCoV, capable of causing significant enteric disease in the absence of coinfection have recently been reported [110], as well as pantropic strains that cause a fatal systemic disease involving lethargy, inappetence, vomiting, hemorrhagic diarrhea, ataxia, and seizures [111–113]. CCoV has also been detected in a number of wild canids, including foxes and raccoon dogs in China [114] and wolves in Alaska [115] and Europe. Remarkably, sequences of the CCoVs found in European wolves were up to 98–99% homologous to known CCoV sequences isolated from domestic dogs [116].

### 4.2. Virology

Similar to FECV, two serotypes of the CCoV exist: serotypes I and II. Mixed infections with strains of both serotypes are common [117]. Like the feline coronavirus serotype II, CCoV serotype II strains replicate well in tissue culture and use APN as an entry receptor. The cellular receptor for serotype I viruses has not been determined, as these viruses are much more difficult to propagate in tissue culture systems. CCoV serotypes I and II share close to 96% nucleotide identity throughout most of their genome, while the gene encoding the S protein is much more divergent, with only 56% sequence identity. It is likely that FECV serotype I and CCoV serotype I arose from a common viral ancestor, while CCoV serotype II arose via recombination with an unknown coronavirus, in the process acquiring an antigenically distinct S gene [83].

The continuing evolution of canine enteric coronaviruses with altered virulence and tropism is likely a result of changes in the genome due to random point mutations and periodic genetic recombination. Genetic recombination between serotype II CCoV and other coronaviruses resulted in the emergence of canine coronavirus variants with spike protein N-terminal domains that are largely homologous to transmissible gastroenteritis virus (TGEV), a coronavirus of pigs [118].

### 4.3. Pathology

Similar to the pathology of other enteric coronaviruses, CCoV infects and replicates in the apical and lateral enterocytes of the intestinal villi (mature enterocytes), resulting in cellular degeneration and/or necrosis characterized by atrophy of enterocytes, loss of the cellular brush border, and sloughing of necrotic cells into the intestinal lumen. Degeneration and destruction of mature enterocytes at the villous tips can lead to villous atrophy, ultimately resulting clinically in maldigestion, malabsorption and diarrhea [119].

A more severe form of enteritis in puppies infected with CCoV has also been reported, in the absence of co-infection. Gross pathology in one case revealed moderate, diffuse, hemorrhagic enteritis, and in another, severe ileo-cecal intussusception and segmental necrotic enteritis. Histologically, mild, lymphocytic and plasmacytic enteritis was present in the first case, along with necrosis and enteric and splenic lymphoid depletion. In the second case, depletion of gut associated lymphoid tissues was also noted, along with diffuse villous blunting and crypt necrosis [110]. A case report of pantropic CCoV described lesions in multiple organs, including a fibrinopurulent bronchopneumonia, renal cortical

infarcts, severe coalescing centrilobular hepatic fatty change, and multifocal hemorrhage in the spleen with lymphoid depletion. Chronic diffuse enteritis in this case was associated with the presence of adult ascarids in addition to CCoV [120].

## 5. Canine Respiratory Coronavirus

### 5.1. Epidemiology and Clinical Features

First discovered in 2003 in dogs housed at a rehoming kennel in the United Kingdom [121], canine respiratory coronavirus (CRCoV) is a coronavirus with worldwide distribution [122–125] and a significant etiologic component of canine infectious respiratory disease (CIRD) or “kennel cough” [126]. CIRD is a highly contagious, polymicrobial respiratory disease syndrome associated with a number of bacterial and viral agents and is readily transmitted via aerosols between dogs housed in relatively high-density groups, like shelters or kennels. Pathogens associated with CIRD include CRCoV, canine adenovirus 2 (CAV-2), canine parainfluenza virus (CPIV), *Bordetella bronchiseptica*, canine herpesvirus, canine pneumovirus (CnPnV), *Streptococcus equi* subsp. *zooepidemicus*, and *Mycoplasma* spp [127,128]; infection by one or a combination of these pathogens may result in disease.

CRCoV has also been shown to be capable of causing disease on its own [4] and is thought to play a role in early CIRD infection by damaging the mucociliary elevator. Affected dogs have an impaired ability to clear pathogens and foreign material from the lower respiratory tract, predisposing them to secondary infections and more severe clinical disease [129]. CRCoV is spread by aerosol transmission and is most commonly associated with mild signs of upper respiratory disease, including nasal discharge, sneezing, and coughing [4]. As is true of SARS CoV-2, CRCoV can also be associated with more severe clinical signs, inappetence, and bronchopneumonia. Disease occurs most frequently in fall to winter months [130], and populations most at risk are dogs densely housed in shelter, kennel, or group environments [131]. CRCoV has been proposed as a naturally occurring animal model of SARS-CoV-2 infection in humans, due to parallels in pathogenesis and early host immune response [132].

### 5.2. Virology

CRCoV is a betacoronavirus, genetically distinct from the alphacoronavirus, canine enteric coronavirus. Based on the polymerase gene sequence, the two canine coronaviruses have sequence identity of 68.5%, but only 21.1% similarity based on the Spike gene [123]. Among betacoronaviruses, CRCoV has the highest sequence identity with the polymerase gene of bovine coronavirus (BCoV) (98.8%) and human “common cold” coronavirus OC43 (98.4%), all of which cause mild to moderate upper respiratory disease in their respective hosts [126]. As is true for other betacoronaviruses, CRCoV binds initially to sialic acids and heparan sulfate on the cell surface for attachment, prior to cell entry via caveolin-dependent endocytosis [133]. Human leukocyte antigen class I (HLA-1), a human transmembrane glycoprotein, has been shown to act as the entry receptor for the in vitro infection of human airway epithelial cells by both CRCoV and BCoV [134].

### 5.3. Pathology

Histopathological lesions are most significant in the trachea and nasal cavity, where infection with CRCoV causes inflammation and damage to the ciliated respiratory epithelium, impairing the clearance of particulate matter in the lower respiratory tract and predisposing individuals to secondary bacterial infection of the lungs. Histological examination following experimental infection with CRCoV has demonstrated that the epithelia of the respiratory tract is disordered and devoid of cilia and goblet cells, and inflammatory cells infiltrate within the epithelium and subjacent lamina propria [4]. The trachea and nasal tonsil are the most common sites of CRCoV infection and are reported to have the highest viral loads, detected by quantitative RT-PCR. Though infrequent, CRCoV has also been detected in the spleen, mesenteric lymph node, and colon of infected dogs; while this may indicate the potential of

CRCoV to display a dual tropism, it is likely that the detection of CRCoV outside the respiratory tract is a result of passive transport from the respiratory tract through the ingestion of saliva and respiratory secretions. [135].

## 6. Equine and Alpaca Coronaviruses

### 6.1. Epidemiology and Clinical Features

Equine coronavirus (ECoV) is an enteric coronavirus originally reported in 2000 in a neonatal foal with enterocolitis [136]. Sporadic outbreaks in riding, racing, and show horses have been reported in the USA, Europe, and Japan with increasing frequency. Clinically, ECoV is associated with anorexia, fever, and lethargy, and in some cases, diarrhea, colic, and neurologic signs [137]. While ECoV infections are generally self-limiting, severe damage to the intestinal mucosa and subsequent loss of barrier function can lead to mortality due to secondary endotoxemia, septicemia, and hyperammonemia-associated encephalopathy [138]. Signs of encephalopathy associated with ECoV infection have been reported in 3% of clinical cases and include circling, head pressing, ataxia, proprioceptive deficits, nystagmus, recumbency, and seizures [138,139]. Hyperammonemia may be caused by increased ammonia production due to enteric microbiome dysbiosis associated with ECoV infection or increased absorption of ammonia from the gastrointestinal tract due to breakdown of the normal intestinal mucosal barrier function [137]. Similar to CRCoV, infections appear to be increased during colder months. While mainly affecting adult horses, infection in foals is associated with more severe gastrointestinal disease. Transmission is fecal-oral [140,141], and it is likely that subclinical horses play a role in transmission of the virus [142].

Alpaca enteric coronavirus is associated with outbreaks of diarrhea in llamas and alpacas; an Oregon study found alpaca enteric coronavirus to be the most common pathogen causing diarrhea in unweaned crias. Alpaca enteric coronavirus was noted to cause diarrhea throughout the year and was involved in outbreaks affecting adult animals as well as unweaned crias ranging in age from 1 to 7 months old [143].

A strong epidemiologic association has been made between alpaca respiratory coronavirus and an outbreak of alpaca respiratory syndrome (ARS) in alpacas in 2007. ARS is characterized by acute respiratory signs ranging in severity from mild upper respiratory disease to severe respiratory distress, high fever, and death [144]. Though all signalments can be affected, ARS is primarily reported in pregnant alpacas; severe fetal hypoxia in alpacas with ARS can result in abortion [145].

### 6.2. Virology

Equine coronavirus is a betacoronavirus, classified in the same genus as canine respiratory coronavirus. The cellular entry receptor has not been identified. Complete genome sequences have been determined for three ECoV isolates from Japan and one from the USA [146,147]. All three isolates from Japan were genetically similar to the isolate from the USA (NC99), with a sequence identity between 98.2 to 98.7% [147]. ECoV is phylogenetically related to a wide variety of coronaviruses including bovine coronavirus, human coronavirus OC43, and porcine hemagglutinating encephalomyelitis virus. Compared to these three coronaviruses, the ECoV nsp3 protein, a critical component of the replicase-transcriptase complex, is the most divergent, containing 3 amino acid deletions and 55 amino acid insertions, though the functional significance of these insertions and deletions has not been clarified [146].

Similar to equine coronavirus, the enteric alpaca coronavirus is a betacoronavirus, first recognized as causing severe diarrhea in llamas and alpacas in 1998 [148]. The enteric alpaca coronavirus is most closely related to bovine coronavirus (>99.5% nucleotide identity), human coronavirus OC43 (>96% identity), and porcine hemagglutinating encephalomyelitis virus (>93% identity), with the most significant differences present in the spike protein sequences [149]. CRCoV, ECoV, and alpaca

betacoronavirus are all either thought to descend from BCoV or have a common ancestor, likely a rat betacoronavirus [7,150].

A novel alpaca coronavirus belonging to the alphacoronavirus genus was isolated in 2007 and associated with acute respiratory disease rather than enteric disease [144]. Complete genome sequencing revealed less than 50% nucleotide identity with the previously reported enteric alpaca coronavirus but a much higher 92.2% nucleotide identity with the human coronavirus (HCoV) 229E, with striking similarity between the HCoV 229E and alpaca respiratory coronavirus spike proteins. Comparison of spike gene sequences revealed that alpaca respiratory coronavirus is most similar to HCoV 229E strains isolated between the 1960s and 1980s, suggesting the possibility that a transmission event may have occurred between alpacas and humans [151].

### 6.3. Pathology

The pathology of equine coronavirus in two horses and one donkey ranging in age from 6 months to 11 years old has been described. The naturally infected equids had severe diffuse necrotizing enteritis characterized by marked villous attenuation, necrosis of apical enterocytes in the small intestinal villi, pseudomembrane formation, and hemorrhage and microthrombosis within the mucosa and submucosa (Figure 5B). In contrast to enteric coronavirus infections in the carnivores, ECoV infection in horses has also been associated with crypt necrosis. In cases of hyperammonemia-associated encephalopathy, Alzheimer type II astrocyte hypertrophy and hyperplasia were observed diffusely throughout the cerebral cortex [2].

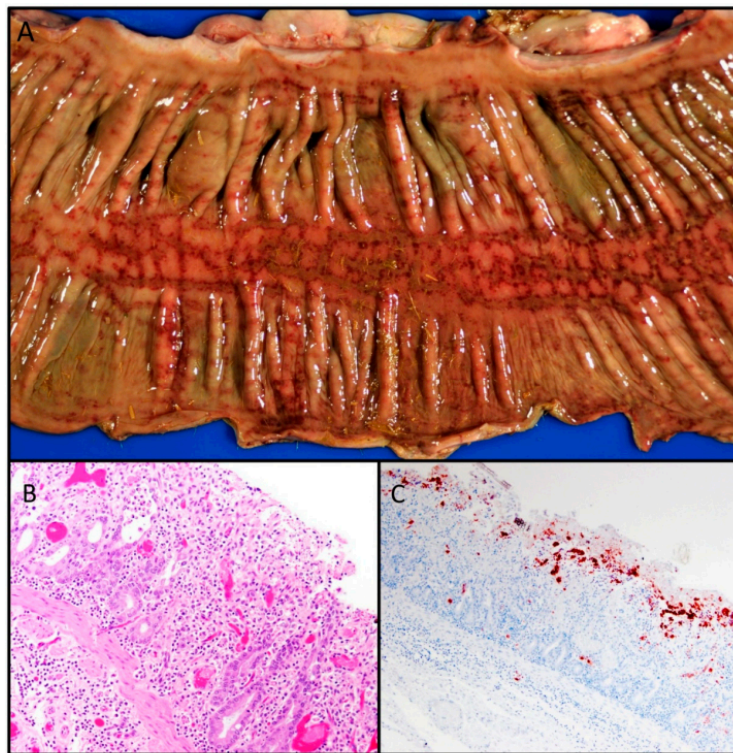


**Figure 5.** (A) Equine coronavirus-associated colitis, colon, horse. Moderate, necrohemorrhagic colitis. Image courtesy of Silvia Siso. (B) Equine coronavirus-associated enteritis, jejunum, horse. Mixed inflammatory enteritis with crypt ectasia and necrosis (crypt “abscesses”) and microvascular thrombi. (C) Equine coronavirus-associated enteritis, jejunum, horse. Diffuse immunoreactivity at the tips of necrotic villi using bovine coronavirus antiserum (immunohistochemistry). Figure 5B,C courtesy of Federico Giannitti.

Gross pathology has been reported in one adult alpaca infected with enteric alpaca coronavirus; gross findings included diffuse thickening of the wall of the third gastric compartment, enlarged dark red mesenteric lymph nodes, and watery intestinal contents mixed with mucous. Histopathological lesions in the small intestine included moderate diffuse edema of the lamina propria and submucosa, multifocal petechiae of the mucosa and submucosa in several sections, moderate autolysis, and small amounts of necrotic debris present within crypts. Mesenteric lymph node sinusoids were hemorrhagic, with fibrinopurulent exudate present in the lymph node parenchyma and lymphatics. Nutritional stress, copper, and other mineral deficiencies may have played a role in the severity of disease seen in this 4-year old alpaca [148].

Alpaca respiratory coronavirus pathology has been reported in 11 naturally infected alpacas: Gross findings included severe pulmonary congestion and edema in combination with marked pleural effusion. Histologically, pulmonary congestion and edema were associated with marked, diffuse interstitial to bronchointerstitial pneumonia focused on terminal airways, including intraluminal fibrin deposition and hyaline membrane formation. Epithelial necrosis and regenerative hyperplasia between terminal airways and alveolar ducts and macrophage infiltrates within the septa and lumen were also noted in several cases [144].

## 7. Zoonotic Coronaviruses

Coronaviridae is a highly successful family of viruses that infects many different vertebrate classes and orders, including humans, causing diseases that range from localized respiratory or enteric infections to systemic disease. Coronaviruses cause significant morbidity and mortality in companion and agricultural animal species, including dogs, cats, ferrets, horses, alpacas, pigs, bovids, and poultry, as well as numerous species of wild animals. Cross-species transmission of canine enteric coronavirus to cats, leading to genetic recombination between FECV serotype I and CCoV serotype II, resulted in the emergence of FECV serotype II [81]. Similarly, recombination between serotype II CCoV and other coronaviruses resulted in the emergence of canine coronavirus variants with spike protein N-terminal domains that are largely homologous to transmissible gastroenteritis virus (TGEV), a coronavirus of pigs [118]. Viral polymerase error-driven point mutations, genetic recombination between different strains and species of coronaviruses, and the incorporation of genes from other viral taxa via nonhomologous recombination [152] demonstrate the genetic plasticity of coronaviruses and contribute to the alarming ability of coronaviruses to “jump species” [153]. Over the past 20 years, three human coronaviral pandemics (SARS, MERS, and most recently, COVID-19) all thought to originate from bat coronaviruses [8], demonstrate the zoonotic potential of coronaviruses. Progressive pathogen emergence along with amplified rates of global dissemination [154] represent a profound threat to global health and world economies. In alignment with the concept of “One Health,” a more thorough understanding of the coronaviruses of companion animals, their biological properties, their ability to recombine and to acquire new biological attributes, and their capacity for cross-species transmission has the potential to improve prevention and control measures for future emerging zoonotic coronaviruses [155].

**Funding:** This work was supported by the Students Training in Advanced Research (STAR) Program at the University of California, Davis, and National Institutes of Health T35 OD010956.

**Acknowledgments:** The authors thank Federico Giannitti, Chrissy Eckstrand, Jordi Jimenez, and Mike Garner for contributing some of the images.

**Conflicts of Interest:** The authors declare no conflict of interest.

## References

1. Gnirs, K.; Quinton, J.F.; Dally, C.; Nicolier, A.; Ruel, Y. Cerebral pyogranuloma associated with systemic coronavirus infection in a ferret. *J. Small Anim. Pract.* **2016**, *57*, 36–39. [[CrossRef](#)] [[PubMed](#)]

2. Giannitti, F.; Diab, S.; Mete, A.; Stanton, J.B.; Fielding, L.; Crossley, B.; Sverlow, K.; Fish, S.; Mapes, S.; Scott, L.; et al. Necrotizing Enteritis and Hyperammonemic Encephalopathy Associated with Equine Coronavirus Infection in Equids. *Vet. Pathol.* **2015**, *52*, 1148–1156. [[CrossRef](#)]
3. Kipar, A.; Kremendahl, J.; Addie, D.D.; Leukert, W.; Grant, C.K.; Reinacher, M. Fatal enteritis associated with coronavirus infection in cats. *J. Comp. Pathol.* **1998**, *119*, 1–14. [[CrossRef](#)]
4. Mitchell, J.A.; Brooks, H.W.; Szlodovits, B.; Erles, K.; Gibbons, R.; Shields, S.; Brownlie, J. Tropism and pathological findings associated with canine respiratory coronavirus (CRCoV). *Vet. Microbiol.* **2013**, *162*, 582–594. [[CrossRef](#)]
5. Coronaviridae. In *Fenner's Veterinary Virology*; Elsevier: Amsterdam, The Netherlands, 2017; pp. 435–461.
6. Woo, P.C.Y.; Lau, S.K.P.; Lam, C.S.F.; Lau, C.C.Y.; Tsang, A.K.L.; Lau, J.H.N.; Bai, R.; Teng, J.L.L.; Tsang, C.C.C.; Wang, M.; et al. Discovery of Seven Novel Mammalian and Avian Coronaviruses in the Genus Deltacoronavirus Supports Bat Coronaviruses as the Gene Source of Alphacoronavirus and Betacoronavirus and Avian Coronaviruses as the Gene Source of Gammacoronavirus and Deltacoronavirus. *J. Virol.* **2012**, *86*, 3995–4008. [[CrossRef](#)] [[PubMed](#)]
7. Decaro, N.; Lorusso, A. Novel human coronavirus (SARS-CoV-2): A lesson from animal coronaviruses. *Vet. Microbiol.* **2020**, *244*, 108693. [[CrossRef](#)]
8. Fan, Y.; Zhao, K.; Shi, Z.-L.; Zhou, P. Bat Coronaviruses in China. *Viruses* **2019**, *11*, 210. [[CrossRef](#)]
9. Shi, J.; Wen, Z.; Zhong, G.; Yang, H.; Wang, C.; Huang, B.; Liu, R.; He, X.; Shuai, L.; Sun, Z.; et al. Susceptibility of ferrets, cats, dogs, and other domesticated animals to SARS–coronavirus 2. *Science* **2020**, *368*, 1016–1020. [[CrossRef](#)]
10. Belouzard, S.; Millet, J.K.; Licitra, B.N.; Whittaker, G.R. Mechanisms of Coronavirus Cell Entry Mediated by the Viral Spike Protein. *Viruses* **2012**, *4*, 1011–1033. [[CrossRef](#)]
11. Freundt, E.C.; Yu, L.; Park, E.; Lenardo, M.J.; Xu, X.-N. Molecular Determinants for Subcellular Localization of the Severe Acute Respiratory Syndrome Coronavirus Open Reading Frame 3b Protein. *J. Virol.* **2009**, *83*, 6631–6640. [[CrossRef](#)]
12. Zhang, X.; Kousoulas, K.G.; Storz, J. The hemagglutinin/esterase gene of human coronavirus strain OC43: Phylogenetic relationships to bovine and murine coronaviruses and influenza C virus. *Virology* **1992**, *186*, 318–323. [[CrossRef](#)]
13. Zeng, Q.; Langereis, M.A.; van Vliet, A.L.W.; Huizinga, E.G.; de Groot, R.J. Structure of coronavirus hemagglutinin-esterase offers insight into corona and influenza virus evolution. *Proc. Natl. Acad. Sci. USA* **2008**, *105*, 9065–9069. [[CrossRef](#)] [[PubMed](#)]
14. De Groot, R.J. Structure, function and evolution of the hemagglutinin-esterase proteins of corona- and toroviruses. *Glycoconj. J.* **2006**, *23*, 59–72. [[CrossRef](#)] [[PubMed](#)]
15. Wickramasinghe, I.N.A.; de Vries, R.P.; Gröne, A.; de Haan, C.A.M.; Verheije, M.H. Binding of avian coronavirus spike proteins to host factors reflects virus tropism and pathogenicity. *J. Virol.* **2011**, *85*, 8903–8912. [[CrossRef](#)]
16. Walls, A.C.; Tortorici, M.A.; Snijder, J.; Xiong, X.; Bosch, B.-J.; Rey, F.A.; Veerler, D. Tectonic conformational changes of a coronavirus spike glycoprotein promote membrane fusion. *Proc. Natl. Acad. Sci. USA* **2017**, *114*, 11157–11162. [[CrossRef](#)]
17. Schiller, J.J.; Kanjanahaluethai, A.; Baker, S.C. Processing of the coronavirus MHV-JHM polymerase polyprotein: Identification of precursors and proteolytic products spanning 400 kilodaltons of ORF1a. *Virology* **1998**, *242*, 288–302. [[CrossRef](#)]
18. Sawicki, S.G.; Sawicki, D.L.; Siddell, S.G. A Contemporary View of Coronavirus Transcription. *J. Virol.* **2007**, *81*, 20–29. [[CrossRef](#)]
19. Narayanan, K.; Huang, C.; Makino, S. Coronavirus Accessory Proteins. *Nidoviruses* **2008**, 235–244. [[CrossRef](#)]
20. Imbert, I.; Snijder, E.J.; Dimitrova, M.; Guillemot, J.-C.; Lécine, P.; Canard, B. The SARS-Coronavirus PLnc domain of nsp3 as a replication/transcription scaffolding protein. *Virus Res.* **2008**, *133*, 136–148. [[CrossRef](#)]
21. Agostini, M.L.; Andres, E.L.; Sims, A.C.; Graham, R.L.; Sheahan, T.P.; Lu, X.; Smith, E.C.; Case, J.B.; Feng, J.Y.; Jordan, R.; et al. Coronavirus Susceptibility to the Antiviral Remdesivir (GS-5734) Is Mediated by the Viral Polymerase and the Proofreading Exoribonuclease. *mBio* **2018**, *9*, e00221–e03188. [[CrossRef](#)]
22. Gordon, C.J.; Tchesnokov, E.P.; Feng, J.Y.; Porter, D.P.; Götte, M. The antiviral compound remdesivir potently inhibits RNA-dependent RNA polymerase from Middle East respiratory syndrome coronavirus. *J. Biol. Chem.* **2020**, *295*, 4773–4779. [[CrossRef](#)] [[PubMed](#)]

23. Minskaia, E.; Hertzog, T.; Gorbalenya, A.E.; Campanacci, V.; Cambillau, C.; Canard, B.; Ziebuhr, J. Discovery of an RNA virus 3'→5' exoribonuclease that is critically involved in coronavirus RNA synthesis. *Proc. Natl. Acad. Sci. USA* **2006**, *103*, 5108–5113. [[CrossRef](#)] [[PubMed](#)]
24. Sawicki, S.G.; Sawicki, D.L. A New Model for Coronavirus Transcription. In *Coronaviruses and Arteriviruses*; Enjuanes, L., Siddell, S.G., Spaan, W., Eds.; Advances in Experimental Medicine and Biology; Springer US: Boston, MA, USA, 1998; pp. 215–219, ISBN 978-1-4615-5331-1.
25. Fehr, A.R.; Perlman, S. Coronaviruses: An Overview of Their Replication and Pathogenesis. In *Coronaviruses: Methods and Protocols*; Maier, H.J., Bickerton, E., Britton, P., Eds.; Methods in Molecular Biology; Springer: New York, NY, USA, 2015; pp. 1–23, ISBN 978-1-4939-2438-7.
26. Song, Z.; Xu, Y.; Bao, L.; Zhang, L.; Yu, P.; Qu, Y.; Zhu, H.; Zhao, W.; Han, Y.; Qin, C. From SARS to MERS, Thrusting Coronaviruses into the Spotlight. *Viruses* **2019**, *11*, 59. [[CrossRef](#)] [[PubMed](#)]
27. Krueger, D.K.; Kelly, S.M.; Lewicki, D.N.; Ruffolo, R.; Gallagher, T.M. Variations in Disparate Regions of the Murine Coronavirus Spike Protein Impact the Initiation of Membrane Fusion. *J. Virol.* **2001**, *75*, 2792–2802. [[CrossRef](#)] [[PubMed](#)]
28. Su, S.; Wong, G.; Shi, W.; Liu, J.; Lai, A.C.K.; Zhou, J.; Liu, W.; Bi, Y.; Gao, G.F. Epidemiology, Genetic Recombination, and Pathogenesis of Coronaviruses. *Trends Microbiol.* **2016**, *24*, 490–502. [[CrossRef](#)] [[PubMed](#)]
29. Pirc, K.; Dijkman, R.; Deng, L.; Jebbink, M.F.; Ross, H.A.; Berkhout, B.; van der Hoek, L. Mosaic Structure of Human Coronavirus NL63, One Thousand Years of Evolution. *J. Mol. Biol.* **2006**, *364*, 964–973. [[CrossRef](#)]
30. Denison, M.R.; Graham, R.L.; Donaldson, E.F.; Eckerle, L.D.; Baric, R.S. Coronaviruses. *RNA Biol.* **2011**, *8*, 270–279. [[CrossRef](#)] [[PubMed](#)]
31. Meli, M.; Kipar, A.; Müller, C.; Jenal, K.; Gönczi, E.; Borel, N.; Gunn-Moore, D.; Chalmers, S.; Lin, F.; Reinacher, M.; et al. High viral loads despite absence of clinical and pathological findings in cats experimentally infected with feline coronavirus (FCoV) type I and in naturally FCoV-infected cats. *J. Feline Med. Surg.* **2004**, *6*, 69–81. [[CrossRef](#)]
32. Herrewegh, A.A.; de Groot, R.J.; Cepica, A.; Egberink, H.F.; Horzinek, M.C.; Rottier, P.J. Detection of feline coronavirus RNA in feces, tissues, and body fluids of naturally infected cats by reverse transcriptase PCR. *J. Clin. Microbiol.* **1995**, *33*, 684–689. [[CrossRef](#)]
33. Pedersen, N.C.; Allen, C.E.; Lyons, L.A. Pathogenesis of feline enteric coronavirus infection. *J. Feline Med. Surg.* **2008**, *10*, 529–541. [[CrossRef](#)]
34. Pedersen, N.C.; Boyle, J.F.; Floyd, K.; Fudge, A.; Barker, J. An enteric coronavirus infection of cats and its relationship to feline infectious peritonitis. *Am. J. Vet. Res.* **1981**, *42*, 368–377. [[PubMed](#)]
35. Riemer, F.; Kuehner, K.A.; Ritz, S.; Sauter-Louis, C.; Hartmann, K. Clinical and laboratory features of cats with feline infectious peritonitis—A retrospective study of 231 confirmed cases (2000–2010). *J. Feline Med. Surg.* **2016**, *18*, 348–356. [[CrossRef](#)] [[PubMed](#)]
36. Worthing, K.A.; Wigney, D.I.; Dhand, N.K.; Fawcett, A.; McDonagh, P.; Malik, R.; Norris, J.M. Risk factors for feline infectious peritonitis in Australian cats. *J. Feline Med. Surg.* **2012**, *14*, 405–412. [[CrossRef](#)]
37. Pesteanu-Somogyi, L.D.; Radzai, C.; Pressler, B.M. Prevalence of feline infectious peritonitis in specific cat breeds. *J. Feline Med. Surg.* **2006**, *8*, 1–5. [[CrossRef](#)] [[PubMed](#)]
38. Foley, J.E.; Pedersen, N.C. The inheritance of susceptibility to feline infectious peritonitis in purebred catteries. *Feline Pract.* **1996**, *24*, 14–22.
39. Heeney, J.L.; Evermann, J.F.; McKeirnan, A.J.; Marker-Kraus, L.; Roelke, M.E.; Bush, M.; Wildt, D.E.; Meltzer, D.G.; Colly, L.; Lukas, J. Prevalence and implications of feline coronavirus infections of captive and free-ranging cheetahs (*Acinonyx jubatus*). *J. Virol.* **1990**, *64*, 1964–1972. [[CrossRef](#)]
40. Colby, E.D.; Low, R.J. Feline infectious peritonitis. *Vet. Med. Small Anim. Clin.* **1970**, *65*, 783–786.
41. Stephenson, N.; Swift, P.; Moeller, R.B.; Worth, S.J.; Foley, J. Feline Infectious Peritonitis in a Mountain Lion (*Puma concolor*), California, USA. *J. Wildl. Dis.* **2013**, *49*, 408–412. [[CrossRef](#)]
42. Tuch, K.; Witte, K.H.; Wüller, H. Feststellung der Felinen Infektiösen Peritonitis (FIP) bei Hauskatzen und Leoparden in Deutschland. *Zentralblatt Für Veterinärmedizin Reihe B* **1974**, *21*, 426–441. [[CrossRef](#)]
43. Poelma, F.G.; Peters, J.C.; Mieog, W.H.C.; Zwart, P. Infektiöse Peritonitis bei Krakal (*Felis Caracal*) und Nordluchs (*Felis Lynx Lynx*). In Proceedings of the Erkrankungen der Zootiere, 13th International Symposium of Zoo Veterinarians, Helsinki, Finland, 2–6 June 1974; pp. 249–253.
44. Juan-Salles, C.; Domingo, M.; Herraiz, P.; Fernandez, A.; Segales, J.; Fernandez, J. Feline infectious peritonitis in servals (*Felis serval*). *Vet. Rec.* **1998**, *143*, 535–536. [[CrossRef](#)]

45. Watt, N.J.; MacIntyre, N.J.; McOrist, S. An extended outbreak of infectious peritonitis in a closed colony of european wildcats (*Felis silvestris*). *J. Comp. Pathol.* **1993**, *108*, 73–79. [[CrossRef](#)]
46. Theobald, J. Felidae. In *Zoo Wild Animal Medicine*, 4th ed.; Fowler, M.E., Ed.; W.B. Saunders Co: Philadelphia, Pennsylvania, 1978; pp. 614–656.
47. Pedersen, N.C. A review of feline infectious peritonitis virus infection: 1963–2008. *J. Feline Med. Surg.* **2009**, *11*, 225. [[CrossRef](#)] [[PubMed](#)]
48. Chang, H.-W.; Egberink, H.F.; Halpin, R.; Spiro, D.J.; Rottier, P.J.M. Spike Protein Fusion Peptide and Feline Coronavirus Virulence. *Emerg. Infect. Dis.* **2012**, *18*, 1089–1095. [[CrossRef](#)] [[PubMed](#)]
49. Licitra, B.N.; Millet, J.K.; Regan, A.D.; Hamilton, B.S.; Rinaldi, V.D.; Duhamel, G.E.; Whittaker, G.R. Mutation in spike protein cleavage site and pathogenesis of feline coronavirus. *Emerg. Infect. Dis.* **2013**, *19*, 1066–1073. [[CrossRef](#)]
50. Bank-Wolf, B.R.; Stallkamp, I.; Wiese, S.; Moritz, A.; Tekes, G.; Thiel, H.-J. Mutations of 3c and spike protein genes correlate with the occurrence of feline infectious peritonitis. *Vet. Microbiol.* **2014**, *173*, 177–188. [[CrossRef](#)]
51. Porter, E.; Tasker, S.; Day, M.J.; Harley, R.; Kipar, A.; Siddell, S.G.; Helps, C.R. Amino acid changes in the spike protein of feline coronavirus correlate with systemic spread of virus from the intestine and not with feline infectious peritonitis. *Vet. Res.* **2014**, *45*, 49. [[CrossRef](#)]
52. Felten, S.; Hartmann, K. Diagnosis of Feline Infectious Peritonitis: A Review of the Current Literature. *Viruses* **2019**, *11*, 1068. [[CrossRef](#)]
53. Pedersen, N.C. An update on feline infectious peritonitis: Diagnostics and therapeutics. *Vet. J. Lond. Engl.* **1997** **2014**, *201*, 133–141. [[CrossRef](#)]
54. Timmann, D.; Cizinauskas, S.; Tomek, A.; Doherr, M.; Vandeveld, M.; Jaggy, A. Retrospective analysis of seizures associated with feline infectious peritonitis in cats. *J. Feline Med. Surg.* **2008**, *10*, 9–15. [[CrossRef](#)]
55. Diaz, J.V.; Poma, R. Diagnosis and clinical signs of feline infectious peritonitis in the central nervous system. *Can. Vet. J.* **2009**, *50*, 1091–1093.
56. Kipar, A.; Meli, M.L. Feline infectious peritonitis: Still an enigma? *Vet. Pathol.* **2014**, *51*, 505–526. [[CrossRef](#)]
57. Berg, A.-L.; Ekman, K.; Belák, S.; Berg, M. Cellular composition and interferon- $\gamma$  expression of the local inflammatory response in feline infectious peritonitis (FIP). *Vet. Microbiol.* **2005**, *111*, 15–23. [[CrossRef](#)]
58. Kipar, A.; May, H.; Menger, S.; Weber, M.; Leukert, W.; Reinacher, M. Morphologic features and development of granulomatous vasculitis in feline infectious peritonitis. *Vet. Pathol.* **2005**, *42*, 321–330. [[CrossRef](#)] [[PubMed](#)]
59. Drechsler, Y.; Alcaraz, A.; Bossong, F.J.; Collisson, E.W.; Diniz, P.P.V.P. Feline Coronavirus in Multicat Environments. *Vet. Clin. N. Am. Small Anim. Pract.* **2011**, *41*, 1133–1169. [[CrossRef](#)] [[PubMed](#)]
60. Jacobse-Geels, H.E.; Daha, M.R.; Horzinek, M.C. Antibody, immune complexes, and complement activity fluctuations in kittens with experimentally induced feline infectious peritonitis. *Am. J. Vet. Res.* **1982**, *43*, 666–670. [[PubMed](#)]
61. Paltrinieri, S.; Parodi, M.C.; Cammarata, G.; Mambretti, M. Type IV Hypersensitivity in the Pathogenesis of FIPV-Induced Lesions. *J. Vet. Med. Ser. B* **1998**, *45*, 151–159. [[CrossRef](#)] [[PubMed](#)]
62. Eggleton, P. Hypersensitivity: Immune Complex Mediated (Type III). In *ELS*; John Wiley & Sons Ltd.: Chichester, UK, 2001; pp. 1–9. [[CrossRef](#)]
63. Petersen, N.C.; Boyle, J.F. Immunologic phenomena in the effusive form of feline infectious peritonitis. *Am. J. Vet. Res.* **1980**, *41*, 868–876. [[PubMed](#)]
64. Takano, T.; Ohyama, T.; Kokumoto, A.; Satoh, R.; Hohdatsu, T. Vascular endothelial growth factor (VEGF), produced by feline infectious peritonitis (FIP) virus-infected monocytes and macrophages, induces vascular permeability and effusion in cats with FIP. *Virus Res.* **2011**, *158*, 161–168. [[CrossRef](#)] [[PubMed](#)]
65. Warrington, R.; Watson, W.; Kim, H.L.; Antonetti, F.R. An introduction to immunology and immunopathology. *Allergy Asthma Clin. Immunol. Off. J. Can. Soc. Allergy Clin. Immunol.* **2011**, *7*, S1. [[CrossRef](#)]
66. Ziółkowska, N.; Paździor-Czapula, K.; Lewczuk, B.; Mikulska-Skupień, E.; Przybylska-Gornowicz, B.; Kwiecińska, K.; Ziółkowski, H. Feline Infectious Peritonitis: Immunohistochemical Features of Ocular Inflammation and the Distribution of Viral Antigens in Structures of the Eye. *Vet. Pathol.* **2017**, *54*, 933–944. [[CrossRef](#)]
67. Foley, J.E.; Lapointe, J.; Koblik, P.; Poland, A.; Pedersen, N.C. Diagnostic Features of Clinical Neurologic Feline Infectious Peritonitis. *J. Vet. Intern. Med.* **1998**, *12*, 415–423. [[CrossRef](#)] [[PubMed](#)]

68. Crawford, A.H.; Stoll, A.L.; Sanchez-Masian, D.; Shea, A.; Michaels, J.; Fraser, A.R.; Beltran, E. Clinicopathologic Features and Magnetic Resonance Imaging Findings in 24 Cats With Histopathologically Confirmed Neurologic Feline Infectious Peritonitis. *J. Vet. Intern. Med.* **2017**, *31*, 1477–1486. [[CrossRef](#)] [[PubMed](#)]
69. Redford, T.; Al-Dissi, A.N. Feline infectious peritonitis in a cat presented because of papular skin lesions. *Can. Vet. J.* **2019**, *60*, 183–185.
70. Declercq, J.; De Bosschere, H.; Schwarzkopf, I.; Declercq, L. Papular cutaneous lesions in a cat associated with feline infectious peritonitis. *Vet. Dermatol.* **2008**, *19*, 255–258. [[CrossRef](#)] [[PubMed](#)]
71. Cannon, M.J.; Silkstone, M.A.; Kipar, A.M. Cutaneous lesions associated with coronavirus-induced vasculitis in a cat with feline infectious peritonitis and concurrent feline immunodeficiency virus infection. *J. Feline Med. Surg.* **2005**, *7*, 233–236. [[CrossRef](#)]
72. Andre, N.M.; Miller, A.; Whittaker, G.R. Feline Infectious Peritonitis Virus-Associated Rhinitis in a Cat. 2020. Available online: <http://creativecommons.org/licenses/by-nc-nd/4.0/> (accessed on 28 July 2020).
73. Foster, R.A.; Caswell, J.L.; Rinkardt, N. Chronic fibrinous and necrotic orchitis in a cat. *Can. Vet. J.* **1996**, *37*, 681–682. [[PubMed](#)]
74. Sigurðardóttir, Ó.G.; Kolbjørnsen, Ø.; Lutz, H. Orchitis in a Cat Associated with Coronavirus Infection. *J. Comp. Pathol.* **2001**, *124*, 219–222. [[CrossRef](#)]
75. Rota, A.; Paltrinieri, S.; Jussich, S.; Ubertalli, G.; Appino, S. Priapism in a castrated cat associated with feline infectious peritonitis. *J. Feline Med. Surg.* **2008**, *10*, 181–184. [[CrossRef](#)]
76. Kitagawa, M.; Okada, M.; Sato, T.; Kanayama, K.; Sakai, T. A feline case of isolated fourth ventricle with syringomyelia suspected to be related with feline infectious peritonitis. *J. Vet. Med. Sci.* **2007**, *69*, 759–762. [[CrossRef](#)]
77. Jaimes, J.A.; Millet, J.K.; Stout, A.E.; André, N.M.; Whittaker, G.R. A Tale of Two Viruses: The Distinct Spike Glycoproteins of Feline Coronaviruses. *Viruses* **2020**, *12*, 83. [[CrossRef](#)]
78. Motokawa, K.; Hohdatsu, T.; Aizawa, C.; Koyama, H.; Hashimoto, H. Molecular cloning and sequence determination of the peplomer protein gene of feline infectious peritonitis virus type I. *Arch. Virol.* **1995**, *140*, 469–480. [[CrossRef](#)] [[PubMed](#)]
79. Hohdatsu, T.; Okada, S.; Ishizuka, Y.; Yamada, H.; Koyama, H. The prevalence of types I and II feline coronavirus infections in cats. *J. Vet. Med. Sci.* **1992**, *54*, 557–562. [[CrossRef](#)] [[PubMed](#)]
80. Addie, D.D.; Schaap, I.A.T.; Nicolson, L.; Jarrett, O. Persistence and transmission of natural type I feline coronavirus infection. *J. Gen. Virol.* **2003**, *84*, 2735–2744. [[CrossRef](#)] [[PubMed](#)]
81. Terada, Y.; Matsui, N.; Noguchi, K.; Kuwata, R.; Shimoda, H.; Soma, T.; Mochizuki, M.; Maeda, K. Emergence of Pathogenic Coronaviruses in Cats by Homologous Recombination between Feline and Canine Coronaviruses. *PLoS ONE* **2014**, *9*, e106534. [[CrossRef](#)] [[PubMed](#)]
82. Herrewegh, A.A.; Smeenk, I.; Horzinek, M.C.; Rottier, P.J.; de Groot, R.J. Feline coronavirus type II strains 79-1683 and 79-1146 originate from a double recombination between feline coronavirus type I and canine coronavirus. *J. Virol.* **1998**, *72*, 4508–4514. [[CrossRef](#)]
83. Lorusso, A.; Decaro, N.; Schellen, P.; Rottier, P.J.M.; Buonavoglia, C.; Haijema, B.-J.; Groot, R.J. de Gain, Preservation, and Loss of a Group 1a Coronavirus Accessory Glycoprotein. *J. Virol.* **2008**, *82*, 10312–10317. [[CrossRef](#)]
84. Tresnan, D.B.; Levis, R.; Holmes, K.V. Feline aminopeptidase N serves as a receptor for feline, canine, porcine, and human coronaviruses in serogroup I. *J. Virol.* **1996**, *70*, 8669–8674. [[CrossRef](#)]
85. Di Matteo, P.; Arrigoni, G.L.; Alberici, L.; Corti, A.; Gallo-Stampino, C.; Traversari, C.; Doglioni, C.; Rizzardi, G.-P. Enhanced expression of CD13 in vessels of inflammatory and neoplastic tissues. *J. Histochem. Cytochem. Off. J. Histochem. Soc.* **2011**, *59*, 47–59. [[CrossRef](#)]
86. Hohdatsu, T.; Izumiya, Y.; Yokoyama, Y.; Kida, K.; Koyama, H. Differences in virus receptor for type I and type II feline infectious peritonitis virus. *Arch. Virol.* **1998**, *143*, 839–850. [[CrossRef](#)]
87. Van Hamme, E.; Desmarests, L.; Dewerchin, H.L.; Nauwynck, H.J. Intriguing interplay between feline infectious peritonitis virus and its receptors during entry in primary feline monocytes. *Virus Res.* **2011**, *160*, 32–39. [[CrossRef](#)]
88. Watanabe, R.; Eckstrand, C.; Liu, H.; Pedersen, N.C. Characterization of peritoneal cells from cats with experimentally-induced feline infectious peritonitis (FIP) using RNA-seq. *Vet. Res.* **2018**, *49*, 81. [[CrossRef](#)] [[PubMed](#)]

89. Olsen, C.W.; Corapi, W.V.; Ngichabe, C.K.; Baines, J.D.; Scott, F.W. Monoclonal antibodies to the spike protein of feline infectious peritonitis virus mediate antibody-dependent enhancement of infection of feline macrophages. *J. Virol.* **1992**, *66*, 956–965. [[CrossRef](#)] [[PubMed](#)]
90. Hohdatsu, T.; Yamada, M.; Tominaga, R.; Makino, K.; Kida, K.; Koyama, H. Antibody-Dependent Enhancement of Feline Infectious Peritonitis Virus Infection in Feline Alveolar Macrophages and Human Monocyte Cell Line U937 by Serum of Cats Experimentally or Naturally Infected with Feline Coronavirus. *J. Vet. Med. Sci.* **1998**, *60*, 49–55. [[CrossRef](#)] [[PubMed](#)]
91. Wan, Y.; Shang, J.; Sun, S.; Tai, W.; Chen, J.; Geng, Q.; He, L.; Chen, Y.; Wu, J.; Shi, Z.; et al. Molecular Mechanism for Antibody-Dependent Enhancement of Coronavirus Entry. *J. Virol.* **2020**, *94*, e02015–e02019. [[CrossRef](#)] [[PubMed](#)]
92. Van Hamme, E.; Dewerchin, H.L.; Cornelissen, E.; Verhasselt, B.; Nauwynck, H.J. Clathrin- and caveolae-independent entry of feline infectious peritonitis virus in monocytes depends on dynamin. *J. Gen. Virol.* **2008**, *89*, 2147–2156. [[CrossRef](#)]
93. Fox, J.G.; Marini, R.P. *Biology and Diseases of the Ferret*; John Wiley & Sons: Hoboken, NJ, USA, 2014; ISBN 978-1-118-78273-6.
94. Williams, B.H.; Kiupel, M.; West, K.H.; Raymond, J.T.; Grant, C.K.; Glickman, L.T. Coronavirus-associated epizootic catarrhal enteritis in ferrets. *J. Am. Vet. Med. Assoc.* **2000**, *217*, 526–530. [[CrossRef](#)]
95. Hoefler, H.L. Gastrointestinal Diseases of Ferrets. *Ferrets Rabbit. Rodents* **2020**, 27–38. [[CrossRef](#)]
96. Wise, A.G.; Kiupel, M.; Maes, R.K. Molecular characterization of a novel coronavirus associated with epizootic catarrhal enteritis (ECE) in ferrets. *Virology* **2006**, *349*, 164–174. [[CrossRef](#)]
97. Garner, M.M.; Ramsell, K.; Morera, N.; Juan-Sallés, C.; Jiménez, J.; Ardiaca, M.; Montesinos, A.; Teifke, J.P.; Löhr, C.V.; Evermann, J.F.; et al. Clinicopathologic features of a systemic coronavirus-associated disease resembling feline infectious peritonitis in the domestic ferret (*Mustela putorius*). *Vet. Pathol.* **2008**, *45*, 236–246. [[CrossRef](#)]
98. Li, T.-C.; Yoshizaki, S.; Kataoka, M.; Doan, Y.H.; Ami, Y.; Suzaki, Y.; Nakamura, T.; Takeda, N.; Wakita, T. Determination of Ferret Enteric Coronavirus Genome in Laboratory Ferrets. *Emerg. Infect. Dis.* **2017**, *23*, 1568–1570. [[CrossRef](#)]
99. Dominguez, E.; Novellas, R.; Moya, A.; Espada, Y.; Martorell, J. Abdominal radiographic and ultrasonographic findings in ferrets (*Mustela putorius furo*) with systemic coronavirus infection. *Vet. Rec.* **2011**, *169*, 231. [[CrossRef](#)] [[PubMed](#)]
100. Autieri, C.R.; Miller, C.L.; Scott, K.E.; Kilgore, A.; Papscoe, V.A.; Garner, M.M.; Haupt, J.L.; Bakthavatchalu, V.; Muthupalani, S.; Fox, J.G. Systemic Coronaviral Disease in 5 Ferrets. *Comp. Med.* **2015**, *65*, 508–516. [[PubMed](#)]
101. Doria-Torra, G.; Vidaña, B.; Ramis, A.; Amarilla, S.P.; Martínez, J. Coronavirus Infection in Ferrets: Antigen Distribution and Inflammatory Response. *Vet. Pathol.* **2016**, *53*, 1180–1186. [[CrossRef](#)] [[PubMed](#)]
102. Duijvestijn, M.; Mughini-Gras, L.; Schuurman, N.; Schijf, W.; Wagenaar, J.A.; Egberink, H. Enteropathogen infections in canine puppies: (Co-)occurrence, clinical relevance and risk factors. *Vet. Microbiol.* **2016**, *195*, 115–122. [[CrossRef](#)] [[PubMed](#)]
103. Dowgier, G.; Lorusso, E.; Decaro, N.; Desario, C.; Mari, V.; Lucente, M.S.; Lanave, G.; Buonavoglia, C.; Elia, G. A molecular survey for selected viral enteropathogens revealed a limited role of Canine circovirus in the development of canine acute gastroenteritis. *Vet. Microbiol.* **2017**, *204*, 54–58. [[CrossRef](#)]
104. Stavisky, J.; Pinchbeck, G.L.; German, A.J.; Dawson, S.; Gaskell, R.M.; Ryvar, R.; Radford, A.D. Prevalence of canine enteric coronavirus in a cross-sectional survey of dogs presenting at veterinary practices. *Vet. Microbiol.* **2010**, *140*, 18–24. [[CrossRef](#)] [[PubMed](#)]
105. Binn, L.N.; Lazar, E.C.; Keenan, K.P.; Huxsoll, D.L.; Marchwicki, R.H.; Strano, A.J. Recovery and characterization of a coronavirus from military dogs with diarrhea. *Proc. Annu. Meet. US Anim. Health Assoc.* **1974**, 359–366.
106. Decaro, N.; Buonavoglia, C. An update on canine coronaviruses: Viral evolution and pathobiology. *Vet. Microbiol.* **2008**, *132*, 221–234. [[CrossRef](#)]
107. Decaro, N.; Martella, V.; Desario, C.; Bellacicco, A.L.; Camero, M.; Manna, L.; d’Aloja, D.; Buonavoglia, C. First detection of canine parvovirus type 2c in pups with haemorrhagic enteritis in Spain. *J. Vet. Med. B Infect. Dis. Vet. Public Health* **2006**, *53*, 468–472. [[CrossRef](#)]

108. Pratelli, A.; Martella, V.; Elia, G.; Tempesta, M.; Guarda, F.; Capucchio, M.T.; Carmichael, L.E.; Buonavoglia, C. Severe enteric disease in an animal shelter associated with dual infections by canine adenovirus type 1 and canine coronavirus. *J. Vet. Med. B Infect. Dis. Vet. Public Health* **2001**, *48*, 385–392. [[CrossRef](#)]
109. Pratelli, A.; Tempesta, M.; Roperto, F.P.; Sagazio, P.; Carmichael, L.; Buonavoglia, C. Fatal Coronavirus Infection in Puppies following Canine Parvovirus 2b Infection. *J. Vet. Diagn. Investig.* **1999**, *11*, 550–553. [[CrossRef](#)]
110. Evermann, J.F.; Abbott, J.R.; Han, S. Canine coronavirus-associated puppy mortality without evidence of concurrent canine parvovirus infection. *J. Vet. Diagn. Investig. Off. Publ. Am. Assoc. Vet. Lab. Diagn. Inc.* **2005**, *17*, 610–614. [[CrossRef](#)] [[PubMed](#)]
111. Buonavoglia, C.; Decaro, N.; Martella, V.; Elia, G.; Campolo, M.; Desario, C.; Castagnaro, M.; Tempesta, M. Canine coronavirus highly pathogenic for dogs. *Emerg. Infect. Dis.* **2006**, *12*, 492–494. [[CrossRef](#)] [[PubMed](#)]
112. Alfano, F.; Fusco, G.; Mari, V.; Occhiogrosso, L.; Miletti, G.; Brunetti, R.; Galiero, G.; Desario, C.; Cirilli, M.; Decaro, N. Circulation of pantropic canine coronavirus in autochthonous and imported dogs, Italy. *Transbound. Emerg. Dis.* **2020**. [[CrossRef](#)] [[PubMed](#)]
113. Alfano, F.; Dowgier, G.; Valentino, M.P.; Galiero, G.; Tinelli, A.; Nicola, D.; Fusco, G. Identification of Pantropic Canine Coronavirus in a Wolf (*Canis lupus italicus*) in Italy. *J. Wildl. Dis.* **2019**, *55*, 504–508. [[CrossRef](#)] [[PubMed](#)]
114. Ma, G.; Lu, C. Two genotypes of Canine coronavirus simultaneously detected in the fecal samples of healthy foxes and raccoon dogs. *Wei Sheng Wu Xue Bao* **2005**, *45*, 305–308. [[PubMed](#)]
115. Zarnke, R.L.; Evermann, J.; Ver Hoef, J.M.; McNay, M.E.; Boertje, R.D.; Gardner, C.L.; Adams, L.G.; Dale, B.W.; Burch, J. Serologic survey for canine coronavirus in wolves from Alaska. *J. Wildl. Dis.* **2001**, *37*, 740–745. [[CrossRef](#)] [[PubMed](#)]
116. Molnar, B.; Duchamp, C.; Möstl, K.; Diehl, P.-A.; Betschart, B. Comparative survey of canine parvovirus, canine distemper virus and canine enteric coronavirus infection in free-ranging wolves of central Italy and south-eastern France. *Eur. J. Wildl. Res.* **2014**, *60*, 613–624. [[CrossRef](#)]
117. Wang, X.; Li, C.; Guo, D.; Wang, X.; Wei, S.; Geng, Y.; Wang, E.; Wang, Z.; Zhao, X.; Su, M.; et al. Co-Circulation of Canine Coronavirus I and IIa/b with High Prevalence and Genetic Diversity in Heilongjiang Province, Northeast China. *PLoS ONE* **2016**, *11*, e0146975. [[CrossRef](#)]
118. Decaro, N.; Mari, V.; Campolo, M.; Lorusso, A.; Camero, M.; Elia, G.; Martella, V.; Cordioli, P.; Enjuanes, L.; Buonavoglia, C. Recombinant canine coronaviruses related to transmissible gastroenteritis virus of Swine are circulating in dogs. *J. Virol.* **2009**, *83*, 1532–1537. [[CrossRef](#)]
119. Licitra, B.; Duhamel, G.; Whittaker, G. Canine Enteric Coronaviruses: Emerging Viral Pathogens with Distinct Recombinant Spike Proteins. *Viruses* **2014**, *6*, 3363–3376. [[CrossRef](#)]
120. Zappulli, V.; Caliani, D.; Cavicchioli, L.; Tinelli, A.; Castagnaro, M. Systemic fatal type II coronavirus infection in a dog: Pathological findings and immunohistochemistry. *Res. Vet. Sci.* **2008**, *84*, 278–282. [[CrossRef](#)] [[PubMed](#)]
121. Erles, K.; Brownlie, J. Canine respiratory coronavirus: An emerging pathogen in the canine infectious respiratory disease complex. *Vet. Clin. North Am. Small Anim. Pract.* **2008**, *38*, 815–825. [[CrossRef](#)] [[PubMed](#)]
122. Priestnall, S.L.; Brownlie, J.; Dubovi, E.J.; Erles, K. Serological prevalence of canine respiratory coronavirus. *Vet. Microbiol.* **2006**, *115*, 43–53. [[CrossRef](#)] [[PubMed](#)]
123. Priestnall, S.L.; Pratelli, A.; Brownlie, J.; Erles, K. Serological Prevalence of Canine Respiratory Coronavirus in Southern Italy and Epidemiological Relationship with Canine Enteric Coronavirus. *J. Vet. Diagn. Investig.* **2007**, *19*, 176–180. [[CrossRef](#)] [[PubMed](#)]
124. Yachi, A.; Mochizuki, M. Survey of Dogs in Japan for Group 2 Canine Coronavirus Infection. *J. Clin. Microbiol.* **2006**, *44*, 2615–2618. [[CrossRef](#)] [[PubMed](#)]
125. Knesl, O.; Allan, F.J.; Shields, S. The seroprevalence of canine respiratory coronavirus and canine influenza virus in dogs in New Zealand. *N. Z. Vet. J.* **2009**, *57*, 295–298. [[CrossRef](#)] [[PubMed](#)]
126. Erles, K.; Toomey, C.; Brooks, H.W.; Brownlie, J. Detection of a group 2 coronavirus in dogs with canine infectious respiratory disease. *Virology* **2003**, *310*, 216–223. [[CrossRef](#)]
127. Decaro, N.; Mari, V.; Larocca, V.; Losurdo, M.; Lanave, G.; Lucente, M.S.; Corrente, M.; Catella, C.; Bo, S.; Elia, G.; et al. Molecular surveillance of traditional and emerging pathogens associated with canine infectious respiratory disease. *Vet. Microbiol.* **2016**, *192*, 21–25. [[CrossRef](#)]

128. Lavan, R.; Knesl, O. Prevalence of canine infectious respiratory pathogens in asymptomatic dogs presented at US animal shelters. *J. Small Anim. Pract.* **2015**, *56*, 572–576. [[CrossRef](#)]
129. Priestnall, S.L.; Mitchell, J.A.; Brooks, H.W.; Brownlie, J.; Erles, K. Quantification of mRNA encoding cytokines and chemokines and assessment of ciliary function in canine tracheal epithelium during infection with canine respiratory coronavirus (CRCoV). *Vet. Immunol. Immunopathol.* **2009**, *127*, 38–46. [[CrossRef](#)] [[PubMed](#)]
130. Arsevska, E.; Priestnall, S.L.; Singleton, D.A.; Jones, P.H.; Smyth, S.; Brant, B.; Dawson, S.; Sánchez-Vizcaíno, F.; Noble, P.J.M.; Radford, A.D. Small animal disease surveillance: Respiratory disease 2017. *Vet. Rec.* **2018**, *182*, 369–373. [[CrossRef](#)] [[PubMed](#)]
131. Wille, M.; Wensman, J.J.; Larsson, S.; van Damme, R.; Theelke, A.-K.; Hayer, J.; Malmberg, M. Evolutionary genetics of canine respiratory coronavirus and recent introduction into Swedish dogs. *Infect. Genet. Evol.* **2020**, *82*, 104290. [[CrossRef](#)] [[PubMed](#)]
132. Priestnall, S.L. Canine Respiratory Coronavirus: A Naturally Occurring Model of COVID-19? *Vet. Pathol.* **2020**, *57*, 467–471. [[CrossRef](#)] [[PubMed](#)]
133. Szczepanski, A.; Owczarek, K.; Milewska, A.; Baster, Z.; Rajfur, Z.; Mitchell, J.A.; Pyrc, K. Canine respiratory coronavirus employs caveolin-1-mediated pathway for internalization to HRT-18G cells. *Vet. Res.* **2018**, *49*, 55. [[CrossRef](#)] [[PubMed](#)]
134. Szczepanski, A.; Owczarek, K.; Bzowska, M.; Gula, K.; Drebot, I.; Ochman, M.; Maksym, B.; Rajfur, Z.; Mitchell, J.A.; Pyrc, K. Canine Respiratory Coronavirus, Bovine Coronavirus, and Human Coronavirus OC43: Receptors and Attachment Factors. *Viruses* **2019**, *11*, 328. [[CrossRef](#)] [[PubMed](#)]
135. Mitchell, J.A.; Brooks, H.; Shiu, K.-B.; Brownlie, J.; Erles, K. Development of a quantitative real-time PCR for the detection of canine respiratory coronavirus. *J. Virol. Methods* **2009**, *155*, 136–142. [[CrossRef](#)]
136. Davis, E.; Rush, B.R.; Cox, J.; DeBey, B.; Kapil, S. Neonatal Enterocolitis Associated with Coronavirus Infection in a Foal: A Case Report. *J. Vet. Diagn. Investig.* **2000**, *12*, 153–156. [[CrossRef](#)]
137. Pusterla, N.; Vin, R.; Leutenegger, C.M.; Mittel, L.D.; Divers, T.J. Enteric coronavirus infection in adult horses. *Vet. J.* **2018**, *231*, 13–18. [[CrossRef](#)]
138. Fielding, C.L.; Higgins, J.K.; Higgins, J.C.; McIntosh, S.; Scott, E.; Giannitti, F.; Mete, A.; Pusterla, N. Disease associated with equine coronavirus infection and high case fatality rate. *J. Vet. Intern. Med.* **2015**, *29*, 307–310. [[CrossRef](#)]
139. Pusterla, N.; Mapes, S.; Wademan, C.; White, A.; Ball, R.; Sapp, K.; Burns, P.; Ormond, C.; Butterworth, K.; Bartol, J.; et al. Emerging outbreaks associated with equine coronavirus in adult horses. *Vet. Microbiol.* **2013**, *162*, 228–231. [[CrossRef](#)]
140. Nemoto, M.; Oue, Y.; Morita, Y.; Kanno, T.; Kinoshita, Y.; Niwa, H.; Ueno, T.; Katayama, Y.; Bannai, H.; Tsujimura, K.; et al. Experimental inoculation of equine coronavirus into Japanese draft horses. *Arch. Virol.* **2014**, *159*, 3329–3334. [[CrossRef](#)]
141. Schaefer, E.; Harms, C.; Viner, M.; Barnum, S.; Pusterla, N. Investigation of an experimental infection model of equine coronavirus in adult horses. *J. Vet. Intern. Med.* **2018**, *32*, 2099–2104. [[CrossRef](#)] [[PubMed](#)]
142. Pusterla, N.; Vin, R.; Leutenegger, C.; Mittel, L.D.; Divers, T.J. Equine coronavirus: An emerging enteric virus of adult horses. *Equine Vet. Educ.* **2016**, *28*, 216–223. [[CrossRef](#)] [[PubMed](#)]
143. Cebra, C.K.; Mattson, D.E.; Baker, R.J.; Sonn, R.J.; Dearing, P.L. Potential pathogens in feces from unweaned llamas and alpacas with diarrhea. *J. Am. Vet. Med. Assoc.* **2003**, *223*, 1806–1808. [[CrossRef](#)] [[PubMed](#)]
144. Crossley, B.M.; Barr, B.C.; Magdesian, K.G.; Ing, M.; Mora, D.; Jensen, D.; Loretto, A.P.; McConnell, T.; Mock, R. Identification of a Novel Coronavirus Possibly Associated with Acute Respiratory Syndrome in Alpacas (*Vicugna Pacos*) in California, 2007. *J. Vet. Diagn. Investig.* **2010**, *22*, 94–97. [[CrossRef](#)] [[PubMed](#)]
145. Pearson, L.K.; Rodriguez, J.S.; Tibary, A. Disorders and Diseases of Pregnancy. *Llama Alpaca Care* **2014**, 256–273. [[CrossRef](#)]
146. Zhang, J.; Guy, J.S.; Snijder, E.J.; Denniston, D.A.; Timoney, P.J.; Balasuriya, U.B.R. Genomic characterization of equine coronavirus. *Virology* **2007**, *369*, 92–104. [[CrossRef](#)]
147. Nemoto, M.; Oue, Y.; Murakami, S.; Kanno, T.; Bannai, H.; Tsujimura, K.; Yamanaka, T.; Kondo, T. Complete genome analysis of equine coronavirus isolated in Japan. *Arch. Virol.* **2015**, *160*, 2903–2906. [[CrossRef](#)]
148. Genova, S.G.; Streeter, R.N.; Simpson, K.M.; Kapil, S. Detection of an Antigenic Group 2 Coronavirus in an Adult Alpaca with Enteritis. *Clin. Vaccine Immunol. CVI* **2008**, *15*, 1629–1632. [[CrossRef](#)]
149. Jin, L.; Cebra, C.K.; Baker, R.J.; Mattson, D.E.; Cohen, S.A.; Alvarado, D.E.; Rohrmann, G.F. Analysis of the genome sequence of an alpaca coronavirus. *Virology* **2007**, *365*, 198–203. [[CrossRef](#)] [[PubMed](#)]

150. Corman, V.M.; Muth, D.; Niemeyer, D.; Drosten, C. Hosts and Sources of Endemic Human Coronaviruses. *Adv. Virus Res.* **2018**, *100*, 163–188. [[CrossRef](#)]
151. Crossley, B.; Mock, R.; Callison, S.; Hietala, S. Identification and Characterization of a Novel Alpaca Respiratory Coronavirus Most Closely Related to the Human Coronavirus 229E. *Viruses* **2012**, *4*, 3689–3700. [[CrossRef](#)] [[PubMed](#)]
152. Lai, M.M.C.; Cavanagh, D. The Molecular Biology of Coronaviruses. In *Advances in Virus Research*; Maramorosch, K., Murphy, F.A., Shatkin, A.J., Eds.; Academic Press: Cambridge, MA, USA, 1997; Volume 48, pp. 1–100.
153. Forni, D.; Cagliani, R.; Clerici, M.; Sironi, M. Molecular Evolution of Human Coronavirus Genomes. *Trends Microbiol.* **2017**, *25*, 35–48. [[CrossRef](#)] [[PubMed](#)]
154. Jones, K.E.; Patel, N.G.; Levy, M.A.; Storeygard, A.; Balk, D.; Gittleman, J.L.; Daszak, P. Global trends in emerging infectious diseases. *Nature* **2008**, *451*, 990–993. [[CrossRef](#)]
155. Cui, J.; Li, F.; Shi, Z.-L. Origin and evolution of pathogenic coronaviruses. *Nat. Rev. Microbiol.* **2019**, *17*, 181–192. [[CrossRef](#)] [[PubMed](#)]

**Chapter 2: Serotype I and II feline coronavirus replication and gene expression patterns of feline cells – building a better understanding of serotype I FIPV biology**

# Serotype I and II Feline Coronavirus Replication and Gene Expression Patterns of Feline Cells—Building a Better Understanding of Serotype I FIPV Biology

Sarah Cook <sup>1,\*</sup>, Diego Castillo <sup>2</sup>, Sonyia Williams <sup>2</sup>, Christine Haake <sup>3</sup>  and Brian Murphy <sup>2</sup> 

<sup>1</sup> Graduate Group Integrative Pathobiology, School of Veterinary Medicine, University of California, Davis, CA 95616, USA

<sup>2</sup> Department of Pathology, Microbiology, and Immunology, School of Veterinary Medicine, University of California, Davis, CA 95616, USA; ldcastillo@ucdavis.edu (D.C.); sywilliams@ucdavis.edu (S.W.); bmurphy@ucdavis.edu (B.M.)

<sup>3</sup> School of Veterinary Medicine, University of California, Davis, CA 95616, USA; cjhaake@ucdavis.edu

\* Correspondence: sestevens@ucdavis.edu



Citation: Cook, S.; Castillo, D.; Williams, S.; Haake, C.; Murphy, B. Serotype I and II Feline Coronavirus Replication and Gene Expression Patterns of Feline Cells—Building a Better Understanding of Serotype I FIPV Biology. *Viruses* **2022**, *14*, 1356. <https://doi.org/10.3390/v14071356>

Academic Editor: Pinghuang Liu

Received: 30 May 2022

Accepted: 21 June 2022

Published: 22 June 2022

**Publisher's Note:** MDPI stays neutral with regard to jurisdictional claims in published maps and institutional affiliations.



**Copyright:** © 2022 by the authors. Licensee MDPI, Basel, Switzerland. This article is an open access article distributed under the terms and conditions of the Creative Commons Attribution (CC BY) license (<https://creativecommons.org/licenses/by/4.0/>).

**Abstract:** Feline infectious peritonitis (FIP) is a disease of domestic cats caused by the genetic variant of the feline coronavirus (FCoV) and feline infectious peritonitis virus (FIPV), currently grouped into two serotypes, I and II. Although serotype I FIPV is more prevalent in cats with FIP, serotype II has been more extensively studied in vitro due to the relative ease in propagating this viral serotype in culture systems. As a result, more is known about serotype II FIPV than the more biologically prevalent serotype I. The primary cell receptor for serotype II has been determined, while it remains unknown for serotype I. The recent development of a culture-adapted feline cell line that more effectively propagates serotype I FIPV, FCWF-4 CU, derived from FCWF-4 cells available through the ATCC, offers the potential for an improved understanding of serotype I FIPV biology. To learn more about FIPV receptor biology, we determined targeted gene expression patterns in feline cells variably permissive to replication of serotype I or II FIPV. We utilized normal feline tissues to determine the immunohistochemical expression patterns of two known coronavirus receptors, ACE2 and DC-SIGN. Lastly, we compared the global transcriptomes of the two closely related FCWF-4 cell lines and identified viral transcripts with potential importance for the differential replication kinetics of serotype I FIPV.

**Keywords:** feline infectious peritonitis; FIP; serotype; cell receptor; coronavirus; viral replication

## 1. Introduction

Feline infectious peritonitis (FIP) is a generally fatal coronaviral disease of domestic cats caused by a genetic variant of the feline coronavirus (FCoV), referred to as the FIP virus (FIPV) [1,2]. FIP is a systemic immune-mediated, inflammatory disease variably characterized by fever, ascites accumulation, fibrinous exudate, pyogranulomatous perivascularitis, and high mortality [3–5]. Virus-associated inflammation may be confined to the abdominal cavity but can also involve the thoracic cavity, lymph nodes, brain, or eye [4].

FCoV is subclassified into two biotypes, feline enteric coronavirus (FECV) and feline infectious peritonitis virus (FIPV), and further classified into two serotypes (serotype I and serotype II), currently taxonomically grouped as a single species of *Alphacoronavirus* based on genomic sequencing [6]. The two distinct serotypes are classified based on variation in the humoral response stemming from marked sequence differences between spike proteins [7]. The coronavirus spike (S) protein serves as the docking ligand for the cell receptor, thereby defining the cellular tropism and tissue-based distribution of the virus. Cellular tropism has been investigated for FIPV through in vitro recombination studies and the generation of viral chimeras to map regions of the S protein that may be

responsible for these differences in cell tropism [8,9]. Serotype II FIPV is the evolutionary result of a recombination event between feline coronavirus and canine enteric coronavirus, resulting in a chimeric FCoV encoding the canine coronavirus *spike* gene [10,11]. However, this taxonomic organization has been challenged by the suggestion that serotype I and II FCoV be redefined as distinct viruses based on distinguishing differences in spike protein structure and function and the pivotal roles that spike plays in biological and clinical outcomes [12].

In nature, serotype I FCoVs, including FIPV I, are more prevalent than FIPV II viruses and are associated with the majority (80–95%) of naturally occurring cases of FIP in cats (serotype I and II FIPVs are hereafter referred to as FIPV I or FIPV II) [13–15]. However, the *in vitro* propagation of FIPV I isolates in tissue culture systems has proven to be problematic, impeding forward progress in tissue-culture-based virology and pathogenesis investigations. While the primary cellular receptor utilized for cell entry by FIPV II has been identified as feline aminopeptidase N (feAPN/CD13), the primary cellular receptor utilized by FIPV I remains to be determined [16–19]. There are conflicting results regarding the possibility of feAPN serving as a primary cell receptor for FIPV I. Tresnan et al. (1996) found that non-permissive mouse or hamster cells, transduced to stably express feAPN, became permissive to both FIPV I and II replication [16]. In contrast, Hohdatsu et al. (1998) found that when applying feAPN antibodies to FIPV permissive cells (FCWF-4), the cells were no longer infectable by FIPV II, while FIPV I was still able to infect the antibody-treated cells [19]. Similarly, Dye et al. (2007) found out through the use of retroviral pseudotypes bearing the type I or type II S glycoprotein that type I S glycoprotein failed to transduce cell lines known to express feAPN (Crandall-Reese feline kidney cells (CRFK), *Felis catus* whole fetus 4 (FCWF-4), and feline kidney fibroblast cells) [18]. These experimental inconsistencies, along with inconsistencies in reported abilities to propagate FIPV I in a number of cell lines (including CRFK and FCWF-4), call into question whether feAPN can be absolutely eliminated as a putative FIPV I receptor.

FIPV II readily replicates in several different feline cell lines (e.g., CRFK and FCWF-4) [20]. The FIPV I Black strain (also referred to as TN406 and hereafter referred to as Black I) was originally isolated from an experimental case of FIP and is one of the few tissue-culture-adapted FIPV I strains [21]. Black I has been successfully propagated in a spontaneously immortalized cell line derived from fetal feline airway epithelial cells (AK-D) [22]. However, FIPV targets feline monocytes/macrophages *in vivo* and not airway epithelium. Thus, a more biologically relevant cell line may provide better insight into the naturally occurring disease in cats [23–25]. The cell line FCWF-4 is a feline macrophage-like cell that is permissive for FIPV I replication [20]. FCWF-4 cells are described as “macrophage-like” based on studies demonstrating nonspecific esterase expression (a cytochemical marker of macrophages), the phagocytic properties of the cells, and the detection of Fc receptors on the FCWF-4 surface membrane [26]. Although permissive to FIPV I, viral replication has been shown to be reduced ( $10^4$  vs.  $10^6$  TCID<sub>50</sub>/mL) and delayed (96 vs. 24 h post-infection) in FCWF-4 cells relative to FIPV II replication [20,22,26–29]. Recently, an FCWF-4-derived cell line established at Cornell University (herein referred to as FCWF-4 CU) demonstrated dramatically improved Black I replication kinetics, with rapidly increased viral titers relative to FCWF-4 obtained directly from the American Type Culture Collection (hereafter referred to as FCWF-4 ATCC) [22]. Possible reasons for improved replication in FCWF-4 CU cells relative to FCWF-4 ATCC cells include variations in antiviral interferon responses, differences in expression and density of the presently undetermined FIPV I receptor [22], or differences in the expression of host cell proteases necessary for coronavirus cell entry or activation.

Different alphacoronaviruses and betacoronaviruses share a discrete collection of receptors for cell entry (Table 1) [16,30–33]. Known cellular receptors of coronaviruses include APN, dendritic cell-specific intercellular adhesion molecule-3-grabbing nonintegrin (DC-SIGN), angiotensin-converting enzyme 2 (ACE2), and dipeptidyl-peptidase 4 (DPP4/CD26). The C-type lectin, DC-SIGN, has been shown to enhance cell entry by FIPV II acting as a co-receptor [24,34]. One study demonstrated that the induction of DC-SIGN

expression in CRFK cells renders them permissive to Black I infection, suggesting that serotype I strains might be dependent upon lectins as a co-receptor and that CRFK cells might express the primary receptor at low levels [24].

**Table 1.** List of known alpha- and betacoronavirus cellular receptors.

Genus	Virus	Species	Receptor
<i>Alpha</i>	HCoV-NL63	Human	ACE2
	229E	Human	APN
	TGEV	Pig	APN
	PRCoV	Pig	APN
	FCoV Serotype I	Cat	ND
	FCoV Serotype II	Cat	APN, DC-SIGN
	CCoV	Dog	APN
	SARS-CoV-1	Human	ACE2
<i>Beta</i>	SARS-CoV-2	Human	ACE2, DC-SIGN
	MERS-CoV	Human	DPP4

ND = not determined; HCoV-NL63 = human coronavirus NL63; 229E = human coronavirus-229E; TGEV = transmissible gastroenteritis virus; PRCoV = porcine respiratory coronavirus; FCoV = feline coronavirus; CCoV = canine coronavirus; SARS-CoV-1 = severe acute respiratory syndrome-coronavirus-1; SARS-CoV-2 = severe acute respiratory syndrome-coronavirus-2; ACE2 = angiotensin-converting enzyme 2; APN = aminopeptidase N; DC-SIGN = dendritic cell-specific intercellular adhesion molecule-3 grabbing nonintegrin; DPP4 = dipeptidyl-peptidase 4 (DPP4).

Here, we characterize FIPV I and II replication in three feline cell lines (CRFK, FCWF-4 ATCC, FCWF-4 CU) and in primary feline monocyte-derived macrophages (feMDMs). Based upon the known coronaviral receptor redundancy, we explored the targeted gene expression patterns in feline cell lines and feMDMs and hypothesized that these expression patterns would facilitate the identification of the FIPV I receptor. Using antibodies targeting two of the investigated feline-specific receptor proteins (DC-SIGN and ACE2), we utilized immunohistochemistry to characterize the feline tissue and cellular distribution patterns of these putative coronaviral receptors. Finally, we hypothesized that the global transcriptome for the two closely related FCWF cell lines would inform the identification of putative viral receptors or other cellular features important for the differential replication kinetics of FIPV I.

## 2. Materials and Methods

### 2.1. FIPV Inoculum for In Vitro Experiments

FIPV II (WSU-79-1146; GenBank DQ010921) was propagated and viral infectivity was quantified in CRFK cells using a biological plaquing assay (median tissue culture infectious dose, TCID<sub>50</sub>); viral RNA was quantified using reverse transcription real-time polymerase chain reaction (RT-qPCR) as previously described [35]. FIPV I (Black I) and FCWF-4 CU cells were kindly donated by Dr. Susan Baker (Loyola University Chicago), originally obtained from Cornell University College of Veterinary Medicine (Dr. Edward Dubovi). Briefly, Black I virus was propagated in FCWF-4 CU cells by inoculating a confluent 75 cm<sup>2</sup> tissue culture flask (Corning, Corning, NY, USA) with Black I virus at a multiplicity of infection (MOI) of 0.1 in 3 mL of minimal essential media (MEM; Sigma, St. Louis, MO, USA) lacking fetal bovine serum (FBS) and incubated for 1 h at 37 °C, tilting the flask every 15 min. The inoculum was then removed, and 10 mL of MEM + 2% FBS was added to the flask and incubated at 37 °C for an additional 24 h before collecting the cultured supernatant and centrifuging the sample at 775 × g rpm for 5 min. The resulting supernatant was aliquoted into 100 or 500 µL volumes and frozen at −80 °C. The determination of the FIPV serotype was confirmed using serotyping primers (FCoV I S For, FCoV II S For, FCoV I and II S Rev; nFCoV I S For, nFCoV II S For, and nFCoV I and II S Rev) targeting a portion of the *spike* gene previously published and listed in Table 2 [36]. All additional primers utilized in this research project can be found in Table 2.

**Table 2.** Primers utilized in all PCR reactions with annealing temperatures and expected amplicon sizes for each primer set.

Target		Sequence (5'-3')	Annealing Temperature (°C)	Size (bp)
FIPV	Forward	GGAAGTTTAGATTGATTTGGCAATGCTAG	58	112
	Reverse	AACAATCACTAGATCCAGACGTTAGCT		
GAPDH	Forward	AAATCCACGGCAGCAAG	58	61
	Reverse	TGATGGGCTTTCATTGATGA		
CD16	Forward	AACCAGCTTCTGCTTCAGTATC	51	98
	Reverse	AGACCTGAGCGCATAGAGTATC		
ACE2	Forward	GACAACAGCCTGGAGTTTCT	51	134
	Reverse	GAGACGATGAGCAGGACAATAC		
DC-SIGN	Forward	GGCCTTAAAGATCCTGAGAGAGA	51	102
	Reverse	GCTGAGACCATCAACAGAAGAAG		
feAPN	Forward	GGTGTTTGACTCCATCTCCTAC	60	134
	Reverse	GGTAGATGGTGTTCCTGATTT		
DPP4	Forward	ATGCAAGCACCGACTTCTAA	55	117
	Reverse	CGTAGCACCTCTAGCCATAAC		
FCoV I S For (Iffs type I)	Forward	GTTTCAACCTAGAAAGCCTCAGAT	50	376
	Reverse	GCCTAGTATTATACCTGACTA		
FCoV II S For (Icfs type II)	Forward	CCACACATACCAAGGCC	47	360
	Reverse	CCTAGAAAAGCCTCAGATGAGTG		
FCoV I and II S Rev (Iubs)	Forward	CAGACCAAACCTGGACTGTAC	47	218
	Reverse	CCAAGGCCATTTTACATA		

## 2.2. RNA Processing

RNA for all experiments was isolated using Invitrogen's PureLink RNA Mini Kit and subsequently treated to remove possible DNA contamination using TURBO DNase from the same manufacturer. Samples in which cDNA was to be generated were reverse transcribed using Applied Biosystem's High-Capacity RNA-to-cDNA Kit, including reactions lacking the reverse transcriptase (RT) enzyme (RT-control) (Thermo Scientific).

## 2.3. Black I and WSU-79-1146 Titers across Cell Types

To determine the relative replication efficiencies of Black I and WSU 79-1146 (FIPV II) in the various cell types (CRFK, FCWF-4 ATCC, FCWF-4 CU, and feline monocyte-derived macrophages (feMDMs)), TCID50 was determined by a biological plaquing assay as previously described and published [35]. Goat synovial membrane (GSM) cells were utilized as a non-permissive negative control cell line. GSM cells were originally derived from fetal goat tissues and were cultured in DMEM/10% FBS [37]. Due to challenges in obtaining complete monolayers of feMDMs necessary for the colorimetric plaquing assay, the replication of Black I and WSU 79-1146 viruses in feMDM cells was determined using RT-qPCR. Using density/centrifugation-based separation, feMDMs were derived from feline peripheral whole blood by isolating peripheral blood mononuclear cells (PBMCs) from approximately 5 to 7 mL of feline whole blood obtained from purposefully bred specific pathogen-free cats from the University California Feline Nutrition Center (UC Davis) in accordance with UC Davis Nutrition Center IACUC protocol and guidelines. Freshly isolated feline PBMCs were resuspended and plated in RPMI-1640 (HyClone) media supplemented with 10% fetal bovine serum (FBS; Gemini, New York, NY, USA), 10% feline serum (Equitech Bio, Kerrville, TX, USA), 100 U/mL penicillin and 0.1 mg/mL streptomycin (Gibco, Waltham, MA, USA), 2 mM GlutaMAX (Gibco), 20 ng/mL recombinant human granulocyte macrophage colony-stimulating factor (GM-CSF; R&D Systems, Minneapolis, MN, USA), and 10 ng/mL recombinant human interleukin-4 (IL-4; Gibco). Culture media was exchanged for fresh media every two days for eight to ten days to allow for adherence and macrophage differentiation based on cytomorphology ("fried-egg" morphology) and the immunofluorescent labeling of the macrophage marker CD14 (BioRad, TUK4; method is described below, Hercules, CA, USA) [38]. Feline MDMs were cultured in a 24-well tissue culture plate and subsequently infected with either Black I or WSU 79-1146 at MOI 0.1 in triplicate wells. Infected cells were incubated for approximately 36 h, at which time cell-associated total RNA was isolated and processed as previously described (Section 2.2).

The copy number for all target genes was determined using Applied Biosystem's QuantStudio 3 Real-Time PCR System and PowerUp SYBR Green Master Mix, following

the manufacturer's protocol for a 10  $\mu$ L reaction. Cycling conditions were as follows: 50 °C for 2 min and 95 °C for 2 min, followed by 40 cycles of 95 °C for 15 s, respective annealing temperature for 30 s (see Table 2), and 72 °C for 1 min. The final step included a dissociation curve to evaluate the specificity of primer binding. All reactions were performed in triplicate with a water template as a negative control and plasmid DNA as a positive control. Copies of target gene cDNA were normalized to  $10^6$  copies of feline *GAPDH* cDNA based on standard curves generated in our laboratory. Results were graphed using Prism 9 (GraphPad), and a Student's *t*-test was performed to determine the significance of differences in the mean viral titer.

#### 2.4. Quantification of FIPV and Cellular Gene Expression by RT-qPCR

Four feline cell types (feMDM, FCWF-4 ATCC, FCWF-4 CU, and CRFK) were evaluated for gene expression patterns of known coronavirus cellular receptors. FeMDMs were cultured as described above. CRFK cells were grown in DMEM/10% FBS. FCWF-4 ATCC and CU cells were grown in MEM supplemented with 1% pen/strep, 1% L-glutamine, 1% HEPES (1M), 1% sodium pyruvate solution, 1% MEM non-essential amino acid solution, and 10% FBS, followed by sterile filtration through a 0.22-micron membrane filter.

In order to assess gene expression patterns of known alpha- and betacoronavirus receptors (ACE2, DC-SIGN, fAPN, and DPP4), the above-listed feline cell types were propagated in tissue culture plates, and total cell-associated RNA was isolated and processed as previously described (Section 2.2). Except for the listed and previously published serotyping primers, all qPCR cycling conditions for all target genes were the same, aside from annealing temperatures, which can be found in Table 2. The copy number for all target genes was determined using Applied Biosystem's QuantStudio 3 Real-Time PCR System and PowerUp SYBR Green Master Mix, following the manufacturer's protocol for a 10  $\mu$ L reaction. All reactions were performed in triplicate with a water template as a negative control and plasmid DNA as a positive control. Copies of target gene cDNA were normalized to  $10^6$  copies of feline *GAPDH* cDNA based on standard curves generated in our laboratory.

#### 2.5. CD14 Immunofluorescence

CD14 immunofluorescence was performed to provide supportive evidence of a histiocytic (macrophage) phenotype for feMDM cells. FeMDM cells were cultured in a 24-well tissue culture plate, as described above. Feline MDM cells were gently washed three times with phosphate-buffered saline (PBS) for 5 min per wash. Cells were then fixed with 100% methanol for 10 min and then incubated with a blocking solution containing 5% bovine serum albumin (tris-buffered saline with 0.1% Tween 20 and 5% bovine serum albumin), rocking it for 1 h at room temperature. Cells were washed three times with PBS and incubated with a primary antibody, mouse anti-human CD14, at a dilution of 1:500 for one hour at room temperature. Cells were washed three times with PBS before incubation with the conjugated secondary antibody (FITC anti-mouse IgG; Vector Laboratories) at 1:1000 dilution for 30 min at room temperature. After washing with PBS three more times, one drop of SlowFade Gold Antifade reagent (Invitrogen, Waltham, MA, USA) containing DAPI was applied to the well. The cells were then assessed visually using fluorescence microscopy with GFP and DAPI light cubes (Life Technologies EVOS digital inverted microscope and cell imaging system). This procedure was repeated for FCWF-4 ATCC, FCWF-4 CU, and CRFK cells.

#### 2.6. Determining the Systemic Distribution of ACE2 and DC-SIGN in Feline Tissues

In order to characterize the feline tissue distribution patterns of ACE2 and DC-SIGN proteins, immunohistochemical staining was performed on formalin-fixed paraffin-embedded (FFPE) tissues derived from a healthy cat. The feline FFPE tissues had been previously archived in our laboratory from an unrelated study.

Heat-induced epitope retrieval (HIER) was performed using citrate buffer (Dako, Carpinteria, CA, USA) before incubation with the primary rabbit polyclonal anti-ACE2 antibody (Abcam) and human monoclonal anti-DC-SIGN antibody (NIH AIDS Reagent Program; 9' E9A8). Immunoreactivity was visualized using the NovaRED Substrate Kit that utilizes horseradish peroxidase (Vector). Slides were assessed by visual inspection performed by a board-certified veterinary pathologist (S. Cook). The antibodies utilized were chosen due to previous use in feline cells or formalin-fixed tissue, and appropriate expression was confirmed using positive control tissues (feline kidney for ACE2 and lymph node for DC-SIGN (dendritic cells)) [34,39]. The ACE2 antibody had been previously published for use in cats and ferrets [40]. The DC-SIGN antibody had been previously published for use in vitro in feline cell lines (CRFK) [34]. A complete set of feline tissues was reviewed, and immunohistochemical staining was recorded for tissue type, cell type expressing the protein, and subcellular localization of immunoreactivity and graded on a semi-quantitative scale of 0 to 3 for intensity of staining. A grade of 0 indicates a complete lack of staining; 3 indicates intense dark staining. Subcellular localization of immunoreactivity was characterized as membranous, cytoplasmic, or both; there was no nuclear immunoreactivity identified. Membranous refers to immunoreactivity primarily localized to the cell membrane while cytoplasmic refers to signals limited to the cytoplasm of the cell. In some cases, immunoreactivity was both membranous and cytoplasmic.

#### 2.7. Gene Expression Profiles of FCWF-4 ATCC and FCWF-4 CU Cell Lines Using RNAseq

Three individual cell cultures representing different passage numbers of both FCWF-4 ATCC and FCWF-4 CU cells were individually processed for total cell-associated RNA using the PureLink RNA mini kit (Invitrogen) and eluted into 50  $\mu$ L of molecular grade water (Invitrogen). Quality and quantity of the RNA were determined using NanoDrop (ThermoScientific, Waltham, MA, USA), and approximately 10  $\mu$ g of RNA from each culture was subsequently treated with DNase (TURBO DNase; Invitrogen), following the manufacturer's protocol. The six total cell-associated RNA samples (3 for each cell line) were stored at  $-80^{\circ}\text{C}$  until the time of submission for 3' Tag-Seq RNA sequencing (RNAseq) at the UC Davis Genome Center as a single batch.

#### 2.8. RNAseq

Barcoded 3' Tag-Seq libraries were prepared using the QuantSeq FWD kit (Lexogen, Vienna, Austria) for multiplexed sequencing according to the recommendations of the manufacturer. The fragment size distribution of the libraries was verified via micro-capillary gel electrophoresis on a Bioanalyzer 2100 (Agilent, Santa Clara, CA, USA). The libraries were quantified by fluorometry on a Qubit instrument (LifeTechnologies, Carlsbad, CA, USA) and pooled in equimolar ratios. Ninety-three libraries were sequenced on one lane of a NextSeq500 sequencer (Illumina, San Diego, CA, USA) with single-end 85 bp reads. The sequencing generated more than 4 million reads per library.

HTStream [41] was used to clean raw sequencing reads, removing PhiX sequences, Illumina adapters, poly AT sequences, low-quality regions (average quality less than 20), and reads below 50 base pairs in length. Unique molecular identifiers (UMIs) were also processed using a custom python script and UMI tools to remove PCR duplicates [42]. The remaining reads were then mapped to the *Felis catus* genome (Felis\_catus\_9.0) using STAR [43], and a counts table was generated using featureCounts [44] and the corresponding Ensembl (version 106) genome annotation. Differential expression analysis was then conducted in R (The R Project for Statistical Computing) [45] with the limma voom pipeline [46,47], which consists of normalization and statistical testing, followed by multiple testing corrections via the Benjamini-Hochberg procedure [48]. Pathway enrichment analysis was also performed, identifying enriched Gene Ontology (GO) terms in topGO [49] (v2.48.0) with the Kolmogorov-Smirnov test [50] and enriched KEGG pathways using the Wilcoxon rank-sum test in KEGGREST (v1.36.0) [51,52]. Heatmaps were prepared from the data matrices of all transcripts and of the differentially expressed genes in R.

### 3. Results

#### 3.1. Comparison of Serotype I and II Titers Produced in Each Cell Line

In order to characterize the viral replication of Black I and WSU 79-1146 among the different cell types, biological plaquing assays were performed in 96-well tissue culture plates (Figure 1). Black I replicated to maximal titers in FCWF-4 CU cells ( $5 \times 10^{6.4}$  TCID<sub>50</sub>/mL) and less efficiently in CRFK cells ( $5 \times 10^{5.2}$  TCID<sub>50</sub>/mL) and demonstrated limited replication in FCWF-4 ATCC cells ( $5 \times 10^{2.1}$ ).

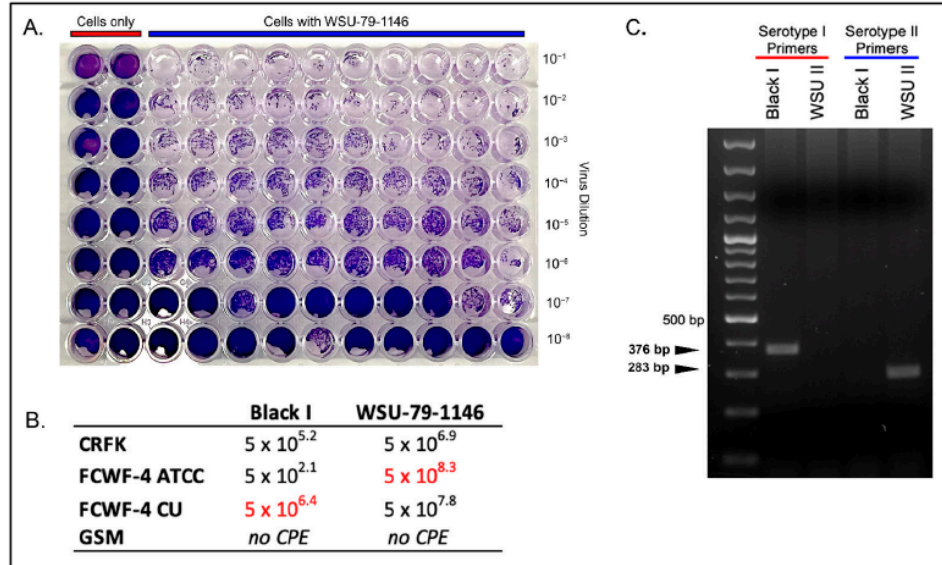


**Figure 1.** TCID<sub>50</sub> results for Black I and WSU-79-1146 in feline cell lines. (A) Representative example of a TCID<sub>50</sub> plate for WSU-79-1146 grown in CRFK cells. Wells are stained with crystal violet stain to evaluate the presence of cytopathic effect (plaque clearing) across serial dilutions of the virus. (B) Summary table of TCID<sub>50</sub> values (TCID<sub>50</sub>/mL) for Black I and WSU-79-1146 grown in four feline cell lines. Numbers highlighted in red represent the maximal TCID<sub>50</sub> achieved for each viral serotype. (C) Agarose gel electrophoresis image confirming the serotype of the two viral stocks. The nested serotyping primers are listed in Table 1 (FCoV I S For, FCoV II S For, and FCoV I and II S Rev; nested primers are nFCoV I S For, nFCoV II S For, and nFCoV I and II S Rev). The nested primer set was not necessary as PCR amplicons were evident using the initial primer set alone. The expected amplicon size for serotypes I and II is 376 and 283 bp, respectively.

Interestingly, WSU 79-1146 replicated most efficiently in FCWF-4 ATCC cells ( $5 \times 10^{8.3}$  TCID<sub>50</sub>/mL), although relatively high viral titers were recovered from CRFK cells ( $5 \times 10^{6.9}$  TCID<sub>50</sub>/mL) and FCWF-4 CU cells ( $5 \times 10^{7.8}$  TCID<sub>50</sub>/mL). These results suggest that CRFK cells may not be the optimal cell line for in vitro propagation of WSU 79-1146 FIPV. Neither virus displayed any evidence of cytopathic effect (plaques) in the non-permissive caprine GSM cell line, consistent with a lack of viral replication (negative control cells).

To genetically confirm the viral serotype, the two viral stocks were “serotyped” using standard PCR targeting spike and the FCoV I S For and Rev primers (listed in Table 2). These PCR reactions yielded the appropriate amplicon sizes of 376 bp (serotype I FIPV) and 283 bp (serotype II FIPV, Figure 1C).

Due to challenges in producing a tightly confluent monolayer of primary feMDMs in tissue culture wells, a comparison of viral replication between Black I and WSU 79-1146 in feMDMs was obtained by quantifying cell-associated viral RNA normalized to *GAPDH* expression. We found that WSU 79-1146 (FIPV II) replicated more efficiently (showed higher copy numbers) than Black I in feMDMs by a factor of almost two logs ( $p = 0.0094$ , *t*-test; Figure 2A).

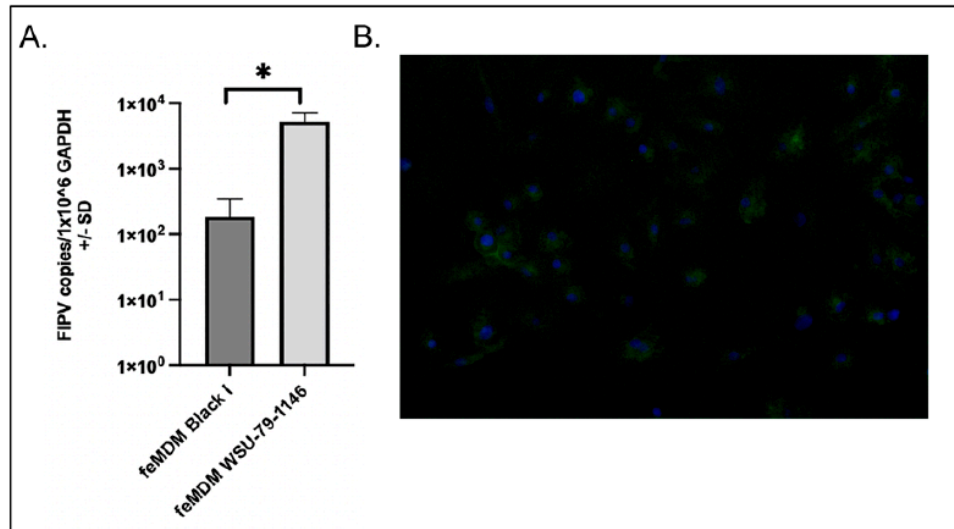


**Figure 2.** feMDM viral growth patterns and CD14 immunofluorescence. (A) Replication of serotype I and II FIPV in feMDM cells was quantified using RT-qPCR and was normalized to the expression of the housekeeping gene, *GAPDH*. Serotype II FIPV (WSU 79-1146) replicated more efficiently than serotype I FIPV (Black I) in feMDM cells (\* indicates significance between groups,  $p = 0.0094$ , Student's *t*-test). (B) Immunofluorescence of CD14 to confirm macrophage differentiation from feline monocytes (green fluorescence). Blue staining represents DAPI staining for cell nuclei. Green fluorescence (FITC) represents membranous CD14 staining.

Positive immunofluorescence with macrophage marker CD14 confirmed a macrophage-type phenotype of the infected feMDM cells (green fluorescence, Figure 2B). As FCWF-4 cells have been described as “macrophage-like”, we also investigated the expression of CD14 in these two cell lines (FCWF-4 CU and FCWF-4 ATCC) and in CRFK cells, which are not expected to demonstrate CD14 expression. As expected, membranous CD14 expression was identified in both of the FCWF-4 cell lines but was not identified in CRFK cells (Figure 3).

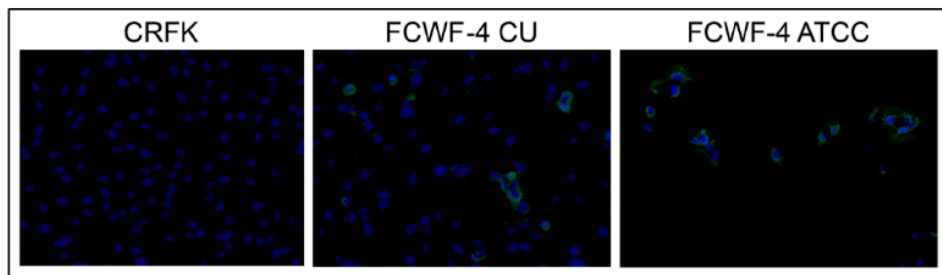


**Figure 3.** Comparison of cellular CD14 expression via immunofluorescence. CRFK cells demonstrate a lack of CD14 expression, and the two FCWF-4 cell line images have variable membranous expression by FCWF-4 cells (green fluorescence). Blue staining represents DAPI staining for cell nuclei. Green fluorescence represents FITC membranous CD14 staining.

### 3.2. Cellular Expression of Known Coronavirus Receptors

Targeted gene expression patterns of known coronavirus receptors in feline cells variably permissive to FIPV replication were determined and normalized to *GAPDH* expression using RT-qPCR. Feline cells known to efficiently propagate FIPV II include CRFK, FCWF-4 ATCC, FCWF-4 CU, and feline monocyte-derived macrophages [22,53]. We found that gene expression of feAPN was greatest in CRFK cells; however, feAPN expression was pronounced in all four of the examined cell types (Figure 4). Since feAPN serves as the

primary cellular receptor for FIPV II, these results are consistent with Figures 1B and 2A (demonstrating efficient replication of FIPV II in all four of these feline cell types).

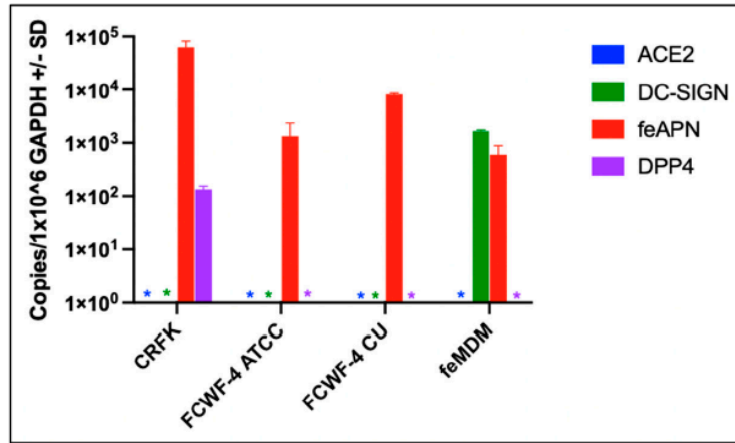


Figure 4. Expression profiles of known coronavirus receptor genes among cell lines permissive to either FIPV I or II tissue-culture-adapted strains, Black I and WSU-79-1146, respectively. Colored asterisks (\*) represent undetected gene expression.

DC-SIGN expression, the receptor previously demonstrated to serve as an optional co-receptor for FIPV II, was not detected in CRFK cells, consistent with the concept that DC-SIGN is not required for FIPV II cell entry [54]. However, DC-SIGN expression was identified in feMDMs (macrophages serving as host cells for FIPV in vivo). Interestingly, ACE2 expression, which has been suggested as a potential FIPV I receptor [55], was not identified in feMDMs or in either of the FCWF-4 cell lines, yet all three of these cell types are permissive to FIPV I replication (Figures 1 and 2). These results suggest that ACE2 does not serve as the primary cellular receptor for FIPV I. DPP4 expression was identified only in CRFK cells and at low levels. If DPP4 served as a primary FIPV I receptor, its expression would be expected in feMDMs and FCWF-4 CU and FCWF-4 ATCC cells.

### 3.3. Feline Tissues and Cellular Distribution of ACE2 and DC-SIGN Proteins via IHC

The systemic distribution of DC-SIGN and ACE2 proteins in feline tissues was determined using immunohistochemistry. In this study, we found no evidence that ACE2 functions as a primary receptor for either FIPV I or II. However, given the interest in ACE2, the primary receptor of SARS-CoV-2, and the role of DC-SIGN as a co-receptor for FIPV II, we chose to characterize the distribution patterns of these proteins in normal feline tissues.

We found that ACE2 was more widely expressed than DC-SIGN in normal feline tissues and cells. ACE2 protein expression was most pronounced in thyroid follicular cells, epithelial cells (particularly tongue, airway, kidney, and small and large intestines), and scattered cells in the intestinal lamina propria. In contrast, DC-SIGN expression (presumably labeling histiocytes based on cell location and morphology) was most pronounced in individualized, scattered cells within the lymph node paracortex, to a lesser extent within the subcapsular sinuses and splenic red pulp, as well as in the intestinal lamina propria (Table 3, Figure 5). The cell labeling with DC-SIGN is presumably labeling histiocytes (dendritic cells and macrophages) based on the location of these cells as well as cell morphology. Dendritic cells are found in tissues involved with immune surveillance and locations in contact with the outside environment, which include lymphoid tissue and the intestinal tract, as we have demonstrated immunohistochemically [56]. Individual cells with ACE2 expression in the lymph node are mostly located within germinal centers, with rare individual cells expressing ACE2 within the paracortex or subcapsular sinuses. ACE2 expression by cells within germinal centers is morphologically consistent with macrophages (Figure 5A). ACE2

expression by macrophages within the spleen and lymph nodes has also been reported in humans [57].

Table 3. List of tissue- and cell-specific immunoreactivity for ACE2 and DC-SIGN in normal feline tissues.

Tissue	Cell	ACE2	DC-SIGN
Cerebrum	Neurons	0	0
	Glial cells	+0-2 (C)	0
Cerebellum	Purkinje cells	0	0
	Granular cells	0	0
Choroid Plexus	Ependymal cells	+1 (C)	0
Meninges	Fibroblasts	+1 (C)	0
Eye	Ganglion cells	+2 (C)	0
	Nuclear layer of retina	+0-1 (C)	0
	Fibroblasts	+2 (C)	0
	Pigmented epithelium	U	U
	Melanocytes	U	U
	Corneal epithelium	+0-1 (C)	0
	Keratocytes	0	0
	Ciliary body epithelium	+0-1 (C)	0
	Lens epithelium	+1 (C)	0
	Optic nerve	Glial cells	+2 (C)
Thyroid	Follicular cells	+2-3 (C)	+2 (C)
	Parafollicular cells	+1 (C)	+0-1 (C)
Parathyroid	Chief and oxyphil cells	0	0
Adrenal gland	Cortex	+0-2 (C)	+1 (C; reticularis)
	Medulla	+1 (C)	0
Lymph node	Paracortex and follicles (scattered cells)	+2 (C)	+3 (C, M)
Adipose tissue	Adipocyte	+2 (C)	+1 (C)
Skeletal muscle	Myocyte	+1 (C)	0
Smooth muscle	Myocyte	+0-1 (C)	0
Tongue	Epithelium	+2-3 (C, M)	0
Esophagus	Epithelium	+2 (M)	0
Trachea	Airway epithelium	+2 (C)	0
	Submucosal gland epithelium	+2 (C)	0
	Bronchial/bronchiolar epithelium	+2-3 (C)	+1-2 (C)
	Type I pneumocyte	+1-2 (U)	+1-2 (U)
Lung	Type II pneumocyte	+2 (C)	+1 (C)
	Submucosal gland epithelium	+1-2 (C)	0
	Myocyte	+0-1 (C)	+0-1 (C)
Heart	Endothelium	+1-2 (C)	0
Vessels	Mural smooth muscle	+2 (C)	0
	Hepatocyte	+1 (C)	0
Liver	Biliary epithelium	0	0
	Cortical tubular epithelium	+3 (M, apical); +1 (C)	0
Kidney	Medullary tubular epithelium	+1 (C)	0
	Red pulp, scattered cells	+1-2 (C)	+2-3 (C)
Spleen	White pulp (rare)	0	+1 (C)
	Acinar cells	+0-1 (C)	0
Pancreas	Islet cells	0	0
	Mucosal epithelium	+2 (C)	0
Stomach	Mucosal epithelium, apical	+3 (M); +1 (C)	0
Small Intestine	Mucosal epithelium, apical	+3 (M); +1 (C)	0
Ileum	Mucosal epithelium	+3 (C)	0
Colon	Mucosal epithelium	+3 (C)	0
Intestine as a whole	Lamina propria, scattered cells	+3 (C)	+3 (C)

0 = absent to nonspecific, +1 = weak, +2 = moderate, +3 = strong, C = cytoplasmic, M = membranous, U = undetermined.

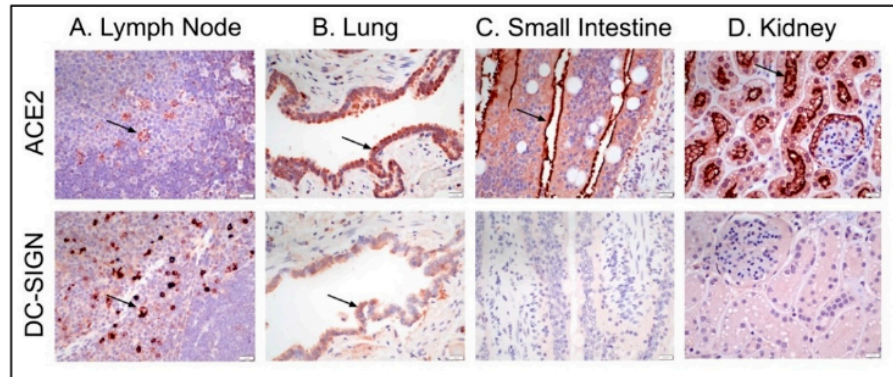


**Figure 5.** ACE2 and DC-SIGN immunohistochemistry panel of representative tissues. Brown immunostaining represents antigen detection of either ACE2 or DC-SIGN (arrows denote examples of antigen detection). (A) Scattered cells with antigen detection for ACE2 in lymphoid follicle germinal centers and paracortex for DC-SIGN. (B) Bronchiolar epithelial antigen detection for ACE2 and weaker signal detected for DC-SIGN. (C) Small intestinal villous epithelial antigen detection for ACE2, particularly along the apical aspect of epithelial cells and absent antigen detection for DC-SIGN. (D) Strong antigen detection for ACE2 within renal cortex tubular epithelium for ACE2 and absent antigen detection for DC-SIGN.

### 3.4. RNAseq Gene Expression Profiles of FCWF-4 ATCC and FCWF-4 CU Cell Lines

RNAseq analyses were performed to determine the global transcriptome of FCWF-4 ATCC and FCWF-4 CU cells. Differentially expressed (DE) genes and the magnitudinal differences in gene expression between these two closely related cell lines were determined. As Black I (FIPV I) replicates with different efficiencies in these two cell lines, we reasoned that identifying DE genes would provide insight into cell factors critical for viral replication (e.g., cell receptors, other cellular factors).

In this transcriptome dataset, the expression of 10,036 feline genes was identified, with 458 significantly DE genes (Figure 6). Visual assessment (cluster analysis heatmap) of the overall differential gene expression covering all detected gene transcripts is depicted in Figure 6A. In Figure 6B, the 458 DE genes are depicted. Minor transcriptional variability was identified between cell passage replicates within each cell line.

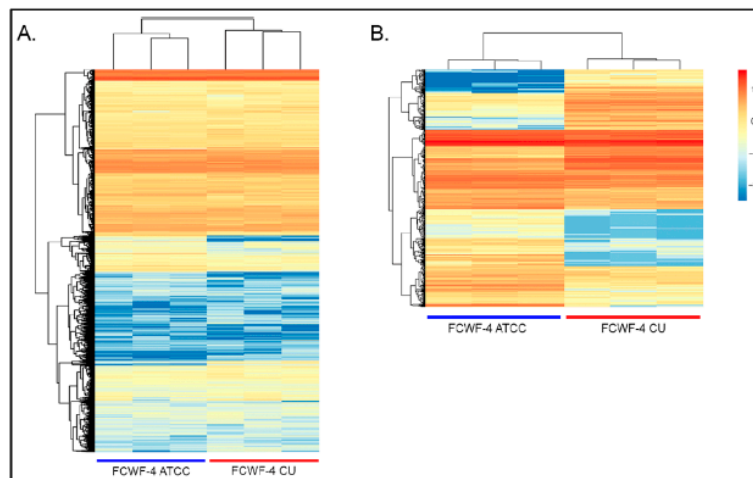


**Figure 6.** Cluster analysis of differential gene expression. (A) Heatmap of 10,036 genes depicting differential gene expression between FCWF-4 ATCC (blue bar) and FCWF-4 CU (red bar) transcriptomes. (B) Heatmap of 458 significantly differentially expressed genes between FCWF-4 and FCWF-4 CU cell lines. Each column represents a different cell passage. Both column and row clustering were applied.

In alignment with the targeted RT-qPCR findings, FCWF-4 CU and FCWF-4 ATCC cell lines both expressed feAPN mRNA, with FCWF-4 CU cells exhibiting a slightly higher transcription level for this receptor transcript, although not significantly greater than FCWF-4 ATCC cells (Figure 7A). Expression of the other three investigated coronavirus receptor transcripts (ACE2, DPP4, and DC-SIGN) was not detected in either cell line, in agreement with the result of the targeted RT-qPCR gene expression (Figure 4).

A detailed evaluation of the 458 significantly DE genes identified six genes of interest that might plausibly be associated with coronavirus cell entry and/or replication (Figure 7B). The expression of these six genes was significantly higher in FCWF-4 CU cells relative to FCWF-4 ATCC cells (Figure 7B–D).

Two of these genes of interest identified in FCWF-4 CU cells are *CTSS* and *CTSC*, cathepsins S and C, respectively. Cathepsins are cysteine proteases involved in the endosomal route of coronaviral cell entry via spike cleavage [58–61]. Two serine proteases were also identified. The first, *TMPRSS7*, or transmembrane serine protease 7, is part of a group of *TMPRSS* proteins associated with early coronavirus cell entry [62]. The other serine protease is *RHBDL2* (the rhomboid-like 2 serine endopeptidase). Although this serine protease is not known to be associated with coronavirus cell entry, some coronaviruses have been shown to utilize serine proteases for cell entry, making this serine protease worthy of further investigation [60,63,64].

The final two significantly upregulated genes possibly associated with coronavirus cell entry or pathogenesis are *EFNB2* and *EFNA1*, ephrin B2 and ephrin A1, respectively. These transcripts are of interest based on the fact that their encoded proteins can serve as entry receptors for a variety of viruses, including Hendra, Nipah, hepatitis C, and Epstein–Barr viruses [65–68]. These gene products have also been shown to serve as an alternative co-receptor for viral entry by SARS-CoV-2, SARS-CoV-1, and Middle Eastern respiratory syndrome (MERS)-CoV [69,70].

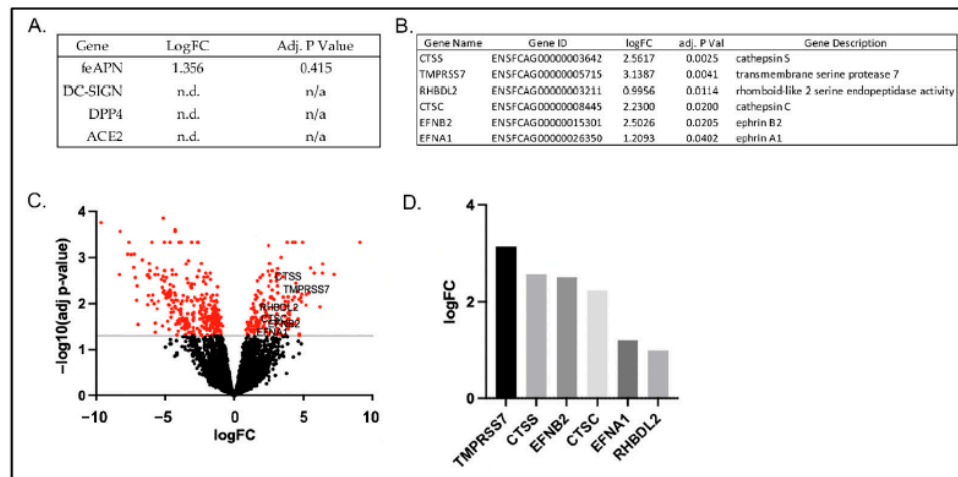


Figure 7. Genes of particular interest associated with coronavirus cell entry and/or pathogenesis. (A) Expression of known coronavirus cellular receptors detected or not detected in FCWF-4 CU and FCWF-4 ATCC cell lines. LogFC represents the log fold change of FCWF-4 CU gene expression relative to FCWF-4 ATCC gene expression. feAPN expression was detected in both FCWF-4 cell lines. (B) Six genes of interest to potentially explain differential FIPV serotype I replication. (C) Volcano plot of whole-transcriptome differentially expressed genes. The transcripts highlighted in red are significantly up- or down-regulated genes in FCWF-4 CU cells relative to FCWF-4 ATCC cells. Genes in (B) are specifically identified. (D) Bar graph depicting log fold change ( $\log_{10}(\text{FC})$ ) of select genes in FCWF-4 CU cells relative to FCWF-4 ATCC cells.

#### 4. Discussion

In this study, we investigated the relative replication efficiencies of culture-adapted FIPVs I and II (Black I and WSU-79-1146) and the expression patterns of a selection of known coronaviral receptors in variably permissive feline cells. We found that feAPN, the FIPV II cellular receptor, is abundantly expressed in all four of the evaluated cell types, with CRFK cells demonstrating the highest level of expression. Although all of the evaluated cell types expressed feAPN, expression in feMDMs and both FCWF-4 cell types was approximately one to two logs less than in CRFK cells. We also found that all four of the examined cell types are permissive to FIPV II replication, consistent with the concept that feAPN serves as the FIPV II receptor. Prior studies have shown that although the receptor DC-SIGN is not required, it can serve as an optional co-receptor by enhancing FIPV II cell entry [34,70]. We only identified DC-SIGN expression in feMDMs, a cell type closely related to the natural host cell of FIPV *in vivo*. Our RNAseq data corroborates these gene expression findings in the two FCWF cell lines, with no transcripts detected for ACE2, DC-SIGN, and DPP4 and a slightly higher expression level of feAPN in FCWF-4 CU cells relative to FCWF-4 ATCC cells (although not significantly different).

DPP4, a type II transmembrane ectopeptidase, serves as the receptor for the zoonotic Middle Eastern respiratory syndrome coronavirus (MERS-CoV) [71]. Here, we detected DPP4 expression only in CRFK cells and, therefore, found no evidence to support DPP4 serving as a primary cellular receptor for FIPV I. ACE2, the cellular receptor for multiple coronaviruses, including HCoV-NL63, SARS-CoV-1, and SARS-CoV-2, is well documented in tissue and cellular distribution in humans and has been shown to be expressed in specific subpopulations of human macrophages [72–76]. Since FIPV infects macrophages *in vivo* and shares some pathogenic features similar to SARS-CoV-2, we reasoned that ACE2 expression should be examined in permissive feline cells and tissues. To our knowledge, there is an absence of peer-reviewed literature focused on ACE2 as a potential receptor for FIPV I. Using IHC, ACE2 expression was detected in a broad range of feline tissues and cell types, with the strongest staining intensity identified within a number of epithelial cells, including respiratory and intestinal epithelium. Interestingly, we detected ACE2 expression within the bronchiolar epithelium, while another recent study reported absent antigen detection for ACE2 within domestic cat bronchiolar epithelium [77]. Here, we further document a more extensive detailed list at both the tissue and cellular levels for ACE2 expression in cats, while previous studies have focused more on the evaluation of intestinal, kidney, and respiratory tissues [40,77,78]. ACE2 expression was also detected in scattered, individualized round cells in lymphoid tissues (lymph node and spleen specifically) within germinal centers and the paracortex and to a much less degree relative to DC-SIGN.

We found that Black I replicated most efficiently in FCWF-4 CU and CRFK cells; however, we did not identify ACE2 gene expression via RT-qPCR in any of the evaluated cell lines (or in the RNAseq data). Although, taken together, these results suggest that ACE2 does not serve as the primary cellular receptor for FIPV I, ACE2's function as a co-receptor cannot be ruled out. It is worth noting that although we found CRFK cells to be permissive to Black I replication, there are experimental inconsistencies with regard to FIPV I replication in CRFK cells. Black (1980) initially reported CRFK permissibility to FIPV I (Black I), while Hohdatsu et al. (1998) were unable to infect CRFK cells with multiple strains of FIPV I (KU-2, Black I, UCD-1). Another study by Van Hamme et al. (2007) documented the inefficient attachment and internalization of Black I in CRFK cells [79]. A definitive explanation for these experimental differences is not available; however, it is possible these variable results relate to genetic changes in either the CRFK cell line or the Black I virus through prolonged subpassaging [19,21,79].

Expression of DC-SIGN, the co-receptor for FIPV II, was also examined using immunohistochemistry in feline tissues. It has been previously shown that antibody-mediated blockade of DC-SIGN greatly reduces FIPV I binding to feline blood monocytes [54]. In our *in vitro* experiments, we detected DC-SIGN expression only in feMDMs. Although these results suggest that DC-SIGN does not function as the primary receptor of FIPV I, a

co-receptor function cannot be excluded. IHC-determined DC-SIGN expression in feline tissues was more limited than ACE2 expression and was predominantly associated with scattered individual round cells in lymphoid tissues, presumed macrophages, and dendritic cells, as discussed within the results. This is consistent with the expectation of histiocytic (dendritic cell and macrophage) expression of DC-SIGN [80].

The markedly different replication kinetics of Black I in the FCWF-4 ATCC and FCWF-4 CU cell lines (a 4-log difference) is interesting, considering that these cell lines are closely related (FCWF-4 CU is passage-derived from FCWF-4 ATCC). We reasoned that the (presumed) genetic similarities of these two feline cell lines and markedly differential viral growth kinetics might facilitate critical insights into FIPV serotype I replication. This was the impetus for pursuing global transcriptome analyses (RNAseq) of the two related cell lines. RNAseq data highlighted the overall similarities in gene expression patterns between the two cell lines, as expected, given their relatedness. RNAseq also identified 458 significantly DE genes. From this subgroup of genes, we identified six genes of particular interest to coronavirus biology.

Four of the six DE genes encode cellular proteases: two are cysteine proteases, cathepsins S (*CTSS*) and C (*CTSC*), and two are transmembrane serine proteases, transmembrane serine protease 7 (*TMPRSS7*) and rhomboid-like 2 serine endopeptidase (*RHBDL2*). Specific viral and host proteases are known to be essential for coronavirus replication and are involved in different steps of the virus life cycle, including cell entry, replication of the virus, protein maturation, and virion assembly [81]. *TMPRSS7* is a member of a larger family of transmembrane serine proteases, one of which (e.g., *TMPRSS2*) is the dominant protease responsible for the proteolytic cleavage of SARS-CoV-2 at the cell surface, thereby triggering fusion of the viral lipid membrane with the host cell membrane [62]. Other transmembrane proteases associated with enhanced entry of SARS-CoV-2 include *TMPRSS11D* and *TMPRSS13* [82]. Although *TMPRSS7* has not been previously identified as a protease associated with coronavirus entry, its identification here warrants further investigation. To the authors' knowledge, *RHBDL2* has not been previously linked with viral cell entry or viral activation, but the DE of this protease in FCWF-4 CU cells warrants further investigation.

The two identified cysteine proteases are lysosomal peptidases (cathepsins), which are the main class of lysosomal peptidases [83]. Cathepsins are involved in virion entry and viral processing after endosomal uptake for a range of viruses, including reoviruses, Ebola virus, and coronaviruses, with cathepsin L being most commonly associated with the activation of coronaviral glycoproteins [84–86]. Of the two cathepsins identified in this research, cathepsin S has been associated with cleavage of the capsid protein during cellular entry in some strains of reovirus [87]. To the authors' knowledge, cathepsin C has not been linked with viral entry or replication for any specific viruses to date; however, the widespread roles of cathepsins with other viruses make the upregulation of this gene in FCWF-4 CU cells notable and worthy of further investigation.

The remaining two DE genes of interest are ephrin B2 and ephrin A1. Ephrins (erythropoietin-producing hepatocellular carcinoma) are the largest family of receptor tyrosine kinases known amongst mammals [88]. Members of the ephrin and ephrin receptor binding pathways have been identified as receptors for multiple RNA and DNA viruses, including paramyxoviruses, flaviviruses, herpesviruses, and retroviruses [67]. Examples include Hendra and Nipah viruses (*Paramyxoviridae*), which utilize ephrin B2 and B3 as viral entry receptors [65,89], as well as the hepatitis C virus, which utilizes ephrin receptor A2 as a co-factor for cell entry [90]. Although ephrin usage by coronaviruses has not been previously reported in the peer-reviewed literature, a recent abstract reported an upregulation of ephrin A1 and B2 in the saliva of COVID-19 patients. The significance of this finding is presently unknown but is being explored as a biomarker for disease severity in COVID-19 patients [91].

Despite decades of study, multiple gaps in our collective understanding of FCoV biology and pathogenesis remain, particularly with regard to FIPV I, the predominant

coronavirus in naturally occurring cases of FIP. A definitive determination of the FIPV I receptor, along with the phenotype of the viral host cell in cats, would likely facilitate the development of targeted treatments and shed mechanistic light on the varied clinical presentations of FIP. Recent success in propagating FIPV I (Black I) in FCWF-4 CU cells provides a tool to explore these questions. The six candidate genes identified in this research should be systematically evaluated for their biological relevance through targeted gene disruption, genetic transduction of non-permissive cell lines, antibody blockade, and pharmacologic inhibition of protease function. The data presented here provide a platform for further exploration of a small group of candidate receptors and proteases.

**Author Contributions:** Conceptualization, S.C. and B.M.; methodology, S.C., D.C., C.H. and S.W.; validation, S.C. and D.C.; investigation, S.C., B.M., S.W. and C.H.; formal analysis, S.C. and B.M.; writing—original draft preparation, S.C. and B.M.; writing—review and editing, S.C., B.M., D.C., S.W. and C.H.; funding acquisition, S.C. and B.M. All authors have read and agreed to the published version of the manuscript.

**Funding:** This research was sponsored by the EveryCat Health Foundation (grant W21-007, 2021–2022), the University of California Davis Peter C. Kennedy Endowed Fellowship, and the University of California Center for Companion Animal Health, School of Veterinary Medicine, University of California, Davis (2020-89-FM).

**Institutional Review Board Statement:** Not applicable.

**Informed Consent Statement:** Not applicable.

**Data Availability Statement:** The raw data supporting the conclusions of this article can be made available by the authors without undue reservation.

**Acknowledgments:** We would like to acknowledge and thank the NIH AIDS Reagent Program, the UC Davis School of Veterinary Medicine Histology Laboratory, and Susan Baker's lab at Loyola University, Chicago. The library preparation and sequencing were carried out at the DNA Technologies and Expression Analysis Core at the UC Davis Genome Center, supported by NIH Shared Instrumentation Grant 1S10OD010786-01.

**Conflicts of Interest:** The authors declare no conflict of interest.

## References

1. Pedersen, N.C.; Liu, H.; Dodd, K.A.; Pesavento, P.A. Significance of coronavirus mutants in feces and diseased tissues of cats suffering from feline infectious peritonitis. *Viruses* **2009**, *1*, 166–184. [CrossRef] [PubMed]
2. Vennema, H.; Poland, A.; Foley, J.; Pedersen, N.C. Feline infectious peritonitis viruses arise by mutation from endemic feline enteric coronaviruses. *Virology* **1998**, *243*, 150–157. [CrossRef] [PubMed]
3. Wolfe, L.G.; Griesemer, R.A. Feline infectious peritonitis. *Vet. Pathol.* **1966**, *3*, 255–270. [CrossRef] [PubMed]
4. Montali, R.J.; Strandberg, J.D. Extraperitoneal lesions in feline infectious peritonitis. *Vet. Pathol.* **1972**, *9*, 109–121. [CrossRef] [PubMed]
5. Kipar, A.; May, H.; Menger, S.; Weber, M.; Leukert, W.; Reinacher, M. Morphologic features and development of granulomatous vasculitis in feline infectious peritonitis. *Vet. Pathol.* **2005**, *42*, 321–330. [CrossRef] [PubMed]
6. King, A.; Adams, M.; Carstens, E.; Lefkowitz, E. Nidovirales. *Virus Taxon.* **2012**, 784–794. Available online: <https://www.sciencedirect.com/science/article/pii/B9780123846846000665> (accessed on 29 May 2022).
7. Fiscus, S.A.; Teramoto, Y.A. Antigenic comparison of feline coronavirus isolates: Evidence for markedly different peplomer glycoproteins. *J. Virol.* **1987**, *61*, 2607–2613. [CrossRef] [PubMed]
8. Rottier, P.J.M.; Nakamura, K.; Schellen, P.; Volders, H.; Haijema, B.J. Acquisition of macrophage tropism during the pathogenesis of feline infectious peritonitis is determined by mutations in the feline coronavirus spike protein. *J. Virol.* **2005**, *79*, 14122–14130. [CrossRef]
9. Haijema, B.J.; Volders, H.; Rottier, P.J.M. Switching species tropism: An effective way to manipulate the feline coronavirus genome. *J. Virol.* **2003**, *77*, 4528–4538. [CrossRef] [PubMed]
10. Terada, Y.; Matsui, N.; Noguchi, K.; Kuwata, R.; Shimoda, H.; Soma, T.; Mochizuki, M.; Maeda, K. Emergence of pathogenic coronaviruses in cats by homologous recombination between feline and canine coronaviruses. *PLoS ONE* **2014**, *9*, e106534. [CrossRef]
11. Herrewegh, A.A.P.M.; Smeenk, I.; Horzinek, M.C.; Rottier, P.J.M.; de Groot, R.J. Feline Coronavirus Type II Strains 79-1683 and 79-1146 originate from a double recombination between feline coronavirus type I and canine coronavirus. *J. Virol.* **1998**, *72*, 4508–4514. [CrossRef] [PubMed]

12. Jaimes, J.A.; Millet, J.K.; Stout, A.E.; André, N.M.; Whittaker, G.R. A tale of two viruses: The distinct spike glycoproteins of feline coronaviruses. *Viruses* **2020**, *12*, 83. [CrossRef] [PubMed]
13. Li, C.; Liu, Q.; Kong, F.; Guo, D.; Zhai, J.; Su, M.; Sun, D. Circulation and genetic diversity of Feline coronavirus type I and II from clinically healthy and FIP-suspected cats in China. *Transbound. Emerg. Dis.* **2019**, *66*, 763–775. [CrossRef] [PubMed]
14. Kummrow, M.; Meli, M.L.; Haessig, M.; Goenczi, E.; Poland, A.; Pedersen, N.C.; Hofmann-Lehmann, R.; Lutz, H. Feline coronavirus serotypes 1 and 2: Seroprevalence and association with disease in Switzerland. *Clin. Diagn. Lab. Immunol.* **2005**, *12*, 1209–1215. [CrossRef] [PubMed]
15. Benetka, V.; Kübber-Heiss, A.; Kolodziejek, J.; Nowotny, N.; Hofmann-Parisot, M.; Möstl, K. Prevalence of feline coronavirus types I and II in cats with histopathologically verified feline infectious peritonitis. *Vet. Microbiol.* **2004**, *99*, 31–42. [CrossRef] [PubMed]
16. Tresnan, D.B.; Levis, R.; Holmes, K.V. Feline aminopeptidase N serves as a receptor for feline, canine, porcine, and human coronaviruses in serogroup I. *J. Virol.* **1996**, *70*, 8669–8674. [CrossRef]
17. Cham, T.-C.; Chang, Y.-C.; Tsai, P.-S.; Wu, C.-H.; Chen, H.-W.; Jeng, C.-R.; Pang, V.F.; Chang, H.-W. Determination of the cell tropism of serotype 1 feline infectious peritonitis virus using the spike affinity histochemistry in paraffin-embedded tissues. *Microbiol. Immunol.* **2017**, *61*, 318–327. [CrossRef] [PubMed]
18. Dye, C.; Temperton, N.; Siddell, S.G. Type I feline coronavirus spike glycoprotein fails to recognize aminopeptidase N as a functional receptor on feline cell lines. *J. Gen. Virol.* **2007**, *88*, 1753–1760. [CrossRef]
19. Hohdatsu, T.; Izumiya, Y.; Yokoyama, Y.; Kida, K.; Koyama, H. Differences in virus receptor for type I and type II feline infectious peritonitis virus. *Arch. Virol.* **1998**, *143*, 839–850. [CrossRef]
20. Pedersen, N.C.; Black, J.W.; Boyle, J.F.; Evermann, J.F.; McKeirnan, A.J.; Ott, R.L. Pathogenic differences between various feline coronavirus isolates. In *Molecular Biology and Pathogenesis of Coronaviruses*; Springer Science & Business Media: Berlin/Heidelberg, Germany, 1984; pp. 365–380.
21. Black, J. Recovery and in vitro cultivation of a coronavirus from laboratory-induced cases of feline infectious peritonitis (FIP). *Vet. Med. Small Anim. Clin.* **1980**, *75*, 811–814. [PubMed]
22. O'Brien, A.; Mettelman, R.C.; Volk, A.; André, N.M.; Whittaker, G.R.; Baker, S.C. Characterizing replication kinetics and plaque production of type I feline infectious peritonitis virus in three feline cell lines. *Virology* **2018**, *525*, 1–9. [CrossRef]
23. Regan, A.D.; Millet, J.K.; Tse, L.V.; Chillag, Z.; Rinaldi, V.; Licitra, B.N.; Dubovi, E.J.; Town, C.D.; Whittaker, G.R. Characterization of a recombinant canine coronavirus with a distinct receptor-binding (S1) domain. *Virology* **2012**, *430*, 90–99. [CrossRef] [PubMed]
24. Regan, A.D.; Ousterout, D.G.; Whittaker, G.R. Feline lectin activity is critical for the cellular entry of feline infectious peritonitis virus. *J. Virol.* **2010**, *84*, 7917–7921. [CrossRef]
25. Hay, R.J.; Williams, C.D.; Macy, M.L.; Lavappa, K.S. Cultured cell lines for research on pulmonary physiology available through the American type culture collection. *Am. Rev. Respir. Dis.* **1982**, *125*, 222–232. [CrossRef] [PubMed]
26. Jacobse-Geels, H.E.L.; Horzinek, M.C. Expression of Feline Infectious Peritonitis Coronavirus Antigens on the Surface of Feline Macrophage-like Cells. *J. Gen. Virol.* **1983**, *64*, 1859–1866. [CrossRef] [PubMed]
27. American Type Culture Collection, 2013. Fcw4 [Fcw4] (ATCC CRL2787). Available online: <https://www.atcc.org/products/crl-2787> (accessed on 1 May 2022).
28. Tekes, G.; Spies, D.; Bank-Wolf, B.; Thiel, V.; Thiel, H.-J. A Reverse genetics approach to study feline infectious peritonitis. *J. Virol.* **2012**, *86*, 6994–6998. [CrossRef]
29. Bálint, A.; Farsang, A.; Zádori, Z.; Hornyák, Á.; Dencső, L.; Almázán, F.; Enjuanes, L.; Belák, S. Molecular characterization of feline infectious peritonitis virus strain DF-2 and studies of the role of ORF3abc in viral cell tropism. *J. Virol.* **2012**, *86*, 6258–6267. [CrossRef]
30. Wang, N.; Shi, X.; Jiang, L.; Zhang, S.; Wang, D.; Tong, P.; Guo, D.; Fu, L.; Cui, Y.; Liu, X.; et al. Complex structure of MERS-CoV RBD with DPP4 986 Structure of MERS-CoV spike receptor-binding domain complexed with human receptor DPP4. *Cell Res.* **2013**, *23*, 986–993.
31. Hofmann, H.; Pyrc, K.; van der Hoek, L.; Geier, M.; Berkhout, B.; Pöhlmann, S. Human coronavirus NL63 employs the severe acute respiratory syndrome coronavirus receptor for cellular entry. *Proc. Natl. Acad. Sci. USA* **2005**, *102*, 7988–7993. [CrossRef]
32. Yeager, C. Identification of Aminopeptidase N as a Cellular Receptor for Human Coronavirus-229E. Ph.D. Thesis, Uniformed Services University of the Health Sciences, Bethesda, MD, USA, 12 May 1992.
33. Li, W.; Moore, M.J.; Vasilieva, N.; Sui, J.; Wong, S.K.; Berne, M.A.; Somasundaran, M.; Sullivan, J.L.; Luzuriaga, K.; Greenough, T.C.; et al. Angiotensin-converting enzyme 2 is a functional receptor for the SARS coronavirus. *Nature* **2003**, *426*, 450–454. Available online: [www.nature.com/nature](http://www.nature.com/nature) (accessed on 4 April 2022).
34. Regan, A.D.; Whittaker, G.R. Utilization of DC-SIGN for entry of feline coronaviruses into host cells. *J. Virol.* **2008**, *82*, 11992–11996. [CrossRef]
35. Cook, S.E.; Vogel, H.; Castillo, D.; Olsen, M.; Pedersen, N.; Murphy, B.G. Investigation of monotherapy and combined anti-coronaviral therapies against feline coronavirus serotype II in vitro. *J. Feline Med. Surg.* **2021**, 1098612X211048647. [CrossRef] [PubMed]
36. Addie, D.D.; Schaap, I.; Nicolson, L.; Jarrett, O. Persistence and transmission of natural type I feline coronavirus infection. *J. Gen. Virol.* **2003**, *84*, 2735–2744. [CrossRef]

37. Klevjer-Anderson, P.; Cheevers, W. Characterization of the infection of caprine synovial membrane cells by the retrovirus caprine arthritis-encephalitis virus. *Virology* 1981, *110*, 113–119. [CrossRef]
38. Landmann, R.; Müller, B.; Zimmerli, W. CD14, new aspects of ligand and signal diversity. *Microbes Infect.* 2000, *2*, 295–304. [CrossRef]
39. Mitani, S.; Yabuki, A.; Sawa, M.; Chang, H.-S.; Yamato, O. Intrarenal distributions and changes of angiotensin-converting enzyme and angiotensin-converting enzyme 2 in feline and canine chronic kidney disease. *J. Vet. Med. Sci.* 2014, *76*, 45–50. [CrossRef]
40. Brand, J.M.A.V.D.; Haagmans, B.L.; Leijten, L.; van Riel, D.; Martina, B.E.E.; Osterhaus, A.D.M.E.; Kuiken, T. Pathology of experimental SARS coronavirus infection in cats and ferrets. *Vet. Pathol.* 2008, *45*, 551–562. [CrossRef]
41. HTStream. Available online: <https://github.com/s4hts/HTStream> (accessed on 22 April 2022).
42. Smith, T.; Heger, A.; Sudbery, I. UMI-tools: Modeling sequencing errors in Unique Molecular Identifiers to improve quantification accuracy. *Genome Res.* 2017, *27*, 491–499. [CrossRef]
43. Dobin, A.; Davis, C.A.; Schlesinger, F.; Drenkow, J.; Zaleski, C.; Jha, S.; Batut, P.; Chaisson, M.; Gingeras, T.R. Sequence analysis STAR: Ultrafast universal RNA-seq aligner. *Bioinformatics* 2013, *29*, 15–21. [CrossRef]
44. Liao, Y.; Smyth, G.K.; Shi, W. Sequence analysis featureCounts: An efficient general purpose program for assigning sequence reads to genomic features. *Bioinformatics* 2014, *30*, 923–930. [CrossRef]
45. R Core Team. *R: A Language and Environment for Statistical Computing*; R Foundation for Statistical Computing: Vienna, Austria, 2017.
46. Ritchie, M.E.; Belinda, P.; Wu, D.; Hu, Y.; Law, C.W.; Shi, W.; Smyth, G.K. limma powers differential expression analyses for RNA-sequencing and microarray studies. *Nucleic Acids Res.* 2015, *43*, e47. [CrossRef]
47. Law, C.W.; Chen, Y.; Shi, W.; Smyth, G.K. Voom: Precision weights unlock linear model analysis tools for RNA-seq read counts. *Genome Biol.* 2014, *15*, 29. [CrossRef] [PubMed]
48. Benjamini, Y.; Hochberg, Y. Controlling the false discovery rate: A practical and powerful approach to multiple testing. *J. R. Stat. Soc. Ser. B* 1995, *57*, 289–300. [CrossRef]
49. Dodge, Y. Kolmogorov-Smirnov Test. In *The Concise Encyclopedia of Statistics*; Springer Science & Business Media: Berlin/Heidelberg, Germany, 2008. [CrossRef]
50. topGO: Enrichment Analysis for Gene Ontology Version from Bioconductor. Available online: <https://rdrr.io/bioc/topGO/> (accessed on 5 May 2022).
51. Haynes, W. Wilcoxon rank sum test BT—Encyclopedia of systems biology. In *Encyclopedia of Systems Biology*; Dubitzky, W., Wolkenhauer, O., Cho, K.-H., and Yokota, H., Eds.; Springer: New York, NY, USA, 2013; pp. 2354–2355.
52. KEGGREST: Client-Side REST Access to the Kyoto Encyclopedia of Genes and Genomes (KEGG) Version 1.30.1 from Bioconductor. Available online: <https://rdrr.io/bioc/KEGGREST/> (accessed on 5 May 2022).
53. Shirato, K.; Chang, H.-W.; Rottier, P.J. Differential susceptibility of macrophages to serotype II feline coronaviruses correlates with differences in the viral spike protein. *Virus Res.* 2018, *255*, 14–23. [CrossRef] [PubMed]
54. Van Hamme, E.; Desmarests, L.; Dewerchin, H.L.; Nauwynck, H.J. Intriguing interplay between feline infectious peritonitis virus and its receptors during entry in primary feline monocytes. *Virus Res.* 2011, *160*, 32–39. [CrossRef] [PubMed]
55. Whittaker, G. Development of Improved Cell Culture Systems for Feline Coronavirus and FIP Vaccine Development. Available online: <https://www.vet.cornell.edu/research/awards/202011/development-improved-cell-culture-systems-feline-coronavirus-and-fip-vaccine-development> (accessed on 26 May 2022).
56. Castell-Rodríguez, A. Dendritic cells: Location, function, and clinical implications. In *Biology of Myelomonocytic Cells*; Piñón-Zárate, G., Ed.; IntechOpen: Rijeka, Croatia, 2017.
57. Xiang, Q.; Feng, Z.; Diao, B.; Tu, C.; Qiao, Q.; Yang, H.; Zhang, Y.; Wang, G.; Wang, H.; Wang, C.; et al. SARS-CoV-2 Induces Lymphocytopenia by Promoting Inflammation and Decimates Secondary Lymphoid Organs. *Front. Immunol.* 2021, *12*, 661052. Available online: <https://www.frontiersin.org/article/10.3389/fimmu.2021.661052> (accessed on 29 May 2022). [CrossRef]
58. Bosch, B.J.; Bartelink, W.; Rottier, P.J.M. Cathepsin L functionally cleaves the severe acute respiratory syndrome coronavirus class I fusion protein upstream of rather than adjacent to the fusion peptide. *J. Virol.* 2008, *82*, 8887–8890. [CrossRef]
59. Qiu, Z.; Hingley, S.T.; Simmons, G.; Yu, C.; Das Sarma, J.; Bates, P.; Weiss, S.R. Endosomal proteolysis by cathepsins is necessary for murine coronavirus mouse hepatitis virus type 2 spike-mediated entry. *J. Virol.* 2006, *80*, 5768–5776. [CrossRef]
60. Millet, J.K.; Whittaker, G.R. Host cell proteases: Critical determinants of coronavirus tropism and pathogenesis. *Virus Res.* 2015, *202*, 120–134. [CrossRef]
61. Peacock, T.P.; Goldhill, D.H.; Zhou, J.; Baillon, L.; Frise, R.; Swann, O.C.; Kugathasan, R.; Penn, R.; Brown, J.C.; David, R.Y.S.; et al. The furin cleavage site in the SARS-CoV-2 spike protein is required for transmission in ferrets. *Nat. Microbiol.* 2021, *6*, 899–909. [CrossRef]
62. Hoffmann, M.; Kleine-Weber, H.; Schroeder, S.; Krüger, N.; Herrler, T.; Erichsen, S.; Schiergens, T.S.; Herrler, G.; Wu, N.H.; Nitsche, A.; et al. SARS-CoV-2 cell entry depends on ACE2 and TMPRSS2 and is blocked by a clinically proven protease inhibitor. *Cell* 2020, *181*, 271–280.e8. [CrossRef]
63. Zhou, Y.; Vedantham, P.; Lu, K.; Agudelo, J.; Carrion, R., Jr.; Nunneley, J.W.; Barnard, D.; Pöhlmann, S.; McKerrow, J.H.; Renslo, A.R.; et al. Protease inhibitors targeting coronavirus and filovirus entry. *Antivir. Res.* 2015, *116*, 76–84. [CrossRef] [PubMed]

64. Sasaki, M.; Itakura, Y.; Kishimoto, M.; Tabata, K.; Uemura, K.; Ito, N.; Sugiyama, M.; Wastika, C.E.; Orba, Y.; Sawa, H. Host serine proteases TMPRSS2 and TMPRSS11D mediate proteolytic activation and trypsin-independent infection in group A rotaviruses. *J. Virol.* **2021**, *95*, e00398-21. [[CrossRef](#)]
65. Bonaparte, M.I.; Dimitrov, A.S.; Bossart, K.N.; Cramer, G.; Mungall, B.A.; Bishop, K.A.; Choudhry, V.; Dimitrov, D.S.; Wang, L.-F.; Eaton, B.T.; et al. Ephrin-B2 ligand is a functional receptor for Hendra virus and Nipah virus. *Proc. Natl. Acad. Sci. USA* **2005**, *102*, 10652–10657. [[CrossRef](#)] [[PubMed](#)]
66. Wang, J.; Zheng, X.; Peng, Q.; Zhang, X.; Qin, Z. Eph receptors: The bridge linking host and virus. *Cell Mol. Life Sci.* **2020**, *77*, 2355–2365. [[CrossRef](#)] [[PubMed](#)]
67. de Boer, E.C.; van Gils, J.M.; van Gils, M.J. Ephrin-Eph signaling usage by a variety of viruses. *Pharmacol. Res.* **2020**, *159*, 105038. [[CrossRef](#)]
68. Zhang, H.; Li, Y.; Wang, H.-B.; Zhang, A.; Chen, M.-L.; Fang, Z.-X.; Dong, X.-D.; Li, S.-B.; Du, Y.; Xiong, D.; et al. Ephrin receptor A2 is an epithelial cell receptor for Epstein-Barr virus entry. *Nat. Microbiol.* **2018**, *3*, 164–171. [[CrossRef](#)] [[PubMed](#)]
69. Zalpoor, H.; Akbari, A.; Samei, A.; Forghani-fidvajani, R.; Kamali, M.; Afzalnia, A.; Manshouri, S.; Heidari, F.; Pornour, M.; Khoshmirsafa, M.; et al. The roles of Eph receptors, neuropilin-1, P2X7, and CD147 in COVID-19-associated neurodegenerative diseases: Inflammasome and JAK inhibitors as potential promising therapies. *Cell Mol. Biol. Lett.* **2022**, *27*, 10. [[CrossRef](#)]
70. Beaudoin, C.A.; Jamasb, A.R.; Alsulami, A.F.; Copoiu, L.; van Tonder, A.J.; Hala, S.; Bannerman, B.P.; Thomas, S.E.; Vedithi, S.C.; Torres, P.H.M.; et al. Predicted structural mimicry of spike receptor-binding motifs from highly pathogenic human coronaviruses. *Comput. Struct. Biotechnol. J.* **2021**, *19*, 3938–3953. [[CrossRef](#)]
71. Raj, V.S.; Mou, H.; Smits, S.L.; Dekkers, D.H.; Müller, M.A.; Dijkman, R.; Muth, D.; Demmers, J.A.; Zaki, A.; Fouchier, R.A.; et al. Dipeptidyl peptidase 4 is a functional receptor for the emerging human coronavirus-EMC. *Nature* **2013**, *495*, 251–254. [[CrossRef](#)]
72. Keidar, S.; Gamliel-Lazarovich, A.; Kaplan, M.; Pavlotzky, E.; Hamoud, S.; Hayek, T.; Karry, R.; Abassi, Z. Mineralocorticoid receptor blocker increases angiotensin-converting Enzyme 2 activity in congestive heart failure patients. *Circ. Res.* **2005**, *97*, 946–953. [[CrossRef](#)]
73. Song, X.; Hu, W.; Yu, H.; Zhao, L.; Zhao, Y.; Zhao, Y. High expression of angiotensin-converting enzyme-2 (ACE2) on tissue macrophages that may be targeted by virus SARS-CoV-2 in COVID-19 patients. *bioRxiv* **2020**, 1–27. [[CrossRef](#)]
74. Song, X.; Hu, W.; Yu, H.; Zhao, L.; Zhao, Y.; Zhao, X.; Xue, H.; Zhao, Y. Little to no expression of angiotensin-converting enzyme-2 on most human peripheral blood immune cells but highly expressed on tissue macrophages. *Cytom. Part A J. Int. Soc. Anal. Cytol.* **2020**, 1–10. [[CrossRef](#)] [[PubMed](#)]
75. Hikmet, F.; Méar, L.; Edvinsson, Å.; Mücke, P.; Uhlén, M.; Lindskog, C. The protein expression profile of ACE2 in human tissues. *Mol. Syst. Biol.* **2020**, *16*, e9610. [[CrossRef](#)] [[PubMed](#)]
76. Hamming, I.; Timens, W.; Bulthuis, M.L.C.; Lely, A.T.; Navis, G.J.; van Goor, H. Tissue distribution of ACE2 protein, the functional receptor for SARS coronavirus. A first step in understanding SARS pathogenesis. *J. Pathol.* **2004**, *203*, 631–637. [[CrossRef](#)] [[PubMed](#)]
77. Lean, F.Z.X.; Núñez, A.; Spiro, S.; Priestnall, S.L.; Vreman, S.; Bailey, D.; James, J.; Wrighlesworth, E.; Suarez-Bonnet, A.; Conceicao, C.; et al. Differential susceptibility of SARS-CoV-2 in animals: Evidence of ACE2 host receptor distribution in companion animals, livestock and wildlife by immunohistochemical characterisation. *Transbound. Emerg. Dis.* **2021**, 1–12. [[CrossRef](#)]
78. Chicchetti, R.; Galiazzo, G.; Fracassi, F.; Giancola, F.; Pietra, M. ACE2 expression in the cat and the tiger gastrointestinal tracts. *Front. Vet. Sci.* **2020**, *7*, 514. [[CrossRef](#)]
79. Van Hamme, E.; Dewerchin, H.L.; Cornelissen, E.; Nauwynck, H.J. Attachment and internalization of feline infectious peritonitis virus in feline blood monocytes and Crandell feline kidney cells. *J. Gen. Virol.* **2007**, *88*, 2527–2532. [[CrossRef](#)]
80. Granelli-Piperno, A.; Pritsker, A.; Pack, M.; Shimeliovich, I.; Arrighi, J.-F.; Park, C.G.; Trumpfheller, C.; Piguet, V.; Moran, T.M.; Steinman, R.M. Dendritic cell-specific intercellular adhesion molecule 3-grabbing nonintegrin/CD209 is abundant on macrophages in the normal human lymph node and is not required for dendritic cell stimulation of the mixed leukocyte reaction. *J. Immunol.* **2005**, *175*, 4265–4273. [[CrossRef](#)]
81. Gioia, M.; Ciaccio, C.; Calligaris, P.; De Simone, G.; Sbardella, D.; Tundo, G.; Fasciglione, G.F.; Di Masi, A.; Di Pierro, D.; Bocedi, A.; et al. Role of proteolytic enzymes in the COVID-19 infection and promising therapeutic approaches. *Biochem. Pharmacol.* **2020**, *182*, 114225.
82. Kishimoto, M.; Uemura, K.; Sanaki, T.; Sato, A.; Hall, W.; Kariwa, H.; Orba, Y.; Sawa, H.; Sasaki, M. TMPRSS11D and TMPRSS13 Activate the SARS-CoV-2 Spike Protein. *Viruses* **2021**, *13*, 384. [[CrossRef](#)]
83. Yadati, T.; Houben, T.; Bitorina, A.; Shiri-Sverdlov, R. The ins and outs of cathepsins: Physiological function and role in disease management. *Cells* **2020**, *9*, 1679. [[CrossRef](#)] [[PubMed](#)]
84. Kawase, M.; Shirato, K.; Matsuyama, S.; Taguchi, F. Protease-mediated entry via the endosome of human coronavirus 229E. *J. Virol.* **2009**, *83*, 712–721. [[CrossRef](#)] [[PubMed](#)]
85. Simmons, G.; Gosalia, D.N.; Rennekamp, A.J.; Reeves, J.D.; Diamond, S.L.; Bates, P. Inhibitors of cathepsin L prevent severe acute respiratory syndrome coronavirus entry. *Proc. Natl. Acad. Sci. USA* **2005**, *102*, 11876–11881. [[CrossRef](#)] [[PubMed](#)]
86. Zhao, M.M.; Yang, W.L.; Yang, F.Y.; Zhang, L.; Huang, W.J.; Hou, W.; Fan, C.F.; Jin, R.H.; Feng, Y.M.; Wang, Y.C.; et al. Cathepsin L plays a key role in SARS-CoV-2 infection in humans and humanized mice and is a promising target for new drug development. *Signal Transduct. Target Ther.* **2021**, *6*, 134. [[CrossRef](#)] [[PubMed](#)]
87. Golden, J.; Bahe, J.A.; Lucas, W.T.; Nibert, M.L.; Schiff, L.A. Cathepsin S supports acid-independent infection by some reoviruses. *J. Biol. Chem.* **2004**, *279*, 8547–8557. [[CrossRef](#)]

88. Tuzi, N.L.; Gullick, W.J. eph, the largest known family of putative growth factor receptors. *Br. J. Cancer* 1994, 69, 417–421. [[CrossRef](#)]
89. Bowden, T.; Aricescu, A.R.; Gilbert, R.; Grimes, J.M.; Jones, Y.; Stuart, D. Structural basis of Nipah and Hendra virus attachment to their cell-surface receptor ephrin-B2. *Nat. Struct. Mol. Biol.* 2008, 15, 567–572. [[CrossRef](#)]
90. Lupberger, J.; Zeisel, M.B.; Xiao, F.; Thumann, C.; Fofana, I.; Zona, L.; Davis, C.; Mee, C.; Turek, M.; Gorke, S.; et al. EGFR and EphA2 are host factors for hepatitis C virus entry and possible targets for antiviral therapy. *Nat. Med.* 2011, 17, 589–595. [[CrossRef](#)]
91. Egal, E.; Helms, M.N.; Liou, T.G.; Mimche, P. Ephrin ligands are upregulated in the saliva of SARS-CoV-2 infected patients. *FASEB J.* 2022, 36. [[CrossRef](#)]

**Chapter 3: Investigation of monotherapy and combined anticoronaviral therapies against feline coronavirus serotype II *in vitro***

# Investigation of monotherapy and combined anticoronaviral therapies against feline coronavirus serotype II in vitro

Journal of Feline Medicine and Surgery

1–11

© The Author(s) 2021

Article reuse guidelines:

sagepub.com/journals-permissions

DOI: 10.1177/1098612X211048647

journals.sagepub.com/home/jfm

This paper was handled and processed

by the American Editorial Office (AAFP)

for publication in *JFMS*



Sarah E Cook<sup>1</sup>, Helena Vogel<sup>2</sup>, Diego Castillo<sup>3</sup>, Mark Olsen<sup>4</sup>, Niels Pedersen<sup>5</sup> and Brian G Murphy<sup>3</sup>

## Abstract

**Objectives** Feline infectious peritonitis (FIP), caused by genetic mutants of feline enteric coronavirus known as FIPV, is a highly fatal disease of cats with no currently available vaccine or US Food and Drug Administration-approved cure. Dissemination of FIPV in affected cats results in a range of clinical signs, including cavitory effusions, anorexia, fever and lesions of pyogranulomatous vasculitis and perivasculitis, with or without central nervous system or ocular involvement. The objectives of this study were to screen an array of antiviral compounds for anti-FIPV (serotype II) activity, determine cytotoxicity safety profiles of identified compounds with anti-FIPV activity and strategically combine identified monotherapies to assess compound synergy against FIPV in vitro. Based upon clinically successful combination treatment strategies for human patients with HIV and hepatitis C virus infections, we hypothesized that a combined anticoronaviral therapy approach featuring concurrent multiple mechanisms of drug action would result in an additive or synergistic antiviral effect.

**Methods** This study screened 90 putative antiviral compounds for efficacy and cytotoxicity using a multimodal in vitro strategy, including plaque bioassays, real-time RT-PCR viral inhibition and cytotoxicity assays.

**Results** Through this process, we identified 26 compounds with effective antiviral activity against FIPV, representing a variety of drug classes and mechanisms of antiviral action. The most effective compounds include GC376, GS-441524, EIDD2081 and EIDD2931. We documented antiviral efficacy for combinations of antiviral agents, with a few examined drug combinations demonstrating evidence of limited synergistic antiviral activity.

**Conclusions and relevance** Although evidence of compound synergy was identified for several combinations of antiviral agents, monotherapies were ultimately determined to be the most effective in the inhibition of viral transcription.

**Keywords:** Feline infectious peritonitis; FIPV; coronavirus; antiviral; combined anti-coronaviral therapy

**Accepted:** 5 September 2021

## Introduction

Feline infectious peritonitis (FIP) is a highly fatal disease of cats with no effective vaccine or US Food and Drug Administration-approved treatment. Although the pathogenesis has not been fully elucidated, FIP is generally understood to develop as a result of specific mutations in the viral genome of the minimally pathogenic and ubiquitous feline enteric coronavirus (FECV), creating the virulent FIP virus (FIPV).<sup>1,2</sup> These FECV mutations result in a virus–host cell tropism switch from intestinal enterocytes to monocytes/macrophages. These two biotypes (FECV and FIPV) are generally considered to exist as two

<sup>1</sup>Graduate Group Integrative Pathobiology, School of Veterinary Medicine, University of California, Davis, CA, USA

<sup>2</sup>School of Veterinary Medicine, University of California, Davis, CA, USA

<sup>3</sup>Department of Pathology, Microbiology and Immunology, School of Veterinary Medicine, University of California, Davis, CA, USA

<sup>4</sup>Department of Pharmaceutical Sciences, College of Pharmacy-Glendale, Midwestern University, Glendale, AZ, USA

<sup>5</sup>Department of Medicine and Epidemiology, School of Veterinary Medicine, University of California, Davis, CA, USA

### Corresponding author:

Sarah E Cook DVM, DACVP, Graduate Group Integrative Pathobiology, School of Veterinary Medicine, University of California Davis, 1 Garrod Drive, Davis, CA 95616-5270, USA  
Email: sestevens@ucdavis.edu

serotypes (I and II); however, this convention has recently been questioned, and suggestions have been made that the 'serotypes' be considered as distinct viruses based on their spike protein differences and expected biologic and clinical outcomes.<sup>3</sup> Regardless of whether these two serotypes represent distinct viruses, both are capable of causing FIP, with serotype I being more prevalent in nature.<sup>4</sup> Although serotype I is more prevalent, it is less well studied than serotype II owing to challenges in propagating this virus *in vitro*.

Productive monocyte/macrophage infection by FIPV, variably widespread anatomic dissemination and immune-mediated perivascularitis results in the highly fatal systemic inflammatory disease, FIP.<sup>5</sup> As a result of viral dissemination, FIP may present with clinical signs reflecting inflammation in a variety of anatomic sites potentially including the abdominal cavity and associated viscera, thoracic cavity, central nervous system and/or eye.<sup>6-9</sup> FIP remains a devastating viral disease of cats owing to its high mortality rate, challenges in establishing a precise etiologic diagnosis, and the current lack of available and effective treatment options.<sup>8,10</sup> The development of an effective vaccine for FIP has been complicated by the role of antibody-dependent enhancement in FIP disease pathogenesis, where the presence of non-neutralizing anticoronaviral antibodies have been shown to exacerbate FIP disease.<sup>11-13</sup>

Recent antiviral clinical trials in both experimentally and naturally FIPV-infected cats have shown promise in treating and curing FIP through the use of GS-441524, a nucleoside analog and metabolite of remdesivir (Veklury; Gilead Sciences), or GC376, a 3C-like protease inhibitor of FIPV (Anavive Lifesciences).<sup>14-16</sup> There have been particular treatment challenges for cats with more complicated and multisystemic forms of FIP, including those with neurologic or ocular involvement. A recent clinical trial of GS-441524 at higher dosages for the treatment of neurologic FIP established the possibility of long-term resolution of disease for some of these more complicated forms of FIP.<sup>17</sup> Despite the recent clinical successes, these antiviral compounds are currently unavailable for legal clinical veterinary use in cats with FIP.

Using a collection of compounds selected based on their proven efficacy in interfering with the replication of other RNA viruses, we identified a subset of compounds with variable anti-FIPV activity against serotype II and characterized their safety and efficacy profiles *in vitro*. Of these compounds, several have been used as treatments for retroviral, hepatitis C or other coronaviral infections, including current investigations as therapies for COVID-19.<sup>18-21</sup> Given the success of combined anti-retroviral therapy (cART) against HIV-1 and combination therapies against hepatitis C virus,<sup>22</sup> it would seem feasible that concurrently targeting FIPV at different steps of the virus lifecycle with a combined anticoronaviral

therapy (cACT) may offer a greater level of sustained and more complete success than has been achieved with monotherapies alone. The inclusion of an antiviral agent in cACT capable of penetrating the blood-brain barrier and/or blood-ocular barrier and achieving pharmacologically relevant tissue concentrations may facilitate system-wide eradication of FIPV.

Here, we describe a set of *in vitro* assays facilitating the identification of effective and safe anticoronaviral compounds. We hypothesized that the combinatorial use of two or more effective antiviral monotherapies with differing mechanisms of action would facilitate the identification of additive or synergistic combinations providing superior anticoronaviral efficacy vs their use as sole agents (monotherapy).

## Materials and methods

### *FIPV inoculum for in vitro experiments*

Crandell-Rees feline kidney cells (CRFK; ATCC) were cultured in T150 flasks (Corning), inoculated with serotype II FIPV (WSU-79-1146; GenBank DQ010921) and propagated in 50ml Dulbecco's Modified Eagle's Medium with 4.5g/l glucose (Corning) and 10% fetal bovine serum (Gemini Bio). After 72h of incubation at 37°C, extensive cytopathic effect (CPE) and large areas of cell clearing/detachment were noted. Flasks were then flash frozen at -70°C for 8mins, thawed briefly at room temperature, and the cells and supernatant were then centrifuged at 1500g for 5mins, followed by a second centrifugation step at 4000g for 5mins, in order to isolate cell-free viral stocks. Supernatant containing the viral stock was divided into 0.5 and 1.0ml aliquots in 1.5ml cryotubes (Nalgene) and stored at -70°C. After freezing, a single tube was thawed, and the viral titer established using both bioassay (tissue culture infectious dose-50 [TCID<sub>50</sub>]) and real-time quantitative RT-PCR (RT-qPCR) methods (below).

The TCID<sub>50</sub> was determined using a viral plaque assay. CRFK cells were grown in a 96-well tissue culture plate (Genesee Scientific) until the CRFK cells achieved approximately 75-85% confluency. Serial 10-fold dilutions were made of FIPV stock and 200µl samples of each dilution were added to 10-well replicates. At 72h post-infection, the cells were fixed with methanol and stained with crystal violet (Sigma-Aldrich). Individual wells were evaluated visually for virus-induced CPE, scored as CPE positive or negative, and the TCID<sub>50</sub> was determined based upon the equation  $\log_{10}TCID_{50} = [\text{total number of wells CPE positive} / \text{number of replicates}] + 0.5$  to reflect infectious virions per milliliter of supernatant.<sup>23</sup>

### *Quantification of FIPV by RT-qPCR*

Cell-free viral RNA was isolated from the viral stock using the QIAamp Viral RNA Mini Kit (Qiagen), following the manufacturer's instructions. The isolated RNA was treated with DNase (TURBO DNase; Invitrogen)

and subsequently reverse transcribed using the High-Capacity RNA-to-cDNA Kit (Applied Biosystems) following the manufacturers' protocols. The copy number of FIPV and feline *GAPDH* cDNA were determined using Applied Biosystem's QuantStudio 3 Real-Time PCR System and PowerUp SYBR Green Master Mix, following the manufacturer's protocol for a 10  $\mu$ l reaction. Each PCR reaction was performed in triplicate with water template as a negative control and plasmid DNA as a positive control. A control reaction excluding reverse transcriptase was included in each real-time PCR assay set. cDNA templates were amplified using the FIPV forward primer, 5'-GGAAGTTTAGATTGATTTGGCAA TGCTAG, and the FIP reverse primer, 5'-AACAATCACT AGATCCAGACGTTAGCT (terminal portion of the FIPV 7b gene).<sup>15</sup> Real-time PCR for the feline *GAPDH* house-keeping gene was performed concurrently using the primers, 5 *GAPDH*, 5'-AAATCCACGGCACAGTCAAG, and 3 *GAPDH*, 5'-TGATGGGCTTCCATTGATGA. Cycling conditions for both FIPV and *GAPDH* amplicons were as follows: 50°C for 2 mins and 95°C for 2 mins, followed by 40 cycles of 95°C for 15s, 58°C for 30s and 72°C for 1 min. The final step included a dissociation curve to evaluate specificity of primer binding. FIPV and *GAPDH* copy numbers were calculated based on standard curves generated in our laboratory. Copies of FIPV cDNA determined via RT-qPCR were normalized per 10<sup>6</sup> copies of feline *GAPDH* cDNA.

#### *Development of anti-helicase chemical fragments*

In general, the drugs examined and described in this study were pre-existing antiviral agents. In contrast, the helicase enzyme of FIPV was cloned, expressed and used as a target for coronavirus and enzyme-specific viral discovery. The target DNA sequence of AviTag-FIP Helicase-HisTag was optimized and synthesized. The synthesized sequence was cloned (Dr Adeyemi Adedeji) into vector pET30a with Avi-His tag for protein expression in *Escherichia coli*. *E. coli* strain BL21(DE3) was transformed with recombinant plasmid. A single colony was inoculated into 11 of auto-induced medium containing antibiotic, and the culture was incubated at 37°C at 200 rpm. When the OD<sub>600</sub> reached about 3, the temperature of the cell culture was changed to 15°C for 16h. Cells were harvested by centrifugation. Cell pellets were resuspended with lysis buffer, followed by sonication. The precipitate after centrifugation was dissolved using denaturing agent. Target protein was obtained by one-step purification using a nickel (Ni) column. Target protein was sterilized by a 0.22  $\mu$ m filter. Yield was 7.2 mg at 0.90 mg/ml, and was stored in phosphate buffered saline, 10% glycerol and 0.5mM L-arginine at pH 7.4. The concentration was determined by Bradford protein assay, with bovine serum albumin as the standard. The protein purity and molecular weight were determined by sodium

dodecyl sulfate polyacrylamide gel electrophoresis with Western blot confirmation.

Surface plasmon resonance (SPR) fragment screening was performed on a ForteBio Pioneer FE SPR platform. A HisCap sensor chip, which contains a nitrilotriacetic acid surface matrix, was used. Channels 1 and 3 were charged with 100  $\mu$ M NiCl<sub>2</sub>, followed by injection of 50  $\mu$ g/ml of FIP protein. Channel 2 was left free of protein, as well as NiCl<sub>2</sub>, as a reference. Channel 1 was immobilized to a density of ~8000 response units (RU), while channel 3 contained about 12,000 RU. Channel 1 was used. The buffer used for immobilization was 10mM HEPES (pH 7.4), 150mM NaCl and 0.1% Tween-20. For the assay, dimethyl sulfoxide (DMSO) was added to a final concentration of 4%. The proprietary compound library was diluted into the same buffer without DMSO, to a final DMSO concentration of 4% DMSO. Library compounds were screened at a concentration of 100  $\mu$ M using the OneStep gradient injection method. Hits were selected based upon RU and kinetics and utilized for cell-based screening.

#### *Viral plaquing assay*

To screen compounds for antiviral activity, infected CRFK cells were treated with compounds in six-well replicates and compared with positive control wells (infected cells), negative controls (uninfected cells) and treatment controls (infected cells treated with a known effective antiviral compound) run concurrently on each tissue culture plate. CRFK cells were grown in 96-well tissue culture plates (Genesee Scientific) containing 200  $\mu$ l of culture media. At ~75–85% cell confluency, the media in the uninfected control wells was aspirated and replaced with 200  $\mu$ l of fresh media. The media in the infected wells was aspirated and replaced with media inoculated with FIPV at a multiplicity of infection (MOI) of 0.004 infectious virions per cell. At 1 h post-infection, each putative antiviral compound was added to six FIPV-infected wells and six uninfected control wells (to screen for compound cytotoxicity). All compounds were initially screened at 10  $\mu$ M, except for the 'chemical fragment' compounds supplied by M Olsen (Midwestern University), which were assessed at 50  $\mu$ M. The tissue culture plates were incubated for 72h at 37°C and subsequently fixed with methanol and stained with crystal violet. Plates were scanned for absorbance at 620nm using an ELISA plate reader (FilterMax F3 [Molecular Devices] and Softmax Pro [Molecular Devices]). The individual well absorbance values along with the average absorbance value and SEM for the six-well experimental replicates were recorded for each treatment condition.

For agents that demonstrated antiviral efficacy in the initial screening at 10 or 50  $\mu$ M (protected from virus-associated CPE), the half-maximal effective concentration (EC<sub>50</sub>) was determined by performing a progressive

two-fold compound dilution series in the viral plaquing assay. For EC<sub>50</sub> determination, CRFK cells were grown in 96-well tissue culture plates similarly to that performed for the antiviral screening assay. Aside from the uninfected control wells, all remaining wells were infected with the FIPV as described above in two-fold dilution series ranging from 20 μM to 0 μM in six-well replicates. The number of dilution steps ranged from six to 14 and was compound dependent. Six-well replicates of uninfected CRFK cells served as a control for normal CRFK cells; six-well replicates of CRFK cells infected with FIPV served as untreated, FIPV-infected control wells; and six-well replicates of FIPV-infected CRFK cells treated with GS-441524 served as control wells for protection against virus-induced cell death based on published data regarding the efficacy of GS-441524 use in vitro in CRFK cells.<sup>16</sup>

Tissue culture plates were incubated for 72 h and subsequently fixed with methanol, stained with crystal violet and scanned for absorbance at 620 nm using an ELISA plate reader. The EC<sub>50</sub> was calculated by plotting a non-linear regression equation (dose–response curve) using Prism 8 (GraphPad).

#### *Viral RNA knock-down assay*

RT-qPCR assays were used to quantify compound inhibition of viral RNA production. CRFK cells were cultured in a six-well tissue culture plate (Genesee Scientific). At approximately 75–85% cellular confluency, the culture media was replenished with fresh media and the cells were infected with FIPV serotype II at a MOI of 0.2. One hour post-infection, FIPV-infected wells were treated with one (monotherapy), two or three (cACT) antiviral compounds performed in triplicate. Compound dosage was based upon the compounds' EC<sub>50</sub> and ranged from 0.001 to 20 μM. Triplicate wells of FIPV-infected and untreated CRFK cells acted as virus-infected controls. All cell culture wells were subsequently incubated for 24 h, and cell-associated total RNA was isolated using the PureLink RNA mini kit (Invitrogen). The RNA was treated with DNase (TURBO DNase; Ambion), reverse transcribed to cDNA using a High-Capacity RNA-to-cDNA Kit (Applied Biosystems) and FIPV cDNA and feline *GAPDH* cDNA were measured using RT-qPCR, as described above. Fold reduction in viral titer was determined by dividing the normalized average FIPV RNA copy number for untreated, FIPV-infected CRFK cells into the normalized average FIPV RNA copy number for treated CRFK cells with the compound(s) of interest. The expected additive effect was determined by adding the fold reduction for each monotherapy treatment used in combination. Foldover additive effect was determined by dividing the predicted additive effect into the combined fold reduction value for the particular combined therapy of interest.

#### *Determination of cytotoxicity safety profiles*

Compound cytotoxicity in feline cells was assessed using the commercially available kit (CellTox Green Cytotoxicity Assay; Promega) according to the manufacturer's instructions. Untreated CRFK cells were used as negative controls and cells treated with a cytotoxic solution provided by the manufacturer was used as the positive toxicity control. Briefly, in addition to the control wells, CRFK cells were plated in 96-well tissue culture plates (Genesee Scientific) in four-well replicates with 5, 10, 25, 50 or 100 μM concentrations of the compound of interest and were incubated for 72 h. After 72 h, the kit DNA binding dye was applied to all wells, incubated at 37°C, shielded from light for 15 mins and the fluorescence intensity determined at 485–500 nm<sub>Ex</sub>/520–530 nm<sub>Em</sub> using a plate reader (FilterMax F3 [Molecular Devices] and Softmax Pro [Molecular Devices]). Compound cytotoxicity at a particular concentration was assumed to be proportional to the intensity of fluorescence based on the selective penetration and binding of the dye to the DNA of degenerate, apoptotic or necrotic cells. The cytotoxicity range was determined by setting the fluorescence value for cells treated with the positive control reagent as 100% and the untreated feline cells as 0% cytotoxicity. The mean fluorescence value for the four wells containing each compound concentration were then interpolated as a percentage (percent cytotoxicity) ranging from 0% to 100%. Clofazimine cytotoxicity was determined by dosing monolayers of CRFK cells in a 96-well plate with serial dilutions of the compound starting at a maximum dose of 100 μM, incubated for 72 h and then stained with crystal violet and scanned for absorbance at 620 nm using an ELISA plate reader. The 50% cytotoxic concentration (CC<sub>50</sub>) was calculated by plotting a non-linear regression equation (dose–response curve) using GraphPad Prism version 8.

## **Results**

### *Compound screening*

In order to identify compounds with anti-FIPV activity, a compilation of 90 compounds (Figure S1 in the supplementary material) from differing drug classes and with a variety of reputed mechanisms of antiviral action were screened for anticoronaviral activity in in vitro assays. Compounds screened included nucleoside polymerase inhibitors (NPIs), non-NPIs, protease inhibitors (PIs), NS5A inhibitors, a set of anti-helicase chemical 'fragments'<sup>24</sup> and a set of compounds with undetermined or multiple antiviral mechanisms of action. From this group of 90 compounds, 26 different compounds were determined to possess antiviral activity against FIPV, including NPIs, PIs, NS5A inhibitors and three compounds with undetermined mechanisms of action (termed 'other'; Figure 1). The antiviral compounds that

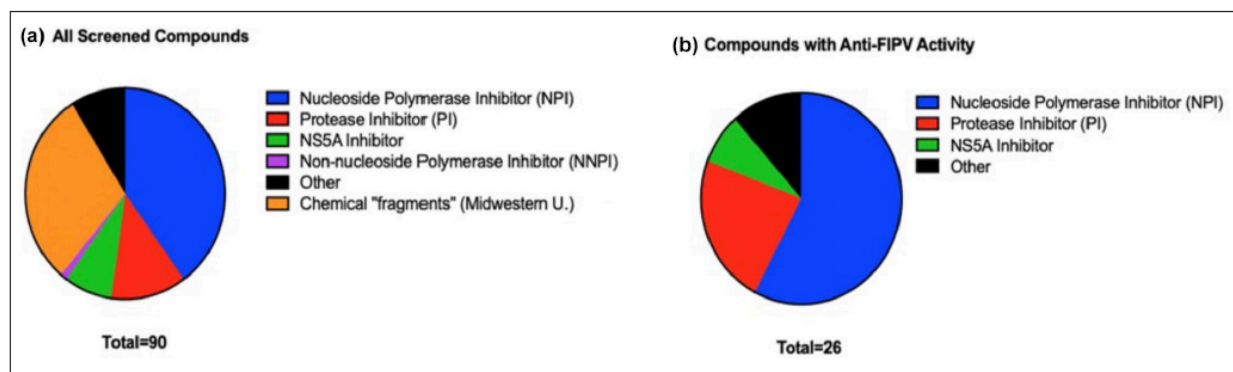


**Figure 1** Compounds screened by mechanism of action. (a) Pie graph depiction of all compounds screened. (b) Compounds identified during screening to possess anti-feline infectious peritonitis virus (FIPV) activity in vitro

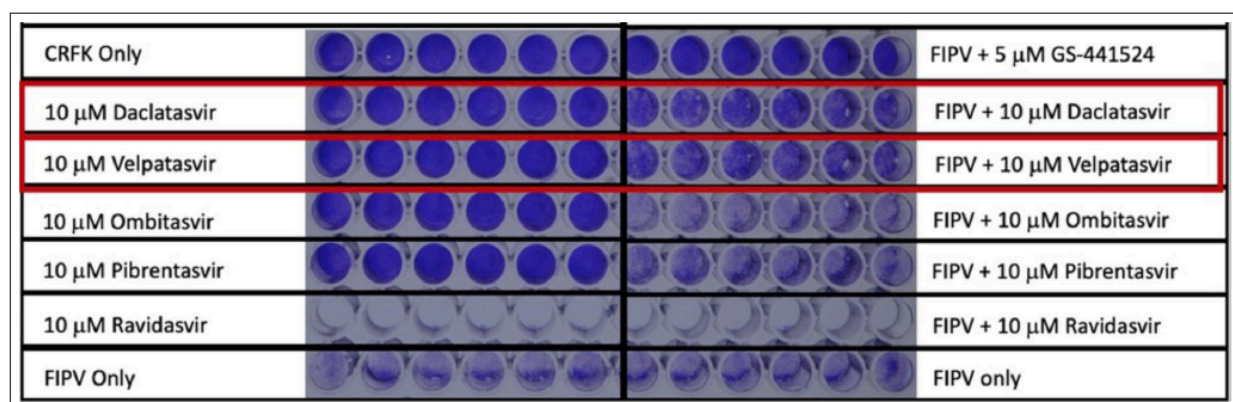


**Figure 2** Example screening plaque assay using crystal violet staining to identify anti-feline infectious peritonitis virus (FIPV) activity at 10µM. The top left row shows control wells with Crandell-Rees feline kidney (CRFK) cells only and no drug or FIPV. The top right row shows a positive control using GS-441524 with known complete protection of CRFK cells against FIPV-induced cell death. The entire bottom row of wells represents CRFK cells infected with FIPV and no drug treatment. The remaining rows are screening wells with the left half assessing for cytotoxicity at 10µM (no FIPV infection) and the right half assessing for anti-FIPV activity at 10µM for any given compound. Loss of staining indicates cell loss. Daclatasvir and velpatasvir demonstrated anti-FIPV activity evidenced by increased crystal violet staining (relatively intact cell monolayers) relative to FIPV-only control wells (bottom row of plate). Ombitasvir, pibrentasvir and ravidasvir demonstrated an absent-to-minimal antiviral effect, with ravidasvir also demonstrating cytotoxicity at 10µM based on the dramatic well clearing seen on the left half of the plate without FIPV

demonstrated efficacy against FIPV included toremifene citrate, daclatasvir, elbasvir, lopinavir, ritonavir, nelfinavir mesylate, K777/K11777, grazoprevir, amodiaquine, EIDD1931, EIDD2801, clofazimine and GS-441524 sourced from three different China-based manufacturers (Figure 2). We tested several nucleoside analog compounds provided by Gilead Sciences structurally related to the nucleoside analogs GS-441524 and remdesivir for their antiviral properties and found several with potential (included in the above-reported 26 identified compounds), but we did not pursue these agents further. As a result, the total number of antiviral agents carried forward for further analyses was 14. This total includes

the previously identified 3-C protease inhibitor, GC376 (Anavive Lifesciences).

#### Determining antiviral efficacy

The  $EC_{50}$  (antiviral efficacy) was determined for 10 antiviral compounds. For these compounds, the  $EC_{50}$  ranged from 0.04µM to 13.47µM (Figure 3). One of the antiviral agents – daclatasvir – demonstrated unacceptable cytotoxicity at 20µM and was removed from further testing. GS-441524 sourced from China (HY-103586; MedChemExpress) was shown to have a comparable  $EC_{50}$  relative to previously published values for GS-441524 sourced from Gilead Sciences,<sup>15</sup> and the  $EC_{50}$  for GC376,

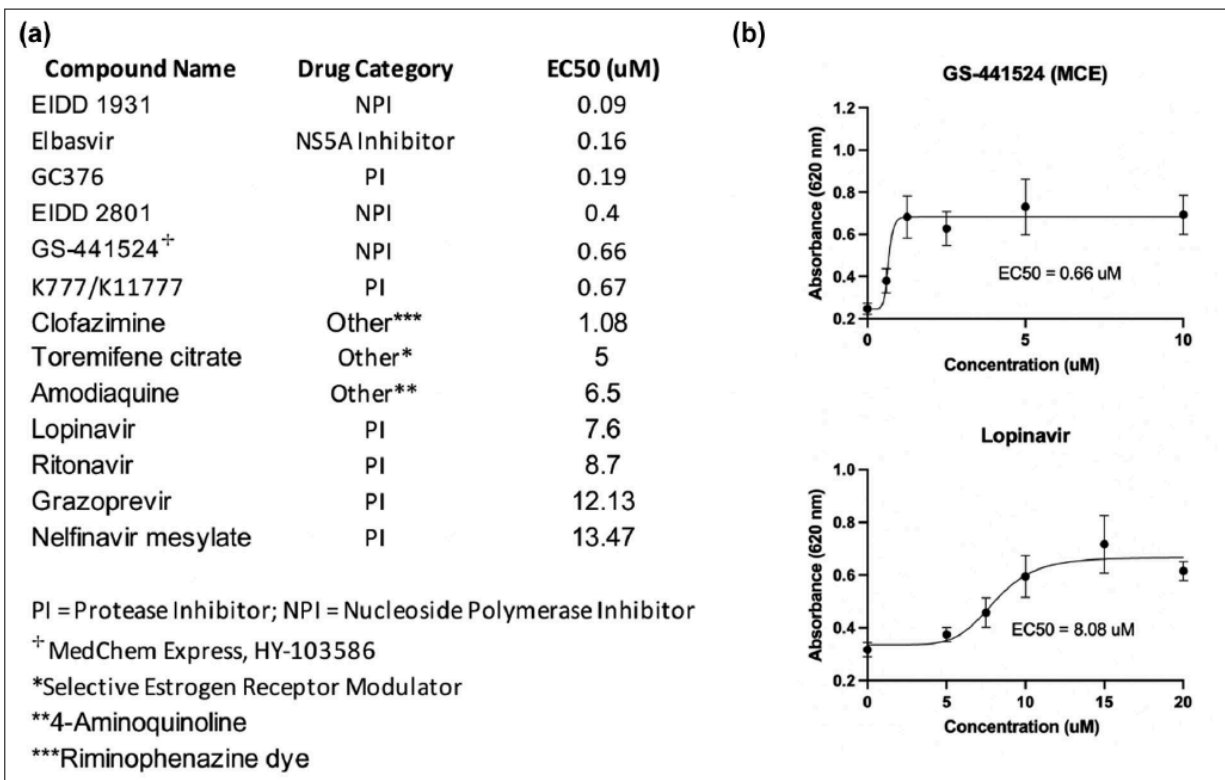


**Figure 3** (a) Half-maximal effective concentration (EC<sub>50</sub>) values and (b) representative non-linear regression analyses for two of the compounds with anti-feline infectious peritonitis virus (FIPV) activity. Serial dilutions of each compound with anti-FIPV activity were performed to identify the EC<sub>50</sub>. GS-441524 results shown here represent the compound sourced from MedChemExpress (MCE)

previously reported as 0.04 μM,<sup>25</sup> was determined in our laboratory to be 0.19 μM.

#### Cytotoxicity safety profiles

Cytotoxicity safety profiles (CSPs) were determined by using the Promega CellTox Green Cytotoxicity Assay for 11 different antiviral compounds in CRFK cells. At 5 μM, seven of the tested compounds demonstrated essentially no cytotoxicity, while two of the antivirals – amodiaquine and toremifene – had 11% and 12% cytotoxicity, respectively (Figure 4). The CC<sub>50</sub> for GC376 has been reported previously as >150 μM.<sup>25</sup> The CC<sub>50</sub> for clofazimine was determined to be 8.3 μM. Interestingly, based upon the Promega CellTox Green Cytotoxicity Assay, the cytotoxicity of both EIDD compounds was essentially undetectable up to 100 μM. However, visual inspection of the EIDD-treated tissue culture wells just prior to fluorescent dye application revealed evidence of agent-associated CPE. The untreated CRFK cells featured an adherent spindle morphology in a closely packed monolayer, while the EIDD-treated wells demonstrated an overt decrease in cellular confluency with variable cell morphology, including rounding and detachment of cells (CPE). The discordance between the subjective visual assessment of

EIDD-treated wells and the results of the fluorescence assay (CellTox Green) remains enigmatic. It is possible that the agent-associated reduction in cell number in EIDD-treated wells resulted in loss and degradation of nucleic acid necessary for fluorescence binding and detection in the CellTox Green assay. These results suggest that the EIDD compounds may be associated with a greater degree of agent-associated cytotoxicity than the CellTox Green assay results indicate.

#### Quantification of compound inhibition of viral RNA production with monotherapy

An RT-qPCR assay was used to measure each antiviral compound's ability to inhibit coronaviral transcription as monotherapy (viral RNA knock-down assay). Compounds demonstrating the greatest inhibition of FIPV RNA production were GC376 (a 3C-like coronavirus protease inhibitor), GS-441524, EIDD1931 and EIDD2801, the latter three all being nucleoside analogs (Figure 5). Those with the least inhibitory effect on viral RNA transcription include elbasvir, nelfinavir and ritonavir. Ritonavir – a protease inhibitor – is used in combination with lopinavir to treat HIV-1 infection (Kaletra; AbbVie). Lopinavir monotherapy has poor oral bioavailability in

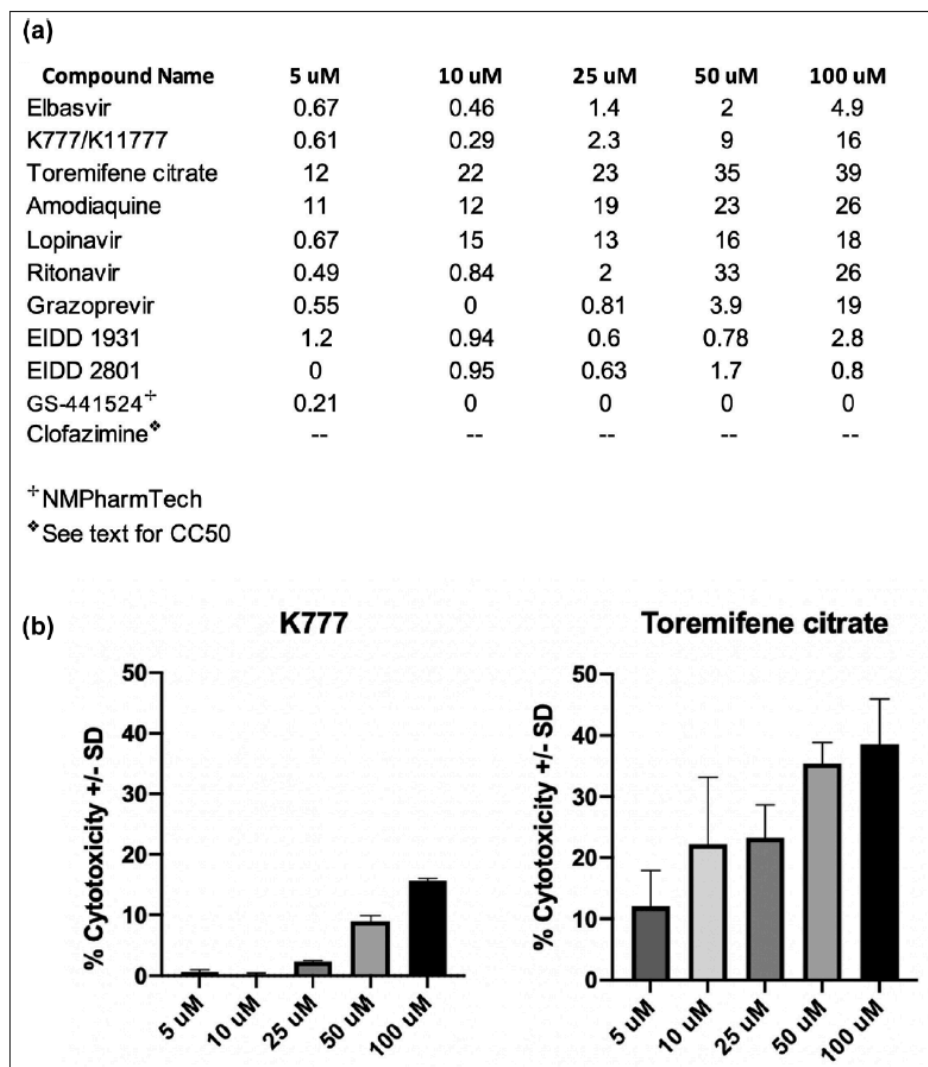


**Figure 4** Cytotoxicity safety profiles and representative graphs. (a) Compounds with demonstrated anti-feline infection peritonitis virus (FIPV) activity and the percent cytotoxicity at 5, 10, 25, 50 and 100  $\mu$ M. (b) Representative percent cytotoxicity bar graphs  $\pm$  SD for two of the compounds with anti-FIPV activity. Percent cytotoxicity values were determined by normalizing cytotoxicity to the positive toxicity control wells (100% cytotoxicity) and untreated Crandell-Rees feline kidney control cells (0% cytotoxicity)

people; however, when used in combination, ritonavir has been demonstrated to markedly improve lopinavir's plasma concentration.<sup>26</sup> Therefore, despite the relatively minimal FIPV inhibition identified with ritonavir as monotherapy, this compound was assessed for combined anticoronaviral efficacy with ritonavir.

#### Quantification of compound inhibition of viral RNA production with cACT

To identify drug combinations with additive or fold-over-additive (synergistic) antiviral activity over monotherapy, combinations of two or more drug compounds were selected based upon: (1) established combinations

used for other viral infections like HIV-1 and HCV; (2) drugs with different mechanisms of action; (3) potential variations in systemic distribution of the compound (eg, predicted ability to penetrate the blood-brain or blood-ocular barriers); and (4) minimal cytotoxicity (based on the CSP). For each cACT, any resulting decrease in FIPV copy number over the calculated additive effect for each drug used as monotherapy was considered to be synergistic (Figure 6).

Owing to the pronounced anti-FIPV activity of GC376, as well as its potential availability for moving forward into in vivo pharmacokinetic studies and clinical applications, this compound was focused on in a series of

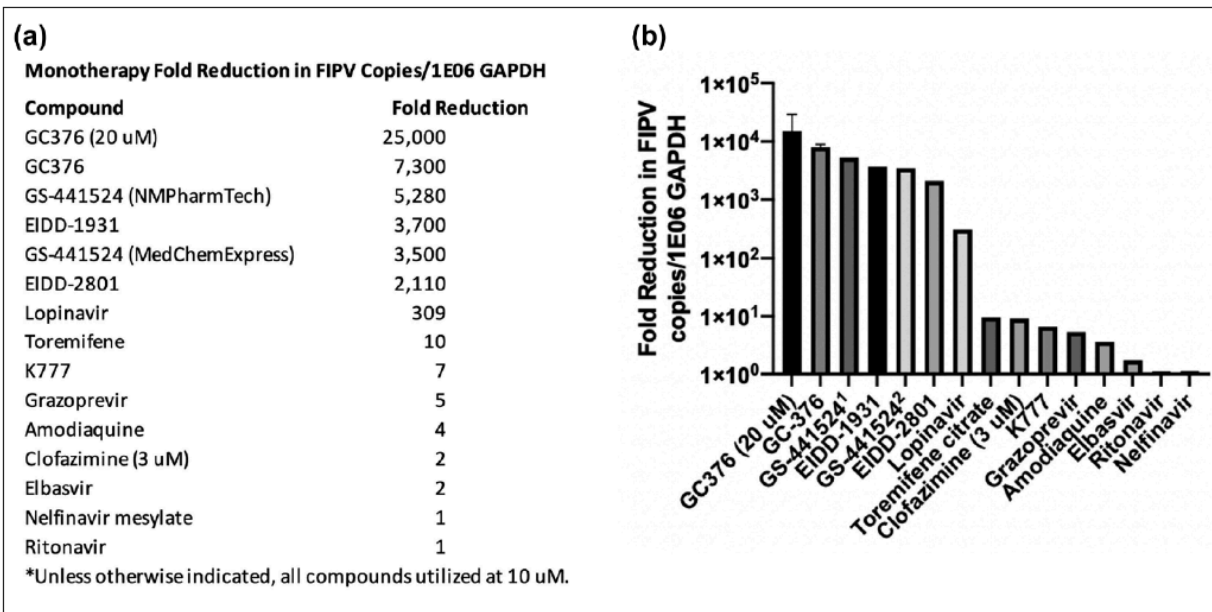


**Figure 5** Fold decrease in feline infectious peritonitis virus (FIPV) RNA copy number using antiviral compounds as monotherapy. (a) FIPV-infected Crandell-Rees feline kidney cells were incubated for 24h with various antiviral compounds. Viral copy number was subsequently determined via quantitative RT-PCR and normalized to feline *GAPDH* copy number, in order to determine the compound's fold decrease effect. All compounds were tested at 10  $\mu$ M unless otherwise specified. All experimental treatments were performed in triplicate wells and the fold decrease calculated by dividing the average experimental, normalized FIPV copy number by the average normalized FIPV copy number determined for untreated, FIPV-infected wells. (b) Graphical representation of fold decrease values in FIPV RNA copy number. Graph bars with SD error bars represent experiments that were repeated. <sup>1</sup>GS-441524 sourced from NMPharmTech (China); <sup>2</sup>GS-441524 sourced from MedChemExpress (China)

mono- and combined viral RNA knock-down assays. Overall, 20  $\mu$ M of GC376 demonstrated superior anti-FIPV activity when used as monotherapy and in combination therapies *in vitro*. Although the combination of elbasvir and lopinavir demonstrated the highest cACT synergy, this combination was ultimately less effective than either GC376 or GS-441524 used as monotherapy. Interestingly, cACT using GC376 or GS-441524 resulted in no or limited detectable synergy.

## Discussion

As there is no currently effective vaccine for FIP, there is an immediate clinical need for effective, affordable and available antiviral treatment options for FIPV-infected cats. Here we describe the *in vitro* screening of 90 compounds, resulting in the identification of 26 antiviral agents with antiviral efficacy against the feline coronavirus, FIPV serotype II. Based on the results of both the plaque and viral RNA inhibition (RT-qPCR) assays, the most effective antiviral compounds that were identified include GC376, GS-441524, EIDD2081 and EIDD2931. Importantly, the agents demonstrating the

least cytotoxicity include GC376 and GS-441524, with no evidence of toxicity up to 100  $\mu$ M.

We also documented antiviral efficacy for combinations of antiviral agents (cACT). A few of the examined drug combinations demonstrated evidence of limited synergistic antiviral activity. cACT synergism, determined using RT-qPCR, was defined as the fold reduction in viral copy number beyond the additive effect (combined reduction in viral copy number for each individual agent). The cACT with the greatest foldover-additive (synergistic) effect was determined to be elbasvir and lopinavir. However, all the cACTs proved to be ultimately less effective than GC376, GS-441524 and both EIDD compounds used as monotherapies. This may be the result of the relative effectiveness of these agents when used as monotherapies in our *in vitro* culture-based systems and an assay-limited inability to identify an antiviral effect beyond a certain level of viral inhibition. Attempts were made to further optimize the detection of compound synergy by modifying the experimental protocol without success. It remains possible that combinations of agents may manifest synergy in *in vivo* studies. In addition,

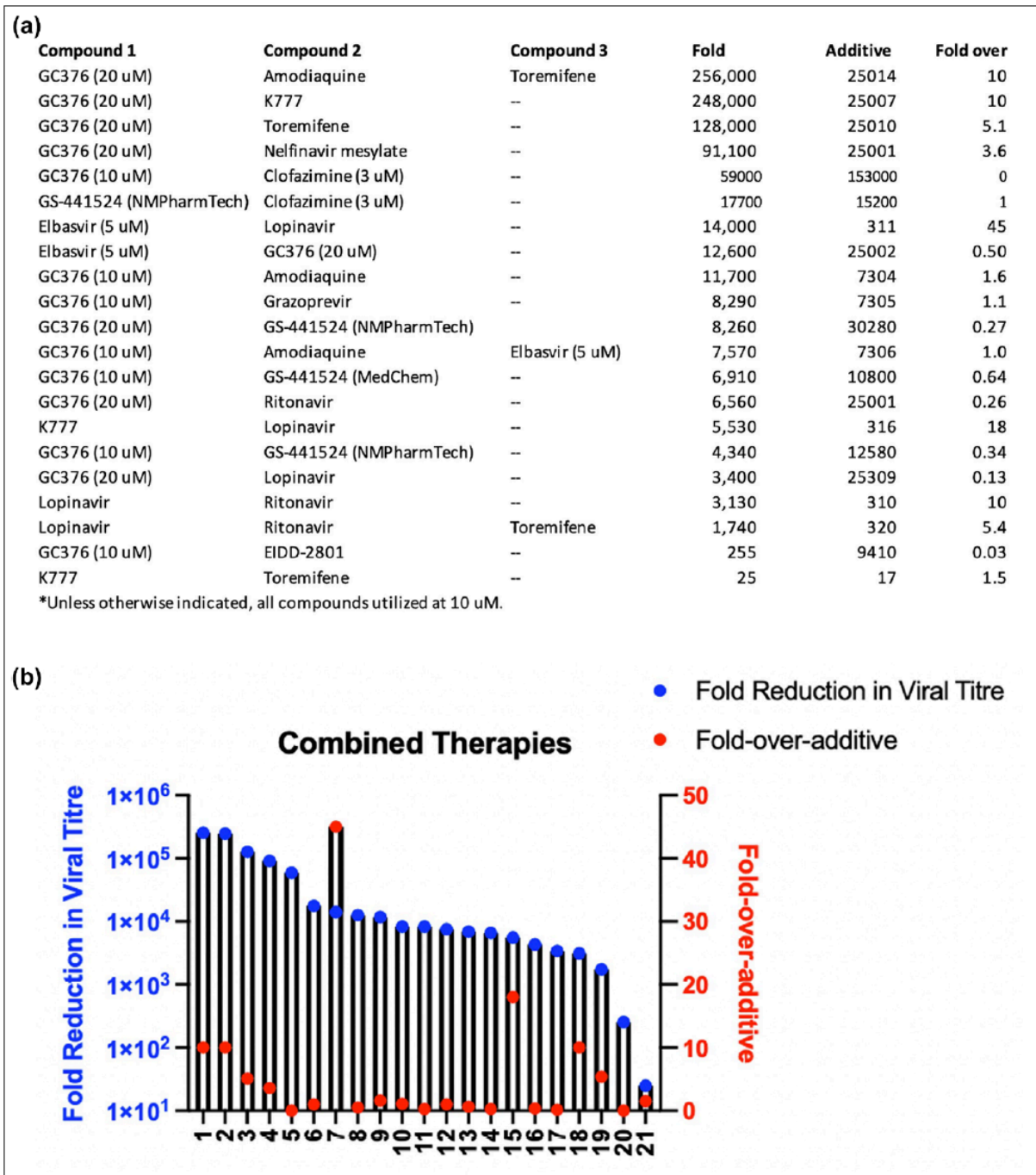


**Figure 6** Additive and foldover-additive reduction in feline infectious peritonitis virus (FIPV) viral RNA copy number using combined anticoronaviral therapy. The expected additive effect reflects the sum of the fold reduction in viral RNA based on each agent used as monotherapy (from Figure 5). (a) List of anti-FIPV combinations with associated fold reduction and foldover-additive reduction in FIPV copies normalized to  $1 \times 10^6$  GAPDH copies. (b) Bar graph demonstrating comparison between overall fold reduction in FIPV copies and foldover-additive values. 1 = GC376 (20  $\mu$ M) + amodiaquine + toremifene; 2 = GC376 (20  $\mu$ M) + K777; 3 = GC376 (20  $\mu$ M) + toremifene; 4 = GC376 (20  $\mu$ M) + nelfinavir mesylate; 5 = GC376 (20  $\mu$ M) + clofazimine (3  $\mu$ M); 6 = GS-441524 (NMPharmTech) + clofazimine (3  $\mu$ M); 7 = elbasvir (5  $\mu$ M) + lopinavir; 8 = elbasvir (5  $\mu$ M) + GC376 (20  $\mu$ M); 9 = GC376 (10  $\mu$ M) + amodiaquine; 10 = GC376 (10  $\mu$ M) + grazoprevir; 11 = GC376 (20  $\mu$ M) + GS-441524 (NMPharmTech); 12 = GC376 (10  $\mu$ M) + amodiaquine + elbasvir (5  $\mu$ M); 13 = GC376 (10  $\mu$ M) + GS-441524 (MCE); 14 = GC376 (20  $\mu$ M) + ritonavir; 15 = K777 + lopinavir; 16 = GC376 (10  $\mu$ M) + GS-441524 (NMPharmTech); 17 = GC376 (20  $\mu$ M) + lopinavir; 18 = lopinavir + ritonavir; 19 = lopinavir + ritonavir + toremifene; 20 = GC376 (10  $\mu$ M) + EIDD-2801; 21 = K777 + toremifene

combinatorial therapy may also serve as a method to prevent the development of antiviral resistance. However, this would require further investigation using long-term culture, viral sequencing and in vivo studies, and is beyond the scope of this study.

Repeated plaque assay data indicated that elbasvir prevented the formation of viral plaques with an impressive  $EC_{50}$  of 0.16  $\mu$ M. However, there was essentially no detectable difference in the viral RNA copy number between infected cells treated with or without elbasvir. Subjective visual analysis of FIPV-infected CRFK cells that were treated with elbasvir revealed evidence of CPE. Interestingly, the treated cells with evidence of CPE did not appear to detach from the culture plate and, as a result, the absorbance values acquired in the plaque assay were comparable to uninfected control wells. This discordant result between the plaquing and viral RNA knock-down assay results suggests that the putative antiviral effect of elbasvir may be downstream of viral transcription (eg, translation, virion assembly and other) and, as a result, elbasvir may reduce overall viral replication but not protect cells from the accumulation of viral RNA and cellular injury.

Prior in vivo clinical successes using GS-441524 or GC376 in cats with experimental and naturally occurring FIP demonstrate that an effective antiviral cure for FIP is an achievable goal. However, therapeutic challenges in treating non-effusive (granulomatous), multisystemic neurologic and ocular FIP remain. A cACT utilizing a compound(s) with effective penetration into these anatomic reservoirs (brain and eye) may be required to achieve a cure in multisystemic FIP. The 3C protease inhibitor GC376 has been demonstrated to be effective in the treatment of experimental FIPV infection but appears to be less effective in treating and eradicating the more chronic neurologic or ocular forms of the disease.<sup>13</sup> Optimizing the dose and administration of GC376 to establish an effective tissue distribution in the brain and eye may improve the overall clinical success of this compound.

## Conclusions

This study reports the screening of 90 putative antiviral agents and the identification of 26 compounds with variable anti-FIPV activity. Further, we designed strategic combinations of efficacious anti-FIPV compounds based on differing antiviral mechanisms of action to determine the presence of additive or synergistic activity. Although evidence of compound synergy was identified, overall, the most effective antiviral compounds were determined to be specific monotherapies, mechanistically featuring either a nucleoside analog or protease inhibitor.

**Supplementary material** The following file is available online:

Figure S1: Complete list of compounds screened for anti-FIPV activity.

**Conflict of interest** The authors declared no potential conflicts of interest with respect to the research, authorship, and/or publication of this article.

**Funding** We are grateful for the generous funding provided by the EveryCat Health Foundation (formerly Winn Feline Foundation – W17-020, W19-026 and W20-003) and the University of California, Davis Center for Companion Animal Health (CCAH) through gifts specified for FIP research by multiple individual donors and organizations (SOCK FIP, Davis, CA, USA) and private foundations (Phillip Raskin Fund, Kansas City, KS, USA).

**Ethical approval** This work did not involve the use of animals and therefore ethical approval was not specifically required for publication in *JFMS*.

**Informed consent** This work did not involve the use of animals (including cadavers) and therefore informed consent was not required. No animals or people are identifiable within this publication, and therefore additional informed consent for publication was not required.

**ORCID iD** Sarah E Cook  <https://orcid.org/0000-0001-8778-9195>

Niels Pedersen  <https://orcid.org/0000-0001-6269-929X>

## References

- 1 Pedersen NC, Liu H, Dodd KA, et al. Significance of coronavirus mutants in feces and diseased tissues of cats suffering from feline infectious peritonitis. *Viruses* 2009; 1: 166–184.
- 2 Vennema H, Poland A, Foley J, et al. Feline infectious peritonitis viruses arise by mutation from endemic feline enteric coronaviruses. *Virology* 1998; 243: 150–157.
- 3 Jaimes JA, Millet JK, Stout AE, et al. A tale of two viruses: the distinct spike glycoproteins of feline coronaviruses. *Viruses* 2020; 12: 83.
- 4 Hohdatsu T, Okada S, Ishizuka Y, et al. The prevalence of types I and II feline coronavirus infections in cats. *J Vet Med Sci* 1992; 54: 557–562.
- 5 Rottier PJM, Nakamura K, Schellen P, et al. Acquisition of macrophage tropism during the pathogenesis of feline infectious peritonitis is determined by mutations in the feline coronavirus spike protein. *J Virol* 2005; 79: 14122–14130.
- 6 Diaz JV and Poma R. Diagnosis and clinical signs of feline infectious peritonitis in the central nervous system. *Can Vet J* 2009; 50: 1091–1093.
- 7 Foley JE, Lapointe JM, Koblik P, et al. Diagnostic features of clinical neurologic feline infectious peritonitis. *J Vet Intern Med* 1998; 12: 415–423.
- 8 Pedersen NC. An update on feline infectious peritonitis: diagnostics and therapeutics. *Vet J* 2014; 201: 133–141.
- 9 Stiles J. Ocular manifestations of feline viral diseases. *Vet J* 2014; 201: 166–173.
- 10 Pedersen NC. A review of feline infectious peritonitis virus infection: 1963–2008. *J Feline Med Surg* 2009; 11: 225–258.

- 11 Hohdatsu T, Yamada M, Tominaga R, et al. Antibody-dependent enhancement of feline infectious peritonitis virus infection in feline alveolar macrophages and human monocytic cell line U937 by serum of cats experimentally or naturally infected with feline coronavirus. *J Vet Med Sci* 1998; 60: 49–55.
- 12 Takano T, Yamada S, Doki T, et al. Pathogenesis of oral type I feline infectious peritonitis virus (FIPV) infection: antibody dependent enhancement infection of cats with type I FIPV via the oral route. *J Vet Med Sci* 2019; 81: 911–915.
- 13 Vennema H, de Groot RJ, Harbour DA, et al. Early death after feline infectious peritonitis virus challenge due to recombinant vaccinia virus immunization. *J Virol* 1990; 64: 1407–1409.
- 14 Pedersen NC, Kim Y, Liu H, et al. Efficacy of a 3C-like protease inhibitor in treating various forms of acquired feline infectious peritonitis. *J Feline Med Surg* 2018; 20: 378–392.
- 15 Murphy BG, Perron M, Murakami E, et al. The nucleoside analog GS-441524 strongly inhibits feline infectious peritonitis (FIP) virus in tissue culture and experimental cat infection studies. *Vet Microbiol* 2018; 219: 226–233.
- 16 Pedersen NC, Perron M, Bannasch M, et al. Efficacy and safety of the nucleoside analog GS-441524 for treatment of cats with naturally occurring feline infectious peritonitis. *J Feline Med Surg* 2019; 21: 271–281.
- 17 Dickinson PJ, Bannasch M, Thomasy SM, et al. Antiviral treatment using the adenosine nucleoside analogue GS-441524 in cats with clinically diagnosed neurological feline infectious peritonitis. *J Vet Intern Med* 2020; 34: 1587–1593.
- 18 Sulejmani N, Jafri SM and Gordon SC. Pharmacodynamics and pharmacokinetics of elbasvir and grazoprevir in the treatment of hepatitis C. *Expert Opin Drug Metab Toxicol* 2016; 12: 353–361.
- 19 Kwo P, Gane EJ, Peng C, et al. Effectiveness of elbasvir and grazoprevir combination, with or without ribavirin, for treatment-experienced patients with chronic hepatitis C infection. *Gastroenterology* 2017; 152: 164–175.
- 20 Zhou Y, Vedantham P, Lu K, et al. Protease inhibitors targeting coronavirus and filovirus entry. *Antiviral Res* 2015; 116: 76–84.
- 21 Dyall J, Coleman CM, Hart BJ, et al. Repurposing of clinically developed drugs for treatment of Middle East respiratory syndrome coronavirus infection. *Antimicrob Agents Chemother* 2014; 58: 4885–4893.
- 22 Nakagawa F, May M and Phillips A. Life expectancy living with HIV: recent estimates and future implications. *Curr Opin Infect Dis* 2013; 26: 17–25.
- 23 Ramakrishnan MA. Determination of 50% endpoint titer using a simple formula. *World J Virol* 2016; 5: 85.
- 24 Erlanson DA. Introduction to fragment-based drug discovery. In: Davies TG and Hyvönen M (eds). *Fragment-based drug discovery and X-ray crystallography*. Berlin: Springer Berlin Heidelberg, 2012, pp 1–32.
- 25 Kim Y, Liu H and Kankanamalage ACG. Reversal of the progression of fatal coronavirus infection in cats by a broad-spectrum coronavirus protease inhibitor. *PLoS Pathog* 2016; 12: e1005531. DOI: 10.1371/journal.ppat.1005531.
- 26 Kumar GN, Jayanti VK, Johnson MK, et al. Metabolism and disposition of the HIV-1 protease inhibitor lopinavir (ABT-378) given in combination with ritonavir in rats, dogs, and humans. *Pharm Res* 2004; 21: 1622–1630.

**Chapter 4: An optimized bioassay for screening combined anticoronaviral compounds for efficacy against feline infectious peritonitis virus with pharmacokinetic analyses of GS-441524, remdesivir, and molnupiravir in cats**

# An Optimized Bioassay for Screening Combined Anticoronaviral Compounds for Efficacy against Feline Infectious Peritonitis Virus with Pharmacokinetic Analyses of GS-441524, Remdesivir, and Molnupiravir in Cats

Sarah Cook <sup>1,\*</sup>, Luke Wittenburg <sup>2</sup>, Victoria C. Yan <sup>3</sup> , Jacob H. Theil <sup>4</sup> , Diego Castillo <sup>1</sup>, Krystle L. Reagan <sup>5</sup> , Sonya Williams <sup>1</sup>, Cong-Dat Pham <sup>3</sup>, Chun Li <sup>3</sup>, Florian L. Muller <sup>6</sup> and Brian G. Murphy <sup>1</sup> 

- <sup>1</sup> Department of Pathology, Microbiology, and Immunology, School of Veterinary Medicine, University of California-Davis, Davis, CA 95616, USA
  - <sup>2</sup> Department of Surgical and Radiological Sciences, School of Veterinary Medicine, University of California-Davis, Davis, CA 95616, USA
  - <sup>3</sup> Department of Cancer Systems Imaging, University of Texas MD Anderson Cancer Center, Houston, TX 77054, USA
  - <sup>4</sup> Office of Research, Campus Veterinary Services, University of California-Davis, Davis, CA 95616, USA
  - <sup>5</sup> Department of Veterinary Medicine and Epidemiology, School of Veterinary Medicine, University of California-Davis, Davis, CA 95616, USA
  - <sup>6</sup> Sporos Bioventures, @JLABS Suite 201, 2450 Holcombe Blvd, Houston, TX 77021, USA
- \* Correspondence: sestevens@ucdavis.edu



**Citation:** Cook, S.; Wittenburg, L.; Yan, V.C.; Theil, J.H.; Castillo, D.; Reagan, K.L.; Williams, S.; Pham, C.-D.; Li, C.; Muller, F.L.; et al. An Optimized Bioassay for Screening Combined Anticoronaviral Compounds for Efficacy against Feline Infectious Peritonitis Virus with Pharmacokinetic Analyses of GS-441524, Remdesivir, and Molnupiravir in Cats. *Viruses* **2022**, *14*, 2429. <https://doi.org/10.3390/v14112429>

Academic Editors: Marina L. Meli and Anja Kipar

Received: 23 September 2022  
Accepted: 28 October 2022  
Published: 1 November 2022

**Publisher's Note:** MDPI stays neutral with regard to jurisdictional claims in published maps and institutional affiliations.



Copyright: © 2022 by the authors. Licensee MDPI, Basel, Switzerland. This article is an open access article distributed under the terms and conditions of the Creative Commons Attribution (CC BY) license (<https://creativecommons.org/licenses/by/4.0/>).

**Abstract:** Feline infectious peritonitis (FIP) is a fatal disease of cats that currently lacks licensed and affordable vaccines or antiviral therapeutics. The disease has a spectrum of clinical presentations including an effusive (“wet”) form and non-effusive (“dry”) form, both of which may be complicated by neurologic or ocular involvement. The feline coronavirus (FCoV) biotype, termed feline infectious peritonitis virus (FIPV), is the etiologic agent of FIP. The objective of this study was to determine and compare the in vitro antiviral efficacies of the viral protease inhibitors GC376 and nirmatrelvir and the nucleoside analogs remdesivir (RDV), GS-441524, molnupiravir (MPV; EIDD-2801), and  $\beta$ -D-N<sup>4</sup>-hydroxycytidine (NHC; EIDD-1931). These antiviral agents were functionally evaluated using an optimized in vitro bioassay system. Antivirals were assessed as monotherapies against FIPV serotypes I and II and as combined anticoronaviral therapies (CACT) against FIPV serotype II, which provided evidence for synergy for selected combinations. We also determined the pharmacokinetic properties of MPV, GS-441524, and RDV after oral administration to cats in vivo as well as after intravenous administration of RDV. We established that orally administered MPV at 10 mg/kg, GS-441524 and RDV at 25 mg/kg, and intravenously administered RDV at 7 mg/kg achieves plasma levels greater than the established corresponding EC<sub>50</sub> values, which are sustained over 24 h for GS-441514 and RDV.

**Keywords:** feline infectious peritonitis; FIPV; coronavirus; antiviral; pharmacokinetics; combined anti-coronaviral therapy

## 1. Introduction

Feline infectious peritonitis (FIP) is a common and generally fatal viral disease of domestic cats caused by various genetic mutants of feline coronavirus (FCoV), collectively referred to as FIP virus (FIPV). Although the complex pathogenesis of FIP remains incompletely understood and involves both pathogen and host factors, FIP disease is thought to result from de novo mutations in the relatively benign coronavirus biotype, feline enteric coronavirus (FECV) [1,2]. A critical switch in viral tropism from intestinal enterocytes to monocytes/macrophages, facilitating systemic spread and inflammation [1,2], results from

these viral mutations. FCoV is also categorized into serotypes I and II, with serotype II evolving as a result of a historic recombination event between FCoV and canine coronavirus (CCoV). This recombination resulted in the stable incorporation of the CCoV *spike* gene within the FCoV genome [3]. The *spike* gene encodes an exposed coronaviral surface protein and serves as a target of antibody production by the infected host [4]. Although FCoVs are currently classified as a single viral species within the *Alphacoronavirus 1* species, given the biological significance of the coronavirus spike protein in host cell tropism and pathogenesis, it has been suggested that the two coronaviral serotypes be considered as distinct viruses [5,6].

The clinical presentation of FIP is a continuum ranging from a predominantly effusive or “wet” form (abdominal or pleural fluid accumulation) to a non-effusive or “dry” form (granulomatous inflammation in organs such as the kidney, brain, eye and lymph nodes) [7]. In both forms of FIP, there may be variable ocular and/or neurologic involvement, although this is less commonly identified with the effusive form [7–9]. Once clinical signs of FIP appear, FIP-associated mortality is high without treatment, with one study reporting an average survival time post-presentation of 21 days for cats with effusive FIP and 38 days for cats with non-effusive FIP [10].

The antiviral compounds GC376 and GS-441524 have been extensively explored in both tissue culture and in vivo studies for their ability to inhibit FIPV replication and to treat cats with experimental or naturally acquired FIP [9,11–17]. Both antiviral agents have variable but generally high success rates in their ability to cure cats with FIP, particularly the effusive form of the disease [9,11–16]. GC376 (Anivive Lifesciences), a 3C-like protease (3CL<sup>Pro</sup>) inhibitor, targets the viral 3CL protease which is also referred to as the main viral protease (M<sup>Pro</sup>). 3CL<sup>Pro</sup> is a cysteine protease and represents an attractive pharmacologic target due to its specific role in viral polyprotein cleavage [17–19]. An initial clinical trial that utilized GC376 in 20 cats with naturally occurring FIP documented remission in seven of the 20 cats [11]. A recent retrospective study found that 29 of 30 cats treated with either GC376 or GS-441524 were clinically cured of FIP [20]. GS-441524 is a nucleoside analog with demonstrated efficacy against feline coronavirus [9,13,14] and SARS-CoV-2 [21,22]. In a study of 10 cats that were experimentally infected with FIPV, GS-441524 treatment resulted in the rapid reversal of clinical signs and disease remission in all 10 cats [14]. In a subsequent clinical trial, 31 cats with naturally occurring FIP were treated with GS-441524, which resulted in 25 of 31 cats healthy and disease free at the time of manuscript publication [13]. A large anecdotal study that surveyed owners of cats with FIP being treated with unlicensed GS-441524 found that 96.7% of the cats (n = 380) were alive at the time of publication and 54.0% of those cats considered cured, while another 43.3% were still being monitored as part of the 12-week observation period [9].

The nucleotide analog remdesivir (RDV), a phosphoramidate prodrug of GS-441524, has been demonstrated to be effective in blocking the replication of multiple families of RNA viruses, including *Coronaviridae* (including SARS-CoV, MERS-CoV, FCoV, SARS-CoV-2) [23–28], *Paramyxoviridae* (including Nipah virus and Hendra virus) [29], and *Filoviridae* (including Ebola virus and Marburg virus) [30]. RDV is currently utilized for the treatment of hospitalized adults and children over 12 years of age infected with SARS-CoV-2 [31]. However, to the authors’ knowledge, there are no peer-reviewed studies describing the in vivo pharmacokinetics of RDV in cats and no published reports evaluating the antiviral efficacy of RDV against FIPV. However, a non-peer reviewed study recently reported that a compounded form of RDV is being successfully and regularly used in Australia via the intravenous (IV) or subcutaneous (SC) route for the treatment of client-owned cats with naturally occurring FIP [32].

Nirmatrelvir is a M<sup>Pro</sup> (or 3CL<sup>Pro</sup>) coronaviral protease inhibitor similar to GC376, which has conditional approval for the treatment of mild to moderate COVID-19 in adults and children over 12 years old [33]. For COVID-19 patients, nirmatrelvir is administered orally in combination with ritonavir, and together are marketed under the name Paxlovid (Pfizer) [33]. The protease inhibitor ritonavir is a cytochrome P450 3A4 (CYP3A4) enzyme

inhibitor, affecting the absorption and metabolism of other protease inhibitors [34]. The use of low-dose ritonavir in combination with other protease inhibitors results in delayed first-pass metabolism and increased dosing intervals for the primary protease inhibitor [35].

The nucleoside analog molnupiravir (MPV; EIDD-2801) has demonstrated anti-coronaviral activity against both FIPV and SARS-CoV-2 [16,36,37]. Although peer-reviewed trials examining the efficacy of MPV in cats with FIP have not been published, the social media group FIP Warriors anecdotally reports that it is highly effective [38]. To our knowledge, there are no peer-reviewed publications documenting the *in vivo* pharmacokinetics in cats. The active metabolite of MPV,  $\beta$ -D-N<sup>4</sup>-hydroxycytidine (NHC; EIDD-1931), has also demonstrated broad-spectrum antiviral activity against multiple coronaviruses, including SARS-CoV-2, MERS-CoV, SARS-CoV-1 [39], multiple bat coronaviruses [39], and FIPV *in vitro* [16].

Some systemic manifestations of FIP, including those with neurologic or ocular involvement, appear to be more difficult to treat, possibly as a result of impaired drug penetration into specific anatomic compartments. However, a study documented successful resolution of disease in 3 of 4 cats with neurological FIP using an escalating dose of GS-441524 [40] and a separate anecdotal study based on owner survey responses reported that 161 of 169 cats with neurological or ocular signs could be successfully treated with GS-441524 [9].

Based on the clinical success of combination therapy for the treatment of certain viral diseases including HIV-1 (e.g., combined antiretroviral therapy or CART) [41] and hepatitis C (e.g., Zepatier, Mavyret) [42,43], it is reasonable to explore combined anticoronaviral therapies (CACT) for the treatment of FIP. In a prior *in vitro* study assessing the efficacy of FIPV antivirals, certain combinations of antiviral drugs demonstrated additive activity against FIPV; however, none of the investigated combinations were more efficacious than GS-441524 or GC376 when used as monotherapy [16]. The study described here builds on the results of this prior study and applies an optimized *in vitro* bioassay for the assessment of combined anticoronaviral efficacy. Here we compare five antiviral agents used as monotherapies and as CACT in *in vitro* screening assays utilizing FIPV serotype I (Black I) and serotype II (WSU-79-1146). Additionally, we performed pharmacokinetic (PK) analyses of MPV (oral), GS-441524 (oral), and RDV (oral, intravenous) in specific pathogen free (SPF) cats *in vivo* to determine a rational feline dosing protocol.

## 2. Materials and Methods

### 2.1. *In Vitro* Propagation of FIPV I and II

Serotype I FIPV strain Black I (GenBank EU186072) and culture adapted *Felis catus* whole fetus 4-Cornell University (FCWF-4 CU) [44] cells were generously donated by Dr. Susan Baker (Loyola University Chicago), originally obtained from Cornell University College of Veterinary Medicine (Dr. Edward Dubovi). Black I virus was propagated in FCWF-4 CU cells, cultured in minimal essential media (MEM; Sigma, St. Louis, MO, USA) with 2% fetal bovine serum (FBS; Gemini Bio, West Sacramento, CA, USA) and viral infectivity quantified using a colorimetric bioassay (median tissue culture infectious dose, TCID<sub>50</sub>) as previously described [45]. FIPV serotype II strain WSU-79-1146 (GenBank DQ010921) was propagated in Crandell-Rees feline kidney cells (CRFK; ATCC, Manassas, VA, USA) in complete Dulbecco's Modified Eagle Medium (DMEM; Gibco, Billings, MT, USA) supplemented with 10% FBS (Gemini Bio) and 1× penicillin/streptomycin (P/S; Gibco). Similar to Black I, viral infectivity was quantified using a colorimetric bioassay (TCID<sub>50</sub>) as previously described [16,45]. Titered virus was aliquoted into 100 or 500  $\mu$ L volumes and stored at  $-80^{\circ}\text{C}$  until further utilized.

### 2.2. Determination of Antiviral Efficacy *In Vitro*

Antiviral compounds were selected based on previous documented efficacy against serotype II FIPV (WSU-79-1146) [14,16,17,46], differing mechanisms of action (nucleoside/nucleotide analog or viral protease inhibitor), and previously documented low to absent evidence of *in vitro* cytotoxicity in feline cells [16]. GC376 was obtained from

Yunjeong Kim (Kansas State University), NHC was sourced from DC Chemicals (dcchemicals.com), and all other antiviral compounds used in the in vitro studies (GS-441524, RDV, nirmatrelvir, and MPV) were sourced from Natural Micron Pharm Tech (NM PharmTech; Tai'an, China). For in vitro experiments, the compounds were received as a powder and stored at 4 °C until reconstituted to 10 mM in DMSO (Sigma Aldrich, St. Louis, MO, USA) and stored at –20 °C.

The half-maximal effective concentration (EC<sub>50</sub>) for each antiviral compound was determined through a colorimetric bioassay to determine the concentration of drug required to obtain 50% of its maximal effect (EC<sub>50</sub>), as a modification of a previously described method [16]. Select FIPV-infected feline cells demonstrate cytopathic effect (CPE), which results in cell injury and loss (or attenuation) of the cell monolayer. Virus-associated CPE can therefore be quantified colorimetrically (loss of absorbance) using a plate reader and can be utilized as a surrogate metric for viral infection. For each assay, a progressive two-fold compound dilution series ranging from 50 to 0.05 μM (10 dilution step series) was performed in tissue culture media [either Minimal Essential Media (MEM)/FBS (FCWF-4 CU cells with Black I) or Dulbecco's MEM/FBS (CRFK cells with WSU-79-1146)]. FCWF-4 CU (Black I) or CRFK cells (WSU-79-1146) were plated in 96-well tissue culture plates at approximately 25,000 cells per well in their respective media (MEM/FBS or DMEM/FBS, respectively), incubated for 24 h, and then infected with either Black I or WSU-79-1146 virus at a multiplicity of infection (MOI) of 0.1 (one infectious virion for every 10 cells). The virus-infected tissue culture plates were incubated for 1 h and then treated with serially diluted antiviral compounds. Control wells included cells only, and cells with virus but no antiviral agents. All experimental treatments were performed in six well replicates. Culture plates were incubated for 72 additional hours at 37 °C in CO<sub>2</sub> incubator, fixed with methanol, stained with crystal violet, and scanned for absorbance at 620 nm using an ELISA plate reader (Softmax Pro, Molecular Devices, Silicon Valley, CA, USA). The absorbance data were graphed and the EC<sub>50</sub> calculated by plotting a non-linear regression equation (inflection point of the dose-response curve) using Prism 9 software (GraphPad, San Diego, CA, USA).

Select antivirals with different mechanisms of action were evaluated for their CACT in blocking the replication of serotype II FIPV (WSU-79-1146). These antiviral combinations included: (i) RDV and GC376, (ii) RDV and nirmatrelvir, and (iii) MPV and nirmatrelvir. Each of these antiviral combinations include a nucleos(t)ide analog (RDV or MPV) along with a viral protease inhibitor (nirmatrelvir or GC376). GS-441524 was not assessed in combination with other compounds as CACT with GS-441524 has been previously reported [16] and this agent faces regulatory challenges with regards to patent protection and advancing to approval for veterinary usage. The combined antiviral efficacy was determined using the colorimetric bioassay and serial 2-fold dilutions of each compound ranging from 50 to 0.05 μM. The EC<sub>50</sub> for the combined therapy and constituent monotherapies were determined concurrently, as described above. To evaluate CACT for evidence of additive or synergistic effect, the compound fractional inhibition was calculated, and synergy calculations were performed with the freely available software program CompuSyn [47]. To calculate fractional inhibition, absorbance data were converted to “viral activity” using cells with no virus as 0% activity and cells with virus only (no drug) as 100% viral activity. Fractional inhibition for each drug concentration (fraction affected) was then calculated as 1-viral activity and used as input for synergy calculations.

### *2.3. Single Dose Pharmacokinetics of Orally Administered MPV, GS-441524, and RDV and Intravenously Administered RDV*

A series of in vivo PK studies to determine the feline-specific pharmacokinetics and metabolism of orally administered MPV, GS-441524, and RDV as well as intravenously administered RDV were performed in healthy, specific pathogen free (SPF) cats sourced from the University of California, Davis' (UC Davis) Feline Nutrition and Pet Care Center. UC Davis is an AAALAC International accredited institution (#000029), and all experi-

mental procedures were approved by the University's Institutional Animal Care and Use Committee (UC Davis IACUC #22839 and #22483). Powdered MPV and GS-441524 was sourced from NM Pharmtech, powdered RDV was sourced from MedKoo Biosciences (Morrisville, NC, USA), and the commercially available intravenous formulation of RDV (Veklury<sup>®</sup>, Gilead, Foster City, CA, USA) was utilized for the RDV IV PK study.

Fasted male cats (N = 3 per group) were enrolled per study and were weighed within 24–48 h prior to receiving the study drug to ensure dosing accuracy. Study drugs were administered at the following doses: 10 mg/kg MPV, 25 mg/kg GS-441524, 25 mg/kg RDV (oral), and 7 mg/kg RDV (IV). Orally administered MPV was formulated as excipient-less powder in size 4 gelatin capsules (Spectrum Scientific, Irvine, CA, USA). Orally administered GS-441524 and RDV were formulated as tightly packed powders in gelatin capsules (size 5, XPRS Nutra). Powdered drug was weighed using Fisherbrand weighing paper and a Metler Toledo AX105 DeltaRange scale, and then transferred with a spatula into capsules.

For intravenously administered RDV, pharmaceutical-grade Veklury<sup>®</sup> (lyophilized powder, 100 mg per vial) was reconstituted in 19 mL of sterile water and diluted to 5 mg/mL in 0.9% saline prior to slow bolus administration per manufacturer's instructions over five minutes [48,49]. All cats were male and approximately 1.5 years old.

For all PK studies, a physical examination was performed on each cat at study initiation (timepoint zero). For orally administered MPV, approximately 2.5 mL of whole blood was obtained from a peripheral vein prior to compound administration (time point 0) to establish a baseline complete blood count and serum biochemistry analysis panel for the MPV study. These panels were repeated 48 h post-MPV administration to assess for acute toxicity. After blood collection, the cat was administered an oral gelatin capsule containing the study drug and then mildly sedated with dexmedetomidine (10–40 µg/kg), butorphanol (0.1–0.4 mg/kg), ketamine (1–3 mg/kg), and midazolam (0.1–0.4 mg/kg) administered subcutaneously. Approximately 0.5–1 mL of whole blood was collected at each of the following time points: 0.25, 0.5, 1, 1.5, 2, 3, 6, 9, 12, and 24 h post-administration of MPV. After the 15-min blood collection, an IV catheter was placed into a cephalic vein, secured in place, and flushed with heparinized saline. For the MPV study, one cat (20-024) required a second peripheral blood collection at the 30 min time point due to the IV catheter not being in place or functional at that time point. For all PK studies, after catheter placement, a heparin lock of 0.1 mL of a 10,000 USP per mL solution was placed. At this time, the sedation was reversed with atipamezole intramuscularly (IM) and recovery took approximately 20 min. Prior to all blood collections, approximately 0.5 mL of blood was collected and discarded to remove the heparin lock. After each blood sample was collected, a fresh 0.1 mL heparin lock was placed into the catheter. Blood collection at the 24 h time point was collected via manual restraint and from the jugular vein.

For orally administered MPV, at each collection time point the blood sample was incubated for 5 min at room temperature to allow for clotting and then centrifuged at 12,000× g for 10 min to separate the serum fraction from the blood cells. One hundred microliters of serum were aliquoted into a 1.5 mL microcentrifuge tube containing 300 µL of acetonitrile to halt compound metabolism by serum esterases and immediately placed in an insulated container with dry ice for temporary storage and freezing. Samples were subsequently stored at –80 °C prior to liquid chromatography tandem-mass spectrometry (LCMSMS) analysis.

GS-441524 is the main systemically circulating metabolite of RDV [48,50] and was thus quantified in plasma for both GS-441524 and RDV studies. For orally administered GS-441524 and RDV, approximately 0.5–1 mL of whole blood was collected at the following timepoints: 0.5, 1, 3, 6, 8, and 24 h post-dose. The encapsulated study drug was orally administered at timepoint zero and then each cat immediately sedated with a combination of ketamine (1–3 mg/kg), butorphanol (0.1–0.4 mg/kg), and midazolam (0.1–0.4 mg/kg) followed by catheter placement. For intravenously administered RDV, approximately 0.5–1 mL of whole blood was collected at the following timepoints: 0.0833, 0.5, 1, 3, 6, 8, and 24 h post-dose. The cats were immediately sedated, followed by catheter placement, and

then IV RDV was administered. Whole blood sampled at each time point was centrifuged at  $500\times g$  for 5 min, the plasma transferred to a clean 1.5 MCT tube, and centrifuged a second time at  $1000\times g$  for 5 min. The resulting plasma was stored at  $-20\text{ }^{\circ}\text{C}$  prior to LCMSMS analysis.

#### 2.4. LCMSMS Quantitation of Serum MPV Concentrations and Pharmacokinetic Analysis

Analysis of serum MPV and its main metabolite, NHC (EIDD-1931), was performed by modification of a previously validated and published method for human samples [51]. Briefly, stock solution of MPV (EIDD-2801; NM Pharmtech, 99.0% purity) and NHC (EIDD-1931; MedChemExpress, Monmouth Junction, NJ, USA, 99.73% purity) were prepared at 2 mg/mL in methanol and stored at  $-80\text{ }^{\circ}\text{C}$ . Stock solutions were further diluted in methanol to produce calibration standards for a low concentration curve at 1, 5, 10, 50, and 100 ng/mL of MPV and NHC combined and a high concentration curve at 250, 500, 750, 1000, 2500 and 5000 ng/mL of NHC alone. Calibration curves were generated by fortification of blank feline serum obtained from the clinical pathology laboratory at the UC Davis Veterinary Teaching Hospital (pooled from 6 individuals). Quality control samples were generated at 10 and 100 ng/mL (MPV and NHC combined) and at 500 ng and 2500 ng (NHC only). Calibrator and QC serum samples (100  $\mu\text{L}$ ) were added to 300  $\mu\text{L}$  acetonitrile (as was done for samples in the *in vivo* PK study) and then all calibrators, QCs and unknown samples were vortex mixed for 5 min followed by centrifugation at  $10,000\times g$  for 5 min at  $4\text{ }^{\circ}\text{C}$ . After centrifugation, 275  $\mu\text{L}$  of supernatant was removed, transferred to clean 2 mL microcentrifuge tubes, and evaporated to dryness (approximately 1 h) in a SpeedVac (Eppendorf, Hamburg, Germany). Samples were reconstituted in 100  $\mu\text{L}$  of starting HPLC mobile phase (98% 1 mM ammonium acetate pH 4.3 and 2% acetonitrile containing 1 mM ammonium acetate). For analysis, 5  $\mu\text{L}$  was injected into the LC-MS/MS system.

#### 2.5. Mass Spectrometry and Liquid Chromatography Conditions

Negative ion electrospray ionization mass spectra were obtained on a Sciex 6500+ Q-TRAP triple quadrupole mass spectrometer (AB Sciex LLC, Framingham, MA, USA) with a turbo ionspray source coupled to the Sciex ExcionLC™ UHPLC system with a cooled ( $15\text{ }^{\circ}\text{C}$ ) autosampler. Chromatographic separation was carried out on a Luna® Phenyl-hexyl 3.0  $\mu\text{m}$  column ( $50\times 2.0\text{ mm}$ ) with a filter frit guard column (both from Phenomenex, Inc., Torrance, CA, USA). A gradient mobile phase was employed consisting of 1 mM ammonium acetate pH 4.3 (mobile phase A) and acetonitrile containing 1 mM ammonium acetate (mobile phase B). Separation was carried out by holding mobile phase B constant at 2% for 1.2 min, increasing linearly to 90% at 2.2 min, holding at 90% until 3.5 min, decreasing linearly back to 2% from at 3.75 min and equilibrating at 2% until 5.0 min. Analytes were identified by monitoring the ion transitions for MPV ( $m/z$  328.1  $\rightarrow$  126.0 and 168.1) and for NHC ( $m/z$  257.9  $\rightarrow$  125.9 and 107.9). Quantitation was performed by linear regression of analyte peak areas in unknown samples with calibrator samples using  $1/x^2$  weighting.

#### 2.6. LC-MS/MS Quantification of GS-441524 in Plasma

Plasma levels of GS-441524 were analyzed at Covance, Inc. (Princeton, NJ, USA) on a fee-for-service basis using a liquid chromatography mass spectrometry (LC-MS/MS) assay described previously [48]. Briefly, For plasma samples, a 25  $\mu\text{L}$  aliquot was treated with 200  $\mu\text{L}$  of 100% acetonitrile with 20 nM 5-(2-aminopropyl)indole (5-IT; as the internal standard). Samples were filtered through an Agilent Captiva 96-well 0.2  $\mu\text{m}$  filter plate. Filtered samples were then dried down completely for approximately 30 min and reconstituted with 250  $\mu\text{L}$  water. A 10  $\mu\text{L}$  aliquot was then injected for LC-MS/MS analysis. Analytes were separated on a Phenomenex Synergi Hydro-RP 30A column (150  $\text{\AA}$ ~2.0 mM, 4.0  $\mu\text{m}$ ) at  $25\text{ }^{\circ}\text{C}$  using a Waters Acquity Ultra Performance LC (Waters Corporation, Milford, MA, USA), a flow rate of 0.26 mL/min, and a gradient from mobile phase A (Water containing 0.2% formic acid) and 1% mobile phase B (acetonitrile/water, 95:5, containing 0.2% formic

acid) over 4.5 min. MS/MS analyses used a Waters Xevo TQ-S triple quadrupole mass spectrometer (Waters Corporation) with a electrospray probe and analytes were detected in positive ion mode with a multiple reaction monitoring (MRM) method ( $m/z$  292→163 for GS-441524 and 393 → 261 for 5-IT). Plasma concentrations were determined using an 8-point calibration curve spanning a concentration range of over three orders of magnitude (6.9 to 3430 nM). Quality control samples were run at the beginning and end of the run to ensure accuracy and precision within 20%.

### 2.7. Pharmacokinetic Analysis

Pharmacokinetic parameters for both MPV and NHC were examined following oral dosing of MPV and were estimated by noncompartmental analysis using the commercially available software program Phoenix WinNonlin v8.3 (Certara Inc., Princeton, NJ, USA) and estimation of  $T_{1/2}$  was made using three to four timepoints. For GS-441524 and RDV studies, data from all were analyzed using PKSolver 2.0 using non-compartmental parameters using two elimination timepoints and graphs were generated using GraphPad Prism 8.

## 3. Results

### 3.1. All of the Antiviral Agents Effectively Block the In Vitro Replication of Both Serotype I and II FIPV as Monotherapies

A plate-based colorimetric bioassay was used to determine the antiviral  $EC_{50}$  values for the nucleoside analogs GS-441524, RDV, MPV, NHC, and the protease inhibitors GC376 and nirmatrelvir against both FIPV I and II. Used as monotherapies, all of the tested compounds were determined to be potent inhibitors of FIPV I and II replication with  $EC_{50}$  values close to 1  $\mu$ M or less (Figure 1). GC376 was determined to be the compound with the lowest  $EC_{50}$  (highest antiviral efficacy) for FIPV I (0.01  $\mu$ M) while the NHC had the lowest  $EC_{50}$  for FIPV II FIPV (0.11  $\mu$ M). All of the tested antiviral compounds consistently demonstrated lower  $EC_{50}$  values for FIPV I relative to FIPV II with nirmatrelvir demonstrating the greatest differential efficacy (nearly 100-fold). Evidence of CPE was not identified in the control wells (cells only) and marked CPE (clearance of the well monolayer) was identified within wells with cells and virus only (no antiviral agent).

### 3.2. Select Antiviral Agents Have a Synergistic Effect When Used in Combination

Individual antiviral combinations were selected based on differing mechanisms of action (e.g., nucleoside analog paired with a protease inhibitor). NHC (EIDD-1931) was not utilized in combination antiviral assessment based on a progressive reduction in absorbance (presumed cytotoxicity) appreciated above 1.5  $\mu$ M in the monotherapy assessment above (Figure 1, NHC).  $EC_{50}$  values were as follows: (A) nirmatrelvir alone—1.313  $\mu$ M, MPV alone—0.693  $\mu$ M, nirmatrelvir combined with MPV—0.5640  $\mu$ M. (B)  $EC_{50}$  values: GC376 alone—0.406  $\mu$ M, remdesivir alone—0.181  $\mu$ M, GC376 combined with remdesivir—0.046  $\mu$ M. (C)  $EC_{50}$  values: remdesivir alone—6.416  $\mu$ M, nirmatrelvir alone—2.936  $\mu$ M, and RDV combined with nirmatrelvir—1.670  $\mu$ M (Figure 2, left column).

Similarly, fractional inhibition curves are shifted left for every drug combination evaluated except for nirmatrelvir combined with RDV between 1 and 2  $\mu$ M (Figure 2, middle column). Further, these curves show that the combination of GC376 and remdesivir reached almost complete fractional inhibition at the lower range of compound concentration, nirmatrelvir combined with MPV only reached approximately 50% fractional inhibition, and nirmatrelvir combined with RDV approached 100% fractional inhibition at approximately 2.5  $\mu$ M.

Compound synergy was calculated and determined to be present for the following antiviral combinations: (1) nirmatrelvir with MPV, (2) GC376 with RDV, and (3) nirmatrelvir with RDV. Synergy was indicated by combination index (CI) values of <1 for the three antiviral combinations (Figure 2, right column).

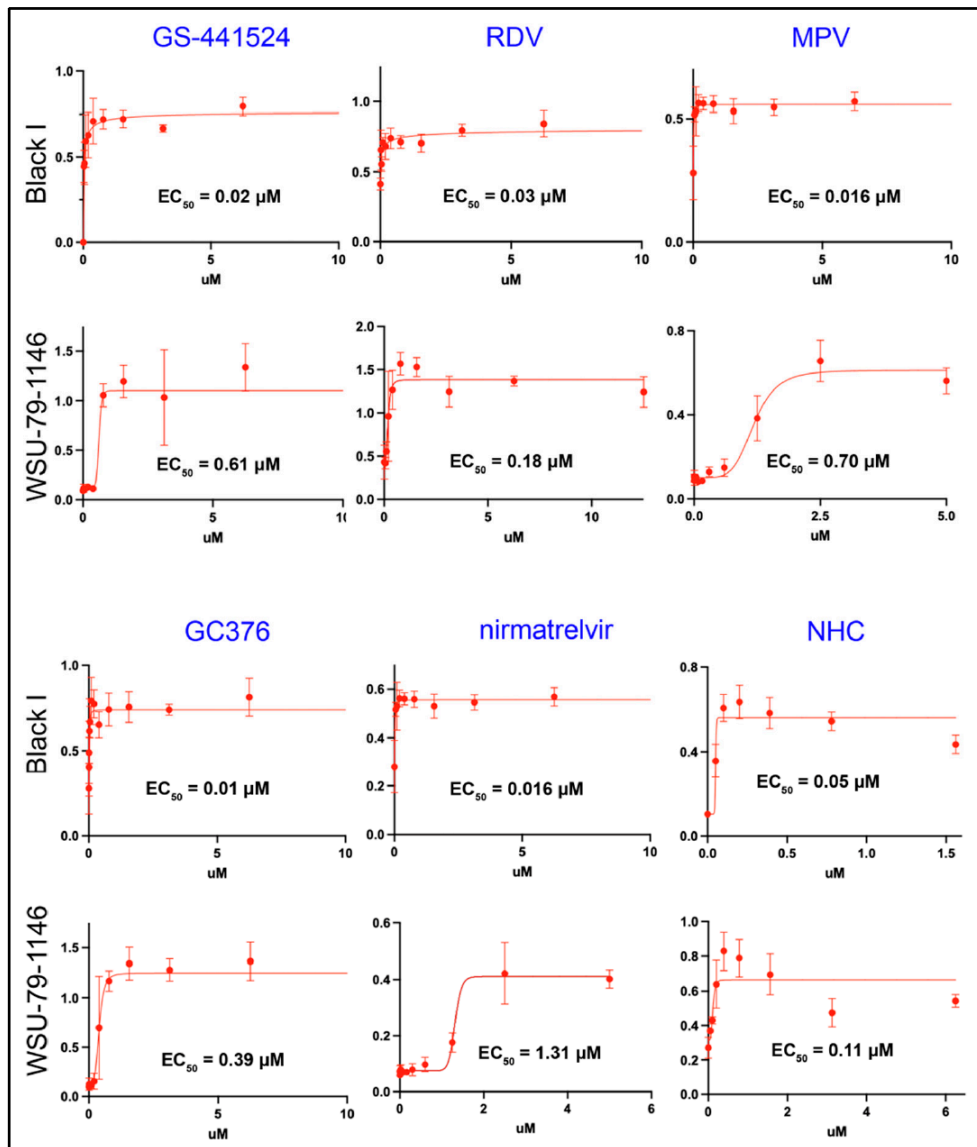


**Figure 1.** Compound inhibition of serotype I and II FIPV as monotherapies. Half-maximal effective concentration ( $EC_{50}$ ) values for the tested nucleoside analogs and protease inhibitors against either Black I (serotype I FIPV) or WSU-79-1146 (serotype II FIPV) and corresponding non-linear regression analyses; all plate absorbance values obtained at 620 nm. For each compound concentration, the absorbance value is the mean of 6 independent wells and error bars reflect the standard deviation. Serial dilutions of each compound were performed to determine the  $EC_{50}$ .

### 3.3. Pharmacokinetics of Oral MPV in Cats

An abbreviated method validation was performed to ensure the method adapted from human plasma was reproducible in feline serum. Blank feline serum did not have a signal at the retention time for the analytes. The calibration curve ( $n = 11$  non-zero concentrations) was linear with an  $r > 0.99$  and accuracy of each concentration within 10% of nominal. The quality control (QC) samples had accuracies within 15% of nominal and precision of calibrators and QC samples was within 10%. A single freeze–thaw cycle was performed at 50 ng/mL (NHC and MPV) and 1000 ng/mL (NHC) and demonstrated stability of NHC and MPV (when combined with acetonitrile) in feline serum with calculated concentrations within 5% of original concentration.

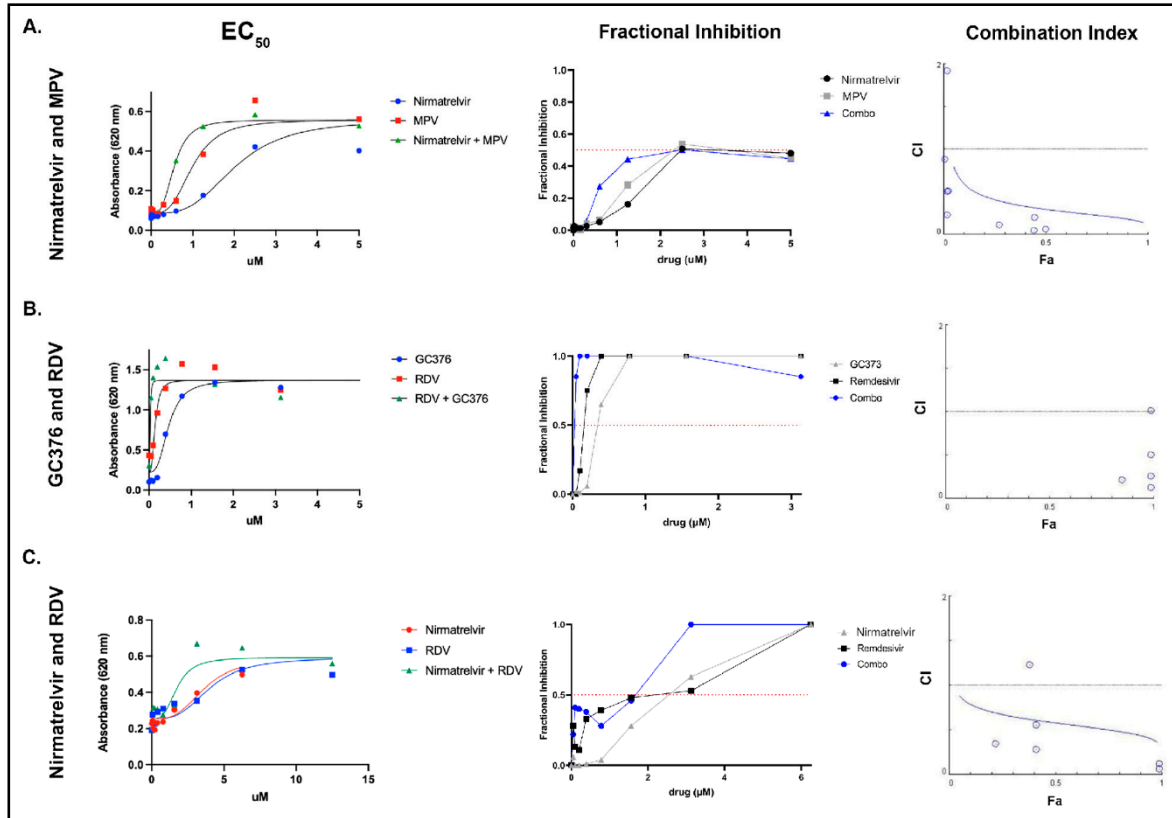


**Figure 2.** EC<sub>50</sub>, fractional inhibition values, and isobologram plots (combination index) representing the three evaluated compound combinations. Left column visually demonstrating individual nonlinear regression curves overlain with combination nonlinear regression curves for the three listed combinations. EC<sub>50</sub> values: (A) Nirmatrelvir alone—1.313 μM, MPV alone—0.693 μM, nirmatrelvir combined with MPV—0.5640 μM. (B) GC376 alone—0.406 μM, remdesivir alone—0.181 μM, GC376 combined with remdesivir—0.046 μM. (C) remdesivir alone—6.416 μM, nirmatrelvir alone—2.936 μM, and RDV combined with nirmatrelvir—1.670 μM. The middle column shows fractional inhibition curves demonstrating the increased fractional inhibition for antiviral combinations at the corresponding drug concentrations. The right column includes isobologram plots that illustrate CI values generally below 1 for all three antiviral compounds, consistent with compound synergy (horizontal line). Fraction affected (Fa) shown on x axis.

We found no evidence of MPV-associated acute organ toxicity in any of the cats based on the pre- and post-treatment complete blood count (CBC) and serum biochemistry panels (Supplementary Tables S1–S3). However, all three of the MPV-treated cats demonstrated variable signs of nausea, including hypersalivation and/or vomiting, after oral administration of MPV (10 mg/kg). Cat 20-024 demonstrated hypersalivation at 1.5 h post administration, had a small amount of vomitus at 2 h, and maintained hypersalivation until 3 h post-administration, at which point the cat regained an appetite. Cat 20-025 exhibited lip licking between 1.5- and 2-h post-administration and lacked an appetite until approximately 6 h post-administration. Cat 20-031 had marked hypersalivation at 1-h post-administration and regained an appetite at 5.5 h post-administration of MPV.

The MPV prodrug was detected in the serum of all three cats at low levels in the first 12 h post-administration while the NHC metabolite was detected at much higher concentrations between 12 to 24 h post-administration. Marked variability in detected NHC levels was present between individual cats (Figure 3A). For cat 20-024, the peak detection level for NHC and MPV occurred at the 3-h time point with NHC detected at

a 10-fold greater level than MPV. For cat 20-031, peak detection levels occur at the 1.5-h time point, with MPV nearly 100-fold below NHC. The peak detection levels occurred for cat 20-025 at the 9-h time point with NHC detected nearly 100-fold over MPV. NHC was more consistently and quantifiably detected over the 24-h time period, aside for cat 20-031, for which NHC was no longer detected (based on limit of detection) after 12 h post-administration. MPV, however, was not consistently detected at the early time points nor after the 12-h time point.

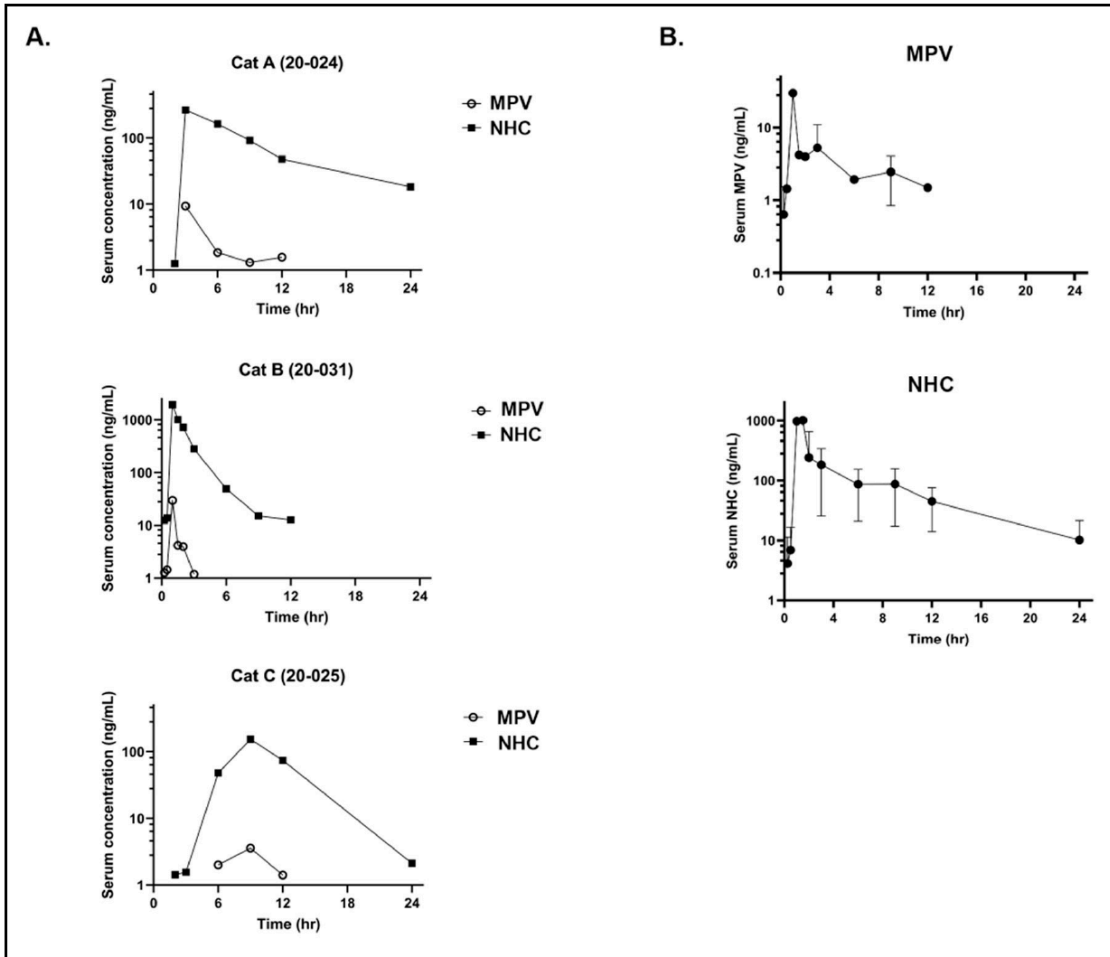


**Figure 3.** Serum detection of prodrug MPV and the metabolite NHC over a 24-h time period in cats. (A) Detection of MPV and NHC in the serum (ng/mL) of each individual cat over 24 h. (B) Combined detection of MPV and NHC in three cats over 24 h.

In aggregate, the data for the three cats (Figure 3B) indicate that peak detection time points for MPV and NHC occur at approximately 1.5 and 2 h post MPV administration. MPV was not detected after the 12-h time point, consistent with rapid metabolic conversion to NHC in vivo.

For orally administered MPV at 10 mg/kg, the PK parameters for the parent drug (MPV) showed a mean maximal concentration of drug in plasma ( $C_{max}$ ) of 14.237 ng/mL (0.043  $\mu$ M; SD  $\pm$  13.781) and an average exposure [measured as area under the curve ( $AUC_{0-t}$ ) where t = last measurable concentration] value of 27.546 h\*ng/mL (0.085  $\mu$ M\*h) (Table 1).

**Table 1.** Pharmacokinetic parameters for parent drug (MPV) from noncompartmental analysis following a 10 mg/kg oral dose of molnupiravir in three cats.

Cat ID	C <sub>max</sub> (ng/mL; μM)	AUC (h*ng/mL)	Vz/F (L/kg)	Cl/F (L/h/kg)	MRT (h)
20-024	9.3 (0.03)	39.6	1101.7	209.0	4.4
20-025	3.6 (0.01)	21.7	1229.4	381.8	8.1
20-031	29.8 (0.09)	21.4	312.4	449.6	1.2
Mean	14.2 (0.04)	27.5	881.1	346.8	4.6
SD	13.8	10.4	405.5	101.3	3.4

C<sub>max</sub>: maximum serum concentration; AUC: area under the MPV serum concentration-time curve; Vz (apparent volume of distribution) and Cl (apparent clearance) are reported as Vz/F and Cl/F as only oral dose data were collected. MRT: mean residence time.

For orally administered MPV at 10 mg/kg, the PK parameters for the NHC metabolite demonstrated an average plasma C<sub>max</sub> of 790 ng/mL (3.05 μM; SD ± 1006) at a corresponding average time of maximum concentration (T<sub>max</sub>) of 4.3 h with an average AUC value of 1779.7 h\*ng/mL (6.87 μM\*h) (Table 2). In all three cats, serum exposure reached levels greater than the NHC EC<sub>50</sub> (0.05 μM for Black I, which is equivalent to 12.9 ng/mL) early in the 24-h time period, and in one cat fell to approximately the level of the EC<sub>50</sub> by the 12-h time point.

**Table 2.** Pharmacokinetic parameters for metabolite (NHC) from noncompartmental analysis following a single 10 mg/kg dose of molnupiravir in three cats.

Cat ID	C <sub>max</sub> (ng/mL; μM)	T <sub>max</sub> (h)	K <sub>el</sub> (1/h)	T <sub>1/2</sub> (h)	AUC (h*ng/mL)	MRT (h)
20-024	265 (1.02)	3.0	0.12	6	1709.47	8.33
20-025	154 (0.15)	9.0	0.29	2.4	950.03	10.51
20-031	1950 (7.52)	1.0	0.26	2.65	2679.57	2.46
Mean	790 (3.05)	4.3	0.2	3.1	1779.7	7.1
SD	1006	4.2	0.1	1.2	866.9	4.2

K<sub>el</sub>: terminal elimination rate; T<sub>1/2</sub>: half-life. Half-life is reported as the harmonic mean and pseudo standard deviation.

### 3.4. Pharmacokinetics of GS-441524 after Administration of GS-441524 or RDV in Cats

No clinical abnormalities were noted in the GS-441524 or IV RDV group. However, mild ptialism, nausea, and lethargy were observed in 2 of 3 cats after oral RDV treatment; these symptoms eventually subsided, and the cats were determined to be clinically normal by the end of the day (~12 h later).

Across all treatment groups, plasma levels of GS-441524 were high (Figure 4). In the oral GS-441524 cohort, plasma concentrations reached an average C<sub>max</sub> value of 10,290 ng/mL (35 μM) (Table 3). The time-of-maximum concentration (T<sub>max</sub>) occurred at 3 h for two of the cats; however, one cat exhibited a T<sub>max</sub> at 8 h, which could be attributed to fractious behavior during dose administration. Drug exposure was AUC<sub>0-24</sub> of 89,708 h\*ng/mL (308 μM\*h) and a 24 h concentration (herein referred to as C<sub>24</sub>) of approximately 664 ± ng/mL (2.3 ± 1.4 μM).

In the oral RDV cohort, GS-441524 exhibited an average plasma C<sub>max</sub> of 2480 ng/mL (7.9 μM) at a corresponding T<sub>max</sub> of 6 h. The average AUC<sub>0-24</sub> value was found to be 32,038 h\*ng/mL (110 μM\*h; average C<sub>24</sub> = 302 ± 75.7 ng/mL, 1 ± 0.26 μM) (Table 4). Finally, in the IV RDV cohort, GS-441524 exhibited an average plasma C<sub>max</sub> of 2003 ng/mL (6.9 μM) at a corresponding T<sub>max</sub> of 0.83 h and an average AUC<sub>0-24</sub> value of 131,645 h\*ng/mL (45 μM\*h; average C<sub>24</sub> = 64 ± 32 ng/mL, 0.22 ± 0.11 μM) (Table 5). In general, plasma exposure to GS-441524 was above the EC<sub>50</sub> for all treatment groups, with 0.22–2 μM of GS-441524 remaining 24 h post-treatment. Average percent oral bioavailability (F%) of

GS-441524 when either GS-441524 or RDV were orally administered was high, exceeding that observed for IV administered GS-441524 (Tables 3 and 4) [14].

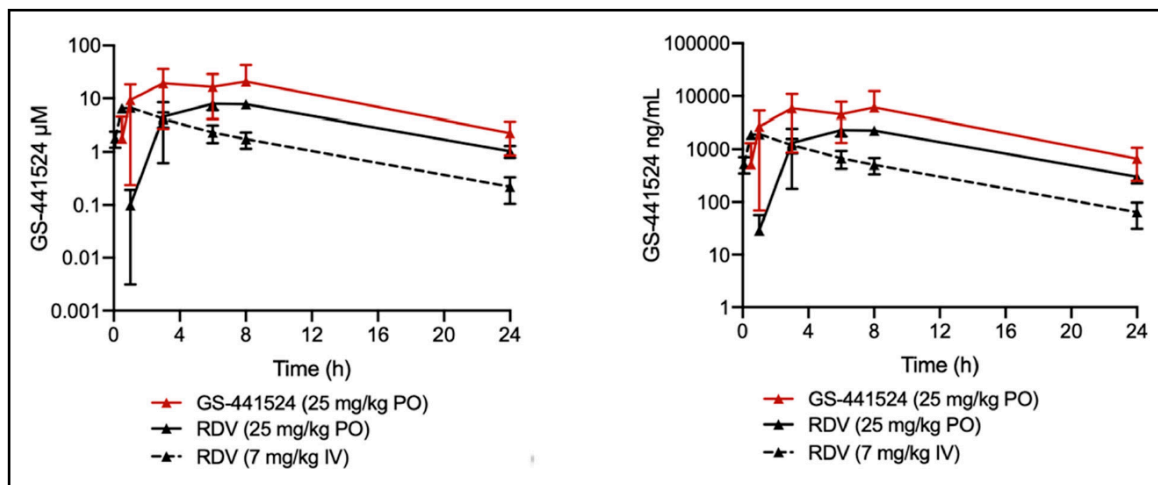


**Figure 4.** Detection of the metabolite, GS-441524, in the plasma of cats administered either oral GS-441524 (25 mg/kg, red line), oral RDV (25 mg/kg, solid black line), or intravenous RDV (7 mg/kg, dashed black line) over 24 h. Data are shown as the mean  $\pm$  SD (N = 3) per drug cohort.

**Table 3.** Pharmacokinetic parameters for GS-441524 after a single oral dose of GS-441524 (25 mg/kg) in 3 cats.

Cat ID	C <sub>max</sub> (ng/mL; $\mu$ M)	T <sub>max</sub> (h)	T <sub>1/2</sub> (h)	AUC (h*ng/mL)	F% *
20-036	13,300 (45.66)	8	4.5	132,232	235
20-044	9100 (31.24)	3	8.8	54,756	100
20-046	8470 (29.08)	3	5.6	82,135	145
Mean	10,290 (35.33)	4.7	6.3	89,708	160
SD	2625 (9.01)	2.9	2.2	39,028	69

\* Relative to 5 mg/kg IV GS-441524 [14].

**Table 4.** Pharmacokinetic parameters for GS-441524 after a single oral dose of RDV (25 mg/kg) in 3 cats.

Cat ID	C <sub>max</sub> (ng/mL; $\mu$ M)	T <sub>max</sub> (h)	T <sub>1/2</sub> (h)	AUC (h*ng/mL)	F% *
20-003	2100 (7.21)	8	5.9	31,747	120
20-024	2390 (8.21)	8	4.6	28,252	103
20-031	2950 (10.13)	6	6.0	36,116	137
Mean	2480 (8.51)	7.3	5.5	32,038	120
SD	432 (1.48)	1.2	0.8	4077	17

\* Relative to 5 mg/kg IV GS-441524 [14].

**Table 5.** Pharmacokinetic parameters for GS-441524 after a single IV dose of RDV (7 mg/kg) in 3 cats.

Cat ID	C <sub>max</sub> (ng/mL; $\mu$ M)	T <sub>max</sub> (h)	T <sub>1/2</sub> (h)	AUC (h*ng/mL)
20-045	1730 (5.94)	0.5	5.3	14,271
21-001	1960 (6.73)	1	5.7	15,291
21-004	2320 (7.97)	1	4.5	99,312
Mean	2003 (6.88)	0.83	5.2	131,645
SD	297 (1.0)	0.29	0.6	2854

#### 4. Discussion

Through a series of in vitro assays, these data demonstrate the feasibility of CACT for the treatment of FIP in cats based on evidence of synergy in select antiviral combinations in vitro. We have also provided data on the in vivo pharmacokinetics and metabolism in cats of MPV administered orally, GS-441524 administered orally, and RDV administered orally or intravenously. Further, we have documented the in vivo detection of the MPV active metabolite, NHC, over a 24-h time period.

A selection of antiviral compounds (nucleoside analogs and viral protease inhibitors) with either previously determined evidence of antiviral efficacy against FIPV serotype II or promising anecdotal evidence of antiviral efficacy were comparatively evaluated using an in vitro colorimetric plate bioassay in order to determine efficacy against FIPV serotype I (Black I) and serotype II (WSU-79-1146) [11,13,14,16]. We found that all of the evaluated compounds, with the exception of nirmatrelvir, had EC<sub>50</sub> values below 1 μM when tested against FIPV serotype II (WSU-79-1146). For serotype I FIPV, all compounds consistently demonstrated greater efficacy (lower EC<sub>50</sub> values) relative to serotype II FIPV (2- to 84-fold). The cause of this consistent difference in EC<sub>50</sub> values between the two viral serotypes was not definitively determined, however, it may reflect differences in viral growth kinetics and a differential temporal manifestation of CPE between the two viruses and their respective permissive cell lines. The EC<sub>50</sub> values for GC376, GS-441524, MPV, and NHC against WSU-79-1146 propagated in CRFK cells were comparable to values previously determined in our laboratory (0.39, 0.61, 0.7 and 0.11 μM, respectively) [16]. A prior study reported an EC<sub>50</sub> for GC376 against FIPV II of 0.9 μM, relatively comparable to the findings reported here (0.39 μM) [52]. The EC<sub>50</sub> for GS-441524 against serotype II FIPV has also been previously reported to be 0.78 μM [14], similar to the results described here (0.61 μM).

The antiviral compounds were evaluated in vitro at concentrations ranging up to 50 μM. For NHC, there was a notable and progressive decrease in well absorbance values at concentrations greater than 1.5 μM in FCWF-4 CU cells, consistent with direct compound-associated cell injury (cytotoxicity). NHC-associated cytotoxicity has been demonstrated in other cells lines with a 50% cytotoxic concentration (CC<sub>50</sub>) of 7.5 μM when used in the CEM/C1 human cell line [53]. NHC-associated cytotoxicity has also been documented in CRFK cells using a fluorescence methodology [16]. More in-depth evaluations of potential NHC cytotoxicity in both in vitro and in vivo experiments are warranted, including evaluation of repeat dosing and long-term monitoring of systemic parameters in cats, such as CBC and serum biochemistry panels.

Based on the monotherapy results demonstrating a predictable and consistently lower EC<sub>50</sub> for antivirals against the Black I tissue culture strain relative to WSU-79-1146, we performed select combination experiments in vitro against WSU-79-1146 (CACT). The three evaluated combinations were (1) nirmatrelvir combined with MPV, (2) GC376 combined with RDV, and (3) RDV combined with nirmatrelvir. All three antiviral combinations demonstrated a nonlinear regression curve shift to the left indicating increased efficacy when the antivirals were used in combination. Consistent with the improved EC<sub>50</sub> values for antiviral combinations, there was a similar left shift in fractional inhibition (the fraction of cells protected from death appreciated via absorbance). Interestingly, the combination of nirmatrelvir and MPV only reached approximately 50% fractional inhibition, suggesting that this combination may be less attractive with regards to overall antiviral efficacy. GC376 combined with RDV was the most effective combination when considering fractional inhibition, as this combination approached 100% fractional inhibition at the lowest range of compound concentrations utilized. Combination index (CI) values were also plotted in order to identify evidence of compound synergy at different fractions affected (indicating the fraction of cells inhibited after drug exposure). The CI values were <1 at almost all data points, consistent with compound synergy. Antiviral synergy suggests that CACT may offer an alternative approach to the use of monotherapies for the treatment of FIP. Further investigations are needed to define if CACT may result in increased cure rates for FIP,

particularly for those cats with neurologic or ocular involvement or those cats experiencing therapeutic relapse.

The GS-441524 dose was selected based on earlier findings that once-daily oral administration at 25 mg/kg yielded curative efficacy in cats with FIP (personal communication, unpublished), although dosages in the literature and in practice vary [9]. Oral RDV dosage was selected based on a combination of peer-reviewed publications documenting differences in pharmacokinetics and oral bioavailability between RDV and GS-441524 in mice as well as non-peer reviewed recommendations put forth by veterinarians in Australia who have been successfully treating cats with FIP [32,54]. Although the molecular weight (MW) of RDV is approximately twice that of GS-441524, bioavailability differences between the two compounds negate these differences in MW and require relatively higher doses of RDV [54]. This is supported by comparing pharmacokinetics data of GS-441524 and RDV *in vitro* and after oral administration in mice [54]. The IV RDV dose corresponds to the allometrically scaled 200 mg first dose used for treating COVID-19 human patients [55].

Although we found no evidence of acute toxicity in the MPV-treated cats based on complete blood count and blood chemistry assessments, all three cats had clinical signs consistent with nausea for several hours post administration. This suggests an association between administration of MPV and nausea in cats. However, all cats were sedated after administration of the drug in order to place an indwelling IV catheter for subsequent blood collections so nausea secondary to sedation cannot be completely ruled out. The cats were also fasted prior to receiving MPV, which might play a role in the development of nausea. In a first-in-human study with MPV, a food effect on the rate of absorption was observed; however, the therapeutic exposures under fasted and fed states were comparable [56]. Due to the emergence of these treatment-related events, a higher oral dose of RDV equimolar to 25 mg/kg GS-441524 was not investigated.

Similar to what has been identified in humans, we found that MPV is rapidly metabolized in feline plasma to the active metabolite, NHC [56]. We detected the NHC metabolite at early timepoints and at markedly higher levels than the administered prodrug, MPV. In all three cats, we established that serum exposure rapidly reached levels greater than the NHC EC<sub>50</sub>, and in one cat fell to approximately the level of the EC<sub>50</sub> by the 12-h time point. We also found marked interindividual variability in MPV metabolism. A definitive cause for the metabolic variability between individual cats is presently undetermined but possible causes could include minor variability in the timing between centrifugation of individual whole blood samples between cats and the timing of the transfer of feline serum into acetonitrile. Variation in genetic polymorphisms related to metabolic pathways, such as the cytochrome P450 system, might also play a role in this variability [57,58]. One study focused on the administration of clopidogrel in cats found that high interindividual variability was associated with sex and cytochrome P450 2C genetic polymorphisms [59]. With a determined NHC half-life of approximately 3 h, we predict that twice daily dosing should not lead to accumulation of drug within the plasma.

The PK data demonstrate that GS-441524 and RDV have sufficient oral bioavailability and that this route of administration can yield therapeutic plasma levels of GS-441524 for treatment of FIP. Peak plasmatic concentrations of GS-441524 were > 30 µM after oral administration of GS-441524 at 25 mg/kg with no treatment-related adverse events; this is approximately 3-fold higher than the C<sub>max</sub> when GS-441524 is subcutaneously administered at the 5 mg/kg (~10 µM). Multiple clinical studies have used ~5 mg/kg as the therapeutic dose, although higher doses are now commonly used with an approximate range of 2–16 mg/kg [9,13,14]. A significant clinical advantage for oral administration of GS-441524 is the elimination of injection site reactions associated with the pH 1.5 solution required for solvating the compound. This suggests that oral GS-441524 may be more amenable for long-term treatment of neurological or ocular FIP [13,40]. The data indicate that oral administration of RDV for systemic delivery of GS-441524 is feasible. When cats were administered 25 mg/kg RDV orally, plasma C<sub>max</sub> values of GS-441524 were approximately 10 µM, which is similar to that observed with 5 mg/kg subcutaneously administered

GS-441524. Further investigation into the nausea and ptyalism observed in 2 of 3 cats in the oral RDV group is warranted and loading/maintenance dose modification similar to that used for RDV in humans should be explored to circumvent these treatment-related events [55].

While some of the studied antivirals have prior demonstrated success in the treatment of FIP in vivo [9,11,13,14] or hold promise based on in vitro data [14,16], the differing forms of FIP and clinical presentations indicate that a “one-size-fits-all” monotherapy approach to treatment may be overly simplistic. Determination of optimal combination therapies and consideration of a compound’s ability to penetrate into certain viral anatomic niches (e.g., CNS and/or ocular compartments) should be determined in order to optimize therapeutic approaches to cats that experience therapeutic relapse. Although multiple non-peer reviewed clinical strategies for treating FIP are readily available, there are limited rigorously designed clinical trials focused on the treatment of cats with naturally occurring FIP in the peer-reviewed literature. Further, there are little to no PK data for many of these antiviral agents and essentially no information regarding the penetration of various compounds into feline tissues. Such pharmacologic information serves as a critical and rational foundation for designing clinical trials aimed at treating cats with refractory FIP.

Additional in vivo pharmacokinetic studies (CACT assessment), assessment of compound penetration into tissues and rigorously designed and peer reviewed clinical trials focused on both monotherapies and CACT are needed to further optimize and individualize the successful treatment of this historically fatal disease in cats, now demonstrated to be amenable to a variety of antiviral therapies.

**Supplementary Materials:** The following supporting information can be downloaded at: <https://www.mdpi.com/article/10.3390/v14112429/s1>, Table S1: Baseline and 48 h post-MPV complete blood count and biochemistry panel for 20-024; Table S2: Baseline and 48 h post-MPV complete blood count and biochemistry panel for 20-025; Table S3: Baseline and 48 h post-MPV complete blood count and biochemistry panel for 20-031.

**Author Contributions:** Conceptualization, S.C., K.L.R., V.C.Y. and B.G.M.; methodology, S.C., L.W., V.C.Y., J.H.T., D.C., K.L.R., C.-D.P., C.L., F.L.M. and B.G.M.; formal analysis, S.C., L.W., V.C.Y., C.-D.P., C.L., F.L.M. and B.G.M.; investigation, S.C., L.W., V.C.Y., J.H.T., D.C., S.W., C.-D.P., C.L., F.L.M. and B.G.M.; writing—original draft preparation, S.C. and B.G.M.; writing—review and editing, S.C., L.W., V.C.Y., J.H.T., D.C., K.L.R., S.W. and B.G.M.; visualization, S.C., L.W., B.G.M. and V.C.Y.; funding acquisition, S.C., L.W., V.C.Y. and B.G.M. All authors have read and agreed to the published version of the manuscript.

**Funding:** This research was funded by the EveryCat Health Foundation (grant W21-007, 2021–2022), the University of California, Davis Peter C. Kennedy Endowed Fellowship (2021–2022), the University of California Center for Companion Animal Health (2020-89-FM) and the NIH/NIAID (R21AI159246-01 to C.L.). Wittenburg is supported by the National Institutes of Health NIH 5K01OD026526.

**Institutional Review Board Statement:** The animal study protocols were approved by the UC Davis Institutional Animal Care and Use Committee (IACUC #22839 and #22483).

**Informed Consent Statement:** Not applicable.

**Data Availability Statement:** Not applicable.

**Acknowledgments:** FCWF-4 CU cells and Black I virus were generously donated by Susan Baker (Loyola University Chicago), originally obtained from Cornell University College of Veterinary Medicine (Edward Dubovi). GC376 was generously donated by Yunjeong Kim (Kansas State University). We would like to thank the UC Davis Feline Nutrition and Pet Care Center and Maria Montano for their assistance in the live animal portion of this study.

**Conflicts of Interest:** The authors declare no conflict of interest.

## References

1. Pedersen, N.C.; Liu, H.; Dodd, K.A.; Pesavento, P.A. Significance of coronavirus mutants in feces and diseased tissues of cats suffering from feline infectious peritonitis. *Viruses* **2009**, *1*, 166–184. [[CrossRef](#)]
2. Vennema, H.; Poland, A.; Foley, J.; Pedersen, N.C. Feline infectious peritonitis viruses arise by mutation from endemic feline enteric coronaviruses. *Virology* **1998**, *243*, 150–157. [[CrossRef](#)]
3. Herrewegh, A.A.; Smeenk, I.; Horzinek, M.C.; Rottier, P.J.; De Groot, R.J. Feline coronavirus type II strains 79-1683 and 79-1146 originate from a double recombination between feline coronavirus type I and canine coronavirus. *J. Virol.* **1998**, *72*, 4508–4514. [[CrossRef](#)]
4. Premkumar, L.; Segovia-Chumbez, B.; Jadi, R.; Martinez, D.R.; Raut, R.; Markmann, A.J.; Cornaby, C.; Bartelt, L.; Weiss, S.; Park, Y. The receptor-binding domain of the viral spike protein is an immunodominant and highly specific target of antibodies in SARS-CoV-2 patients. *Sci. Immunol.* **2020**, *5*, eabc8413. [[CrossRef](#)]
5. Whittaker, G.R.; André, N.M.; Millet, J.K. Improving virus taxonomy by recontextualizing sequence-based classification with biologically relevant data: The case of the alphacoronavirus 1 species. *MSphere* **2018**, *3*, e00463-17. [[CrossRef](#)]
6. Jaimes, J.A.; Millet, J.K.; Stout, A.E.; André, N.M.; Whittaker, G.R. A tale of two viruses: The distinct spike glycoproteins of feline coronaviruses. *Viruses* **2020**, *12*, 83. [[CrossRef](#)]
7. Montali, R.; Strandberg, J. Extraperitoneal lesions in feline infectious peritonitis. *Vet. Pathol.* **1972**, *9*, 109–121. [[CrossRef](#)]
8. Foley, J.E.; Lapointe, J.M.; Koblik, P.; Poland, A.; Pedersen, N.C. Diagnostic features of clinical neurologic feline infectious peritonitis. *J. Vet. Intern. Med.* **1998**, *12*, 415–423. [[CrossRef](#)]
9. Jones, S.; Novicoff, W.; Nadeau, J.; Evans, S. Unlicensed GS-441524-like antiviral therapy can be effective for at-home treatment of feline infectious peritonitis. *Animals* **2021**, *11*, 2257. [[CrossRef](#)]
10. Tsai, H.-Y.; Chueh, L.-L.; Lin, C.-N.; Su, B.-L. Clinicopathological findings and disease staging of feline infectious peritonitis: 51 cases from 2003 to 2009 in Taiwan. *J. Feline Med. Surg.* **2011**, *13*, 74–80. [[CrossRef](#)]
11. Pedersen, N.C.; Kim, Y.; Liu, H.; Galasiti Kankanamalage, A.C.; Eckstrand, C.; Groutas, W.C.; Bannasch, M.; Meadows, J.M.; Chang, K.-O. Efficacy of a 3C-like protease inhibitor in treating various forms of acquired feline infectious peritonitis. *J. Feline Med. Surg.* **2018**, *20*, 378–392. [[CrossRef](#)] [[PubMed](#)]
12. Perera, K.D.; Rathnayake, A.D.; Liu, H.; Pedersen, N.C.; Groutas, W.C.; Chang, K.-O.; Kim, Y. Characterization of amino acid substitutions in feline coronavirus 3C-like protease from a cat with feline infectious peritonitis treated with a protease inhibitor. *Vet. Microbiol.* **2019**, *237*, 108398. [[CrossRef](#)] [[PubMed](#)]
13. Pedersen, N.C.; Perron, M.; Bannasch, M.; Montgomery, E.; Murakami, E.; Liepnieks, M.; Liu, H. Efficacy and safety of the nucleoside analog GS-441524 for treatment of cats with naturally occurring feline infectious peritonitis. *J. Feline Med. Surg.* **2019**, *21*, 271–281. [[CrossRef](#)]
14. Murphy, B.G.; Perron, M.; Murakami, E.; Bauer, K.; Park, Y.; Eckstrand, C.; Liepnieks, M.; Pedersen, N.C. The nucleoside analog GS-441524 strongly inhibits feline infectious peritonitis (FIP) virus in tissue culture and experimental cat infection studies. *Vet. Microbiol.* **2018**, *219*, 226–233. [[CrossRef](#)]
15. Krentz, D.; Zenger, K.; Alberer, M.; Felten, S.; Bergmann, M.; Dorsch, R.; Matiasek, K.; Kolberg, L.; Hofmann-Lehmann, R.; Meli, M.L. Curing cats with feline infectious peritonitis with an oral multi-component drug containing GS-441524. *Viruses* **2021**, *13*, 2228. [[CrossRef](#)] [[PubMed](#)]
16. Cook, S.E.; Vogel, H.; Castillo, D.; Olsen, M.; Pedersen, N.; Murphy, B.G. Investigation of monotherapy and combined anticoronaviral therapies against feline coronavirus serotype II in vitro. *J. Feline Med. Surg.* **2021**, *24*, 1098612X2110486. [[CrossRef](#)]
17. Kim, Y.; Liu, H.; Galasiti Kankanamalage, A.C.; Weerasekara, S.; Hua, D.H.; Groutas, W.C.; Chang, K.-O.; Pedersen, N.C. Reversal of the progression of fatal coronavirus infection in cats by a broad-spectrum coronavirus protease inhibitor. *PLoS Pathog.* **2016**, *12*, e1005531.
18. Yan, S.; Wu, G. Potential 3-chymotrypsin-like cysteine protease cleavage sites in the coronavirus polyproteins pp1a and pp1ab and their possible relevance to COVID-19 vaccine and drug development. *FASEB J.* **2021**, *35*, e21573. [[CrossRef](#)]
19. Weiss, S.R.; Hughes, S.A.; Bonilla, P.J.; Turner, J.D.; Leibowitz, J.L.; Denison, M.R. *Coronavirus Polyprotein Processing*; Springer: Vienna, Austria, 1994; pp. 349–358.
20. Yin, Y.; Li, T.; Wang, C.; Liu, X.; Ouyang, H.; Ji, W.; Liu, J.; Liao, X.; Li, J.; Hu, C. A retrospective study of clinical and laboratory features and treatment on cats highly suspected of feline infectious peritonitis in Wuhan, China. *Sci. Rep.* **2021**, *11*, 5208. [[CrossRef](#)]
21. Li, Y.; Cao, L.; Li, G.; Cong, F.; Li, Y.; Sun, J.; Luo, Y.; Chen, G.; Li, G.; Wang, P.; et al. Remdesivir Metabolite GS-441524 Effectively Inhibits SARS-CoV-2 Infection in Mouse Models. *J. Med. Chem.* **2022**, *65*, 2785–2793. [[CrossRef](#)]
22. Yan, V.C.; Muller, F.L. Advantages of the parent nucleoside GS-441524 over remdesivir for COVID-19 treatment. *ACS Med. Chem. Lett.* **2020**, *11*, 1361–1366. [[CrossRef](#)] [[PubMed](#)]
23. Agostini, M.L.; Andres, E.L.; Sims, A.C.; Graham, R.L.; Sheahan, T.P.; Lu, X.; Smith, E.C.; Case, J.B.; Feng, J.Y.; Jordan, R. Coronavirus susceptibility to the antiviral remdesivir (GS-5734) is mediated by the viral polymerase and the proofreading exoribonuclease. *MBio* **2018**, *9*, e00221-18. [[CrossRef](#)] [[PubMed](#)]
24. Olender, S.A.; Perez, K.K.; Go, A.S.; Balani, B.; Price-Haywood, E.G.; Shah, N.S.; Wang, S.; Walunas, T.L.; Swaminathan, S.; Slim, J. Remdesivir for severe coronavirus disease 2019 (COVID-19) versus a cohort receiving standard of care. *Clin. Infect. Dis.* **2021**, *73*, e4166–e4174. [[CrossRef](#)] [[PubMed](#)]

25. Sheahan, T.P.; Sims, A.C.; Leist, S.R.; Schäfer, A.; Won, J.; Brown, A.J.; Montgomery, S.A.; Hogg, A.; Babusis, D.; Clarke, M.O. Comparative therapeutic efficacy of remdesivir and combination lopinavir, ritonavir, and interferon beta against MERS-CoV. *Nat. Commun.* **2020**, *11*, 222. [CrossRef] [PubMed]
26. De Wit, E.; Feldmann, F.; Cronin, J.; Jordan, R.; Okumura, A.; Thomas, T.; Scott, D.; Cihlar, T.; Feldmann, H. Prophylactic and therapeutic remdesivir (GS-5734) treatment in the rhesus macaque model of MERS-CoV infection. *Proc. Natl. Acad. Sci. USA* **2020**, *117*, 6771–6776. [CrossRef]
27. Yethindra, V. Role of GS-5734 (Remdesivir) in inhibiting SARS-CoV and MERS-CoV: The expected role of GS-5734 (Remdesivir) in COVID-19 (2019-nCoV)-VYTR hypothesis. *Int. J. Res. Pharm. Sci.* **2020**, *11*, 1–6. [CrossRef]
28. Bohm, M. Successful treatment of a South African cat with effusive feline infectious peritonitis with remdesivir. *J. S. Afr. Vet. Assoc.* **2022**, *93*, 1–4. [CrossRef]
29. Lo, M.K.; Feldmann, F.; Gary, J.M.; Jordan, R.; Bannister, R.; Cronin, J.; Patel, N.R.; Klena, J.D.; Nichol, S.T.; Cihlar, T. Remdesivir (GS-5734) protects African green monkeys from Nipah virus challenge. *Sci. Transl. Med.* **2019**, *11*, eaau9242. [CrossRef]
30. Lo, M.K.; Jordan, R.; Arvey, A.; Sudhamsu, J.; Shrivastava-Ranjan, P.; Hotard, A.L.; Flint, M.; McMullan, L.K.; Siegel, D.; Clarke, M.O. GS-5734 and its parent nucleoside analog inhibit Filo-, Pneumo-, and Paramyxoviruses. *Sci. Rep.* **2017**, *7*, 43395. [CrossRef]
31. U.S. Food and Drug Administration. *FDA Approves First Treatment for COVID-19*; FDA News Release: Silver Spring, MD, USA, 2020.
32. Malik, R. Treatment of FIP in Cats with Subcutaneous Remdesivir Followed by Oral GS-441524 Tablets. 2022. Available online: <https://www.zenbycat.org/blog/treatment-of-fip-in-cats-with-subcutaneous-remdesivir-followed-by-oral-gs-441524-tablets> (accessed on 19 July 2022).
33. U.S. Food and Drug Administration. Fact Sheet for Healthcare Providers: Emergency Use Authorization for Paxlovid. 2021. Available online: <https://www.fda.gov/media/155050/download> (accessed on 19 July 2022).
34. Acosta, E.P. Pharmacokinetic enhancement of protease inhibitors. *J. Acquir. Immune Defic. Syndr.* **2002**, *29*, S11–S18. [CrossRef]
35. Zeldin, R.K.; Petruschke, R.A. Pharmacological and therapeutic properties of ritonavir-boosted protease inhibitor therapy in HIV-infected patients. *J. Antimicrob. Chemother.* **2004**, *53*, 4–9. [CrossRef] [PubMed]
36. Wahl, A.; Gralinski, L.E.; Johnson, C.E.; Yao, W.; Kovarova, M.; Dinnon, K.H.; Liu, H.; Madden, V.J.; Krzystek, H.M.; De, C.; et al. SARS-CoV-2 infection is effectively treated and prevented by EIDD-2801. *Nature* **2021**, *591*, 451–457. [CrossRef] [PubMed]
37. U.S. National Library of Medicine. The Safety of Molnupiravir (EIDD-2801) and Its Effect on Viral Shedding of SARS-CoV-2 (END-COVID). Identifier NCT04405739. 28 May 2020–21 March 2022. Available online: <https://clinicaltrials.gov/ct2/show/NCT04405739?id=NCT04405739&draw=2&rank=1&load=cart> (accessed on 25 August 2022).
38. Warriors, F. EIDD-2801. Available online: <https://www.fipwarriors.eu/en/eidd-2801-molnupiravir/> (accessed on 19 July 2022).
39. Sheahan, T.P.; Sims, A.C.; Zhou, S.; Graham, R.L.; Hill, C.S.; Leist, S.R.; Schäfer, A.; Dinnon, K.H.; Montgomery, S.A.; Agostini, M.L. An orally bioavailable broad-spectrum antiviral inhibits SARS-CoV-2 and multiple endemic, epidemic and bat coronavirus. *Biorxiv* **2020**, *12*, eabb5883.
40. Dickinson, P.J.; Bannasch, M.; Thomasy, S.M.; Murthy, V.D.; Vernau, K.M.; Liepnieks, M.; Montgomery, E.; Knickelbein, K.E.; Murphy, B.; Pedersen, N.C. Antiviral treatment using the adenosine nucleoside analogue GS-441524 in cats with clinically diagnosed neurological feline infectious peritonitis. *J. Vet. Intern. Med.* **2020**, *34*, 1587–1593. [CrossRef] [PubMed]
41. Lima, V.D.; Harrigan, R.; Bangsberg, D.R.; Hogg, R.S.; Gross, R.; Yip, B.; Montaner, J.S. The combined effect of modern highly active antiretroviral therapy regimens and adherence on mortality over time. *J. Acquir. Immune Defic. Syndr.* **2009**, *50*, 529. [CrossRef] [PubMed]
42. Poordad, F.; Lawitz, E.; Kowdley, K.V.; Cohen, D.E.; Podsadecki, T.; Siggelkow, S.; Heckaman, M.; Larsen, L.; Menon, R.; Koev, G. Exploratory study of oral combination antiviral therapy for hepatitis C. *N. Engl. J. Med.* **2013**, *368*, 45–53. [CrossRef]
43. Fabrizi, F.; Dixit, V.; Martin, P.; Messa, P. Combined antiviral therapy of hepatitis C virus in dialysis patients: Meta-analysis of clinical trials. *J. Viral Hepat.* **2011**, *18*, e263–e269. [CrossRef]
44. O'Brien, A.; Mettelman, R.C.; Volk, A.; André, N.M.; Whittaker, G.R.; Baker, S.C. Characterizing replication kinetics and plaque production of type I feline infectious peritonitis virus in three feline cell lines. *Virology* **2018**, *525*, 1–9. [CrossRef]
45. Cook, S.; Castillo, D.; Williams, S.; Haake, C.; Murphy, B. Serotype I and II Feline Coronavirus Replication and Gene Expression Patterns of Feline Cells—Building a Better Understanding of Serotype I FIPV Biology. *Viruses* **2022**, *14*, 1356. [CrossRef]
46. Rathnayake, A.D.; Zheng, J.; Kim, Y.; Perera, K.D.; Mackin, S.; Meyerholz, D.K.; Kashipathy, M.M.; Bataile, K.P.; Lovell, S.; Perlman, S.; et al. 3C-like protease inhibitors block coronavirus replication in vitro and improve survival in MERS-CoV-infected mice. *Sci. Transl. Med.* **2020**, *12*, eabc5332. [CrossRef]
47. Chou, T.-C. Drug Combination Studies and Their Synergy Quantification Using the Chou-Talalay Method Synergy Quantification Method. *Cancer Res.* **2010**, *70*, 440–446. [CrossRef] [PubMed]
48. Warren, T.K.; Jordan, R.; Lo, M.K.; Ray, A.S.; Mackman, R.L.; Soloveva, V.; Siegel, D.; Perron, M.; Bannister, R.; Hui, H.C. Therapeutic efficacy of the small molecule GS-5734 against Ebola virus in rhesus monkeys. *Nature* **2016**, *531*, 381–385. [CrossRef] [PubMed]
49. Sheahan, T.P.; Sims, A.C.; Graham, R.L.; Menachery, V.D.; Gralinski, L.E.; Case, J.B.; Leist, S.R.; Pyrc, K.; Feng, J.Y.; Trantcheva, I. Broad-spectrum antiviral GS-5734 inhibits both epidemic and zoonotic coronaviruses. *Sci. Transl. Med.* **2017**, *9*, eal3653. [CrossRef] [PubMed]

50. Humeniuk, R.; Mathias, A.; Cao, H.; Osinusi, A.; Shen, G.; Chng, E.; Ling, J.; Vu, A.; German, P. Safety, tolerability, and pharmacokinetics of remdesivir, an antiviral for treatment of COVID-19, in healthy subjects. *Clin. Transl. Sci.* **2020**, *13*, 896–906. [[CrossRef](#)]
51. Amara, A.; Penchala, S.D.; Else, L.; Hale, C.; FitzGerald, R.; Walker, L.; Lyons, R.; Fletcher, T.; Khoo, S. The development and validation of a novel LC-MS/MS method for the simultaneous quantification of Molnupiravir and its metabolite  $\beta$ -d-N4-hydroxycytidine in human plasma and saliva. *J. Pharm. Biomed. Anal.* **2021**, *206*, 114356. [[CrossRef](#)]
52. Vuong, W.; Khan, M.B.; Fischer, C.; Arutyunova, E.; Lamer, T.; Shields, J.; Saffran, H.A.; McKay, R.T.; Van Belkum, M.J.; Joyce, M.A.; et al. Feline coronavirus drug inhibits the main protease of SARS-CoV-2 and blocks virus replication. *Nat. Commun.* **2020**, *11*, 4282. [[CrossRef](#)]
53. Sticher, Z.M.; Lu, G.; Mitchell, D.G.; Marlow, J.; Moellering, L.; Bluemling, G.R.; Guthrie, D.B.; Natchus, M.G.; Painter, G.R.; Kolykhalov, A.A. Analysis of the potential for N 4-hydroxycytidine to inhibit mitochondrial replication and function. *Antimicrob. Agents Chemother.* **2020**, *64*, e01719-19. [[CrossRef](#)]
54. Xie, J.; Wang, Z. Can remdesivir and its parent nucleoside GS-441524 be potential oral drugs? An in vitro and in vivo DMPK assessment. *Acta Pharm. Sin. B* **2021**, *11*, 1607–1616. [[CrossRef](#)]
55. Beigel, J.H.; Tomashek, K.M.; Dodd, L.E.; Mehta, A.K.; Zingman, B.S.; Kalil, A.C.; Hohmann, E.; Chu, H.Y.; Luetkemeyer, A.; Kline, S.; et al. Remdesivir for the Treatment of COVID-19—Final Report. *N. Engl. J. Med.* **2020**, *383*, 1813–1826. [[CrossRef](#)]
56. Painter, W.P.; Holman, W.; Bush, J.A.; Almazedi, F.; Malik, H.; Eraut, N.C.; Morin, M.J.; Szewczyk, L.J.; Painter, G.R. Human safety, tolerability, and pharmacokinetics of molnupiravir, a novel broad-spectrum oral antiviral agent with activity against SARS-CoV-2. *Antimicrob. Agents Chemother.* **2021**, *65*, e02428-20. [[CrossRef](#)]
57. O'Malley, K.; Crooks, J.; Duke, E.; Stevenson, I.H. Effect of Age and Sex on Human Drug Metabolism. *BMJ* **1971**, *3*, 607–609. [[CrossRef](#)] [[PubMed](#)]
58. Kraemer, S.D.; Testa, B. The Biochemistry of Drug Metabolism—An Introduction: Part 6. Inter-Individual Factors Affecting Drug Metabolism. *Chem. Biodivers.* **2008**, *5*, 2465–2578. [[CrossRef](#)] [[PubMed](#)]
59. Lee, P.M.; Faus, M.C.L.; Court, M.H. High interindividual variability in plasma clopidogrel active metabolite concentrations in healthy cats is associated with sex and cytochrome P450 2C genetic polymorphism. *J. Vet. Pharmacol. Ther.* **2019**, *42*, 16–25. [[CrossRef](#)] [[PubMed](#)]

**Chapter 5: Assessing safety and efficacy of a lentivirus-vectored feline erythropoietin gene therapy strategy in tissue culture and rodent models**

## **Assessing safety and efficacy of a lentivirus-vectored feline erythropoietin gene therapy strategy in tissue culture and rodent models**

SE Cook<sup>a</sup>, D Castillo<sup>b</sup>, T Wolf<sup>b</sup>, C Hillman<sup>c</sup>, K Bauer<sup>d</sup>, S Williams<sup>b</sup>, BG Murphy<sup>b</sup>

<sup>a</sup> Graduate Group Integrative Pathobiology, School of Veterinary Medicine, University of California, 1 Garrod Dr., Davis, CA, USA

<sup>b</sup> Department of Pathology, Microbiology, and Immunology, School of Veterinary Medicine, University of California, 1 Garrod Dr., Davis, CA, USA

<sup>c</sup> National Institute of Allergy and Infectious Disease, Hamilton, MT, USA

<sup>d</sup> Department of Biomedical Sciences, College of Veterinary Medicine, Cornell University, 602 Tower Rd, Ithaca, NY, USA

\*Corresponding author: Sarah E. Cook, DVM, DACVP

*E-mail:* sestevens@ucdavis.edu (SEC)

Gene therapy, feline chronic renal disease, anemia, erythropoietin, lentivirus

### **ABSTRACT**

Chronic renal disease (CRD) is a common disease of aged cats, often associated with clinically significant nonregenerative anemia as a result of reduced renal production of erythropoietin (EPO). Multiple medical approaches have been attempted to manage feline CRD-associated anemia including periodic blood transfusions, parenteral treatment with recombinant EPO, and a variety of gene therapy strategies. We designed a series of third-generation lentivirus-based vectors to encode and produce the feline EPO (feEPO) gene product in tissue culture cells *in vitro* and in rodent models *in vivo*. These vectors incorporated a genetic mechanism to facilitate the pharmacologic termination of the therapeutic effect in the event of

supraphysiologic polycythemia, the herpes simplex virus thymidine kinase (HSV-TK) “suicide gene”. We hypothesized that feline cells transduced *in vitro* by a lentiviral vector encoding native feline erythropoietin would express feEPO mRNA and biologically active feEPO protein and that this expression could be terminated by the administration of ganciclovir (GCV, the nontoxic substrate of HSV-TK). The *in vitro* assays facilitated optimization of the vector for *in vivo* studies in mice and rats in which we demonstrated a progressive, lentiviral dose-dependent significant elevation of blood packed cell volume (PCV) in treated animals. Despite *in vitro* evidence supporting functional efficacy of the suicide gene, administration of GCV *in vivo* did not abrogate the elevated PCV effect of the lentiviral vector.

## **INTRODUCTION**

Gene therapy involves the transfer of genetic material for a broad range of therapeutic applications including cancer, tissue regeneration and functional gene replacement[1-4]. Although more limited in its use in veterinary medicine relative to human medicine, it continues to gain attention in veterinary medicine, with a recent review identifying particular areas of gene therapy applications, including cardiovascular disease, ocular disease, neoplasia, skin disease, and blood/hematopoietic disorders, such as anemia secondary to chronic renal disease, among others[5]. Chronic renal disease (CRD) is a common, progressive disease reported in up to 50% of aged domestic cats[6]. Although the pathogenesis is not completely understood, the causes of CRD are numerous, inter-related, and complex with disease development thought to be an outcome of a combination of genetic, environmental, and individual animal factors[7-11]. Cats presenting with chronic CRD are typically older animals with clinical evidence of weight loss, altered kidney size and shape, dehydration, polyuria, and polydipsia. Abnormalities in serum

chemistry panels and urinalyses typically include azotemia, hyperphosphatemia, and unconcentrated urine in the face of dehydration (isosthenuria)[12]. Grossly, affected kidneys are typically small and have an irregular to spherical shape with surface pitting. Histologically, CRD lesions are generally restricted to the tubulointerstitial compartment with variable secondary involvement of glomeruli[13]. Microscopic lesions often include an interstitial mononuclear cell infiltrate, tubular degeneration, tubular loss, and interstitial fibrosis with a loss of renal parenchyma[13].

With progression of CRD, approximately 30-65% of affected cats will develop a clinically significant nonregenerative anemia[14, 15]. Anemia secondary to CRD is a result of decreased production of kidney-associated erythropoietin (EPO), the principal hormonal regulator of erythropoiesis. Spliced feline EPO mRNA is 579 nucleotides long (GenBank accession #JQ413414.1) and encodes a 192 amino acid protein (30-40 kD, GenBank accession #AFN85670.1) produced by peritubular fibroblast-like cells in the kidney[16-19]. CRD-associated reduction in EPO production results in a loss of bone marrow erythroid progenitor cells and nonregenerative anemia characterized by decreased reticulocyte production and decreased packed cell volume (PCV) of circulating red blood cells [20, 21].

Therapeutic approaches to CRD-associated nonregenerative anemia include whole blood transfusions, parenteral administration of exogenous recombinant EPO (replacement therapy), and a variety of gene therapy strategies utilizing either non-viral (plasmid) or viral vectors encoding the EPO transgene. Cats have been successfully treated parenterally with human erythropoietin (EPOGEN, epoetin alfa, Amgen) and longer-acting darbepoetin (Aranesp, darbepoetin alpha, Amgen)[22, 23]. However, this approach often requires repeated injections and the therapeutic response can become attenuated over time, possibly as a result of antibody

production directed against the human EPO transprotein[22, 23]. Approximately 25-30% of cats treated with EPOGEN develop pure red cell aplasia (PRCA), a severe adverse event in which neutralizing antibodies produced against the human EPO transprotein cross-react and neutralize endogenous feline EPO resulting in a severe and progressive anemia[22]. A recombinant feline-specific EPO protein product was developed[24] in an attempt to avoid the immunologic complications associated with administration of the human specific transprotein. Investigators found that administration of this exogenous feline specific EPO reestablished erythropoiesis in most cats with CRD, although the risk of PRCA was not eliminated[24].

The use of viral vectors offers improved efficiency of gene delivery (transduction) and can be engineered to target specific cell types. Disadvantages of viral vectors include a more complex production process, potential limitations in packaging capacity, and certain immunologic obstacles[3, 25, 26]. Several published studies have explored the use of adeno-associated viral vectors as a method to deliver and produce native feline EPO in cats. In one study involving six clinically normal cats, administration of a recombinant adeno-associated viral (rAAV) vector encoding the feline EPO gene resulted in a dose-responsive and statistically significant increase in mean PCV from 31.2% to 59.5% approximately 6-8 weeks post-treatment [27]. A separate study involving a different rAAV vector also reported an increase in the PCV of the treated cats, however, several adverse events occurred including the development of PRCA in one cat and persistent erythrocytosis in a second animal that failed to respond to surgical excision of the injection site[28]. These rAAV studies lacked a predictable therapeutic response and method of reliably terminating the effect of the feEPO transgene. Importantly, the reported sequence of the feline EPO transgene utilized in both of these studies had a single nucleotide misincorporation resulting in an amino acid substitution at the 44<sup>th</sup> codon of the feline EPO gene

(glycine for glutamic acid)[29]. Whether this amino acid misincorporation had any effect in the study outcome is unknown.

To the authors' knowledge, there are no peer-reviewed studies focused on the parenteral administration of plasmid DNA encoding the feline EPO gene as a therapeutic approach to CRD-associated anemia. Plasmid vectors encoding feline EPO are attractive in that the method is relatively inexpensive and plasmids can be designed to encode large amounts of genetic material. However, the efficiency of gene transfer with plasmid-based therapies can be poor[25].

Optimal gene therapy approaches for cats with CRD-associated anemia should induce a persistent and physiologically appropriate effect, eliminating the need for frequent therapeutic injections to maintain normal PCV. The inclusion of additional safety mechanisms within the viral vector, so-called *suicide genes*, facilitate the pharmacologically mediated and selective elimination of the vector-transduced cells. In the event of an adverse supraphysiologic response (excessively elevated PCV), the suicide gene product (*Herpes simplex virus thymidine kinase*, HSV-TK) phosphorylates the non-toxic prodrug ganciclovir (GCV) into the cytotoxic metabolite GCV triphosphate. GCV triphosphate is subsequently incorporated into host cell genomic DNA during cell replication, thereby inhibiting DNA synthesis and resulting in apoptosis of the transduced cell[30]. Therefore, in the event of supraphysiologic polycythemia, the administration of GCV results in targeted cell death of the transduced cells [31, 32].

Third generation lentiviral vectors are capable of efficiently packaging a relatively large transgene (approximately 9 kb), permanently integrate into the host cell genome, can transduce both dividing and non-dividing cells, can be pseudotyped to selectively transduce specific cell types and have not been reported to be associated with insertional mutagenic events[33-35]. Permanent integration of the vector into the host genome is beneficial in that the introduced

(transduced) transgene functions like host cell genetic material and is passed on to daughter cells during subsequent cell divisions. As a result, the incorporation of the transgene into the host genome should facilitate a persistent therapeutic effect.

We have previously reported on the efficacy of a lentiviral vector system encoding native feline EPO using *in vitro* assays[29]. In this previous work, feline peripheral blood mononuclear cells, human 293H cells, and feline CRFK cells were transduced with a lentiviral vector encoding the native feline EPO cDNA; transcription of feline EPO mRNA and production of bioactive feline EPO protein were confirmed using multiple techniques[29]. Here we describe the further optimization of the vector construct, including promoter selection and the incorporation of a tandemly expressed HSV-TK gene as a safety mechanism for terminating the effect. We document the efficacy and safety of the lentiviral gene therapy strategy in a variety of cell types *in vitro*. These *in vitro* studies were followed by a series of *in vivo* experiments in multiple rodent models, including normal rats and genetically modified EPO-deficient anemic mice.

## **METHODS and MATERIALS**

### *Design and packaging of lentiviral vectors*

Feline EPO (feEPO) mRNA was previously PCR-amplified from feline renal tissue-derived RNA and the resulting reverse transcribed cDNA was incorporated into an initial lentiviral vector system, referred to here as Vector A [29]. The feEPO gene (cDNA) was subsequently utilized in the design and construction of three third-generation, replication-defective lentiviral vectors, Vectors B, C and D. A UC Davis Biological Use Authorization (BUA; #895) was approved for the use of lentiviral vectors A, B, C, and D.

The plasmid encoded feEPO cDNA was confirmed by sequencing (GenBank JQ413414). The construct design was similar for Vector B, C and D but varied in the promoter regulating feEPO transgene expression (Fig 1). All of the lentiviral vectors feature a HIV-derived and gene-deleted backbone with one of three internal promoters regulating expression of feEPO: the constitutively active human cytomegalovirus immediate-early enhancer and promoter (CMV, Vector B), a hypoxia-inducible promoter (9X- hypoxia response element (HRE)-SV40 mini, Vector C), or the early promoter of simian virus 40 (SV40, Vector D).

The CMV promoter is a commonly used element for the production of high levels of recombinant protein[36, 37]. The CMV promoter is a powerful, constitutively active promoter; however, a potential disadvantage is that it is prone to transcriptional silencing over time after transduction (attenuation of promoter effect), suspected to be a result of promoter methylation[36, 38-40]. Given that reduced oxygenation and delivery of blood to the kidney is a key signal in the induction of renal erythropoietin production, the hypoxia-inducible promoter (9X-HRE-SV40 mini) is a rational and physiologically relevant synthetic promoter [41, 42]. Hypothetically, this promoter should function as an oxygen-regulated promoter for the physiologically appropriate production of erythropoietin *in vivo*- once sufficient EPO production occurs and anemia resolves, promoter function should cease. The SV40 promoter (Vector D) was selected as a constitutively active promoter with moderately attenuated function relative to the CMV promoter[43].

All three of the promoters were situated directly 5' to the cloned feEPO gene (cDNA) which was linked through an internal ribosome entry site (IRES) to the herpes simplex virus thymidine kinase gene (suicide gene) [44]. A Control Vector was also designed based on the HIV-derived backbone and featured the EF1A promoter regulating expression of the reporter

gene mCherry (Figure 1). The Control Vector also featured a second internal promoter (CMV) regulating expression of the enhanced green fluorescent protein (EGFP) and an antibiotic resistance gene (puromycin-N-acetyltransferase gene, Puro) linked to EGFP through an autocleaving 2A site[45]. The plasmid constructs for each vector were assembled by VectorBuilder (VectorBuilder.com) and confirmed by sequencing.

Plasmid constructs were packaged into pseudotyped (VSV-G), single-cycle infectious lentiviral particles using a set of packaging plasmids (Invitrogen) transfected into human 293FT cells as described previously[29] and were utilized for all of the Vector B and C *in vitro* studies. For Vector D *in vitro* and *in vivo* rodent experiments, infectious lentiviral vectors were packaged and titered by VectorBuilder as transducing units per mL (TU/mL). Ultra-purified lentiviral vectors were shipped frozen from VectorBuilder on dry ice to Davis, California in HBSS buffer.

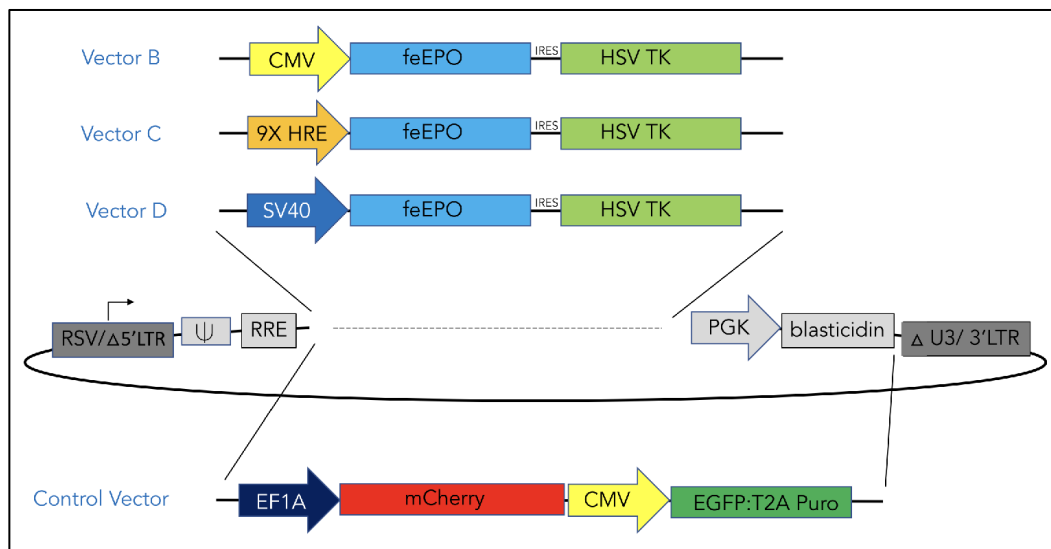


**Figure 1. Vector construct schematics.** Vector B, C, and D with different promoter sequences regulating transcription of the feline EPO and HSV TK genes.

*RNA isolation and RT-PCR assays*

For *in vitro* experiments using Vector B and C, RNA was isolated using TRIzol reagent (Invitrogen) and further processed with the RNeasy Kit (Qiagen). RNA was DNase treated (TURBO DNase, Ambion) and reverse transcribed to complimentary DNA (cDNA) using the First Strand cDNA Synthesis System (Origene) following the manufacturers' protocols. Standard RT-PCR was performed to determine the presence of feline EPO mRNA using the primers EPO short forward 5'- AAC CTC TGC TGC TCC ACT CC and EPO reverse 5'- CCT GTC TCC TCT TCG GCA GGC and Invitrogen's recombinant *Taq* DNA polymerase following the manufacturer's protocol for a 50  $\mu$ L reaction. Expected amplicon size is 130 bp. Cycling conditions as follows; 95°C for 2 min followed by 40 cycles of 95°C for 15 s, 56°C for 30 s, 72°C for 30 s, and a final extension step of 72°C for 5 min. PCR amplicons were electrophoresed on 1% agarose gels, stained with ethidium bromide and digitally imaged.

For experiments utilizing Vector D, total cell-associated RNA was isolated with the PureLink RNA mini kit (Thermo Fisher Scientific), DNase treated, and reverse transcribed as described above. Quantitative reverse transcription PCR (RT-qPCR) was utilized to determine copy number for feline EPO and feline glyceraldehyde-3-phosphate dehydrogenase (GAPDH) using Applied Biosystems' QuantStudio 3 Real-Time PCR System and PowerUp SYBR Green Master Mix, following the manufacturer's protocol for a 10  $\mu$ L reaction. The primers utilized for amplifying the feline EPO gene were EPO forward 5'- AAC CTC TGC TGC TCC ACT CC, EPO reverse 5'- TCA CCT GTC TCC TCT TCG GCA G (amplicon size of 130 bp). RT-qPCR was performed concurrently for amplifying the feline housekeeping gene GAPDH using the following primers: GAPDH forward 5'- AAA TTC CAC GGC ACA GTC AAG, and GAPDH reverse 5'- TGA TGG GCT TTC CAT TGA TGA primers (amplicon size of 61 bp) [46]. Cycling conditions for both feline EPO and feline GAPDH amplicons were 50°C for 2 min,

95°C for 2 min, followed by 40 cycles of 95°C for 15 s, 58°C for 30s and 72°C for 1 min. The final step for both reactions included a dissociation curve to evaluate specificity of primer binding. All PCR reactions were performed in triplicate alongside a water template negative control, a reaction lacking reverse transcriptase (RT-) and a positive control reaction using feline EPO and feline GAPDH plasmid DNA. The resulting feline EPO copy number was normalized to 10<sup>6</sup> copies of feline GAPDH as described previously [46].

A set of three primers was utilized for genotyping the EPO-deficient anemic mice, facilitating the differentiation of wildtype, heterozygous and homozygous EPO disrupted animals. The 3 genotyping primers were used in a set of two real time PCR reactions and each reaction included a water template as a negative control and positive controls (DNA controls from previously genotyped wildtype, heterozygous, and homozygous EPO disrupted mice). Wildtype murine EPO primers included mEPO forward – 5'-CGC ACA CAC AGC TTC ACC C and mEPO reverse – 5'-CTG TAG GGC CAG ATC ACC. The primers for the EPO disrupted gene included the mEPO forward primer paired with the SV40T reverse primer – 5'-GCC TAG GCC TCC AAA AAA GC. The wildtype PCR cycling conditions were as follows: 50°C for 2 min, 95°C for 2 min, followed by 40 cycles of 95°C for 15 s, 56°C for 15 s, 72°C for 15 s. The EPO disrupted PCR cycling conditions were as follows: 50°C for 2 min, 95°C for 2 min, followed by 40 cycles of 95°C for 15 s, 63°C for 15 s, 72°C for 15 s. The final step for both reactions included a dissociation curve to evaluate specificity of primer binding. Expected amplicon sizes for mice with the wildtype EPO amplicon were 228 bp and 200 bp for mice with the EPO disrupted genotype (SV40-mutant amplicon). Heterozygous mice possessing both a wildtype murine EPO allele and an EPO disrupted allele were expected to exhibit both amplicons.

### *Detection of feEPO protein using western blot assays*

A series of western blot (WB) assays were performed to identify the presence of feEPO protein in tissue culture cells and/or culture supernatants. For each WB, controls included 5  $\mu$ L (10 U) of human recombinant EPO protein (Epoetin alpha, EPOGEN, positive control) and lysates from non-transfected/non-transduced cells (negative control).

Either cell lysates, culture supernatants or both were collected for WB analyses. Cultured cells were detached from the plate with 0.25% Trypsin-EDTA (Gibco), washed with phosphate-buffered saline (PBS; Gibco), centrifuged at 500 g for 5 min and resuspended in lysis buffer (150mM NaCl, 50 mM Tris base, 1% NP-40, 0.25% deoxycolic acid, 0.1% SDS, pH 7.4) and protease inhibitor complex (PIC; Thermo Scientific). Cell lysate samples were then incubated on ice for 30 min, centrifuged at 16,000g for 10 min, and the cleared extract transferred to a new tube. Culture supernatants were centrifuged at 500g for 5 min, transferred to a clean tube, and centrifuged at 3000g for 5 min before storage in -20°C prior to WB analysis.

In preparation for electrophoresis, 13  $\mu$ L of extracted protein or processed supernatant was mixed with 5  $\mu$ L of 4X LDS Sample Buffer RunBlue (Abcam) and 2 $\mu$ L of 10X DTT Reducer RunBlue (Abcam). Lysate samples were incubated for 10 min at 70°C. The molecular weight marker, cell lysates, culture supernatant samples, positive and negative control samples were electrophoresed on a 4-20% SurePAGE, Bis-Tris polyacrylamide gel (GenScript) at 150 V for 50 min using a PowerPack 200 Universal Power Supply (BioRad) and then transferred to a PVDF membrane (BioRad) using a Mini-PROTEAN Tetra electrophoresis system (BioRad) at 5°C for 12 hours at 50 V with constant stirring. The PVDF membrane was washed three times with tris-buffered saline 0.1% tween-20 (TBS-T) and placed in blocking buffer consisting of

TBS-T 5% non-fat dry milk for 1 hour at room temperature. The PVDF membrane was washed three times with TBS-T before incubation with rabbit anti-human erythropoietin antibody (Bio Rad) at a dilution of 1:1000, rocking overnight at 5°C. The membrane was subsequently washed three times with 10mL of TBS-T prior to incubation with a goat anti-rabbit IgG-HRP Immunopure antibody (Thermo Fisher Scientific) at a dilution of 1:10,000 for one hour at room temperature. Antibodies were diluted in TBS-T with 5% bovine serum albumin.

For experiments utilizing Vectors B and C, protein-antibody interactions were treated with Pierce SuperSignal WestPico Chemiluminescent Substrate (Perbio Science) enhanced chemiluminescence reagent and visualized via autoradiograph using Kodak BioMax MS Film and developed using a medical film processor (Konica Minolta Medical & Graphic). For experiments utilizing Vector D, the blots were treated with Prometheus ProSignal Femto Chemiluminescent HRP substrate (Genesee Scientific) and imaged with a Protein Simple FluorChem E System.

#### *MTT assay*

An MTT cell-proliferation bioassay was utilized to evaluate the bioactivity of the feline EPO transprotein in culture supernatants derived from transduced feline PBMCs. In this assay, proliferation of the human TF-1 erythroblastic leukemia cell line (ATCC) is induced by the presence of EPO protein and proliferation is detected by absorbance (optical density) using a plate reader. The assay was performed according to a previously published protocol[29]. Untreated cells served as a negative control. Supernatants derived from control (untransfected) and Vector B transduced cells (MOI of 5) were collected on days 4, 6, and 12. The MTT assays

were performed in triplicate for each sample and the optical density of the wells was determined at 595 nm using a Thermomax microplate reader (Molecular Devices).

### *Statistics*

For the MTT assay, Student's t-tests were performed for each sample time point comparing the control and transduced samples. For the *in vivo* studies where there were more than two treatment groups involved, a one-way ANOVA was performed for each dataset (timepoint) in order to identify significant differences between the three treatment groups followed by Tukey's multiple comparisons test. When only two experimental groups were present, a Student's t-test was performed for each dataset timepoint. Significance was defined as  $p \leq 0.05$ .

### *In vitro Vector B experiments*

A series of *in vitro* experiments were performed in human and feline cells to assess feEPO mRNA and bioactive protein production in cells treated with Vector B. In an initial plasmid DNA transfection experiment, human embryonal kidney (HEK) 293FT cells (Thermo Fisher Scientific) were cultured in 10 cm diameter culture dishes (Corning) in complete Dulbecco's Modified Eagle Medium (DMEM; Gibco) supplemented with 10% fetal bovine serum (FBS; Gemini Bio) and 1x penicillin/streptomycin (P/S; Gibco) to approximately 90% confluency in 37°C and 5% CO<sub>2</sub>. Sixty µL of Lipofectamine 2000 (Thermo Fisher Scientific) was combined with 1.5 mL of DMEM and incubated at room temperature for 5 minutes. Twenty-four µg of Vector B plasmid DNA was added to the DMEM/Lipofectamine 2000 reagent and incubated at room temperature for 20 minutes. The mixture was then added to the

293FT cells and incubated for 24 hours in 37°C and 5% CO<sub>2</sub>. Untreated 293FT cells served as negative control samples. The culture media was then replaced with complete DMEM and incubated for an additional 24 hours. Media was centrifuged at 500g for 5 min, transferred to a new tube, and centrifuged at 3000 g for 5 min before storage in -20°C prior to WB analysis. The remaining adherent 293FT cells were detached with trypsin-EDTA (Gibco), washed with 8 mL of PBS (Gibco), and centrifuged at 500g for 5 min, washed in 10 mL PBS and enumerated using a hemacytometer. Thirty million cells were processed for evaluation of feEPO protein expression using WB analysis as described previously.

In a subsequent transduction experiment with human 293H cells (Gibco), cells were plated at  $2 \times 10^6$  cells per well in a 6-well tissue culture plate (Corning) in complete DMEM. Cells were transduced with Vector B lentivirus at either 0.1 MOI, 0.01 MOI, or 0 MOI (negative control). Transduced cells were incubated for 72 hours in 37°C 5% CO<sub>2</sub> at which point supernatant and cell lysates were harvested for WB analyses as described previously.

Freshly isolated feline peripheral blood mononuclear cells (fePBMC) were transduced with Vector B and assessed for feEPO mRNA production (RT-qPCR), protein production (WB) and bioactivity of the feEPO transprotein (MTT assay). Briefly, feline specific pathogen-free (SPF) PBMC were isolated by density centrifugation using Hystopaque-1077 (Sigma-Aldrich)[47]. Four  $\times 10^6$  PBMC were added to a 25 cm<sup>2</sup> tissue culture flask (Corning) with complete peripheral blood leukocyte (PBL) media consisting of Roswell Park Memorial Institute (RPMI) 1640 Medium (Gibco) with 10% fetal bovine serum (FBS, Gemini Bio), 1x Penicillin/Streptomycin (Gibco), 1% L-Glutamine (Gibco), 1% HEPES (Gibco), 100 U/mL recombinant human IL-2 (Hoffman-La Roche), 0.05 mM 2-Mercaptoethanol (MP Biomedicals). FePBMC were transduced (infected) with Vector B lentivirus at an MOI of 5. Non-transduced

fePBMC cultured under the same conditions served as a negative control. Samples of culture supernatant were collected on days 4, 6, and 12 after transduction. After the final collection of supernatants on day 12, the remaining culture cells were detached with 0.25% Trypsin-EDTA (Gibco), washed in PBS (Gibco) and enumerated using a hemacytometer. Two million cells were used for RNA processing and subsequent RT-qPCR analysis for the detection of feEPO mRNA as described while the remaining cells were lysed and processed for WB analysis as described. Negative controls were non-transduced cells and recombinant human EPO protein (Epoietin alpha, EPOGEN) was used as a positive control.

#### *In vitro Vector C experiments*

A series of *in vitro* experiments were performed in human and feline cells to assess the hypoxia-associated regulation of feEPO expression in Vector C. Human 293T cells (ATCC) were grown to confluency in four 25 cm<sup>2</sup> tissue culture flasks. In two of the flasks, Lipofectamine 2000 (Thermo Fisher Scientific) was used to transfect 8 µg of Vector C plasmid DNA following the manufacturer's protocol. The transfected culture flasks were incubated overnight at 37°C and then expanded into 75 cm<sup>2</sup> culture flasks. One non-transfected control flask and one Vector C-transfected flask were incubated in normoxic conditions (37°C, ~21% O<sub>2</sub>, 5% CO<sub>2</sub>), while the other non-transfected control and Vector C transfected flask were incubated in a hypoxia chamber (Stemcell Technologies) for 72 hours (37°C, 1% O<sub>2</sub>, 5% CO<sub>2</sub>). Culture supernatants were then collected, and cells were processed for WB and RT-qPCR analyses, as described.

In a subsequent transduction experiment using feline cells, 4.0 x 10<sup>6</sup> fePBMCs were cultured in four T-25 tissue culture flasks with complete PBL media and 5 µg/mL concanavalin

A (ConA) (Sigma-Aldrich) under previously described normoxic and hypoxic conditions for 48 hours. One normoxic and one hypoxic flask were transduced with  $2.0 \times 10^7$  viral particles each (Vector C, MOI 5). The remaining two flasks served as controls. One set of infected and control flasks were incubated under normoxic conditions while the other set was incubated under hypoxic conditions, as described above. Cell culture supernatants were harvested 24- and 72-hours post-transduction via centrifugation at 500 g for 5 min and the culture media was replaced with fresh media. On day 12 post-transduction, both cells and supernatants were harvested. Two million cells were used for DNA and RNA extraction using QIAGEN's AllPrep DNA/RNA Kit and  $3 \times 10^6$  cells were processed for protein extraction (WB analysis). Isolated total cellular RNA was used for RT-qPCR analysis of feEPO mRNA production as well as GAPDH expression, as described previously.

#### *In vitro Vector D experiments*

An *in vitro* experiment was performed to evaluate the Vector D SV40 promoter-regulated expression of feEPO and to assess functionality of the HSV-TK suicide gene system. Crandell-Rees Feline Kidney (CRFK) cells were cultured in DMEM/10%FBS in 12-well tissue culture plates (Corning) at a concentration of  $4.5 \times 10^5$  cells per well and incubated at 37°C and 5% CO<sub>2</sub>. Experimental groups included i) non-transduced CRFK control cells, ii) CRFK cells transduced with the Control Vector lentivirus (MOI of 10), iii) CRFK cells transduced with Vector D lentivirus (MOI of 10), and iv) CRFK cells transduced with Vector D lentivirus (MOI of 10) and subsequently treated with ganciclovir (GCV, ThermoFisher) at a concentration of 25 µM, 24 hours post-transduction for 3 consecutive days. The concentration of GCV utilized was based on the determination of cytotoxicity for GCV used alone with CRFK cells, which was not

observed at 25  $\mu\text{M}$  (50% cytotoxicity concentration [ $\text{CC}_{50}$ ] determined to be 52.3  $\mu\text{M}$ ). All experimental conditions were carried out in triplicate wells. Cells were transduced 24 hours after plating the CRFK cells by aspirating off the culture media and replacing with the appropriate amount of Vector D or Control Vector lentivirus diluted in 2 mL fresh media.

An inverted fluorescent microscope (Life technologies, EVOS digital inverted microscope and cell imaging system) was used to visualize cell morphology at 24-, 48-, 72-, and 96-hour post-transduction using bright-field illumination. Visual assessment was performed to assess cytotoxicity in the wells treated with GCV. For wells transduced with the Control Vector, GFP and mCherry fluorescence was used to confirm lentiviral transduction of CRFK cells qualitatively.

At each timepoint (24-, 48-, 72-, and 96-hours post-transduction), supernatants were aspirated from the wells and centrifuged at 500g for 5 min, transferred to a new tube, and centrifuged at 3000g for 5 min before storage in  $-20^{\circ}\text{C}$  prior to determination of feEPO protein production via WB analyses as previously described. All of WB analyses utilized the same volume culture supernatant from wells seeded with a constant cell density. After processing the supernatant, cell-associated RNA was collected from the cells in the same wells, as described previously using PureLink (Invitrogen) RNA Mini Kit and following the manufacturer's instructions. Isolated RNA was stored at  $-80^{\circ}\text{C}$  until utilized for feEPO and GAPDH RT-qPCR reactions, as described above.

### *In vivo* rodent experiments

In order to demonstrate the *in vivo* efficacy, longevity of effect, and safety of the feEPO lentiviral gene therapy system, a series of rodent studies were performed. An initial pilot study

using Fischer rats was followed by a series of lentiviral dose-escalation studies utilizing genetically modified EPO-deficient (disrupted EPO gene) anemic mice. For these experiments, packaged, concentrated and ultra-purified Vector D ( $1.94 \times 10^9$  TU/mL) and Control Vector ( $8.52 \times 10^8$  TU/mL) lentivirus were obtained from VectorBuilder.

### *Rat study*

A pilot rat study was performed in order to demonstrate the *in vivo* efficacy of Vector D (UC Davis Institutional Animal Care and Use Committee [IACUC] #19202; Biological Use Authorization [BUA] #R2033). Eight 15-week-old female Fischer rats (Charles River) between 147 and 183 grams in weight were randomized into three experimental groups: (Group A) Vector D plasmid DNA-treated (n=3), (Group B) inoculated with Vector D lentivirus (n=3), and (Group C) untreated control rats (n=2). Group A rats were injected intramuscularly (IM) into the hamstring muscles of the right caudal thigh with 100 ug sterile Vector D plasmid DNA diluted in Tris EDTA (TE) buffer (70  $\mu$ L). Group B rats were each injected with  $6.32 \times 10^5$  TU Vector D divided into two injection sites (180  $\mu$ L divided between right and left caudal thigh). The remaining two rats (Group C) served as untreated controls.

Using either a sterile #10 scalpel blade or a lancet (Medipoint) to create a small nick in the tail tip, peripheral blood samples were obtained once per week and loaded into one or two heparinized capillary tubes (Fisher Scientific). For each peripheral blood sample, the red blood cell packed cell volume (PCV) was determined by centrifuging the capillary tubes at 12,000g for 5 minutes (Beckman Microfuge 11) and determining the percentage of packed RBC in the total blood volume (PCV). The peripheral PCV was determined for each rat for the two weeks prior to treatment in order to establish baseline values. The peripheral PCV and body weights were

assessed on a weekly basis for each animal over a period of 12 weeks post-inoculation. All of the *in vivo* experimental manipulations were approved and in alignment with the UC Davis Office of Research and IACUC.

At the 12-week terminus of the experiment, the rats were euthanized by isoflurane anesthesia followed by CO<sub>2</sub> asphyxiation and whole blood exsanguination via cardiocentesis (no anticoagulant; approximately 3-5 mL blood obtained per rat). The terminal blood sample was allowed to clot, serum separated, and the serum frozen at -80°C. Unclothed terminal whole blood was also collected into heparinized capillary tubes and utilized for a final PCV determination. A complete necropsy was performed for each rat with tissues collected and preserved in 10% neutral buffered formalin (NBF). Targeted fresh tissue samples (spleen, liver, kidney, and skeletal muscle of the caudal thigh) were frozen and archived in RNALater (Ambion) at -80°C. Formalin-fixed tissues were fixed for 24-72 hours, routinely sectioned, embedded into paraffin blocks using standard protocols, stained with hematoxylin and eosin, and examined microscopically by a board-certified pathologist (SEC).

#### *Genetically modified anemic mouse studies*

A series of *in vivo* studies using an EPO-deficient mouse model was approved and carried out under the UC Davis IACUC protocol #20925 and a Biological Use Authorization (BUA R2033). A mixed colony of wild type (WT), heterozygous (Het), and homozygous (Hom) genetically EPO-deficient mice (EPO-tag<sup>h</sup>) was obtained as a gift of Dr. J. Solnick (UC Davis) originally sourced from France (N. Voituron)[48]. The EPO-tag<sup>h</sup> mice have the gene encoding the SV40 Large T antigen integrated into and disrupting the regulatory sequence of the endogenous murine *EPO* gene resulting in targeted disruption of murine erythropoietin

expression and subsequent chronic anemia[48, 49]. Mice were maintained in a vivarium managed by the UC Davis Teaching and Research Animal Care Services (TRACS) where the mice were bred in order to produce the required number of EPO-deficient mice (homozygous EPO disruption) for the two murine studies detailed below. Founder mice were genotyped using PCR by the Solnick laboratory, who provided 15 mice total. The mice were genotyped by obtaining an approximately 1-2 mm long tail tip between 19 and 21 days of age for DNA isolation using the QIAamp DNA mini kit (Qiagen) following the manufacturer's protocol for DNA purification from tissues. Isolated DNA samples were stored in microcentrifuge tubes at -20°C prior to PCR analysis. Mice were genotyped using qPCR as described previously and were phenotyped in parallel using their tail blood to determine blood PCV. Wildtype mice have a PCV of approximately 55%, heterozygous mice approximately 40%, and homozygous EPO-tag<sup>h</sup> mice have a PCV of approximately 20%[50]. Two of the founder mice were determined to be WT (lacking a disrupted EPO gene), six were homozygous EPO-deficient (EPO-tag<sup>h</sup>), and seven of the mice were heterozygous for the disrupted EPO gene.

#### *Murine experiment #1*

The initial murine study was performed to evaluate the efficacy of feEPO transduction and longevity of effect when inoculated with a high dose of Vector D lentivirus (vector to body weight ratio, relative to the rat study). All of the mice were approximately 13 weeks old at initiation of the experiment. Twenty-four genetically confirmed homozygous EPO-deficient mice with an average PCV of approximately 20% were divided into two groups: Group A mice were inoculated intramuscularly with Vector D lentivirus (16 mice, 10 males and 6 females) and Group B mice were inoculated intramuscularly with Control Vector lentivirus (8 mice, 5 female

and 3 males). Group A mice each received  $7.75 \times 10^7$  transducing units (TU) Vector D in a total volume of 50  $\mu\text{L}$  diluted with sterile phosphate buffered saline (PBS) delivered into the right hamstring musculature. Group B mice each received  $8.5 \times 10^6$  TU Control Vector diluted with sterile PBS in a total volume of 50  $\mu\text{L}$  also delivered into the hamstring musculature of the right thigh.

Mouse behavior and body weight were serially assessed, and peripheral blood was collected from the tail tip into heparinized hematocrit tubes, centrifuged at 12,000g for 5 minutes (Beckman Microfuge 11), and a peripheral blood PCV was determined for each animal on a weekly basis. At the end of the nine-week study, the mice were euthanized using isoflurane anesthesia followed by  $\text{CO}_2$  asphyxiation and cardiac exsanguination (approximately 0.5 to 1 mL per mouse). Terminal blood was used to determine PCV, and serum separated by centrifugation and serum stored at  $-80^\circ\text{C}$ . A complete necropsy was performed for all animals and tissues were preserved in 10% neutral buffered formalin (NBF). Select tissues (caudal thigh skeletal muscle, spleen, liver, and kidney) were collected fresh in 700  $\mu\text{L}$  RNAlater solution (Ambion) and a duplicate set of tissues was archived at  $-80^\circ\text{C}$ . Tissues collected in formalin were fixed for a minimum of 24 hours prior to trimming into cassettes, embedded in paraffin wax, cut into 4  $\mu\text{M}$  sections, mounted on glass slides, and stained with hematoxylin and eosin (HE) for histologic evaluation. For bone marrow evaluation, both right and left femora were fixed in 10% NBF for a minimum of 24 hours and then decalcified in 15% formic acid for approximately 48 to 72 hours prior to processing for histologic evaluation as described above. All murine tissues were examined by a board-certified veterinary pathologist (SEC).

*Murine experiment #2*

In the second murine experiment, the inoculating dose of Vector D lentivirus was increased to  $1 \times 10^8$  TU/mouse, one group of mice received a second dose of the lentiviral vector (same amount as initial), and the *in vivo* functionality of the HSV-TK suicide gene was assessed via the intraperitoneal administration of the GCV substrate. This murine study was approved under the UC Davis IACUC #22226 and BUA R2033.

Fifteen genetically confirmed EPO-deficient anemic mice were randomly divided into three groups of 5 animals each: Group A control mice were inoculated with Control Vector lentivirus (two females, three males), Group B mice were inoculated with two serial doses of Vector D lentivirus (two females, three males), and Group C mice were inoculated with a single dose of Vector D lentivirus followed by GCV treatment (two males, three females).

The inoculating doses of both the Control Vector and Vector D lentiviruses were increased to  $1 \times 10^8$  TU/mouse, administered intramuscularly in the same manner and location as the first murine study with Group A control mice receiving the Control Vector diluted in sterile PBS in a total volume of 39  $\mu$ L and Group B and C mice receiving Vector D in a volume of 53  $\mu$ L. Peripheral blood was obtained from the tail tip and PCV determined along with body weight on a weekly basis. Each Group B mouse was re-inoculated with a second dose of Vector D lentivirus ( $1 \times 10^8$  TU/mouse) when an individual animal's PCV fell below 25%. Based on published protocols [51], Group C mice received 50 mg/kg of GCV (Hospira, reconstituted with sterile water) beginning three weeks after inoculation with Vector D for five consecutive days via the intraperitoneal route. At the time of GCV treatment in Group C mice, the PCV was determined to be elevated relative to the control animals and averaged 47.4%. Re-inoculated Group B mice were euthanized at 5 weeks post-reinoculation. Group C mice were euthanized when their PCV values dropped below 25%, aside from one mouse, which was maintained to 31

weeks post-inoculation (PCV of 28% at time of euthanasia). Mice were euthanized using isoflurane anesthesia followed by CO<sub>2</sub> asphyxiation and cardiac exsanguination when their PCV had returned to near baseline (PCV <25%). A complete necropsy, tissue collection and histologic examination were performed for each mouse as described for the first murine study.

## RESULTS

### *Transfection and transduction experiments using Vector B*

WB analyses of cell lysates and supernatants from human 293FT cells transfected with Vector B plasmid demonstrate feEPO protein production within both the culture supernatant and the cell lysates (Fig 2A, lanes 3 and 5). An appropriate-sized feline EPO protein band was detected in the positive control lane (Fig 2A, faint band, lane 1, human rEPO) and was not detected in the untransfected negative control samples (Fig 2A, supernatant and cell lysate, lanes 2 and 4).

For 293FT cells transduced with Vector B lentivirus at an MOI of 0.1 or 0.01, feEPO protein was detected within the culture supernatants (Fig 2B, lanes 4 and 6) but was not detected in the cell lysates (Fig 2B, lanes 3 and 5). These results suggest that once feEPO protein is produced in Vector B transduced cells, it is secreted into the extracellular fluid. A qualitatively greater amount of feEPO protein was detected in supernatants derived from cells transduced at an MOI of 0.1 relative to 0.01 (the same volume of supernatant was utilized for each assay). Feline EPO protein was not detected in the non-transduced negative control samples (Fig 2B, lanes 1 and 2) and an appropriate-sized band was detected in the positive control sample (Fig 2B, human rEPO protein, lane 7).

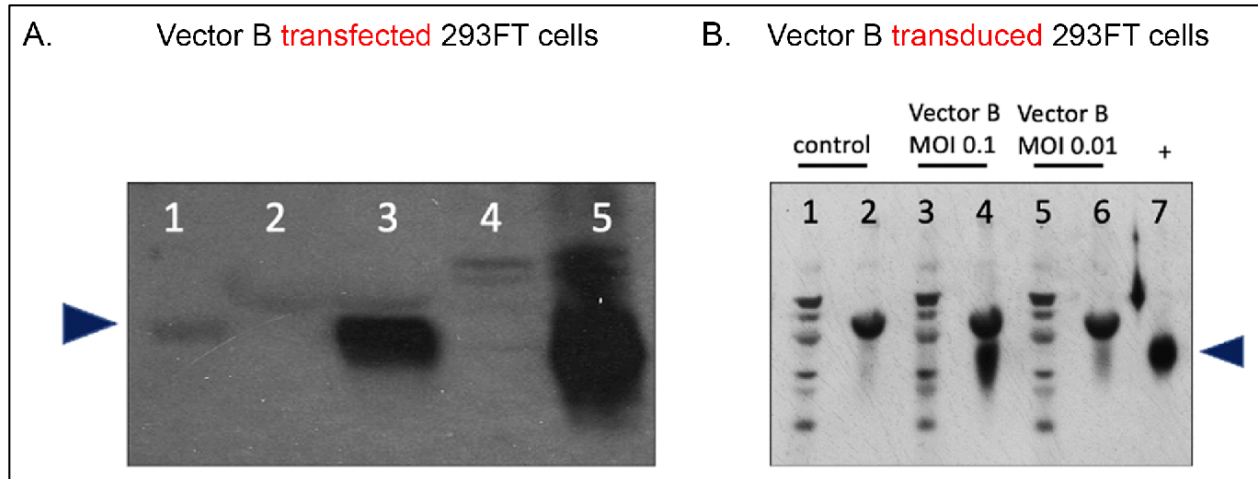


**Figure 2.** Western blot images demonstrating protein detection in 293FT cells. (A) 293FT cells transfected with Vector B plasmid. Lane 1- human rEPO (EPOGEN; positive control), lane 2- untransfected control cell supernatant, lane 3- culture supernatant from Vector B-transfected cells, lane 4- untransfected control cell lysate, lane 5- cell lysate from Vector B-transfected cells. (B) 293FT cells transduced with Vector B infectious viral particles. Lanes 1, 3, and 5- cell lysates, lanes 2, 4, and 6- supernatant, lane 7- human rEPO (EPOGEN; positive control). Arrowhead for A and B: 34 kDa (approximate size of EPO protein).

Feline PBMC transduced with Vector B lentivirus transiently produce feEPO mRNA and bioactive feEPO protein. Feline EPO mRNA (Fig 3A, lane 3) and protein (Fig 3B, lanes 2 and 3) were detected in the cell-associated RNA (standard RT-PCR, cDNA) and supernatant (WB, protein) of feEPO transduced cells 4 days post infection, but not at 6- or 12-days post infection (data for 6- and 12-days post infection are not shown for RT-PCR reaction). The results for the positive and negative controls (standard RT-PCR and WB assays) were appropriate. Feline EPO protein bioactivity was detectable in supernatants derived from the transduced PBMC at days 4 and 6, but not day 12 relative to control supernatants (MTT assay, Figure 3C). Collectively, these

results suggest that fePBMC transduced with Vector B produces feEPO mRNA and biologically active protein and that the CMV promoter function of Vector B becomes attenuated over time.

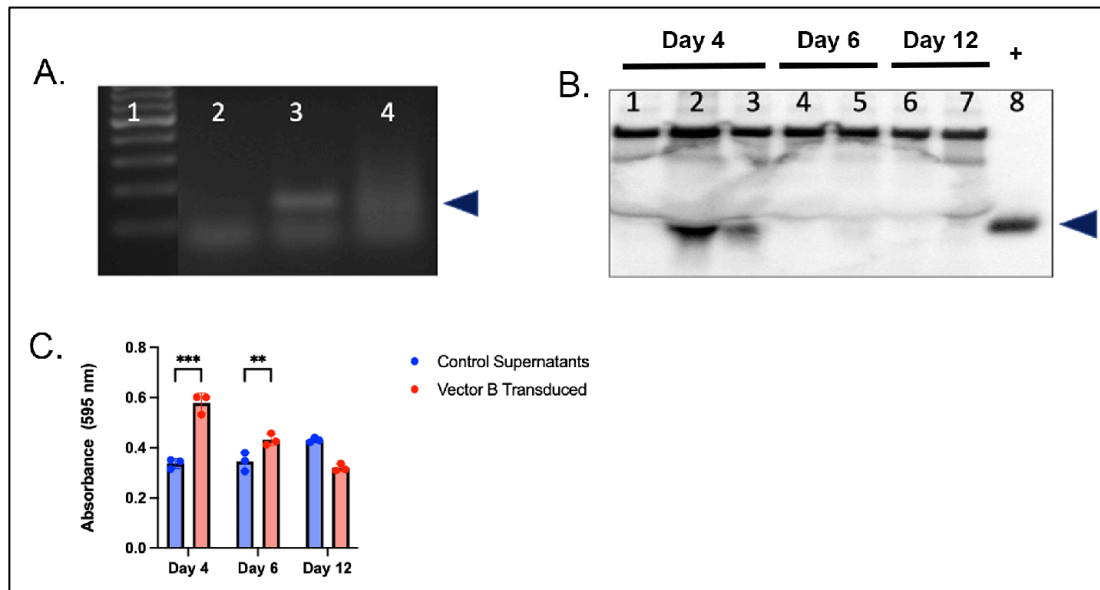


**Figure 3.** Feline PBMCs transduced with Vector B. (A) Gel image from feEPO standard RT-PCR demonstrating detection of cell-associated feEPO mRNA (cDNA). Lane 1- molecular weight marker, lane 2- negative control water template, lane 3- feEPO-transduced PBMCs, lane 4- RT- (negative control); arrowhead = 130 bp. (B) Western blot image demonstrating feEPO protein detection in the supernatant of transduced PBMCs. Lane 1- negative control/non-transduced cells, lane 2- supernatant derived from transduced PBMCs on day 4, lane 3- supernatant derived from transduced PBMCs on day 4 at 1:2 dilution, lane 4- supernatant derived from negative control/non-transduced cells, lane 5- supernatant derived from transduced PBMCs on day 6, lane 6- supernatant derived from negative control/non-transduced cells on day 12, lane 7- supernatant derived from transduced PBMCs on day 12, and lane 8- positive control (human rEPO, EPOGEN). Arrowhead: 34 kDa (approximate size of EPO protein). (C) MTT assay absorbance values demonstrating transient EPO bioactivity (cell replication). Day 4 and day 6,  $p = 0.0007$  and  $p = 0.026$ , respectively.

*Infection experiments using Vector C in human and feline cells*

Using Vector C, feEPO mRNA was detectable in both human 293T (transfected) and fePBMC (transduced) and feEPO protein was detected in supernatants derived from transduced fePBMC cultured in either normoxic or hypoxic conditions (Fig 4). Cell associated RNA derived from 293T cells transfected with Vector C and cultured under normoxic (lane 4) or hypoxic (lane 6) conditions demonstrate feEPO mRNA expression (Fig 4A). Cell associated RNA derived from fePBMCs transduced with Vector C lentivirus also demonstrate feEPO mRNA transcription under both normoxic (lane 4) and hypoxic (lane 6) conditions with no appreciable difference in signal intensity (Fig 4B). Control GAPDH reactions were appropriate (data not shown).

In fePBMC transduced with Vector C lentivirus, feEPO protein is detectable in supernatants (Fig 4C) under both normoxic and hypoxic culture conditions. Feline EPO protein was not detected in supernatants from control cells. For the treated supernatant samples (same volume added per lane), there is subjectively less feEPO protein in the samples derived from normoxic (lane 3) vs hypoxic (lane 5) culture conditions, suggesting some functionality of the HRE promoter (oxygenation-associated regulation).

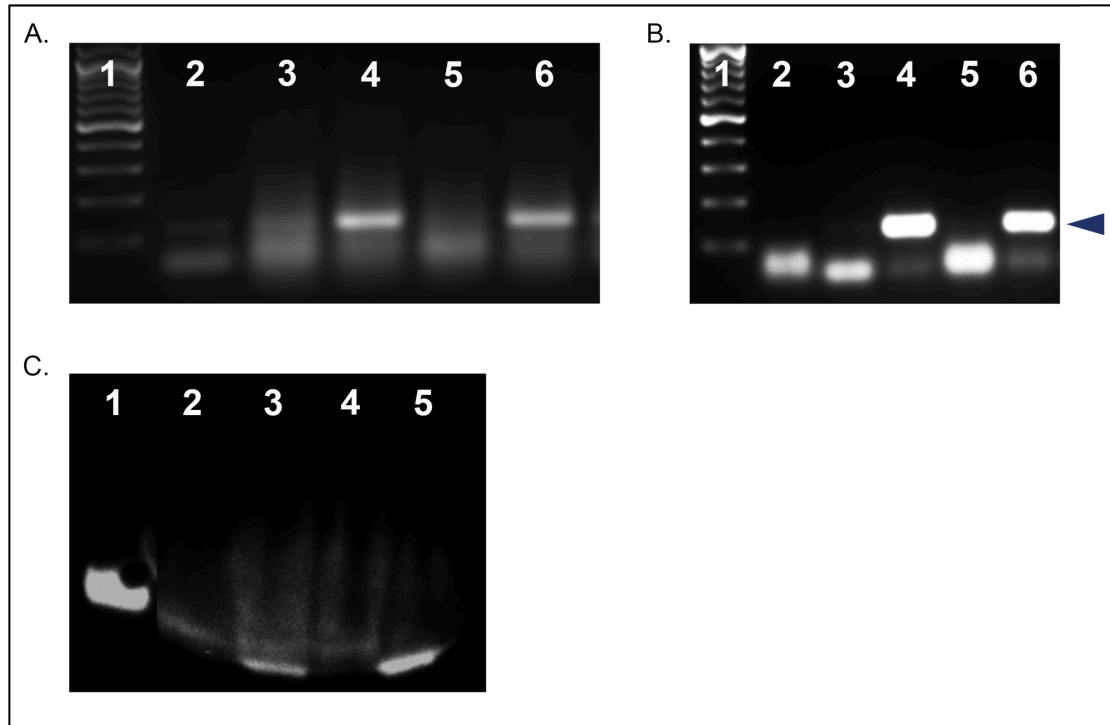


**Figure 4.** Vector C transfection and transduction of 293T cells. (A) RT-PCR gel electrophoresis for feEPO mRNA from Vector C-transfected PBMCs under normoxic and hypoxic conditions. Lane 1- molecular weight marker, lane 2- water control template (negative control), lane 3- normoxic control, lane 4- normoxic transfected with Vector C, lane 5- hypoxic control, and lane 6- hypoxic transfected with Vector C. (B) RT-PCR for feEPO mRNA 4 days post-transduction of fePBMCs with Vector C. Lane 1- MWM, lane 2- water control template, lane 3- hypoxic control, lane 4- hypoxia transduction with Vector C, lane 5- normoxic control, lane 6- normoxic transduction with Vector C. Expected amplicon size is 130 bp (arrowhead). (C) WB assay for EPO protein in supernatants-derived from transduced fePBMCs. Lane 1- positive control (human rEPO, EPOGEN), lane 2- normoxic control, lane 3- normoxic transduced with Vector C, lane 4- hypoxic control, lane 5- hypoxic transduced with Vector C.

*Vector D transduction of feline CRFK cells*

The efficient transduction of feline CRFK cells by the Control Vector (MOI 10) was confirmed using immunofluorescent microscopy. CRFK cells exhibited cytoplasmic GFP immunofluorescence in approximately 80-90% of the cells, confirming cell transduction (Fig 5a, data for mCherry not shown). Visual evaluation of CRFK cells at 96 hours post Vector D transduction and treated with GCV (bottom right of Fig 5A) demonstrate morphologic evidence of cytotoxicity seen as rounding and occasional detachment of cells. These findings suggest that the CRFK cells were effectively transduced with Vector D lentivirus and that the HSV-TK gene product converted GCV into its toxic metabolite. Transduced CRFK cells that were not treated with GCV at the same time point do not demonstrate morphologic evidence of cytotoxicity (uniform monolayer of spindle cohesive cells, upper left and lower left of Fig 5A).

CRFK cells transduced with Vector D lentivirus (MOI 10) exhibit pronounced expression of feEPO mRNA at each time point (24-96 hours), regardless of whether the cells were treated with GCV (real-time RT-PCR, Fig 5B). However, in a WB assay performed with the samples in parallel, supernatants from CRFK cells transduced with Vector D lentivirus demonstrate progressively increased production of feEPO protein over time (24-96 hours post transduction) which becomes markedly attenuated with GCV treatment (Fig 5C). EPO protein was not detected in CRFK cells transduced with the Control Vector (Vector) nor the non-transduced CRFK cells (CRFK) and an appropriate-sized band was detected for the EPO positive control lane.

These results indicate that GCV treatment abrogated feEPO protein production but did not have an apparent attenuating effect on feEPO mRNA production. A definitive explanation for this discordant result was not determined; however, it is possible that transduced cells undergoing apoptosis as a result of GCV treatment had inhibition of protein synthesis, a feature

known to occur in the face of apoptosis[52]. All of WB analyses were derived from the same volume of supernatant from wells seeded with a constant cell seeding density to control for protein amounts.

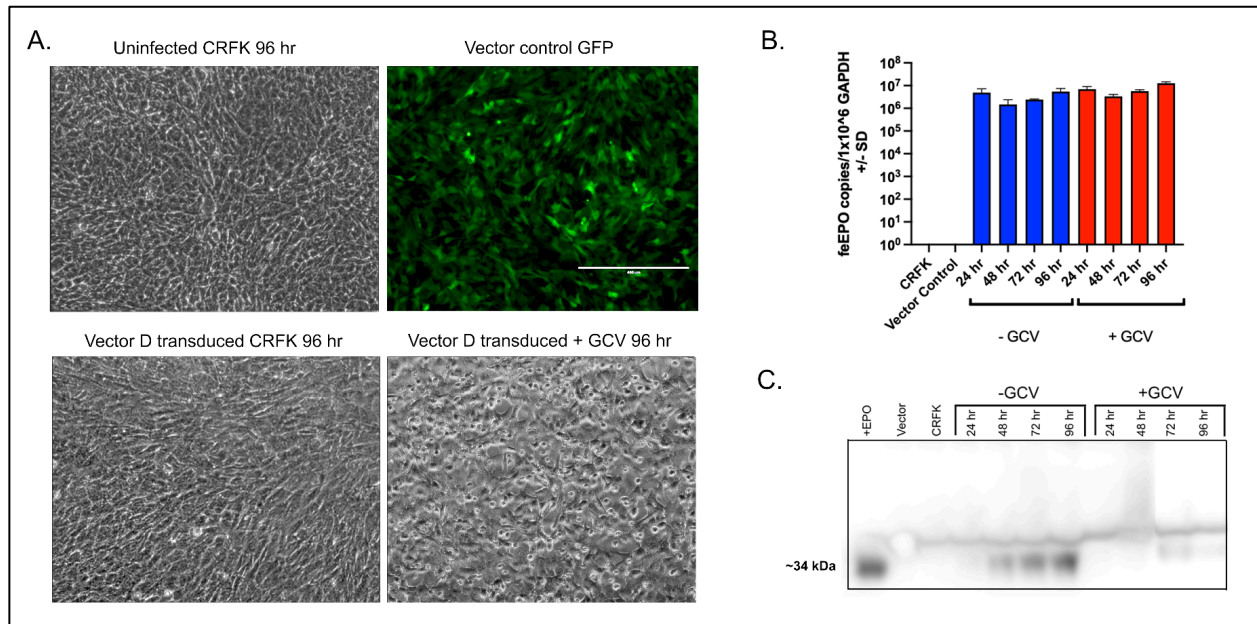


**Figure 5.** Vector D transduction (MOI 10) of CRFK cells. (A) Representative images of non-transduced CRFK cells and those transduced with Vector D lentivirus with or without GCV treatment 96 hours post-transduction. (B) Feline EPO mRNA copy numbers detected per 1 x 10<sup>6</sup> copies of GAPDH from cell-associated derived RNA from CRFK cells transduced with Vector D or uninfected cells (CRFK). (C) Western blot image showing EPO protein detection from supernatants from the transduced CRFK cells. An appropriately sized band detected for the positive control (EPOGEN), and no bands detected for the Vector Control and non-transduced CRFK cells.

*Rats treated with Vector D lentivirus have a significant but transient increase in blood PCV*

Fisher rats inoculated intramuscularly with Vector D lentivirus demonstrated a significant increase in blood PCV relative to uninoculated control animals and rats treated with Vector D plasmid DNA (Fig 6). The PCV effect was statistically significant relative to the two other groups, but was transient, persisting for only two weeks post inoculation. The mean PCV values at one- and two-weeks post-treatment were 52.3, 59.2, and 50.3% for the uninoculated control, Vector D lentivirus treated, and plasmid DNA-treated groups at 1-week post-treatment, and 51.2, 58.0, and 51.3%, for week 2 post-treatment, respectively. These results provide evidence that inoculation with Vector D lentivirus results in a transient increase in PCV in normal rats *in vivo*. After the two-week time point there was no significant differences in PCV detected between the three groups. No significant changes in behavior or weight gain/loss were identified in any of the study animals, although one rat in the plasmid-treated group died prematurely for an undetermined reason two days prior to the termination of the experiment.

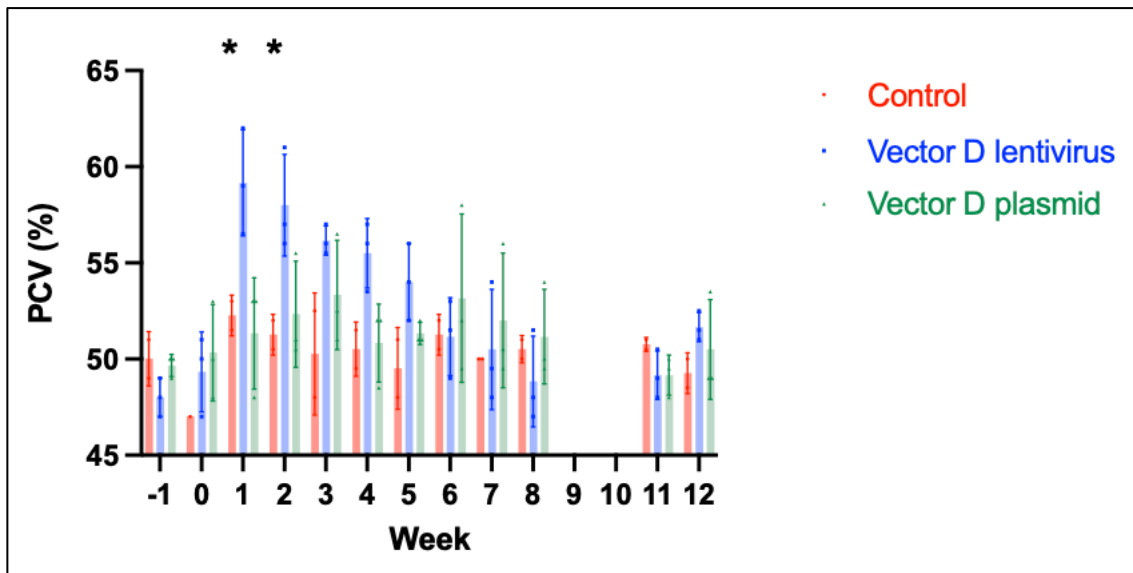


**Figure 6.** Mean PCV values vs. time for the different rat treatment groups (error bars +/- standard deviation). A significant difference between the treatment groups is identified at one-

and two-weeks post-treatment (ANOVA,  $p=0.026$ ). A Tukey's multiple comparisons test identified a significant difference in the mean PCV values between the Vector D treatment group and the plasmid treatment group ( $p=0.03$ ) and no statistical significance when comparing the control group against the Vector D plasmid-treated group ( $p=0.07$ ).

Histologic evaluation of the rat tissues collected at the termination of the study did not identify any pathologic trends in the rats and no significant lesions were identified within the pelvic limb musculature from the injection sites in any of the experimental groups (Figure 7A). Two rats, one control animal and one plasmid-treated animal, had mild focal lesions of myositis or myodegeneration in the inoculation site of the caudal hindlimb musculature characterized by a mild mononuclear inflammation or focal myocyte degeneration and regeneration. These lesions in the skeletal muscle were considered to be incidental (Fig 7B). One rat in the plasmid-treatment group died idiopathically two days prior to euthanizing the remaining rats. The cause of death for this animal was not determined from either the subsequent gross or microscopic examinations.

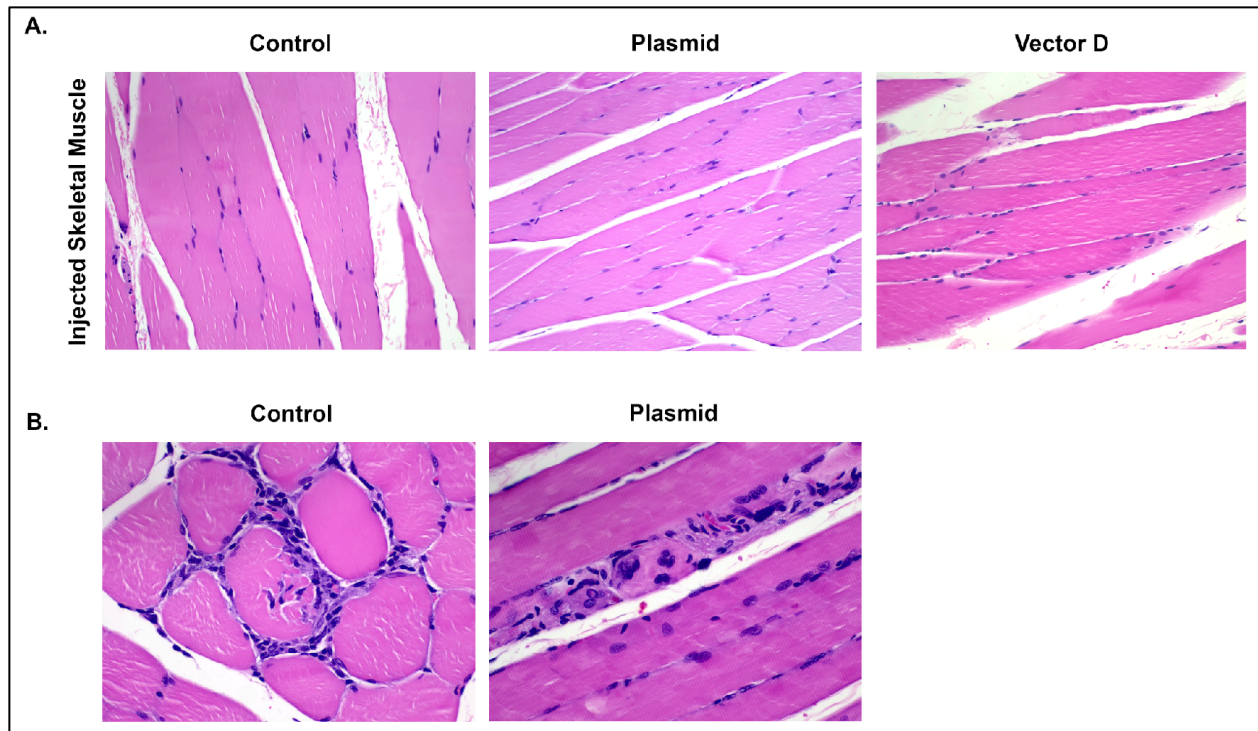


**Figure 7.** Representative histologic images from the injected pelvic limb musculature of control and experimental rats. (A) Representative images from control, plasmid and Vector D-treated rats demonstrating normal skeletal musculature. Images at 200x magnification, hematoxylin and eosin (HE) stain. (B) Histologic images of rare incidental lesions identified within the injected musculature of the Control (myositis) and plasmid-treated (myocyte degeneration/regeneration) rats. Images at 400x magnification, HE stain.

*EPO-deficient anemic mice treated with Vector D lentivirus demonstrate a significant and variably persistent increase in blood PCV relative to control animals*

For the genetically EPO-deficient anemic mouse studies, mouse genotypes were confirmed by demonstrating that the individuals enrolled in the study were homozygous for the SV40 transgene inserted into the murine EPO promoter allele (homozygous EPO disrupted). The DNA from each group (e.g., WT, Het, and Hom) were utilized in PCR reactions with either

primers designed to amplify the WT murine EPO gene or the SV40 mutant gene. Figure 8A demonstrates mouse genotyping- agarose gel electrophoresis of PCR amplicons using DNA obtained from wild type mouse (WT, PCR amplicon only evident with wildtype primers), heterozygous mouse (Het, PCR amplicons present with both WT and SV40 mutant primers) and homozygous mutant mouse (Hom, PCR amplicon only evident with the SV40 mutant primers).

In the preliminary murine study (experiment #1), the inoculating dose of Vector D lentivirus was  $7.75 \times 10^7$  TU/mouse. PCV values were determined for two weeks prior to transduction. Anemic mice treated intramuscularly with Vector D lentivirus had a significantly increased mean PCV relative to control mice treated with the Control Vector lentivirus that persisted for 5 weeks post-inoculation (mean PCV values for treated vs. untreated mice  $\pm$  standard deviation, Fig 8B). However, two of the Vector D-treated mice had elevated PCV values out to week nine post-inoculation relative to the untreated animals in the Control group.

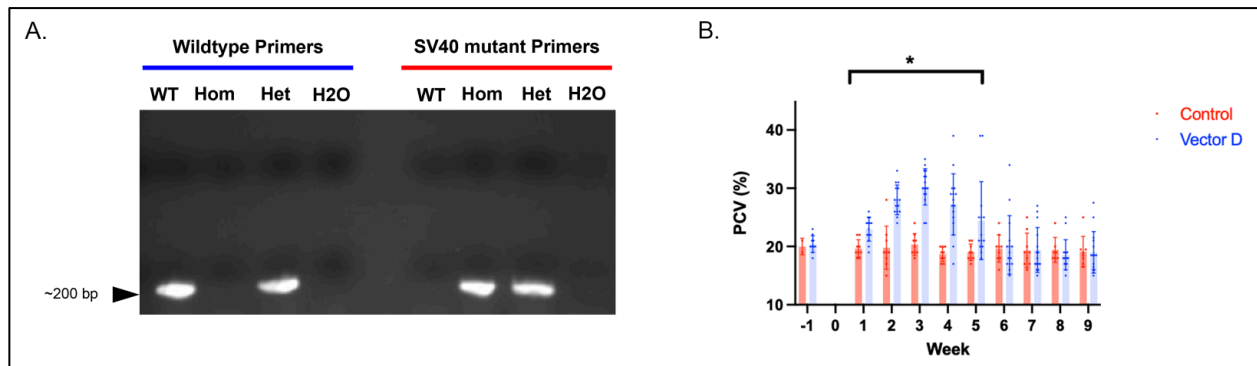


**Figure 8.** Genotyping of mice and effect of Vector D lentivirus inoculation on EPO-deficient mouse PCV. (A) Agarose gel electrophoresis depicting PCR genotyping results for wildtype mice (WT), heterozygous mice (Het) and for mice homozygous for disrupted EPO (Hom). All of the mice have the appropriate-sized PCR amplicons. A negative control (H<sub>2</sub>O, water template) was used for both sets of primers. (B) Mean blood PCV for mice treated with either the

Control Vector or Vector D lentivirus over time. Mice treated with Vector D had significantly elevated mean PCV for weeks 1 through 5 compared to control mice (Student's t-test,  $p=0.0002$ ,  $0.0001$ ,  $0.0001$ ,  $0.0001$ , and  $0.0292$ , respectively).

The second murine study was designed to determine i) the effect of a higher inoculating dose of Vector D lentivirus ( $1 \times 10^8$  TU/mouse), ii) the effect of a second administration of Vector D lentivirus after the PCV returned to near baseline ( $< 25\%$ ), and iii) the functionality of the HSV-TK suicide gene system through the *in vivo* administration of GCV three weeks after initial Vector D administration. Similar to the result of the first murine study, mice treated with the escalated dose of Vector D lentivirus had a significantly elevated PCV relative to control mice for five weeks post inoculation (Fig 9A). However, the magnitude of the effect on PCV between the two studies was markedly different. For the first study, the lentivirus-treated group had a 51% mean increase in PCV (30.25%) over the control group, while in the second study, there was a 144% increase in mean PCV (47%) relative to the control group (at peak elevation in PCV, 3 weeks post-inoculation).

Interestingly, for mice reinoculated with the same dose of Vector D lentivirus (Group B), serial weekly PCV assessments failed to identify any evidence that the second dose of Vector D resulted in an increase in PCV relative to control animals (Fig 9B). A single reinoculated mouse exhibited lethargy, pale mucous membranes, and progressive weight loss. PCV analyses demonstrated a progressive and profound anemia for this animal. The mouse was euthanized four weeks post-reinoculation (4% PCV nadir at time of euthanasia). Histologic evaluation of the mouse's tissues identified an increase in brown intracytoplasmic pigment within macrophages of the spleen consistent with blood-derived hemosiderin deposition (Fig 9C). The bone marrow had

a marked decrease in hematopoietic precursor cellularity consistent with a non-regenerative anemia. The few hematopoietic cells that were identified were most consistent with myeloid lineage cells rather than erythroid precursors (Fig 9C). These clinical and pathological findings are consistent with the development of red cell aplasia and associated splenic sequestration of hemosiderin.

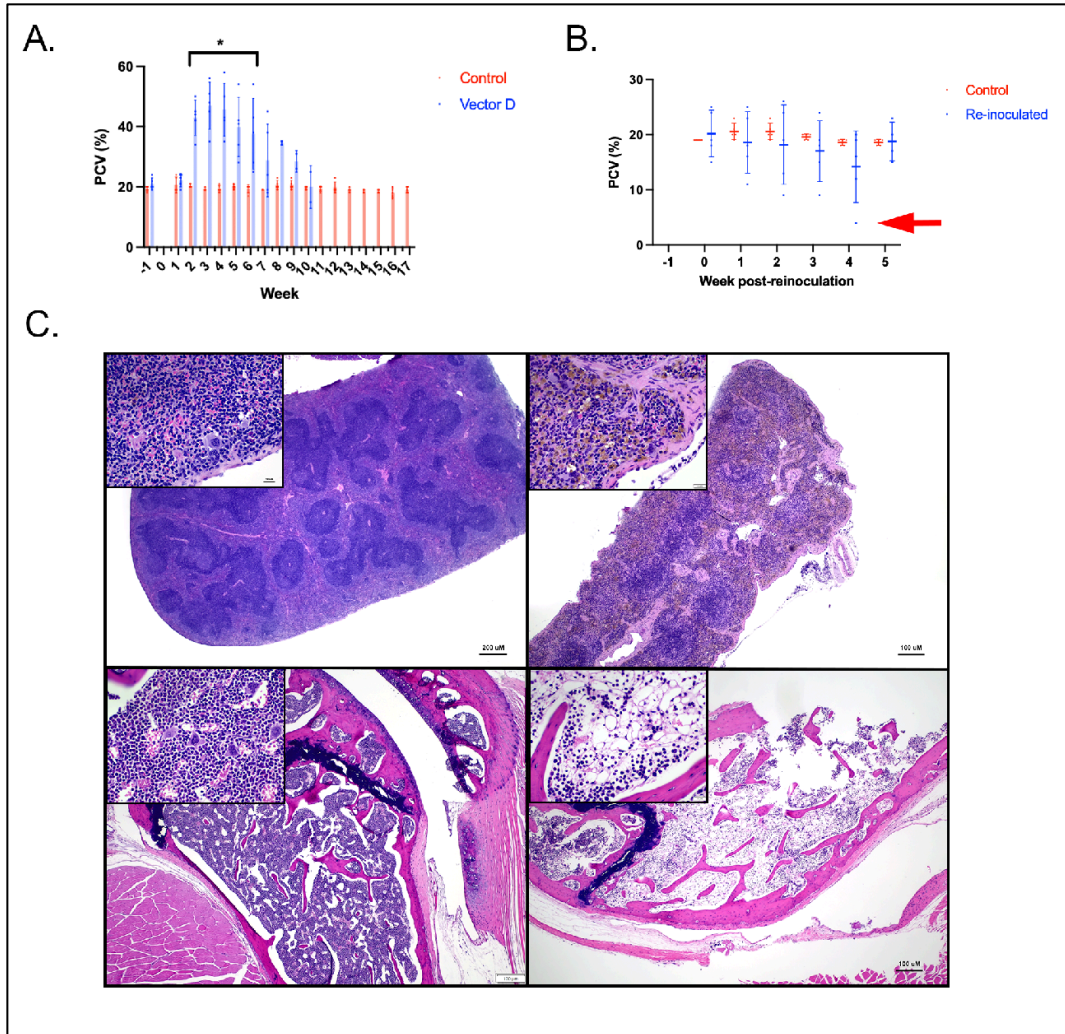


**Figure 9.** EPO-deficient mice administered Vector D once and then readministered Vector D after PCV returns to baseline. (A) PCV over time post-administration of Vector D once. Bar with asterisks represents weeks in which there was significant difference in PCV between the two groups. (Student's t-test, weeks 2 through 6 post-administration,  $p < 0.0001$ ,  $0.0002$ ,  $0.0002$ ,

0.0019, and 0.0087, respectively). (B) PCV for the same mice after receiving a second dose of Vector D lentivirus indicating no increase in PCV relative to control animals. The red arrow indicates a single mouse with a steadily declining PCV after re-administration of Vector D and the time point of euthanasia (4 weeks post Vector D readministration). (C) Representative histologic images with high power insets of spleen and tibia with bone marrow from a control group mouse (left images) and mouse that developed red cell aplasia (right images).

The third objective of murine experiment #2, to test the effect of the HSV-TK suicide gene through the *in vivo* intraperitoneal administration of GCV, was assessed 3 weeks after administration of Vector D lentivirus. At 3 weeks post inoculation, while the mean PCV was still elevated relative to control mice (47.4% vs 20%), this murine cohort was treated intraperitoneally for 5 consecutive days with 50 mg GCV/kg body weight. A precipitous decline in PCV was not identified in the GCV-treated mice suggesting that the administered dose of GCV did not abrogate the effect of Vector D lentivirus. Unexpectedly, two of the Vector D inoculated and subsequent GCV-treated mice had a markedly prolonged elevation in PCV values relative to the non-GCV treated mice (Group B), with one GCV-treated mouse maintaining an elevation in PCV for 7.5 months post treatment (Fig 10A).

Histologic evaluation of tissues collected from male mice treated with GCV demonstrated bilateral, severe, tubular degeneration and atrophy within the seminiferous tubules of the testes. These lesions were characterized by loss of germ cells (spermatogonia) with preservation of supportive Sertoli cells (Fig 10B). No gross or microscopic lesions were identified within the female mice receiving GCV and no other relevant or significant histologic findings were identified in any of the mouse groups. GCV is known to cause tubular

degeneration and atrophy of spermatogonia[53]. The histological findings of testicular tubular degeneration confirm that the GCV was properly administered at a pharmacologically appropriate dose but still failed to abrogate the effect of Vector D gene therapy.

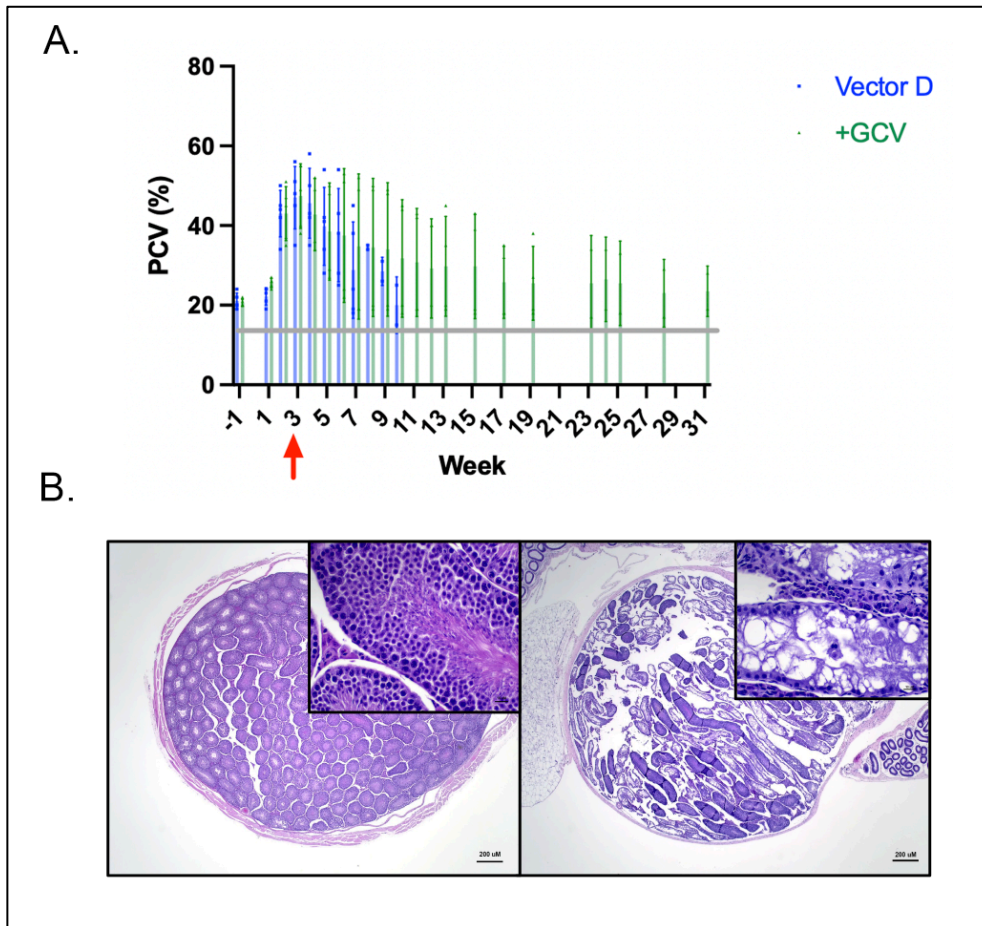


**Figure 10.** Mice receiving Vector D at time point Week 0 and PCV over time. (A) Red arrow indicates time point at which one group (+GCV) received ganciclovir for 5 consecutive days intraperitoneally at 50 mg/kg. (B) Histologic images with higher power images (insets) of the testis from a control mouse (left) and severe tubular degeneration and atrophy in an experimental mouse that received GCV treatment.

## DISCUSSION

This study builds on previous results demonstrating the effectiveness of a replication-defective lentiviral gene therapy vector as a method of efficiently delivering the feEPO gene *in vitro* [29]. A set of replication defective, third generation lentiviral vectors with different promoters regulating expression of the feEPO gene and suicide gene HSV-TK were serially generated and functionally evaluated *in vitro*. Treatment of human and feline cells with Vector B, utilizing the potent and constitutively active CMV promoter regulating feEPO expression, resulted in expression of feEPO mRNA and protein. However, feEPO expression attenuated over time. Studies indicate that the powerful CMV promoter can be methylated and transcriptionally silenced by the transfected/transduced host cell [54, 55]. As a result, we concluded that the CMV promoter may not be ideal and the functionality of other promoters regulating feEPO expression was explored.

In mammals, EPO expression in health is physiologically regulated by oxygen levels, predominantly in the cells of the renal interstitium. Promoter hypoxia-response elements function as oxygen-sensing regulatory elements that has the potential to attenuate transcription when adequate erythropoiesis and tissue oxygenation are achieved. Here we found that Vector C, utilizing a synthetic hypoxia-response promoter (9X HRE) seemed to function constitutively when evaluated with RT-PCR (feEPO mRNA production) while feEPO protein production appeared to be minimally affected by the hypoxic conditions (subjectively reduced protein production in cells incubated in normoxic conditions relative to hypoxic culture conditions). These results were not considered to be sufficiently impressive to warrant *in vivo* experiments, and an alternative promoter was sought for the rodent studies.

Vector D features the constitutively active SV40 promoter which is functionally attenuated relative to the CMV promoter. Prior studies have shown more stable, long term transgene expression with the SV40 promoter relative to with the CMV promoter[43]. We confirmed successful lentiviral vector transduction via fluorescence (Control vector), feEPO mRNA detection in Vector D transduced cells, and feEPO protein production using WB analyses. Further, we demonstrated a marked decrease in feEPO protein production in Vector D transduced CRFK cells that were subsequently treated with GCV relative to cells that were not treated with GCV. These findings suggest that the HSV-TK suicide gene functioned as anticipated by either killing the transduced cells or inhibiting protein production. Interestingly, GCV-treated cells did not demonstrate a commensurate reduction in feEPO mRNA production. An explanation for this finding was not conclusively determined. The Vector D transduced cells treated with GCV demonstrated cytological evidence of cytotoxicity, however, extensive cell death was not identified (loss of cell monolayer). However, in order for GCV to cause cell death, the cell must be undergoing active cell division. In the confluent monolayers of Vector D transduced cells, cell division may have been minimal. Further, it is possible that the *in vitro* 3-day GCV dosing regimen was only marginally adequate, and a more prolonged dosing regimen would be more optimal. It has also been shown that mRNA expression does not always correlate with protein expression as protein expression can also be regulated at the level of translation[56]. Cells undergoing apoptosis can also have substantial inhibition of protein synthesis[52].

Based on the *in vitro* tissue culture studies, the project was extended to a pilot rat study *in vivo*. We found that rats inoculated with Vector D lentivirus had a significant, but transient increase in PCV relative to untreated rats and rats treated with Vector D plasmid DNA. The

results of this pilot rat study provided an impetus for moving forward with Vector D lentivirus into additional rodent models.

To better evaluate the efficacy and persistence of Vector D treatment, a more biologically relevant anemic mouse model was utilized in a series of *in vivo* experiments. The genetically modified anemic mice treated (inoculated/transduced) with Vector D lentivirus had a statistically significant but transient increase in blood PCV relative to control mice. For the rats, the maximum effect was an increase in average PCV from approximately 50% to 58% (16% increase over control), while for murine study #1, PCV rose from approximately 20% to 30% (51% increase), and in murine study #2 the PCV rose from approximately 20% to 47 (144% increase). These magnitudinal differences in PCV are likely a reflection of the progressive lentiviral dose escalation with each new study with the rats receiving  $3.81 \times 10^3$  TU per gram (g) of body weight (BW), the mice in the first murine experiment receiving  $3.15 \times 10^6$  TU/g of BW, and the mice in the final murine study receiving  $4.30 \times 10^6$  TU/g of BW.

The gradual attenuation of the PCV augmentation over time *in vivo* may have several possible explanations, including host-directed immune-mediated destruction of the feline specific EPO transprotein, eventual loss or destruction of the transduced skeletal myocytes, or loss of signaling efficiency by the feEPO transprotein in these xenogenic rodent models. Transduced cells can signal to the host immune system that transgenic material has been detected resulting in destruction of the transduced cells[57]. There is generally high sequence conservation of the erythropoietin gene among mammals[58] with the feline EPO gene (ENSFCAG00000006850) being 81.25% similar to mouse (*Mus musculus*; ENSMUSG00000029711) and 82.29% similar to rat (*Rattus norvegicus*; ENSRNOG00000001412). An immunologic attack on transduced cells is less likely to be the mechanism of attenuation in the rodents based on a lack of histopathologic

lesions detected in the inoculated muscle tissue; however, it cannot be completely ruled out as it remains possible that focal myocyte inflammation or loss was not adequately sampled or examined microscopically. Attempts to validate an ELISA in order to detect serum antibodies in the inoculated rodents directed against recombinant feline EPO (Kingfisher Biotech) were not successful (data not shown).

Similar to other studies delivering feline EPO to cats using an AAV vector, the development of pure red cell aplasia appears to have occurred in a single mouse when administered a second dose of Vector D lentivirus. We suspect that the profound anemia (PCV 4%) resulted from the development of murine antibodies directed against the feline EPO product which subsequently cross-neutralized the endogenous mouse EPO (produced at very low levels in the EPO disrupted transgenic mice). However, we do not anticipate that immunologic clearance will be a significant problem in cats treated with their own native feEPO gene.

We identified *in vitro* evidence that the construct HSV-TK/GCV suicide gene system abrogated feEPO protein production when transduced CRFK cells were treated with GCV. However, decreased blood PCV was not observed *in vivo* in Vector D inoculated mice that were subsequently treated with GCV intraperitoneally. However, the HSV-TK/GCV system is designed to function in replicating cells as the GCV end product (GCV triphosphate) gets incorporated into DNA during cell replication leading to the inhibition of DNA synthesis and resulting in cell death[59, 60]. Therefore, skeletal myocytes may not represent the ideal transduction target as myocytes are generally long-lived with limited ongoing cell replication. Further, the histologic evidence of degeneration and cell death in the replicating germ cells of the testes confirmed that GCV was successfully administered as GCV is known to be toxic for these germ cells. Endogenous mammalian TK, which has been shown to be synthesized at a 10-fold

greater rate in cells in S phase compared to G1 phase[61], makes highly mitotic cells (such as germ cells in the testes) particularly sensitive to the drug, ganciclovir[62].

Collectively, these results provide a justification for a lentiviral gene therapy approach to treating non-regenerative anemia associated with chronic renal disease in cats.

### Acknowledgements

We would like to acknowledge and thank the UC Davis School of Veterinary Medicine Histology Laboratory, Dr. Jay Solnick's lab (UC Davis), and the UC Davis Teaching and Research Animal Care Services (TRACS).

### Funding

This research was sponsored by Morris Animal Foundation (*in vitro* experiments only; D13FE-30), the University of California Davis Peter C. Kennedy Endowed Fellowship, the University of California Center for Companion Animal Health, School of Veterinary Medicine, UC Davis (2017-19-R; 2020-43-R; 2022-68-R), and EveryCat Health Foundation (W21-007).

### **References**

1. Mendell, J.R., et al., *Current clinical applications of in vivo gene therapy with AAVs*. Molecular Therapy, 2021. **29**(2): p. 464-488.
2. Anguela, X.M. and K.A. High, *Entering the modern era of gene therapy*. Annu Rev Med, 2019. **70**(1): p. 273-288.
3. Young, L.S., et al., *Viral gene therapy strategies: from basic science to clinical application*. The Journal of Pathology: A Journal of the Pathological Society of Great Britain and Ireland, 2006. **208**(2): p. 299-318.
4. Bulaklak, K. and C.A. Gersbach, *The once and future gene therapy*. Nature communications, 2020. **11**(1): p. 1-4.
5. Zakirova, E.Y., et al., *Genetic Therapy in Veterinary Medicine*. BioNanoScience, 2022.

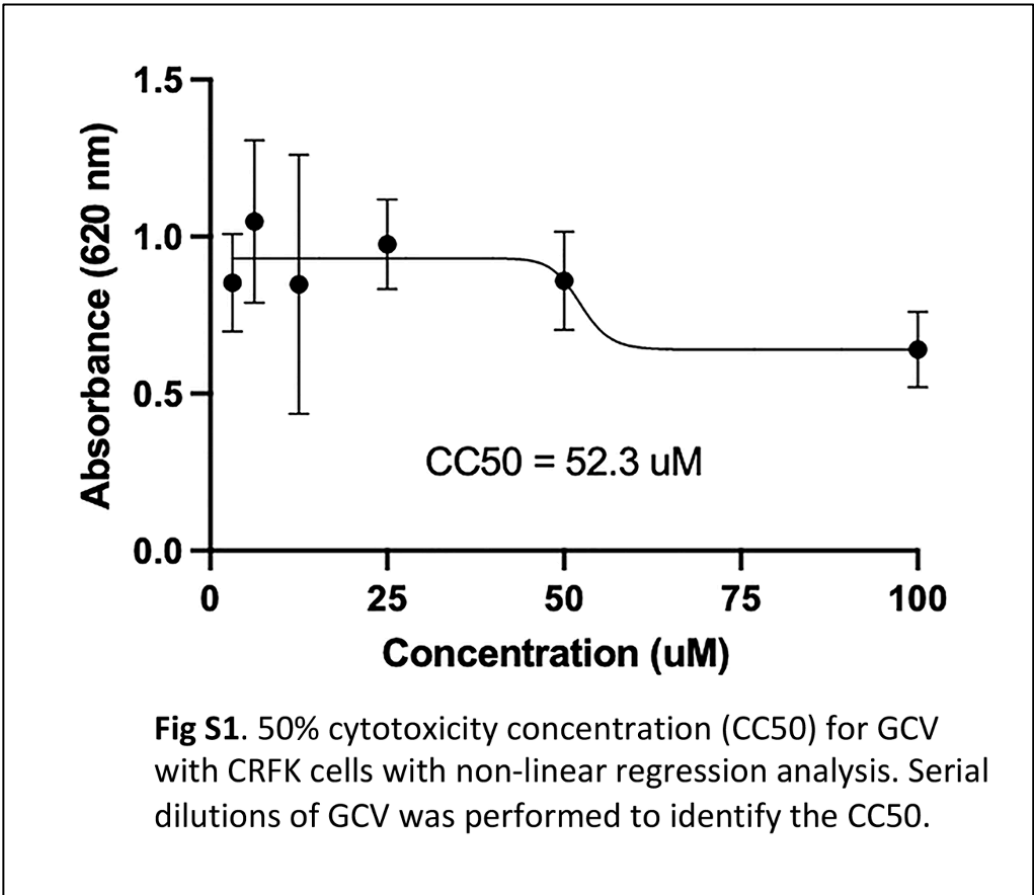
6. Marino, C.L., et al., *Prevalence and classification of chronic kidney disease in cats randomly selected from four age groups and in cats recruited for degenerative joint disease studies*. Journal of feline medicine and surgery, 2014. **16**(6): p. 465-472.
7. Jepson, R.E., *Current understanding of the pathogenesis of progressive chronic kidney disease in cats*. Veterinary Clinics: Small Animal Practice, 2016. **46**(6): p. 1015-1048.
8. Quimby, J.M., et al., *Feline chronic kidney disease is associated with shortened telomeres and increased cellular senescence*. American Journal of Physiology-Renal Physiology, 2013. **305**(3): p. F295-F303.
9. Greene, J.P., et al., *Risk factors associated with the development of chronic kidney disease in cats evaluated at primary care veterinary hospitals*. Journal of the American Veterinary Medical Association, 2014. **244**(3): p. 320-327.
10. Elliott, J., et al., *Survival of cats with naturally occurring chronic renal failure: effect of dietary management*. Journal of Small Animal Practice, 2000. **41**(6): p. 235-242.
11. Hughes, K., et al., *Diet and lifestyle variables as risk factors for chronic renal failure in pet cats*. Preventive veterinary medicine, 2002. **55**(1): p. 1-15.
12. Sparkes, A.H., et al., *ISFM consensus guidelines on the diagnosis and management of feline chronic kidney disease*. Journal of feline medicine and surgery, 2016. **18**(3): p. 219-239.
13. Brown, C., et al., *Chronic kidney disease in aged cats: clinical features, morphology, and proposed pathogeneses*. Veterinary pathology, 2016. **53**(2): p. 309-326.
14. Elliott, J. and P. Barber, *Feline chronic renal failure: clinical findings in 80 cases diagnosed between 1992 and 1995*. Journal of Small Animal Practice, 1998. **39**(2): p. 78-85.
15. DiBartola, S., et al., *Clinicopathologic findings associated with chronic renal disease in cats: 74 cases (1973-1984)*. Journal of the American Veterinary Medical Association, 1987. **190**(9): p. 1196-1202.
16. Koury, S.T., et al., *Quantitation of erythropoietin-producing cells in kidneys of mice by in situ hybridization: correlation with hematocrit, renal erythropoietin mRNA, and serum erythropoietin concentration*. 1989.
17. Koury, S.T., M.C. Bondurant, and M.J. Koury, *Localization of erythropoietin synthesizing cells in murine kidneys by in situ hybridization*. Blood, 1988. **71**(2): p. 524-527.
18. Lacombe, C., et al., *Peritubular cells are the site of erythropoietin synthesis in the murine hypoxic kidney*. The Journal of clinical investigation, 1988. **81**(2): p. 620-623.
19. Bachmann, S., M. Le Hir, and a.K.-U. Eckardt, *Co-localization of erythropoietin mRNA and ecto-5'-nucleotidase immunoreactivity in peritubular cells of rat renal cortex indicates that fibroblasts produce erythropoietin*. Journal of Histochemistry & Cytochemistry, 1993. **41**(3): p. 335-341.
20. Koury, M.J. and M.C. Bondurant, *Maintenance by erythropoietin of viability and maturation of murine erythroid precursor cells*. Journal of cellular physiology, 1988. **137**(1): p. 65-74.
21. Koury, M.J. and M.C. Bondurant, *Erythropoietin retards DNA breakdown and prevents programmed death in erythroid progenitor cells*. Science, 1990. **248**(4953): p. 378-381.
22. Cowgill, L.D., et al., *Use of recombinant human erythropoietin for management of anemia in dogs and cats with renal failure*. Journal of the American Veterinary Medical Association, 1998. **212**(4): p. 521-528.

23. Chalhoub, S., C. Langston, and J. Farrelly, *The use of darbepoetin to stimulate erythropoiesis in anemia of chronic kidney disease in cats: 25 cases*. Journal of Veterinary Internal Medicine, 2012. **26**(2): p. 363-369.
24. Randolph, J.F., et al., *Expression, bioactivity, and clinical assessment of recombinant feline erythropoietin*. American journal of veterinary research, 2004. **65**(10): p. 1355-1366.
25. Nayerossadat, N., T. Maedeh, and P.A. Ali, *Viral and nonviral delivery systems for gene delivery*. Advanced biomedical research, 2012. **1**.
26. Collins, M. and A. Thrasher, *Gene therapy: progress and predictions*. Proceedings of the Royal Society B: Biological Sciences, 2015. **282**(1821): p. 20143003.
27. Beall, C., et al., *Transfer of the feline erythropoietin gene to cats using a recombinant adeno-associated virus vector*. Gene therapy, 2000. **7**(6): p. 534-539.
28. Walker, M.C., et al., *Expression of erythropoietin in cats treated with a recombinant adeno-associated viral vector*. American journal of veterinary research, 2005. **66**(3): p. 450-456.
29. Vapniarsky, N., et al., *A lentiviral gene therapy strategy for the in vitro production of feline erythropoietin*. 2012.
30. Dey, D. and G. Evans, *Suicide gene therapy by herpes simplex virus-1 thymidine kinase (HSV-TK)*. Targets Gene Therapy, 2011. **65**.
31. Beltinger, C., et al., *Herpes simplex virus thymidine kinase/ganciclovir-induced apoptosis involves ligand-independent death receptor aggregation and activation of caspases*. Proceedings of the National Academy of Sciences, 1999. **96**(15): p. 8699-8704.
32. Karjoo, Z., X. Chen, and A. Hatefi, *Progress and problems with the use of suicide genes for targeted cancer therapy*. Advanced drug delivery reviews, 2016. **99**: p. 113-128.
33. Dull, T., et al., *A third-generation lentivirus vector with a conditional packaging system*. Journal of virology, 1998. **72**(11): p. 8463-8471.
34. Zufferey, R., et al., *Self-inactivating lentivirus vector for safe and efficient in vivo gene delivery*. Journal of virology, 1998. **72**(12): p. 9873-9880.
35. Naldini, L., et al., *In vivo gene delivery and stable transduction of nondividing cells by a lentiviral vector*. Science, 1996. **272**(5259): p. 263-267.
36. Boshart, M., et al., *A very strong enhancer is located upstream of an immediate early gene of human cytomegalovirus*. cell, 1985. **41**(2): p. 521-530.
37. Costa, A.R., et al., *Guidelines to cell engineering for monoclonal antibody production*. European Journal of Pharmaceutics and Biopharmaceutics, 2010. **74**(2): p. 127-138.
38. Foelckig, M.K. and H. Hofstetter, *Powerful and versatile enhancer-promoter unit for mammalian expression vectors*. Gene, 1986. **45**(1): p. 101-105.
39. Bailey, L.A., et al., *Determination of Chinese hamster ovary cell line stability and recombinant antibody expression during long-term culture*. Biotechnology and bioengineering, 2012. **109**(8): p. 2093-2103.
40. Hsu, C.-C., et al., *Targeted methylation of CMV and E1A viral promoters*. Biochemical and biophysical research communications, 2010. **402**(2): p. 228-234.
41. Viault, F., *Sur l'augmentation considerable du nombre des globules rouges dans sang chez les habitants des haut plateaux de l'Amerique de Sud*. Comp rend Acad d sc, 1890. **111**: p. 917-918.

42. Goldberg, M.A., et al., *The regulated expression of erythropoietin by two human hepatoma cell lines*. Proceedings of the National Academy of Sciences, 1987. **84**(22): p. 7972-7976.
43. Wang, X.-Y., et al., *Impact of different promoters on episomal vectors harbouring characteristic motifs of matrix attachment regions*. Scientific reports, 2016. **6**(1): p. 1-10.
44. Wagner, M.J., J.A. Sharp, and W.C. Summers, *Nucleotide sequence of the thymidine kinase gene of herpes simplex virus type 1*. Proceedings of the National Academy of Sciences, 1981. **78**(3): p. 1441-1445.
45. Yan, J., et al., *Signal sequence is still required in genes downstream of "autocleaving" 2A peptide for secretory or membrane-anchored expression*. Analytical biochemistry, 2010. **399**(1): p. 144-146.
46. Cook, S.E., et al., *Investigation of monotherapy and combined anticoronaviral therapies against feline coronavirus serotype II in vitro*. Journal of Feline Medicine and Surgery, 2021: p. 1098612X2110486.
47. Murphy, B., et al., *FIV establishes a latent infection in feline peripheral blood CD4+ T lymphocytes in vivo during the asymptomatic phase of infection*. Retrovirology, 2012. **9**(1): p. 1-17.
48. Pichon, A., et al., *Erythropoietin and the use of a transgenic model of erythropoietin-deficient mice*. Hypoxia, 2016. **4**: p. 29.
49. Maxwell, P.H., et al., *Identification of the renal erythropoietin-producing cells using transgenic mice*. Kidney international, 1993. **44**(5): p. 1149-1162.
50. Macarlapu, J., et al., *Time course of ventilatory acclimatisation to hypoxia in a model of anemic transgenic mice*. Respiratory physiology & neurobiology, 2006. **153**(1): p. 14-22.
51. Blumenthal, M., et al., *Effective suicide gene therapy for leukemia in a model of insertional oncogenesis in mice*. Molecular Therapy, 2007. **15**(1): p. 183-192.
52. Clemens, M., et al., *Translation initiation factor modifications and the regulation of protein synthesis in apoptotic cells*. Cell Death & Differentiation, 2000. **7**(7): p. 603-615.
53. Rayburn, E.R., et al., *FDA-approved drugs that are spermatotoxic in animals and the utility of animal testing for human risk prediction*. Journal of Assisted Reproduction and Genetics, 2018. **35**(2): p. 191-212.
54. Brooks, A.R., et al., *Transcriptional silencing is associated with extensive methylation of the CMV promoter following adenoviral gene delivery to muscle*. The Journal of Gene Medicine: A cross-disciplinary journal for research on the science of gene transfer and its clinical applications, 2004. **6**(4): p. 395-404.
55. Ngai, S.C., et al., *DNA methylation and histone modifications are the molecular lock in lentivirally transduced hematopoietic progenitor cells*. BioMed research international, 2015. **2015**.
56. Guo, Y., et al., *How is mRNA expression predictive for protein expression? A correlation study on human circulating monocytes*. Acta Biochimica et Biophysica Sinica, 2008. **40**(5): p. 426-436.
57. Zhou, H.s., D.p. Liu, and C.c. Liang, *Challenges and strategies: the immune responses in gene therapy*. Medicinal research reviews, 2004. **24**(6): p. 748-761.
58. Wen, D., et al., *Erythropoietin structure-function relationships: high degree of sequence homology among mammals*. 1993.
59. van Dillen, I.J., et al., *Influence of the bystander effect on HSV-tk/GCV gene therapy. A review*. Current gene therapy, 2002. **2**(3): p. 307-322.

60. Dachs, G.U., et al., *Bystander or no bystander for gene directed enzyme prodrug therapy*. *Molecules*, 2009. **14**(11): p. 4517-4545.
61. Sherley, J. and T.J. Kelly, *Regulation of human thymidine kinase during the cell cycle*. *Journal of Biological Chemistry*, 1988. **263**(17): p. 8350-8358.
62. Meyer, K.B., et al., *Identification of a critical window for ganciclovir-induced disruption of testicular development in rats*. *Toxicological Sciences*, 2018. **162**(2): p. 488-498.

Supplementary Figure



## Chapter 6. Conclusion

Despite many decades of study, feline infectious peritonitis (FIP) continues to be a challenging, fascinating, and clinically frustrating viral disease of domestic cats. Multiple facets of feline coronaviral virology, disease immunopathogenesis, and antiviral treatment strategies remain to be fully explained. The goals of this dissertation were: i) investigate FIPV serotype I cell receptor usage using RNA expression in variably permissive cell lines and immunohistochemistry studies using archived feline tissues, ii) compare and contrast FIPV serotype I and II replication kinetics in feline cells, iii) identify antiviral compounds effective against FIPV serotype I and II replication, and iv) perform pharmacokinetic analyses on select antiviral agents in healthy, SPF cats *in vivo* (in order to establish therapeutic dose). A parallel lentiviral gene therapy project was carried out using both *in vitro* cell lines and *in vivo* animal models that also explored viral cell entry, dissemination, and persistence in the host cells and rodents. We developed and tested a lentiviral-vectored gene therapy system with the ultimate goal of treating cats with chronic renal disease-associated anemia.

To achieve these objectives, in Chapter 2, serotype I and II FIPV were propagated in a selection of feline cells in order to document differential replication kinetics between the two tissue-culture adapted FIP viral serotypes. In these studies, we contrasted the gene expression profiles for multiple known coronavirus receptors in the variably FIPV permissive cell types FCWF4- CU and FCWF-4. The primary cell receptor for FIPV serotype II has been previously determined to be feline aminopeptidase N (feAPN), while the primary cell receptor for FIPV serotype I is currently unknown. The recent development of a feline cell line that efficiently propagates FIPV serotype I (FCWF-4 CU) contrasted to the marginally permissive and closely related FCWF-4 cell line provides an *in vitro* system for leveraging information from the differential viral replication patterns. We determined the global gene expression patterns (RNAseq) for these two feline cell lines and identified six differentially expressed transcripts with potential to explain the differential replication efficiencies. Candidate differentially expressed

cellular genes include cathepsin S and C, transmembrane serine protease 7 (TMPRSS7), rhomboid-like 2 serine endopeptidase (RHBDL2), ephrin A1, and ephrin B2.

Although dramatic pharmaceutical advances have been made recently in antiviral therapies for a number of infectious agents, there still remains a lack of affordable, readily available and licensed antiviral treatments for FIP. Although currently only obtained through “black market” channels in North America and Europe, the nucleoside analog GS-441524 nevertheless remains one of the most effective antiviral therapies for use in cats with naturally occurring FIP. Unfortunately, there are currently multiple regulatory challenges to the legal use of GS-441524 in veterinary settings. Therefore, in Chapter 3, we screened 90 putative antiviral compounds for efficacy against FIPV serotype II (WSU-79-1146) using real-time RT-PCR based assays and identified 26 compounds with antiviral activity representing differing drug classes and mechanisms of action. In addition, we approached antiviral assessment in Chapter 4 using an optimized biological colorimetric assay to compare the efficacy of the protease inhibitors, GC376 and nirmatrelvir and the nucleoside/nucleotide analogs, remdesivir, GS-441524, molnupiravir (MPV; EIDD-2801), and  $\beta$ -D-N4-hydroxycytidine (NHC; EIDD-1931) against both FIPV serotype I and II as monotherapies as well as in strategic combined therapies. We found GS-441524, remdesivir (RDV), MPV, GC376, nirmatrelvir, and NHC to be potent inhibitors of replication for both viral serotypes and that all of the tested antiviral compounds predictably demonstrated lower EC<sub>50</sub> values for FIPV I relative to FIPV II. Three select antiviral combinations, each including a nucleoside analog combined with a viral protease inhibitor, were assessed against FIPV serotype II to determine evidence for additive and/or synergistic antiviral effects. Compound synergy was identified for all three of the antiviral combinations, which included (1) nirmatrelvir combined with MPV, (2) GC376 combined with RDV, and (3) nirmatrelvir combined with RDV. The antiviral efficacy against both serotypes coupled with antiviral synergy supports the proposed application for combined therapy in cats with naturally

occurring FIP, particularly those cats with more challenging clinical presentations (brain and/or eye) or refractory disease (treatment failure).

As an additional step towards establishing effective and rational clinical therapy, we also determined the pharmacokinetic properties (metabolism) of molnupiravir (MPV), GS-441524, and remdesivir (RDV) administered orally and/or intravenously. Similar to what has been identified in humans, we found that MPV is rapidly metabolized in feline plasma *in vivo* to the metabolite NHC. We detected the NHC metabolite at early timepoints in the 24-hour time period and at markedly higher levels than the administered prodrug, MPV. There was sufficient oral bioavailability of MPV to yield serum levels of the active metabolite, NHC, greater than the half maximal concentration ( $EC_{50}$ ) when administered at 10 mg/kg. For GS-441524 and RDV, there was sufficient oral bioavailability, which yields therapeutic plasma levels of GS-441524 for treatment of FIP when administered at 25 mg/kg (both compounds).

As a parallel adjunct study in Chapter 5, we created a lentiviral-vectored gene therapy system as a model for treating cats with chronic renal disease (CRD)-associated anemia. CRD is a common condition in aged cats that results from a reduced renal production of erythropoietin (EPO). We designed a series of replication defective, third-generation lentivirus-based vectors to encode and produce the native feEPO protein in tissue culture experiments and in multiple rodent models *in vivo*. The vectors were designed to include a genetic-pharmacologic safety mechanism through the incorporation of the “suicide gene” HSV-TK in the gene therapy vector. The HSV-TK gene product allows for the pharmacologic termination of the therapeutic effect in the event of supraphysiologic polycythemia. Using an optimized lentiviral vector encoding the feline EPO gene we (i) demonstrated successful transduction of human and feline cells *in vitro* via the detection of bioactive feEPO mRNA transcripts using real-time RT-PCR and protein production (western blot), (ii) demonstrated the *in vivo* relevance of this method in a rat pilot study through the documentation of elevated packed cell volumes

(PCV) in treated rats, and (iii) demonstrated a prolonged and magnitudinally greater effect on PCV in a more biologically-relevant EPO-deficient anemic mouse model. Collectively, the results of these gene therapy studies provide a justification for a lentiviral gene therapy approach to treating non-regenerative anemia associated with CRD in cats.